Universidade de Trás-os-Montes e Alto Douro

SILICA NANOPARTICLES IN ORAL PEPTIDE DELIVERY FOR DIABETES *MELLITUS* CONTROL AND TREATMENT

TESE APRESENTADA PARA OBTENÇÃO DO GRAU DE DOUTOR EM CIÊNCIAS QUÍMICAS E BIOLÓGICAS

Tatiana Andreani

Orientadora: Professora Doutora Eliana B. Souto
Coorientadora: Professora Doutora Amélia M. Lopes Dias da Silva

Vila Real, 2014

Universidade de Trás-os-Montes e Alto Douro

SILICA NANOPARTICLES IN ORAL PEPTIDE DELIVERY FOR DIABETES *MELLITUS* CONTROL AND TREATMENT

TESE APRESENTADA PARA OBTENÇÃO DO GRAU DE DOUTOR EM CIÊNCIAS QUÍMICAS E BIOLÓGICAS

Tatiana Andreani

Orientadora: Professora Doutora Eliana B. Souto
Coorientadora: Professora Doutora Amélia M. Lopes Dias da Silva

Composição do Júri:

_____
_____
_____
_____
_____
_____
_____

Vila Real, 2014

Tatiana Andreani

Silica nanoparticles in oral peptide delivery for Diabetes *Mellitus* control and treatment

Thesis submitted to the Universidade de Trás-os-Montes e Alto Douro in fulfillment of the requirements for the degree of Philosophy Doctor, in the Field of Chemical and Biological Sciences, under the guidance of Professors Eliana B. Souto and Amélia M. Silva

Acknowledgements

I express my deep sense of gratitude and reverence to God for every moment experienced in Portugal and especially for the opportunity of learning during the whole PhD.

I am extremely grateful to my dear parents who support me over the distance and always believe in me. Thanks also to my sisters (Juli and Fabi), so loving and that always gave me motivation to follow my dreams - without all of you, none of this would have been possible.

Special thanks to Marco, my eternal love, for his supreme sacrifice, unwavering support and affection and for giving me optimism to never giving up.

I am grateful to my dear friend Joana Fangueiro for her friendship and for spending countless hours with me writing scientific papers and thesis and mainly for helping me in several down moments in my life.

I similarly extend heartfelt thanks to my friend and collaborators at Universidade Estadual Paulista (UNESP). Thank you – Professor Maria Palmira, Ana Luiza, Charlene, Leonardo and Esteban for receiving me and for acclimating me to the laboratory. Thank you for constant help and valuable advices. Without them would be difficult to carry out this work.

I would like to thank to my colleagues from UTAD and Fernando Pessoa University (UFP), Vânia, Ana Sofia, Bruno and Slavomira for their moral support, help and encouragement.

I would like to thank to my friends at Department of Geology – Mizé, Rui and Paula for our fun lunches at the canteen.

Thanks to technicians and professors at Department of Biology and Environment (UTAD) and at UFP for their help and support during the period of my project.

I would like to thank Lisete Fernandes from Microscopy Unit for her help with TEM images and X-Ray analysis. I also would like to thanks to Professor Verónica Bermudez and Mariana Almeida for their constant help in DSC studies and for interesting discussions about sol-gel technology.

Big thanks to Professor Maria Luiza García from Barcelona University, for receiving me in her laboratory and for her invaluable help in my investigation when I really needed it.

I wish to express my most sincere, heartfelt thanks to my supervisors and friends, Professors Eliana B. Souto and Amélia M. Silva, for their excellence guidance, constant encouragement and unending enthusiasm about our work. Their friendship and support made my PhD experience exciting and fruitful, and for this I will be forever grateful.

Finally, I would like to acknowledge the Fundação para Ciência e Tecnologia (FCT, Portugal) for financial support, grating me a PhD scholarship (SFRH/BD/60640/2009). FCT is also acknowledged under the reference PTDC/SAU-FAR/113100/2009 and PEst-C/AGR/UI4033/2011.

Resumo

O presente trabalho visou o desenvolvimento de nanopartículas de sílica (SiNP, do inglês "silica nanoparticles") com a finalidade de explorar o potencial destes sistemas para a administração oral de péptidos, usando a insulina como fármaco modelo.

As SiNP foram produzidas a partir da hidrólise e condensação do silicato de tetraetila (TEOS) pelo método sol-gel e otimizadas usando um desenho fatorial 2^2. O tamanho médio (Z-Ave) e o índice de polidispersão (PI) das nanopartículas foram influenciados pela concentração de TEOS e pela velocidade de agitação durante a síntese das mesmas. Foram obtidas nanopartículas com 0,43 $mol.L^{-1}$ de TEOS e uma velocidade de homogeneização de 5000 rpm, revelando um Z-Ave de 256,6 nm e um PI de 0,218. Trealose, manitol e sorbitol foram utilizados como crioprotetores a fim de melhorar a estabilidade das nanopartículas durante a liofilização. Calorimetria diferencial de varrimento (DSC) e raio-X revelaram que as SiNP na presença dos crioprotetores apresentaram uma forma cristalina. No entanto, a trealose foi a mais adequada para a manutenção da integridade das nanopartículas após a sua reconstituição em água, uma vez que este dissacarídeo oferece maior resistência das camadas em torno das nanopartículas, a qual promove maior interação com os grupos SiOH presentes na superfície da sílica.

O revestimento das SiNP com quitosano, alginato de sódio, PEG 6000 e PEG 20000 foi realizado para desenvolver uma formulação destinada à administração oral de insulina por meio da combinação das vantagens das SiNP e das propriedades mucoadesivas desses polímeros. A associação da insulina às nanopartículas foi realizada por adsorção após a produção das mesmas. No caso das nanopartículas revestidas, a insulina foi previamente dissolvida na solução polimérica e posteriormente adicionada às SiNP.

Estudos de DSC revelaram que os picos endotérmicos e exotérmicos dos polímeros puros foram deslocados para temperaturas mais elevadas nas SiNP revestidas, provavelmente devido à interação de ligação de hidrogénio entre os grupos de SiOH das SiNP e os grupos funcionais específicos do PEG (OH), do quitosano (NH) ou do alginato de sódio (COOH). Esta alteração resultou em maior estabilidade das nanopartículas. A difração de raio-X mostrou que as SiNP revestidas exibiram uma estrutura menos ordenada comparado com os polímeros puros. A associação da insulina às nanoparticulas resultou numa estrutura mais cristalina, provavelmente devido à solubilização da insulina nas soluções poliméricas

originando a cristalização das nanoparticulas durante o armazenamento. A análise por infravermelho por transformada de Fourier (FTIR) também mostrou a eficiência do revestimento das nanopartículas, além das bandas de absorção de amida que são características essenciais dos espectros de proteínas. Análises por dicroísmo circular (CD) demonstraram que a estrutura da insulina foi ligeiramente afetada pelo revestimento durante a síntese das nanopartículas.

Termogramas obtidos por nano DSC mostraram que as SiNP não revestidas podem promover melhor interação com os grupos polares dos liposomas. Além disso, as SiNP e o PEG 6000 foram mais eficazes em proteger a insulina contra a desnaturação térmica.

A mucoadesividade das nanopartículas foi avaliada *in vitro* pela interação com mucina a pH gástrico e intestinal. SiNP revestidas com quitosano ou alginato apresentaram melhor capacidade de adsorver a mucina, em comparação com as SiNP não revestidas e as SiNP revestidas com PEG (SiNP-PEG 6000).

O revestimento das nanopartículas resultou numa libertação da insulina mais rápida tanto a pH 2,0 como a pH 6,8, comparando com as nanopartículas não revestidas, devido à baixa interação entre a insulina e os grupos SiOH da superfície da sílica. O perfil de libertação de insulina foi afetado apenas pelas SiNP não revestidas e pelas SiNP-PEG 6000 em relação à solução de insulina. Embora as SiNP não revestidas e as SiNP-PEG 6000 tenham provocado redução da libertação de insulina a pH gástrico, 60% da insulina foi libertada após 2 horas de incubação.

Os estudos *in vitro* de permeação da insulina foram realizados por meio do saco intestinal invertido de ratos, comparando as nanopartículas não revestidas e SiNP-PEG 6000 e SiNP-PEG 20000. No entanto, a presença do PEG não alterou significativamente o comportamento da permeação da insulina na mucosa intestinal de ratos.

As nanopartículas mostraram baixa toxicidade nas linhagens celulares testadas (HepG2 e Caco-2) nas concentrações de 50-500 μg/mL. A incorporação da insulina nas nanopartículas não afetou a viabilidade celular. Doses mais elevadas de SiNP-PEG 6000 apresentaram toxicidade nas linhas celulares selecionadas. Imagens obtidas por microscopia óptica revelaram a presença de vacúolos no interior das células Caco-2, indicando uma possível endocitose dessas nanopartículas.

As SiNP podem ser consideradas como sistemas promissores para a dministração oral da insulina aplicando uma tecnologia simples, de baixo-custo e sem danos ao ambiente.

Palavras-chave: Nanopartículas de sílica, insulina, polímeros mucoadesivos, administração oral, citotoxicidade

Abstract

The present work has been focused on the synthesis of silica nanoparticles (SiNP) intended to oral peptide delivery for Diabetes *mellitus* control and treatment, using insulin as model drug.

SiNP were synthesized from the hydrolysis and condensation of tetraethyl orthosilicate (TEOS) by sol-gel technology. Nanoparticles were optimized using a 2^2factorial design approach. The mean particle size (Z-Ave) and polydispersity index (PI) were influenced by TEOS concentration and by stirring speed during nanoparticle synthesis. Optimized SiNP were obtained using 0.43 $mol.L^{-1}$of TEOS and the homogenization speed of 5000 rpm, depicting a Z-Ave of 256.6 nm and a PI of 0.218.

Trehalose, mannitol and sorbitol were used as cryoprotectants to improve SiNP stabilization during lyophilization. Differential scanning calorimetry (DSC) and X-ray studies demonstrated that SiNP in the presence of different cryoprotectans showed a crystalline behavior. However, trehalose was more suitable in maintaining particle integrity after reconstitution of lyophilized nanoparticles in water, due to the higher spatial resistance of its layers around the nanoparticles, leading to stronger interaction with SiOH groups in comparison to mannitol or sorbitol.

After formulation optimization, the next step was to coat SiNP with chitosan, sodium alginate, PEG 6000 and PEG 20000 to develop a system for oral insulin administration by combining the SiNP advantages and the mucoadhesive properties of hydrophilic polymers. Insulin was associated to different nanoparticles by adsorption after nanoparticles production. In the case of coated nanoparticles, insulin was previously dissolved in the polymer solution and then added to SiNP.

Interaction between insulin and nanoparticles was assessed by DSC, X-ray and Fourier-transform infrared (FTIR) studies. DSC showed that endothermic and exothermic peaks of pure polymers were shifted to higher temperatures in all coated SiNP, probably due to the interaction by hydrogen bounds between SiNP SiOH groups and specific functional groups of PEG (OH), chitosan (NH) or sodium alginate (COOH), resulting in more stable nanoparticles. X-ray diffraction showed that coated SiNP displayed less ordered structure compared with pure polymers. The association of insulin to nanoparticles resulted in more crystalline structure due to the insulin solubilization into the polymers solutions leading to the

nanoparticles crystallization during storage. FTIR analysis showed the high efficiency nanoparticles coating, as well as amide absorption bands which are characteristic of protein spectra.

Insulin secondary structure was assessed by Circular Dichroism (CD) after protein dissolution into polymer solutions during nanoparticle synthesis, showing that insulin structure was slightly affected by coating.

Nano DSC was used to evaluate the interaction between nanoparticles and the biomembrane models (liposomes), and the thermal insulin stability dissolved in the different polymers. The interaction between nanoparticles and liposomes showed that uncoated SiNP could promote higher interaction with the polar head groups of liposomes. Also, uncoated SiNP were more effective in protecting insulin from thermal denaturation.

The nanoparticles mucoadhesive properties were assessed by *in vitro* interaction with mucin at gastric and intestinal pH. SiNP coated with chitosan or alginate showed better ability in adsorbing to mucin in comparison to uncoated SiNP and PEG-coated SiNP.

It was observed that nanoparticles coated with mucoadhesive polymers resulted in faster insulin release at pH 2.0 and 6.8 in comparison to uncoated nanoparticles due to the low interaction between insulin and SiOH present onto the silica surface. Insulin release profile was only significantly affected by uncoated SiNP and PEG 6000-coated SiNP in comparison to insulin solution. Although, uncoated and PEG-coated SiNP reduced insulin release at gastric pH, 60% of insulin was released at pH 2.0 after 2 h.

In vitro insulin permeation studies were conducted through everted rat intestine comparing uncoated and PEG-coated SiNP. However, the presence of PEG onto the silica surface did not significantly change the permeation behavior of insulin through the intestinal mucosa.

In general, all nanoparticles showed to be biocompatible, revealing low toxicity in different human cancer cell lines (HepG2 and Caco-2) at tested concentrations (50-500 μg/mL). The presence of insulin did not affect the cell viability significantly. Higher toxicities were observed for PEG 6000-coated SiNP at high concentrations. Microscope images revealed the formation of vacuoles in the Caco-2 cell body, indicating a possible endocytosis of these nanoparticles.

The present work allows the conclusion that coating of silica nanoparticles with mucoadhesive polymers influences their physicochemical properties, insulin release, as well as the cell viability. These studies and findings show the feasibility of applying silica

nanoparticles for oral insulin delivery using a simple, cheap and environmentally friendly technology.

Keywords: Silica nanoparticles, insulin, mucoadhesive polymers, oral delivery, cytotoxicity

Thesis Contents

Figure Captions

Table Captions

List of Abbreviations

Adm	Administration
AE	Association efficacy
AFM	Atomic force microscopy
AIC	Akaike information criteria
APC	Allophycocyanin
APDMOS	3-aoryloxypropyl) dimethoxymethylsilane
APS	Adaptor molecules containing PH and SH2 domains
ATP	Adenosine triphosphate
AUC	Area under curve
BMI	Body mass index
BSA	Bovine serum albumin
CBLC	Cas-Br-M (murine) ecotropic retroviral transforming sequence c
CH	Chitosan
CD	Circular dichroism
CTAB	Cetyltrimethyl-ammonium bromide
DGS	Diglyceroxysilane
DLS	Dynamic light scattering
DNA	Deoxyribonucleic acid
DPP-IV	Dipeptidyl peptidase-IV
DPPC	Dipalmitoylphosphatidylcholine
DRG	Dorsal root ganglia
DSC	Differential scanning calorimeter
EDTA	Diaminoethanetetraacetic acid
FDA	Food and Drug Administration
FITC	Fluorescein isothiocyanate
FITR	Fourier-transform infrared
FP	Farmacopéia portuguesa
G6PDH	Glucose-6-phosphate dehydrogenase

Gab1	Grb2-associated binder 1
HbA_{1c}	Glycosylated haemoglobin
GIP	Glucose-dependent insulinotropic polypeptide
GIT	Gastrointestinal tract
GLP-1	Glucagon-like peptide 1
GMNC	Genomagnetic nanocapturers
GPTMS	Glycidoxypropyl trimethoxysilane
h	Hour(s)
HAS	Human serum albumin
HbHNL	Hydroxynitrile lyase
HIM2	Hexyl-insulin monoconjugate
HIV	Human immunodeficiency virus
HP55	Hydroxypropyl methylcellulose phthalate
HPLC	High performance liquid chromatography
HPMCP	Hydroxypropyl methylcellulose phthalate
HRP	Horseradish perosidase
HSH	High shear homogenization
HVD-I	Hepatic-directed vesicle insulin
ICH	International Conference on Harmonization
Ins-CH	Insulin dissolved in chitosan solution
Ins-HCl/KCl	Insulin dissolved in HCl/KCl buffer
Ins-PBS	Insulin dissolved in Phosphate-buffered saline
Ins-PEG 6000	Insulin dissolved in PEG 6000 solution
Ins-PEG 20000	Insulin dissolved in PEG 20000 solution
Ins-SA	Insulin dissolved in sodium alginate solution
Ins-SiNP	Insulin associated to silica nanoparticles
Ins-SiNP-CH	Insulin associated to silica nanoparticles coated with chitosan
Ins-SiNP-PEG 6000	Insulin associated to silica nanoparticles coated with PEG 6000
Ins-SiNP-PEG 20000	Insulin associated to silica nanoparticles coated with PEG 20000
Ins-SiNP-SA	Insulin associated to silica nanoparticles coated with sodium alginate
IRS	Insulin receptor substrate

LCA-CoA	Long-chain fatty acyl CoA
MCM	Mesoporous cristalline materials
μDSC	Micro differential scanning calorimetry
MPS	Mononuclear phagocyte system
MRI	Magnetic resonance image
MSCs	Mesenchymal stem cells
MRT	Mean release time
MSiNP	Mesoporous silica nanoparticles
MWNT	Multi-walled carbon nanotubes
nDSC	Nano differential scanning calorimetry
NIR	Near infra-red
PACA	Poly(alkyl cyanocrylate)
PBS	Phosphate-buffered saline
PC	Phosphatidylcholine
PCL	Poly(ε-caprolactone)
PCS	Photon correlation spectroscopy
PDGF	Platelet Derived Growth Factor
pDNA	Plasmid DNA
PEG	Poly(ethylene glycol)
PEI	Polyethlyenimine
γ-PGA	Poly(γ-glutamic acid)
PH	Pleckstrin homology
PI	Polydispersity index
PLA	Poly(lactide acid)
PLE	Poly(lactic acid-co-ethylene oxide)
PLGA MS	Poly (D, L-lactic-co-glycolic acid) microspheres
PLGA-PEG-PLGA	Poly [(DL-lactide-co-glycolide)-b-ethylene glycol-b-(DL-lactide-coglycolide)]
PPAR-γ	Peroxisome proliferator-activated receptor-gamma
QD	Quantum dots
RES	Reticulo-endothelial system
RITC	Rodhamine B isothiocyanate
RSD	Relative standard deviation

SA	Sodium alginate
SBA	Santa Barbara Amorphous
SD	Standard deviation
SH	Shc
SiNP	Silica nanoparticles
SiNP-Sorb	Silica nanoparticles lyophilized with sorbitol
SiNP-Man	Silica nanoparticles lyophilized with mannitol
SiNP-Tre	Silica nanoparticles lyophilized with trehalose
SiNP-CH	Silica nanoparticles coated with chitosan
SiNP-PEG 6000	Silica nanoparticles coated with PEG 6000
SiNP-PEG 20000	Silica nanoparticles coated with PEG 20000
SiNP-SA	Silica nanoparticles coated with sodium alginate
SiRNA	Small interfering RNA
SLN	Solid lipid nanoparticles
SNAC	Sodium N-(8-[2-hydroxybenzoyl]-amino) caprylic acid)
S/O/O	Solid-in-oil-in-oil
SUR1	Sulfonylurea receptor 1
T2DM	Type 2 diabetes *mellitus*
TEOS	Tetraethyl ortosilicate
$\boldsymbol{Tg}$	Glass transition temperature
TEM	Transmission electron microscope
TFA	Trifluoroacetic acid
TL	Tomato lectin
$\boldsymbol{T_m}$	Transition temperature
TMC	Trimethyl chitosan
TMOS	Tetramethyl ortosilicate
UEA1	*Ulex europaeus* agglutinin 1
UI	Under investigation
UV	Ultraviolet
VEGF	Vascular endothelium growth factor
XRD	X-ray diffraction
Z-Ave	Mean particle size
ZP	Zeta potential

W/O	Water-in-oil
WGA	Wheat germ agglutinin
WHO	World Health Organization

Chapter I
General Introduction

1. A critical review on development of silica matrices and their biomedical applications

1.1. Sol-gel technology

The sol-gel technology, for a long time, has been used for synthesizing a variety of silica materials, either crystalline or amorphous of controlled porosity, as well as fibers (Turinske et al., 2013), films (Ghach et al., 2013), glasses (Ferrer et al., 2002) and nanoparticles (Deng et al., 2005) due to its ability to form products at mild conditions. This technology involves hydrolysis and condensation of metal alkoxysilanes precursors ($Si(OR)_4$), such as tetraethyl orthosilicate (TEOS), tetramethyl orthosilicate (TMOS) or inorganic salts, such as sodium silicate (Na_2SiO_3) under acidic or alkaline conditions. The hydrolysis reaction of TEOS can be expressed by the following formulae:

$$Si(OC_2H_5)_4 + H_2O \rightarrow Si(OC_2H_5)_3OH + C_2H_5OH$$

The hydrolysis of TEOS molecules forms silanol groups (SiOH). The condensation between the silanol groups or between silanol groups and alkoxysilanes precursor can lead to particles with siloxane bonds (Si-O-Si). Examples of condensation reactions are given bellow:

Water condensation

$$2Si–(OH)_4 \rightarrow 2\ SiO_2 + 4\ H_2O$$

Alcohol condensation

$$Si\text{-}(OH)_4 + Si\text{-}(OR)_4 \rightarrow SiO_2 + C_2H_5OH$$

Due to the low partial positive charge (δ) of silicon, the introduction of catalytic agents for nucleophilic attack is required. The catalyst most used in sol-gel process is mineral acids or ammonium, but neutral salts and transition metal alkoxides have also been employed.

1.1.1. Silica gel

1.1.1.1. Silica gel and drug release

Sol-gel technology provides several alternatives to synthesize various kinds of silica gel, which structure depends on many parameters, such as type and concentration of precursors, water to precursor ratio, nature and concentration of catalyst agent, solvent, temperature, as well as aging and dry processes (Iller, 1979; Jafarzadeh et al., 2009; Rahman et al., 2004; Sato et al., 1990).

The silica gels obtained by sol-gel process are usually classified according to the dispersion medium used in the gel preparation. Hydrogel consists of hydrophilic polymer networks with three dimension configuration enabling the imbibing of high amounts of water or biological fluids (Gehrke and Lee, 1990; Peppas and Mikos, 1986). In contrast, an alcogel is a colloidal gel which alcohol is the dispersion medium. After gel preparation, gel aging and drying can lead to the production of a xerogel or an aerogel. A xerogel is based on a solid from gel by drying at ambient pressure. This kind of drying usually results in shrinkage of the network, and further expelling of the liquid from the pores. The shrinkage mechanism is generally attributed to the new bond formation through condensation reaction.

Alternatively, when solvent removal occurs under supercritical conditions, the surface tension between liquid and vapor can be avoided and an aerogel is produced without porous collapse (Mohanan et al., 2005). Aerogels consist of pearl-necklace–like network of particles which 99 % of their bulk volume is empty (Pierre and Pajonk, 2002).

Although sol-gel based silica xerogels and aerogels have been exhaustively investigated as drug delivery carriers (Caputo et al., 2012; Costache et al., 2013), the release mechanisms of drugs from the gels have not been elucidated. Data demonstrate that the control release can be based on simple diffusion or a combination of the diffusion and erosion process (Ritger and Peppas, 1987; Wu et al., 2005). These processes are affected by several aspects, such as, molecular size and chemical characteristics of the drug, the matrix size, pH, interactions between the drug and the matrix and the texture of the gel (Prokopowicz, 2009). The hydrolysis and condensation reactions can be influenced by water/alkoxide increasing the surface area that can control and sustain the release of encapsulated compounds (Tan et al., 1996).

Recently, an interesting pH responsive sol-gel hybrid hydro-xerogel for drug release of doxorubicin was reported by Angelopoulou and co-workers (Angelopoulou et al., 2012). For this purpose, the authors used a Si/Ca or Mg based-xerogel with a dextran hydrogel. The hybrid-xerogel showed good apatite deposition properties. For doxorubicin, the release was more pronounced under low pH, reaching ~70 % of drug released after 180 h. In contrast, at neutral pH, only 20 % of doxorubicin was released.

1.1.1.2. Silica gel for biological species immobilization

Enzyme-based electrode has been widely studied for developing sensitive and selective biosensors. The traditional method of enzyme immobilization consists in non-covalent or covalent attachment (Guibault, 1984). However, biosensor development for enzyme immobilization may be limited due to the lack of simple and generic protocols. Thus, a simple and low cost method to immobilize and stabilize enzymes is required.

Sol-gel technology has been used for encapsulating a large number of proteins and cells. The produced sol-gel glasses can protect the biomolecules from denaturation, maintaining their activities, as well as can permit the growth and proliferation of entrapped cells. However, several factors could affect the bio species encapsulation in sol-gel matrices (Carturan et al., 2004; Kuncová et al., 2004). The hydrolysis and condensation of silicon alkoxides lead to the release of alcohol molecules as byproduct, being a potential obstacle for enzyme and cell encapsulation. Many approaches have been adopted to avoid the presence of alcohol. One way, is the alcohol removal via evaporation under vacuum. The alcohol-free route has been used for encapsulating horseradish perosidase (HRP), hydroxynitrile lyase (HbHNL) or allophycocyanin (APC) (Macmillan et al., 2009). However, the removal of alcohol is not complete, since its release can proceed for prolonged periods. Thus, aqueous sol-gel route using sodium silicate as precursors has been developed to avoid the generation of alcohol. The encapsulation is carried out at room-temperature and neutral pH, minimizing the degradation of biomolecules. HRP and glucose-6-phosphate dehydrogenase (G6PDH) were successfully encapsulated in this aqueous route processing (Bhatia et al., 2000). The use of biocompatible alcohols such as polyol-based silanes can also avoid denaturation by alcohol. The stability of entrapped enzymes is improved, since glycerol is produced under hydrolysis reaction. Recently, the use of diglyceroxysilane (DGS) as precursor and poly(ethylene glycol) (PEG) as stabilizer agent has been employed for HRP immobilization in

monodisperse spherical silica nanoparticles. The large PEG molecular weights lead to better steric stabilization and more monodisperse particles (Voss et al., 2007).

Glucose biosensor analysis was developed by combining immobilized glucose oxidase in silica gel with an oxygen sensing film using sol-gel technology (Chang et al., 2010). Even in the presence of high concentrations of ascorbic acid or chloride ion, no interference was detected and the activity of the enzyme was preserved after 2 months of storage. In addition, the evaluation of glucose concentrations was conducted using a 96-well plate and a fluorescence plate reader that permit an optimization of the tests in a laboratory scale.

Table 1.1 summarizes examples of various enzymes entrapped in silica sol-gel matrices for biosensor application.

Another exciting research area is the development of sol-gel based matrices for tissue derived cell growth aiming at cell therapy and at living organism immobilization. However, active cell immobilization still remains a challenge. Cells are more sensitive than biomolecules, requiring material with high biocompatibility, as well as appropriate immobilization methods. In addition, nutrients, oxygen and degradation products should be easily diffused by the material porous (Meunier et al., 2010). Hence, sol-gel matrices can also act as template allowing the growth and proliferation of the host cells and can be remodeled in a living tissue, as well as promote successful immobilization of numerous microorganisms as shown in Table 1.2.

Table 1.1. Recent achievements in biosensing from silica sol-gel matrices.

Sensor preparation	Transducer	Detection range	Sensitivity (μA/mM)	Response time (s)	*Km* (mM)	Reference
Glucose oxidase in chitosan-SiO_2 gel dropped on Pt/MWNT nanoparticles	Amperometric	1 μM to 23mM	5.89	5	14.4	(Zou et al., 2008)
L-lactate oxidase in silica-sol-gel film on Pt/MWNT nanoparticles	Amperometric	0.2 to 2.0 mM	6.36	5	-	(Huang et al., 2008)
Cholesterol oxidase + cholesterol esterase in chitosan-SiO_2/MWCNT bionanocomposite film	Differential pulse voltammetry	0.15 to 7.68 mM	3.8	10	0.052	(Solanki et al., 2009)
Glucose oxidase in silica sol–gel film onto Prussian Blue modified electrode	Amperometric	0 to 4.75 mM	-	12	6.7	(Li et al., 2004)
HRP in sol-gel chitosan –APDMOS film	Amperometric	5.0×10^{-9} to 1.0×10^{-7} M	-	2	1.3×10^{-3}	(Wang et al., 2003)
Acetylcholinesterase/choline oxidase in gold nanoparticles and MWCNTs by silica sol-gel process	Amperometric	0.005 to 0.4 mM	3.395	15	-	(Hou et al., 2012)

Abbreviations: MWNT, Multi-walled carbon nanotubes; APDMOS, (3-aoryloxypropyl) dimethoxymethylsilane.

Table 1.2. Encapsulation of cells into silica matrices.

Cell and/or factors	**Silica source**	**Application**	**Comments**	**Reference**
3T3 mouse fibroblasts and CRL-2595 epithelial cells	TEOS	Wound healing	Survive of cells after encapsulation; cell death due to the lack of cell attachment	(Nieto et al., 2009)
Myoblasts and VEGF	TMOS	Diaphragm repair	VEGF control release; nontoxicity; inflammatory response by high VEGF concentration	(Conconi et al., 2009)
Rat (DRG) neurons	TMOS/ Polyurea	Neural repair	Attachment and growth of DRG neurons on the surface	(Sabri et al., 2010)
SaOs-2 osteosarcoma	GPTMS/γ -PGA	Bone defect	Hybrid with good mechanical properties; Support and growth of cell line without toxicity	(Poologasundaram pillai et al., 2012)
hMSCs	TEOS-PEG-RGD	Neural, muscular and bone repair	Nanocomposite thixotropic gel for 3D cell culture. High expression and differentiation of cells. Differences in cell morphology with stiffness changes	(Pek et al., 2010)

Abbreviations: VEGF, vascular endothelium growth factor; DRG, dorsal root ganglia; GPTMS, glycidoxypropyl trimethoxysilane; γ-PGA, Poly(γ-glutamic acid); MSCs, mesenchymal stem cells.

However, the presence of acidic or alkaline catalysis in the sol-gel technology and the addition or generation of alcohol used to dissolve the silica precursor in the reaction media are highly harmful, affecting, thus, the cell viability (Carturan et al., 2004; Kuncová et al., 2004). To overcome these limitations, several techniques have been employed in sol-gel process, including a sequence of events, such as, low pH hydrolysis, alcohol removal and previous neutral condensation-gelation before the cell entrapment in colloidal silica (Baca et al., 2007; Conroy et al., 2000). The typical procedure to entrapped cells in sol-gel matrices is shown in Figure 1.1.

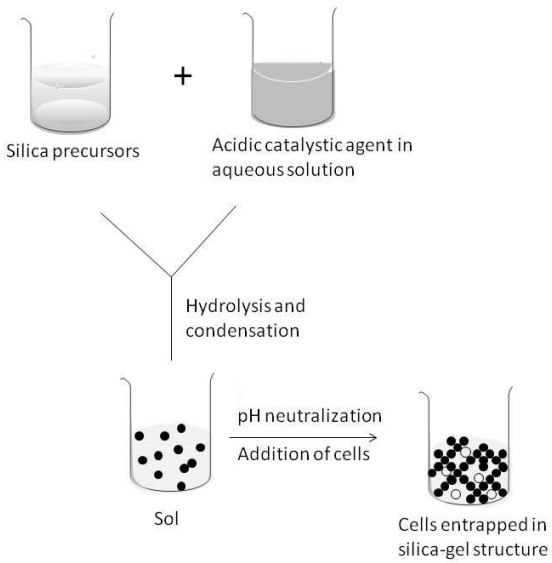

Figure 1.1. Immobilization procedures for cell attachment in sol-gel matrices. The hydrolysis and condensation of silica precursors are carried out at low pH, using HCl as catalytic agent leading to the sol formation. The pH of sol is neutralized and then the cells are added to sol, causing rapid gelation and cell entrapment within a silica-gel structure (Andreani et al., 2012a).

1.1.2. Silica nanoparticles

Silica nanoparticles can be produced mainly by two methods: Stöber method and microemulsion technique.

1.1.2.1. Stöber Method

Many processes can be based on sol-gel reactions to produce silica nanoparticles. One of the most popular is the so-called Stöber method which allows synthesizing monodisperse silica spheres from aqueous alcohol solutions in the presence of ammonium as catalyst agent (Stober et al., 1968). Although some works have performed the production of nanoparticles under acidic conditions (Takahashi et al., 2000), Stöber process has been widely applied for the preparation of colloidal monodispersed silica spheres between 50 and 2000 nm size. The formation of nanometer silica particles highly depends on the reaction parameters. By optimizing the concentration of TEOS, ammonium, water and alcohol, Park and co-workers (Park et al., 2002) synthesized ultra-fine silica particles with a mean size of 13.7 ± 4.5 nm. The effect of these factors on the resulting particle size and distribution of silica particles has

been extensively studied. The particle size can increase with the increase of TEOS and ammonium concentrations. This phenomenon is attributed to the increase of primary particles at the induction period leading to secondary particles and consequently aggregation. The presence of ammonium increases the hydrolysis and condensation rate of TEOS, resulting in the increase of silica nanoparticles (Rahman et al., 2007). However, some works have demonstrated that with increasing the ammonium concentration smaller particles were produced (Bagwe et al., 2004).

The main advantage of Stöber method is the ability to form homogenous spherical silica particles in comparison to the systems catalyzed under acidic conditions which usually result in gel structures (Prokopowicz, 2009).

1.1.2.2. Microemulsion technique (polymerization)

Silica nanoparticles with controlled size can be produced using the compartmentalization of sol-gel solution into nano droplets that work as nano-reactors. To synthesize particles with dimensions comparable to these nano-reactors, two approaches have been employed, such as spray-drying and emulsion polymerization.

Spray-drying process consists in a production of silica microspheres by atomization of pre-hydrolyzed sol-gel solution into a heated reactor, evaporating the fluid within the droplets. The droplets size is usually controlled by many parameters, including sol-gel viscosity and surface tension as well as by flow rate and atomizer characteristics (Barbe et al., 2004). Although this process can produce controlled release microspheres, several limitations can result from this method. Since the spray-dried process produced particles that are non-pores particles, the release rate is controlled by dissolution of the silica matrix in the releasing medium. This phenomenon can lead to a burst release in the sol-gel isoelectric point and when using less water-soluble drugs. The coagulation of the droplets inside the reactor, due to increasing the water to alkoxide ratio, can also occur (Kortesuo et al., 2001; Kortesuo et al., 2002). In addition, the particles synthesized by spray-drying process are limited to the micrometer range, and thus, they cannot be applied in intravenous administration. Finally, the right temperature used during the processing prevents its application for encapsulating biomolecules such as, enzymes and other proteins.

The combination of water-in-oil emulsion (W/O) with alkoxide hydrolysis contributes for a better assembling of these materials and retains the release control of sol-gel technology.

The technique is based on the immiscibility between non-polar organic solvent and polar sol-gel solution leading to a compartmentalization of sol-gel within water droplets stabilized by a surfactant (Figure 1.2). The water droplet size is directly controlled by the emulsion parameters, including the used solvent, nature of surfactant and water/surfactant ratio (Rosen, 1989).

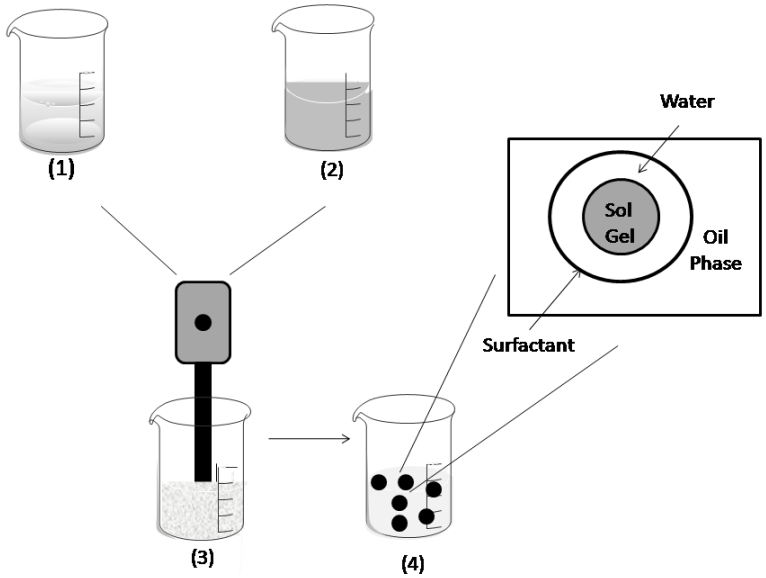

Figure 1.2. Schematic procedure of silica growth in W/O microemulsion technique. (1) Sol-gel solution composed by silica precursor, water and ammonium. (2) Surfactant in organic solvent. (3) Emulsification between the organic phase and the aqueous phase in order to prepare the microemulsion. (4) Compartmentalization of sol-gel within water droplets (Andreani et al. 2012b).

In recent years, some sol-gel/emulsion methods have been adopted to synthesize silica particles (Guo et al., 2012; Hwang et al., 2005; Teng et al., 2010; Zhang et al., 2010). By combining sol-gel technology with emulsion polymerization, Barbé and co-workers (Barbé et al., 2008), demonstrated that silica micro- and nanoparticles can maintain the control of the release rate of encapsulated active agents compared with xerogel monoliths. However, this process is limited to small hydrophilic molecules, and the presence of solvents and surfactants may be harmful for biomolecules encapsulation. Therefore, this technique is always

associated to extensively centrifugation and washing cycles to remove the surfactant and solvent molecules before the contact of biological species.

1.1.2.3. Application of silica nanoparticles in biomedicine

1.1.2.3.1. Cell Imaging

Cellular imaging using fluorescent optical microscopy is an important technique in biomedical application to monitor several tissues, and thus, to recognize defect cells. Quantum Dots (QD), gold nanoparticles, organic dyes and phosphors have been extensively used for tumor detection (Aravind et al., 2012). However, the high production cost of gold nanoparticles and phosphors, as well as the decomposition, short lifetime and accumulation of heavy metal ions in the body, in the case of QD (Atabaev et al., 2012; Derfus et al., 2004b) can limited their use in life sciences. Very recently, Wang and co-workers (Wang et al., 2012) developed a new strategy for the synthesis of near infrared (NIR) PbS-QD functionalized with a silica-polymers dual layer, leading to an improvement of PbS-QD stability, as well as prevention of PbS-QD ionization in Pb^{2+}, eliminating, thus the cytotoxicity events.

Silica nanoparticles can also act as carriers for dye molecules, being a great potential for bioimaging. Compared to a single dye molecule, dye-doped silica nanoparticles demonstrated a highly signal quality with greater sensitivity and photostability without cytotoxic effects (Derfus et al., 2004a; Li et al., 2013; Ow et al., 2004; Yang et al., 2013). Several organic dye molecules can be doped into silica nanoparticles. Recently, Accomasso and co-workers (Accomasso et al., 2012) reported the development of fluorescent silica nanoparticles using cyanine dyes prepared *via* microemulsion method. Cyanine-doped silica nanoparticles easily penetrate into stem cells and do not affect the cell viability and growth which are essential properties for cell tracking agent.

1.1.2.3.2. Biomolecular and cell separation

Magnetic nanoparticles of iron oxide have been widely developed for many applications in, for example, drug and gene delivery (Parveen et al., 2012), magnetic resonance imaging (MRI) (Amiri et al., 2013), magnetic hyperthermia for tumor cells (Sadhukha et al., 2013), biolabelling and biomolecular separation (Herr et al., 2006; Smith et al., 2007). Magnetic separation has the ability to separate biological molecules and cells due

to the external magnetic field exerted in magnetic nanoparticles. However, these nanoparticles tend to aggregate and can lead to the potential toxicity to the biological systems. To circumvent such issues, silica-coated magnetic nanoparticles have been successfully used in bio-separation of nucleic acids, cells and peptides.

In 2003, Zhao and co-workers developed the first bio-separation in a functionalized silica surface (Zhao et al., 2003). The authors created genomagnetic nanocapturers (GMNC) for collection and detection of DNA/mRNA molecules by hybridization events followed by magnetic separation. GMNC is constructed by bioconjugation of DNA probe molecules at magnetic nanoparticles surface via avidin-biotin linkage (Figure 1.3).

Silica-coated magnetic nanoparticles have been also developed to detect the presence of DNA sequences related to human immunodeficiency virus (HIV) (Liang et al., 2007). This strategy is based on the hybridization reaction between Ag/SiO_2 core-shell nanoparticles-based RAMAN tags functionalized with oligonucleotides (detection probe) and the amino groups functionalized silica-coated magnetic nanoparticles (captureprobe). The silica coating demonstrated signal amplification of hybridization assay, allowing better DNA detection sequences by RAMAN spectroscopy.

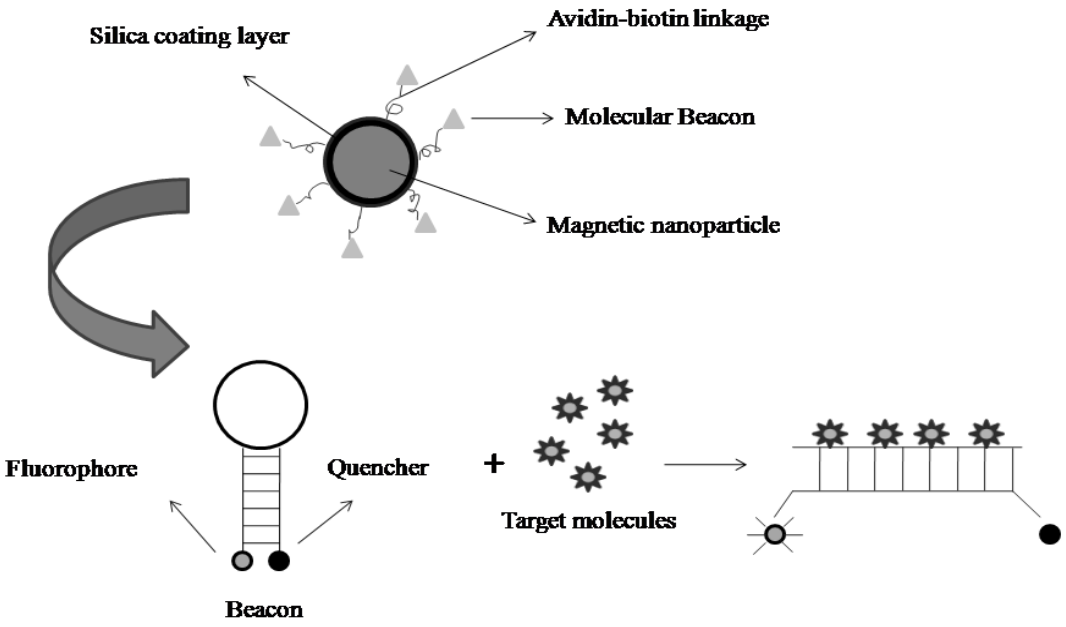

Figure 1.3. Structure and mechanism of GMNC. GMNC is constituted by magnetic nanoparticles, silica coating, avidin-biotin linkage and a molecular beacon. Molecular beacon consists in a loop of nucleic acid with a fluorophore and a quencher group attached at opposite ends. When the beacon is a closed loop mode, the quencher and the fluorophore are held together which causes the quenching of the fluorescent emission of the dye. If the target molecules (DNA or RNA) are complementary to the strand in loop, molecular beacon hybridizes resulting in an opened loop shape and consequently the separation of quencher and fluorophore leads to the fluorescence detection.

1.1.2.3.3. Controlled drug release

After the discovery of mesoporous materials for drug delivery, ordered mesoporous silica nanoparticles (MSiNP) have attracted considerable attention on biomedical application. Mobil Crystalline Materials (MCM-41, MCM-48) and Santa Barbara Amorphous (SBA-15) are examples of mesoporous silica that consist in a honeycomb-like porous structure with mesopores (2-10 nm) suitable for encapsulate large amounts of drug (Slowing et al., 2008).

MCM-41 are the most type of MSiNP used for controlled drug release. Generally, a cationic surfactant, such as cetyltrimethyl-ammonium bromide (CTAB) is employed as template in the synthesis of MCM-41. When CTAB concentration is above the critical micelle concentration (CMC), the surfactant can self-aggregate into micelles. Thus, the silica

precursor is hydrolyzed at the polar region of micelles, leading to the silica matrix around the micelle surface. The removal of CTAB results in MCM-41.

Unlike MCM-41, MCM-48 have bicontinuous channels, which can confer more suitable drug loading and release (Alfredsson and Anderson, 1996). However, the MCM-48 synthesis, under cationic or anionic surfactant as templates and under high temperatures, may produce particles in micrometer dimensions. Methods for circumventing this problem have been suggested, such as utilizing the modified Stöber method at room temperature employing pluronic F127 as surfactant to synthesize monodispersed spherical MCM-48 nanoparticles (Kim et al., 2010).

As alternative to the use of surfactants, amphiphilic triblock and diblock copolymers, under acidic media, have been extensively used as template for synthesizing silica mesoporous, such as SBA-15, which possesses a 2D hexagonal symmetry (p6mm) (Zhao et al., 1998a; Zhao et al., 1998b). In comparison to MCM-41, SBA-15 possesses larger sizes (~200 nm), thicker pore walls and wider pore sizes ranging of 5 to 30 nm.

Due to the easy of introducing of several organic groups onto MSiNP surface by covalent bounding or electrostatic interaction, various interesting hybrid structures have also been investigated. The preparation of single colloidal mesoporous silica nanoparticles coated with an intact supported lipid bilayer using three different kinds of lipids has been reported. The colloidal mesoporous silica nanoparticles were synthesized by sol-gel method using TEOS as silica source and the surfactant CTAB as pore template. The resulting nanoparticles were then suspended in the lipid solution. The hybrid system loaded with the anticancer drug colchicine is readily taken up by cells and lead to the depolymerization of microtubules with remarkably enhanced efficiency as compared to the same dose of drug in solution. The potential use of the hybrid system was demonstrated by delivery of colchicine into HuH7 liver cancer cells. The diffuse release of the drug inside the living cells inhibits, after 120 min, the microtubule polymerization and hence induces cell death, increasing drug efficiency. Also, this novel drug delivery system shows the advantage of providing a stable colloidal suspension in aqueous media, carrying large amounts of drug inside the silica mesoporous (Cauda et al., 2010). Table 1.3 summarizes the several drugs incorporated in silica nanoparticles.

Table 1.3. Examples of drugs incorporated in silica nanoparticles and their properties.

Incorporated drugs	Properties	Reference
Camptothecin	Suppression of tumor growth in mice with low toxicity effects	(Lu et al., 2010)
Camptothecin	Surface functionalization of SiNP with THSC demonstrated high colloidal stability in aqueous medium and internalized by cancer cells leading to the suppression of tumor growth in mice	(Botella et al., 2011)
Rifampin/ Isoniazid	MSiNP coated with PEI or cyclodextrin for rifampin and isoniazid delivery, respectively, showed high internalization efficacy in *M. tuberculosis*-infected macrophages	(Clemens et al., 2012)
Paclitaxel	MSiNP functionalized-PEI for siRNA attachment with enhancing paclitaxel release to pancreatic cancer cells with reduced cytotoxicity	(Xia et al., 2009)
Doxorubicin	Delivering of siRNA simultaneously with doxorubicin into multidrug-resistance human ovarian cancer cells suppress the non-pump resistance and improve the anticancer action of doxorubicin	(Chen et al., 2009)
Ibuprofen	MSiNP-coated chitosan polymer for pH-responsive delivery of ibuprofen. Under low pH, the amino groups on chitosan are protonated and, thus, ibuprofen can be released. In contrast, at physiological conditions, a chitosan insoluble gel is formed, avoiding the release of ibuprofen	(Popat et al., 2012)
Insulin	Insulin release was dependent on porous size. The large porous led to faster release of peptide	(Tozuka et al., 2010)

Abbreviations: SiRNA, small interfering RNA; PEI, polyethlyenimine; SiNP, silica nanoparticles.

Recently, several studies have used PEG coating on the surface of various nanoparticulate systems to make them water-soluble and/or biocompatible (Du et al., 2009; Hervé et al., 2008). PEG is an important polymer used for drug delivery due to its water solubility and its ability to prevent opsonization, consequently increasing circulation lifetime of the drugs or vehicles (Andrade et al., 1996). In order to study the potential application as

intravenous drug delivery vehicle, PEGylated silica spheres have been successfully synthesized. Immobilization of bovine serum albumin was carried out to evaluate the protein adsorption after PEGylation. The addition of PEG onto silica surface can avoid the reticulo-endothelial systems (RES) compared to bare silica. The influence of PEG's chain length was also analyzed, demonstrating that PEG concentrations above 300 g/mol maintain constant the reduction of protein adsorption (Yagüe et al., 2008).

1.1.2.3.4. Gene therapy

Gene therapy has gained more attention as a promising strategy for the treatment of several disorders, such as cancer and infectious diseases. The most challenge in gene delivery processes is the optimization of gene carriers that confers not only gene transfection efficiency but also low toxicity.

The successful plasmid DNA (pDNA) gene delivery was achieved *in vivo*, using rat Achilles tendon and MSiNP (Suwalski et al., 2010). The release of pDNA entrapped in MSiNP was sustained for at least 2 weeks with gradual decrease of the luciferase activity. Plasmid encoded Platelet Derived Growth Factor (PDGF) gene in MSiNP demonstrated high gene transfection in injured tendon, resulting in a strong organization of collagen fibers with no inflammation or necrosis signs (Suwalski et al., 2010).

He and co-workers (He et al., 2011) reported the development of a hybrid for non-viral gene delivery. The hybrid nanoparticles (PEI-SiNP) complexed-DNA showed higher internalization in COS-7 cells in comparison to PEI-DNA complexes. Also, PEI-SiNP demonstrated serum-resistant properties with low cytotoxicity.

Another example involves *in vitro* and *in vivo* SiRNA delivery (using siRNA targeting to VEGF) by an expansion of amine functionalized-MSiNP porous with an average of 23 nm (Na et al., 2012). The expansion of silica pores allowed high loading capacity of siRNA, as well as maintained the chemical stability of the nucleic acid upon exposures to nucleases. Fluorescence microscopy images indicated the suppression of blood vessel by downregulation VEGF, indicating the high efficiency in silencing of the targeted gene.

1.1.3. Multifunctional silica nanoparticles: A new approach in theragnostic nanomedicine

Theragnostic is the treatment that associates diagnostic and therapeutic agents in one single structure. This approach has the ability to integrate imaging and therapy, aiming to improve the response to the treatment by means of optimizing imaging information, drug selection and safety. In this context, multifunctional silica nanoparticles have been developed for simultaneous diagnostic and therapeutic purposes.

Wang and co-workers (Wang et al., 2011) developed a multifunctional system based on mesoporous silica nanocages for imaging, drug delivery and photodynamic therapy. Doxorubicin was loaded into silica porous and released in a sustained behavior at low pH. Fluorescein isothiocyanate (FITC) was used as dye molecules for fluorescent imaging and hematoporphyrin molecules were also covalently attached in the nanocages for photodynamic therapy.

A versatile multifunctional hybrid designed for drug delivery and MRI was reported by Hyeon and co-workers (Kim et al., 2008; Lee et al., 2009). The authors synthesized two kinds of systems using MSiNP coated with Fe_2O_3 nanocrystal nanoparticles or core-shell MSiNP using Fe_2O_3 nanocrystals as core. The multifunctional properties of both systems were demonstrated by fluorescence imaging with FITC or rodhamine B isothiocyanate (RITC) dye molecules. The MRI was allowed by Fe_2O_3 nanocrystals, and the drug delivery was showed by the incorporation of doxorubicin.

Another example developed for multifunctional applications is described by Zhang and co-workers (Zhang et al., 2012a). Fe_2O_3 coated with mesoporous silica nanocapsules were functionalized with PEI for fluorescent imaging and magnetically guided siRNA delivery. Fluorescent dye (e.g., RITC) was incorporated into Fe_3O_4 nanoparticles to obtain fluorescence imaging. PEI was used as cationic polymer for siRNA attachment by electrostatic interactions between PEI amino groups and phosphate groups of siRNA. In comparison with Lipofectamine 2000, a commercial transfection agent, PEI- Fe_2O_3-SiO_2 demonstrated better siRNA delivery.

1.2. Diabetes *mellitus*

Diabetes *mellitus* is a condition which results from a deficiency in the insulin secretion by the pancreas or/and from peripheral resistance to insulin action (Carino and Mathiowitz, 1999; Graves and Eisenbarth, 1999). The chronic hyperglycemia is associated with long-term damage, dysfunction, and failure of different organs, especially the eyes, kidneys, nerves, heart, and blood vessels. Symptoms of hyperglycemia include polyuria, polydipsia, weight loss, polyphagia, and blurred vision (Lawal, 2008).

The prevalence of diabetes *mellitus* worldwide reflects its broad impact on patient´s quality of life, morbidity, health care costs and mortality (Moore, 2000). World Health Organization (WHO) estimates that by the year of 2030 more than 300 million people will be affected reaching epidemic proportions worldwide (Zimmet et al., 2001).

Diabetes *mellitus* can be classified into three main types: Diabetes *mellitus* type 1, Diabetes *mellitus* type 2 and gestational. In type 1 diabetes, previously encompassed by the term insulin-dependent diabetes, there is no production of insulin by pancreatic β-cells, therefore, the patients require exogenous insulin to maintain the blood glucose. This type of diabetes is characterized by autoimmune destruction of insulin secretion and by genetic markers. On the other hand, in type 2 diabetes *mellitus* (previously referred to as non-insulin-dependent diabetes), the most common form of diabetes, is characterized by non-responsiveness to insulin which in turn decline β-cell function. Although the mechanisms are still unclear, insulin resistance plays an important role in type 2 diabetes and is associated to obesity and age leading to an inappropriate use of glucose (Carino and Mathiowitz, 1999). Many researchers have suggested that the accumulation of specific toxic lipid metabolites, such as long-chain fatty acyl CoA (LCA-CoA), diacylglycerol and ceramide in muscles and/or liver tissues can result in insulin resistance by impairing insulin signaling and consequently glucose metabolism (Haus et al., 2009; Itani et al., 2002; Kim et al., 2001; Samuel and Shulman, 2012). As research about the relation between obesity and insulin resistance has intensified, certain fat compartments, in particular visceral fat, have shown to be more functionally active than others (Montague & O'Rahilly, 2000). Visceral fat cells have higher rates of lipolysis than subcutaneous fat cells, resulting in a greater production of free fatty acids, and elevated free fatty acids have been associated with increased insulin resistance. In addition, visceral fat is a prominent source of the adipocytokines IL-6, TNF-α and adiponectin, all of which have been related to insulin resistance (Kadowaki et al., 2006;

Moller, 2000; Rotter et al., 2003). Visceral fat content is highly correlated with waist circumference, suggesting that waist, rather than body mass index (BMI), may be a better predictor of insulin resistance. Another type is the gestational diabetes, which is developed during the pregnancy, but usually disappears after pregnancy.

The subcutaneous administration of insulin has been the main delivery route of insulin for the treatment of diabetes type 1, until now. In the case of type 2 diabetes, a variety of anti-diabetic agents, including sulfonylureas, biguanides and thiazolidinedione has been widely used for many years. Despite their effectiveness in glycaemic control, several adverse effects are associated with the administration of these treatment modalities and in the majority of the patients, combination of oral anti-diabetic drugs and high doses are employed (Table 1.4). In many cases, the type 2 diabetes patients require exogenous insulin, when the combination of anti-diabetic agents has failed. Currently, incretin hormones have received a great deal of attention in the pharmaceutical area due to their efficacy in type 2 diabetes (Peters, 2010).

Table 1.4. Anti-hyperglycemic drugs available, respective mechanisms of action, administration route (Adm) and main side effects.

Drug	**Mechanism of action**	**Adm.**	**Benefits**	**Main side effects**	**Reference**
Biguanides (Metformin)	Improve sensitivity of liver and peripheral tissues to insulin by inhibition of hepatic glucose production through decreased gluconeogenesis; increases the GLP-1 circulating levels	Oral	Long-term safety No weight gain Low hypoglycemia and macro-vascular events risk Low cost	Gastrointestinal intolerance Lactic acidosis. Contraindicated in renal and hepatic dysfunction	(Hermann, 1979)
Meglitinides	Close the β-cells K-ATP channels, competes with sulfonylureas to its receptor (SUR1), but their action and effect duration is shorten than glyburide	Oral	Prandial administration due to its short action	Weight gain	(Black et al., 2007)
Sulfonylureas	Stimulate pancreatic ß-cells by binding to SUR1 receptors; K-ATP channels closure results in more insulin secretion	Oral	Long-term safety Low cost	Hyperinsulinaemia, Risk of hypoglycemia Weight gain	(Ashcroft and Gribble, 1999; Krentz and Bailey, 2005)
Thiazolidinediones	Promote glucose uptake (mainly in muscle). Interaction with PPAR-γ nuclear receptor in adipose tissue, increasing subcutaneous adipogenesis and reducing release of free fatty acids	Oral	Low risk of hypoglycaemia	Peripheral edema Weight gain Risk for heart failure	(Philippe and Raccah, 2009)

Drugs	**Mechanism of action**	**Adm.**	**Benefits**	**Main side effects**	**Reference**
α-glucosidase inhibitors	Inhibit enzyme located on the intestinal brush border reducing hydrolysis disaccharides to monosaccharides	Oral	No weight gain Low cost	Gastointestinal symptoms	(Lebovitz, 1998)
Amylin analogues (Pramlintide)	Reduce postprandial glucose by hypothalamic receptors, suppressing inappropriate glucagon secretion, and slowing gastric emptying	Subcutaneous injection	Weight loss	Hypoglycemia	Kruger and Gloster, 2004
Insulin	Inhibits glucagon release Increases glucose uptake by muscle and liver. Ocasionally used for T2DM patients when other medications fail	Subcutaneous injection	Overcome insulin resistance	Weight gain Hypoglycemia	Philippe, 2010; Wright et al., 2009

Abbreviations: Adm, administration; SUR 1, sulfonylurea receptor 1; ATP, adenosine triphosphate; PPAR-γ, peroxisome-activated receptor gamma; T2DM, type 2 diabetes *mellitus*.

1.2.1. Therapeutic proteins for Diabetes treatment

1.2.1.1. Incretin hormones

Incretins are gut hormones secreted in response to nutrient intake or oral glucose ingestion. Many hormones are considered as possible incretin candidates (Holst and Orskov, 2001), but incretin response is mediated by two peptides, namely glucose-dependent insulinotropic polypeptide (GIP) and glucagon-like peptide-1 (GLP-1) (Brubacker, 2007). Experiments with healthy human volunteers have shown that both GIP and GLP-1 have additive effects to insulin release (Nauck et al., 1993a). However, studies with GIP and GLP-1 secretion in type 2 diabetic individuals have suggested that there is a pronounced impairment of GLP-1, whereas GIP secretion is normal or even higher compared with healthy individuals (Kim and Egan, 2008; Vilsboll et al., 2001) and it does not amplify the insulinotropic activity exerted by GLP-1 (Mentis et al., 2011).

1.2.1.1.1. Glucagon-like-peptide 1

GLP-1 is a product of the preproglucagon gene. It is expressed in pancreatic α-cells and also in the L-cells situated at the distal gastrointestinal tract (GIT) (Bell et al., 1983). Administration of GLP-1 produces several physiological effects in the pancreas. Studies in animals have demonstrated that GLP-1 promotes β-cells neogenesis, and increases islet cell mass, as well as a decreases their apoptosis (Buteau, 2008; Perfetti et al., 2000; Yu and Jin, 2010). In type 2 diabetic individuals, the administration of GLP-1 leads to the insulinotropic effects normalizing fasting and postprandial blood glucose level, increasing insulin release (Nauck et al., 1993b) and reducing glucagon secretion (Gutniak et al., 1992).

Administration of GLP-1 can cause other effects beyond its insulinotropic actions. GLP-1 also exerts effects on the gastrointestinal tract, inhibiting the gastrointestinal secretion and decreasing the gastric emptying (Nauck et al., 1997). In addition, chronic administration of GLP-1 inhibits appetite and food intake, causing a decreased in body weight gain (Verdich et al., 2001).

GLP-1 has also been shown to improve myocardial function in individuals with type 2 diabetes and congestive heart failure (Nikolaidis et al., 2004) and in patients with type 2 diabetes and coronary artery disease, beneficial effect of GLP-1 infusion on endothelial function have been pointed out (Nyström et al., 2004). A study in Dahl salt-sensitive rats,

exhibiting many phenotypic traits associated with salt sensitive hypertension in humans (Yu et al., 2003), showed that chronic GLP-1 treatment possess antihypertensive and cardiac/renoprotective effects, mainly due to its diuretic and natriuretic effects, rather than improving insulin resistance. Some studies with animal models have demonstrated that GLP-1 administration improves learning behavior, and supplies neuroprotection against toxin-induced apoptosis and seizures (During et al., 2003).

Figure 1.4 depicts all GLP-1 functions mentioned above.

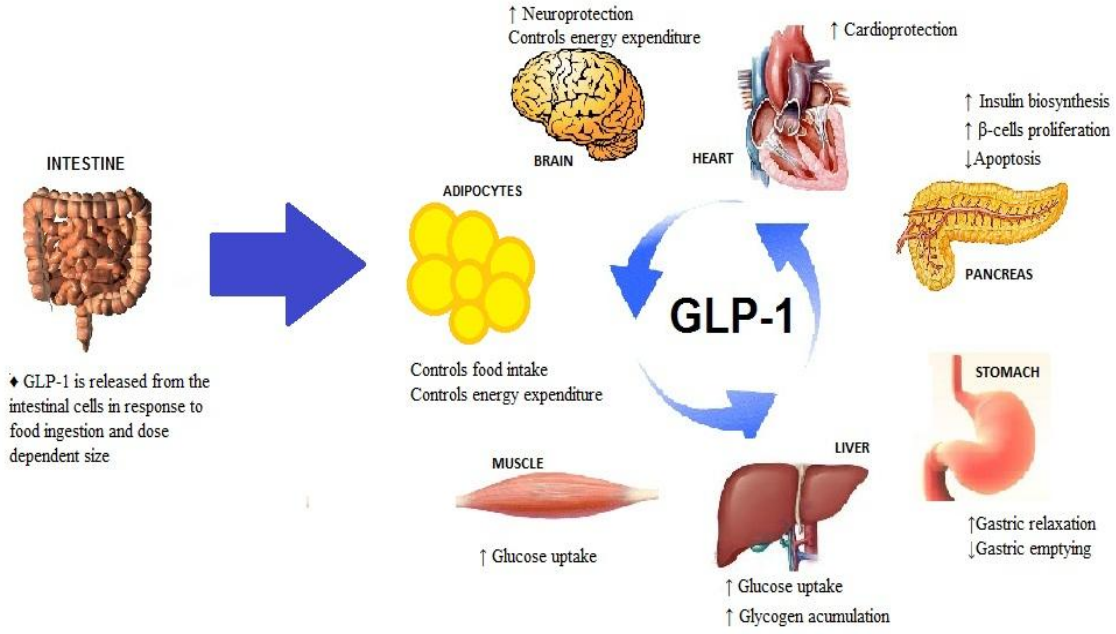

Figure 1.4. GLP-1 release and its main action on several target organ. GLP-1 is released from the intestinal A-cells in response to food ingestion and dose-dependent on meal size. Through the activation of GLP-1 receptors, it slows gastric emptying, induces gastric relaxation and satiety. It induces insulin biosynthesis and secretion, pancreatic beta cell proliferation and reduces cytotoxic-induced apoptosis. It exerts protection of the cardiovascular and neuronal system. GLP-1 acts on the adipocytes and brain centers to control food intake and energy expenditure. It increases glucose uptake by muscle and liver cells.

As a peptide, GLP-1 cannot be administered orally because it is immediately denaturated and inactivated by gastric acid. Subcutaneous or intravenous administration is required for GLP-1 to reach the circulation (Choi et al., 2004). Nevertheless, the peptide cannot be immediately employed because of its extensive and rapid degradation by the ubiquitous dipeptidyl peptidase-IV (DPP-IV) enzyme. A number of pharmacological

strategies have been developed, to provide continuous delivery of GLP-1 and prevent its degradation, including GLP-1 analogues and DPP-IV inhibitors.

Exenatide (Byetta®), a synthetic replica of Exendin-4, is indicated as monotherapy or in combination with metformin or sulfonylurea (Kendall et al., 2005). Two subcutaneous injections per day of appropriate doses (5-10 μg) were derived from various studies (Buse et al., 2004; DeFronzo et al., 2005; Heine et al., 2005), leading to the glycaemic control and weight loss in patients with type 2 diabetes. Clinical studies comparing Exenatide and placebo have reported the efficacy of Exenatide monotherapy in 232 patients with type 2 diabetes naive to anti-diabetic agents and in patients were inadequately controlled with diet and exercise alone (Moretto et al., 2008). Reducing glycosylated haemoglobin (the % of HbA_{1C}) from baseline is beneficial in controlling the body weight and improving pancreatic β-cell function and systolic and diastolic blood pressure. Exenatide has also been associated with improvements in a number of cardiovascular risk factors in adults (Klonoff et al., 2008). The main side effects, such as nausea and vomiting, are dose-dependent but may show some tachyphylaxis, and can decline along the time (Kolterman et al., 2005).

Liraglutide (Victoza®) is another GLP-1 mimetic obtained by substitution of Lys 34 to Arg, and by addition of a C16 fatty acid at position 26 using a γ-glutamic acid spacer (Knudsen et al., 2000). Pharmacokinetic properties of liraglutide point out its suitability for once-daily administration, with a T_{max} of 9–13 h and a $T_{1/2}$ of 13 h. Combination of albumin binding in the circulation leads to the protaction of liraglutide and reduces its susceptibility to DPP-IV degradation (Steensgaard et al., 2008). Liraglutide causes a dose dependent weight loss (Pi-Sunyer, 2008), improves β-cell function and decreases the concentration of HbA_{1C} (Buse et al., 2009; Nauck et al., 2009), as well as reduces the systolic blood pressure (Astrup et al., 2009). As for Exenatide, common side-effects of liraglutide treatment include gastrointestinal effects, such as nausea, diarrhea, and vomiting (Vilsboll et al., 2007).

Sitagliptin (Januvia®) was the first DDP-IV inhibitor on the market followed by Vildagliptin (Galvus®). Saxagliptin (Onglyza™) and Linagliptin (Tradjenta®) have recently been approved by Food and Drug administration (FDA).

When evaluated as monotherapy, these agents demonstrated significant and sustained improvements on glycaemia control (Del Prato et al., 2011; Rosenstock et al., 2008; Scherbaum et al., 2008; Scott et al., 2007). The mechanism of action of DDP-IV inhibitors can be described in Figure 1.5.

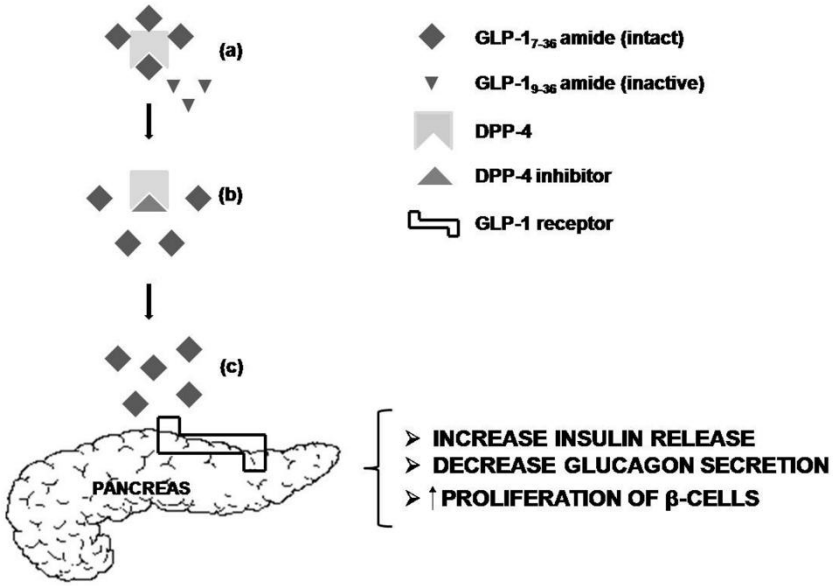

Figure 1.5. Mechanism of action of DDP-IV inhibitors: These drugs inhibit the DDP-IV activity, preventing the enzymatic inactivation of GLP-1. a) The enzyme DDP-IV cleaves the intact GLP-1, producing inactive fragments of GLP-1; b) DDP-IV inhibitors inactivate the enzyme and c) active GLP-1 bind to incretin receptors of pancreatic β-cell, increasing the insulin release, the proliferation of β-cell and decreasing of glucagon secretion (Andreani et al., 2011).

Trials in 273 patients with type 2 diabetes have demonstrated that sitagliptin (100 mg) added to metformin therapy resulted in large reductions of HbA_{1C} after 18 weeks (Scott et al., 2008). Another study performed with sitagliptin in monotherapy and in combination with metformin demonstrated their potential reduction of HbA_{1C}. This study also confirmed the efficiency of the combination of these two drugs and the reduction of side effects commonly associated to the treatment (Miller et al., 2009). Other results from a study involving a treatment with saxagliptin and metformin provided mean baseline HbA_{1C} of 6.5-10 %. During the study period (18-week) the adjusted mean changes in HbA_{1C} following the addition of saxagliptin to stable metformin therapy were −0.52 % (Scheen et al., 2010), confirming that sexagliptin improved glycaemic control in type 2 diabetes patients.

In contrast to the GLP-1 receptor agonists, DDP-IV inhibitors do not cause reduction on body weight. This can be explained by higher circulation of GLP-1 concentration obtained by GLP-1 mimetics compared to that obtained by the DDP-IV inhibitors (Burcelin and Dejager, 2010).

The side effects of the DPP-IV inhibitors have been well documented in clinical trials, demonstrating the incidence of upper respiratory and urinary tract infection, headache, as well as acute pancreatitis (Ravichandran et al., 2008; Richter et al., 2008).

Table 1.5 lists examples of drugs already on the market and others under development for therapy based on GLP-1.

Table 1.5. Drugs on the market and under development for GLP-1 therapies: GLP-1 receptor agonists and DDP-IV inhibitors.

Agent	**Manufacturer**	**Dosing schedule**	**Status**	**Reference**
GLP-1 receptor agonists				
Exenatide	Amylin Pharmaceuticals/Eli Lilly & Co	5-10 µg twice daily	Approved	(DeFronzo et al., 2005)
Liraglutide	NovoNordisk	0.6-1.8 mg once daily	Approved	(Bode, 2012)
Exenatide LAR	Amylin Pharmaceuticals/Eli Lilly & Co/ Alkermes	2 mg once weekly	UI/ Phase III	(Russel-Jones et al., 2012)
Exenatide intra-nasal	Amylin Pharmaceuticals/Eli Lilly & Co/MDRNA	-	UI/ Phase I	(Blase et al., 2008)
Exenatide transdermal	Amylin Pharmaceuticals/Eli Lilly & Co	-	UI/Phase I	(Mevorat-Kaplan et al., 2011)
Albiglutide	GSK	4–30 mg once weekly	UI/ Phase III	(Rosenstock et al., 2009)
Lixisenatide (AVE0010)	Sanofi-Aventis	5–30 µg once or twice daily	UI/ PhaseIII	(Garber, 2012)
Taspoglutide	Ipsen /Roche	20–40 mg once weekly	UI/ Phase III	(Balena et al., 2008; Fonseca et al., 2012; Ratner et al., 2008)
Semaglutide (NN9535)	NovoNordisk	0.1–1.6 mg once weekly	UI/ Phase II	(Anagnostis et al., 2011)
LY2189265	Lilly	0.05–8 mg once weekly	UI/ Phase III	(Barrington et al., 2011; Umpierrez et al., 2011)
CJC1134PC	Conjuchem Biotechnologies	1.5–3.0 mg once or twice weekly	UI/ Phase III	(Ahrén and Burke, 2012)

Agent	Manufacturer	Dosing schedule	Status	Reference
DDP-IV Inhibitors				
Sitagliptin	Merck & Co	25-100 mg once daily	Approved	(Raz et al., 2012)
Vildagliptin	Novartis	50 mg twice daily	Approved	(Bosi et al., 2007)
Saxagliptin	Bristol-Myers Squibb/Astra Zeneca	2.5-5 mg once daily	Approved	(DeFronzo et al., 2009)
Linagliptin	Boehringer Ingelhein	5 mg once daily	Approved	(Del Plato et al., 2011)
Dutogliptin	Phenomix/Forest Laboratories	200-400 mg once daily	UI/Phase III	(Plattzi et al., 2010)
Alogliptin	Takeda Pharmaceuticals Co	12.5-25 mg once daily	UI/ Phase III	(DeFronzo et al., 2008)
Melogliptin	Glenmark Pharmaceuticals	50 mg twice daily/100 mg once daily	UI/ PhaseIII	(Mulakayla et al., 2010)
PF 734200	Pfizer	2–20 mg once daily	UI/ Phase II	(Terra et al., 2011)

Abbreviation: UI, under investigation.

Several strategies are being developed to improve the use of GLP-1 for clinical application. Liposomal formulations of GLP-1 were prepared and characterized by Hanato and co-workers (Hanato et al., 2009). The formulations were based on cationic, anionic or nonionic liposomal GLP-1. Liposomal GLP-1 formulations with the diameter of 130–210 nm were found to be highly dispersible, and the highest encapsulation efficiency was observed in anionic liposomal GLP-1 formulation (~80 %) among all liposomal formulations tested. In particular, anionic liposomal GLP-1 formulation, also exhibited an improvement of pharmacological effects in rats, increasing the serum GLP-1 level and insulin secretion by 260 % and 70 %, respectively as compared to GLP-1 solution.

Gao and co-workers (Gao et al., 2009a) developed a sustained-release formulation using an analogue of GLP-1, the KGLP-1, that resulted from the attachment of a lysine residue at the N-terminal of GLP-1, being, therefore resistant to DPP-IV degradation. KGLP-1-loaded poly (D, L-lactic-co-glycolic acid) microspheres (PLGA MS) were prepared by

solvent extraction using a solid-in-oil-in-oil (S/O/O) dispersion, with an encapsulation efficiency of ~85 %. The KGLP-1-loaded PLGA MS formulation provided a controlled release *in vivo* and exert biological efficacy over a period of 10 days after a single subcutaneous injection. Injection of KGLP-1 MS increased insulin levels to 0.48–0.54 ng/mL, initially, a level that was maintained for several days with a subsequent gradual decrease over 10 days.

Functional experiments have demonstrated that the fusion of KGLP-1 and human serum albumin (HAS), in the form of KGLP-1/HAS, increases KGLP-1 half-life through resistance to DDP-IV, reducing, therefore, the blood glucose levels (Gao et al., 2009b). However, the half-life of KGLP-1/HAS was shorter when compared to HAS alone which, in humans, is about 19 days, indicating that other enzymes can be involved in the inactivation of this incretin (Plamboeck et al., 2005).

Other new drug delivery system based on biodegradable triblock copolymer of poly [(DL-lactide-co-glycolide)-b-ethylene glycol-b-(DL-lactide-coglycolide)] (PLGA-PEG-PLGA was developed to delivery GLP-1 by subcutaneous injection (Choi et al., 2004). The *in vitro* and *in vivo* GLP-1 release showed to be a promising, since there was no initial burst and a constant release was observed for 2 weeks. *In vitro* studies, also suggested that only one injection of the formulation was enough to control adequately the blood glucose level for a 2-week period. These results are very interesting due to the fact that this new delivery system is biocompatible and requires twice-a-month injection, leading to an improvement of patient´s compliance.

Other approach that use the GLP-1 incretin effect on the regulation of type 2 diabetes is based on the gene therapy (Jean et al., 2011; Kim et al., 2012; Oh et al., 2003), where the GLP-1 gene was delivered (*in vitro* and *in vivo*) by means of a new plasmid constructed with a modified GLP-1 (7-37) cDNA. The *in vitro* results showed a dose-dependent increase in GLP-1 levels, while the *in vivo* results showed normalization of insulin secretion and blood glucose levels.

Studies that include new drug delivery systems also explored other routes beyond the subcutaneous administration. The pulmonary administration was exploited using technosphere particles (Leone-Bay et al., 2009). Results suggested a rapid absorption of the pharmacologically active GLP-1 that promoted insulin secretion and controls postprandial glucose hyperglycaemia in a rat model.

Recently, pH-sensitive nanoparticles composed of chitosan and γ-PGA have been developed for oral delivery of therapeutic proteins (Sonaje et al., 2009). Nanoparticles composed of chitosan and γ-PGA have been developed for oral exedin-4 delivery, using an enteric-coated capsule (Nguyen et al., 2011). The administration of exendin-4 was absorbed into the systemic circulation, stimulated the insulin secretion, and provided a prolonged glucose-lowering effect, being the T_{max} of oral nanoparticles containing exedin-4 of 5 h in comparison to 1 h of the subcutaneous administration.

1.2.1.2. Insulin

Insulin was discovered in 1922 by Banting and Best (Banting and Best, 1922). Since then, this discovery not only prolonged the live of diabetic patients but also avoided the severe forms of the disease.

Insulin is produced and secreted as a single polypeptide pro-hormone (pro-insulin) by β-cells of the islet of Langerhans and released into bloodstream after hydrolysis of the peptide-C in response to glucose concentrations. The active hormone is a molecule composed of 51 amino acid residues arranged into two polypeptide chains, the A and B chains which are linked by two inter-chain disulphide bridges A7-B7 and A20-B19. In the A chain, there is an intra-chain cysteine linkage at A6-A11.

Insulin can be isolated from several sources, including human, bovine, porcine and sheep (Peppas and Kavimandan, 2006). Human insulin can be manufactured by recombinant DNA technology or by enzymatic modification of porcine insulin (semi-synthetic synthesis).

In addition to its primary effect on glucose homeostasis, insulin also stimulates the synthesis of glycogen (in the liver and in muscles), proteins (in muscles) and lipids (in the liver and adipose tissues) by promoting intracellular uptake of glucose and amino acids. In addition, insulin can promote the gene transcription and DNA synthesis (Cheatham and Kahn, 1995).

The biological action of insulin is mediated by its interaction to the cell surface receptor leading to many protein activation cascades. The insulin receptor is a transmembrane complex consisting of four subunits: two α-chains (extracellular subunits), responsible for insulin binding and two β-chains (transmembrane subunits) which contain intracellular tyrosine kinase domains (Roth and Cassel, 1983). When reaching its target tissues, insulin binds to the α-subunits. This interaction leads to conformational changes in the receptor

followed by the activation of kinase domains. These kinase domains phosphorylate the tyrosine residues on the β-subunits (Cheatham and Kahn, 1995). The activated insulin receptor phosphorylates a number of substrates, including isoforms of Shc (SH) (Virkamäki et al., 1999), Grb2-associated binder 1 (Gab1) (Virkamäki et al., 1999), Cas-Br-M (murine) ecotropic retroviral transforming sequence c (CBLC) (Baumann et al., 2000), the adaptor molecules containing pleckstrin homology (PH) and SH2 domains (APS) (Moodie et al., 1999) and members of the insulin receptor substrate (IRS) family (Virkamäki et al., 1999). However, the predominant substrates are IRS1 and Shc. IRS1 and its signaling pathway is responsible for most of the metabolic effect of insulin (Cheatham et al., 1994), while Shc promotes the mostly non-metabolic processes induced by insulin, such as cell growth and cell differentiation (Sasaoka and Kobayashi, 2000).

1.2.1.2.1. Novel advances for oral insulin delivery

Recently, significant growth in the biotechnology field has shown several strategies for overcoming the complications of insulin injections, exploiting non-invasive routes to reach a better patient compliance in diabetes treatment, such as oral (Su et al., 2012), nasal (Khafagy et al., 2013), pulmonary (Al-Qadi et al., 2012), buccal (Giovino et al., 2012) and transdermal (Liu et al., 2012). Pulmonary route is known as a favorable via for drug administration due to its large surface area, low level of proteolytic enzymes activity and high blood supply (Todoroff and Vanbever, 2011). Inhaled insulin system (Exubera®, Nektar Therapeutics, Sanofi-Aventis and Pfizer) has received US FDA approval in 2006 for the treatment of adult patients with type 1 and 2 diabetes. However, its production was discontinued in 2007 due to reduced sales and low acceptance by patients and doctors. The treatment safety and efficacy is similar to short-acting subcutaneous insulin, but the inhaled insulin showed an increase of mild-to moderate cough. Also, high costs of the product, as well as the possibility of dosing error during the administration of inhaled insulin (since insulin dose was not given in conventional units but in milligrams) were also an obstacle to success (Heinemann, 2008).

An oral insulin delivery would be the most convenient route due to many reasons, such as better suitability for self-medication, lower production cost, and it would have a great advantage of mimicking the natural insulin secretion pathway, avoiding, thus, the hypoglycemic effect (Owens et al., 2003). However, oral delivery of therapeutic proteins is

hindered by several physical and biochemical barriers which normally protect the organism from microorganism and toxins. The major obstacle is the protein absorption through the GIT membrane. The molecules can cross the GIT barrier via different pathways using paracellular or transcellular route. In transcellular route, the absorption of molecules is carried out by the intestinal epithelial cells and M cells of the Peyer's patches via passive or active process. The most hydrophilic molecules are transported by paracellular pathway. However, the transport though this route is regulated by tight junctions to form a tight membrane and thus, this transport is limited to hydrophilic molecules with small molecular weight (Anderson and Van Itallie, 1995).

The acidic environment in the stomach and the presence of proteolytic enzymes located throughout the GIT are also obstacles faced in the oral insulin delivery. The degradation of therapeutic proteins can be carried out by stomach enzymes, such as pepsin and by intestinal enzymes, such as trypsin, chymotrypsin and carboxypeptidases. The protease enzymatic activity is more pronounced in luminal brush border of small intestine.

Several progresses of innovative oral insulin delivery systems have been reached, including (i) modification of the physicochemical properties of insulin (Shah and Shen, 1996); (ii) functionalization of insulin by permeation enhancers, enteric coatings or retentive devices (Mesiha et al., 1994); (iii) use of enzymatic inhibitors (Agarwal et al., 2000) and (iv) encapsulation or association of insulin in delivery carriers to achieve delayed and controlled release (Reis et al., 2007; Sarmento et al., 2007b; Su et al., 2012; Zhang et al., 2012b).

Table 1.6 shows the oral systems for insulin delivery that are currently investigated in different clinical phases.

Table 1.6. Oral systems for insulin delivery that are currently being investigated in different clinical phases.

Agent	Manufacturer	Current status	Characteristics	Reference
Capsulin™	Diabetology	Phase II completed	Capsule containing a mixture of excipients with absorption-enhancing properties.	(Luzio et al., 2010)
ORMD-0801	Oramed Pharmaceuticals	Phase II	Capsule containing an omega-3 fatty acid as a protease inhibitor and sodium EDTA as absorption enhancer	(Sabetsky and Ekblom, 2010)
HIM2	Nobex corporation	Phase II	Modification of insulin by attachment of PEG moieties and alkyl chains for protein stability against enzymatic degradation	(Clement et al., 2004)
IN-105	Biocon	Phase II	Modification of insulin by methoxy-polyethylene glycol derivates. Stability from enzymatic degradation and improvement of intestinal absorption	(Dave et al., 2008)
SNAC	Emisphere's Eligen™	Phase II	Non-covalent interaction between insulin and organic compounds for improving the lipophilicity and absorption of the protein	(Malkov et al., 2005)
CobOral insulin	Access Pharmaceuticals	Phase I	Vitamin B12-coated dextran nanoparticles	(Heinemann, 2011)
HVD-I	Diasome Pharmaceuticals	Phase II	Small phospholipids vesicles for insulin delivery in a pill or gel cap dosage form	(Geho et al., 2009)

Abbreviations: HIM2, Hexyl-insulin monoconjugate 2; SNAC, Sodium N-(8-[2-hydroxybenzoyl]-amino) caprylic acid); HVD-I, Hepatic-directed vesicle insulin; EDTA, Diaminoethanetetraacetic acid.

1.2.1.2.2. Application of nanotechnology for oral insulin delivery

1.2.1.2.2.1. Liposomes

Zhang and co-workers (Zhang et al., 2005) developed and characterized lectin-modified liposomes for insulin administration. Wheat germ agglutinin (WGA), tomato lectin (TL) or *Ulex europaeus* agglutinin 1 (UEA1) were covalently bound by carbodiimide method. Following the oral administration of insulin to rats, the relative pharmacological bioavailability for liposomes modified with WGA, TL or UEA1were 8.47, 7.29 and 4.85 %, respectively, and the relative bioavailability were 9.12, 7.89 and 5.37 % in comparison to subcutaneous insulin, respectively.

Niu and co-workers (Niu et al., 2012) prepared liposomes containing different kinds of bile salts, such as glycocholate, sodium taurocholate or sodium deoxycholate by reverse-phase evaporation method. The integrity of insulin was preserved after entrapment into the liposomes. Oral administration of these formulations showed higher bioavailability for liposome containing sodium glycocholate (8.5 % and 11.0 % for non-diabetic and diabetic rats, respectively) due to its ability to protect insulin from enzymatic degradation.

1.2.1.2.2.2. Solid lipid nanoparticles

Solid lipid nanoparticles (SLN) containing insulin have also demonstrated effective results in glycaemic control. Sarmento and co-workers (Sarmento et al., 2007a) developed insulin-loaded SLN by a modified solvent emulsification-evaporation method using cetyl palmitate as lipid matrix. The mean particle size, surface charge and association efficiency of loaded nanoparticles were about 360 nm, –8 mV and 43 %, respectively. After oral administration to diabetic rats, insulin-loaded SLN showed a hypoglycemic effect with a bioavailability of 1.6 % in comparison to insulin solution. Surface modification of SLN by chitosan was carried out to improve the mucoadhesivess of the nanoparticles (Fonte et al., 2011). In this context, chitosan showed relative pharmacological bioavailabilities of 8 % and 17 % for uncoated and chitosan-coated SLN, respectively. Also, SLN coated with chitosan was able to avoid the uptake by mononuclear phagocyte system (MPS), probably due to the hydrophilic properties of the polymer (Sarmento et al., 2011).

1.2.1.2.2.3. Polymeric nanoparticles

Polymeric nanoparticles have received considerable attention for oral insulin delivery. These nanoparticles generally consist of biodegradable natural or synthetic polymers, including PLGA, poly(lactide) acid (PLA), poly(ε-caprolactone) (PCL), poly(alkyl cyanocrylate) (PACA), chitosan, alginate and dextran.

Wu and co-workers (Wu et al., 2012) developed a system composed cationic nanoparticles based on PLGA and Eudragit® RS for oral delivery of insulin. These nanoparticles were prepared by multiple emulsion solvent method and showed a mean size of 285 nm, a potential zeta of + 42 mV and an encapsulation efficiency of about 73 %. The nanoparticles were also involved by an enteric capsule coated with hydroxypropyl methylcellulose phthalate (HP55) to control release. This system permits a controlled release of insulin by presenting a primary layer (HPP55) that is insoluble in acidic pH, but is soluble at intestinal pH, allowing the contact of the nanoparticles with intestinal mucosa. The presence of Eudragit® RS has the ability to increase the mucoadhesion of nanoparticles, enhancing the absorption of insulin released. The oral administration of the formulation in diabetic rats (50 U/kg) showed a significant reduction on glucose and a pharmacological availability of 32.9 % and 9.2 %, respectively.

PLA-b-Pluronic-b-PLA (PLA-F127-PLA) vesicles were synthesized and characterized by Xiong and co-workers (Xiong et al., 2007). The vesicles were synthesized by aggregation of amphiphilic block copolymers in aqueous solution. These vesicles showed a high glucose reduction of 25 %, which was maintained until 18.5 h after oral administration in diabetic mice (50 U/kg).

Damgé and co-workers prepared nanoparticles based on blends of PCL and Eudragit® RS (Damgé et al., 2007). According to the results, the formulation can preserve the biological activity of insulin, reducing of the hyperglycemia. These nanoparticles showed a blood glucose reduction in diabetic rats of 52 % and 24 % for aspart-insulin-loaded nanoparticles and regular insulin-loaded nanoparticles, respectively at the dose of 50 U/kg. However, high doses (100 U/kg) showed a reduction on glycaemia only with regular insulin-loaded nanoparticles.

Dextran nanoparticles have also been developed for oral insulin delivery. Insulin-loaded dextran nanoparticles were prepared by Chalasani and co-workers (Chalasani et al., 2007a; Chalasani et al., 2007b). The vitamin B12 was conjugated to nanoparticles in order to

improve their uptake. These nanoparticles showed a mean size ranging from 150 to 300 nm and high efficacy in reducing blood glucose (70-75 %) with prolonged anti-diabetic effects (54 h) and pharmacological availability of 26.5 % in diabetic rats. The authors also reported that minimizing the degree of cross linking the pharmacological availability increased to 29.4 %.

Pharmacological activity of insulin-loaded alginate-chitosan nanoparticles was evaluated after oral administration in diabetic rats at 25, 50 and 100 U/kg doses (Sarmento et al., 2007b). The nanoparticles were prepared by ionotropic pre gelation method. Pharmacological availability was 6.8 and 3.4 % for the dose of 50 and 100 U/kg, respectively with a cumulative hypoglycemic effect of 55 %. In addition, the nanoparticles demonstrated high ability to adhere to intestinal mucosa, being insulin more concentrated on the Peyer's patches region. Reis and co-workers (Reis et al., 2008) also developed alginate-dextran nanoparticles for oral insulin delivery. The nanoparticles were coated with a complex based on chitosan, PEG and albumin. Dextran sulfate prevented insulin release at low pH. Chitosan was used to promote insulin controlled release at intestinal pH and albumin could protect the nanoparticles from enzymatic degradation. After orally administration of insulin-loaded nanoparticles to diabetic rats at 25, 50 and 100 U/kg, the blood glucose was reduced in a dose dependent manner, which was sustained for 24 h. The pharmacological availability was 42, 21 and 10 % for 25, 50 and 100 U/kg, respectively.

Chitosan was modified with hydroxypropyl methylcellulose phthalate (HPMCP) as a pH-sensitive polymer for the oral delivery of insulin (Makhlof et al., 2011). Chitosan-HPMCP nanoparticles improved the intestinal mucoadhesion in comparison to chitosan nanoparticles. The authors also observed that after oral administration in rats, Chitosan- HPMCP nanoparticles increased the hypoglycemic effect of insulin by approximately 9.8 and 2.8-folds as compared to insulin solution and chitosan nanoparticles, respectively. Recent investigations by Sonaje and co-workers (Sonaje et al., 2009) showed that sensitive pH nanoparticles composed of chitosan-γ-PGA could improve the transport of insulin across the Caco-2 monolayers according to pH. Following oral administration of insulin-loaded chitosan-PGA nanoparticles in diabetic rats, the relative bioavailability of insulin was 15 % at a dose of 30 U/kg. Also, the *in vivo* toxicity studies indicated absence of pathological changes in kidney, liver and intestine segments. However, these nanoparticles were found to be instable at low pH. Therefore, the authors optimized the nanoparticles using the freeze-drying process and

filled them in an enteric-coated capsule (Sonaje et al., 2010). After oral administration in diabetic rat models, the capsule preserved the integrity of the nanoparticles at acidic pH in the stomach, but dissolved rapidly in the small intestine. Pharmacokinetics and pharmacodynamics studies showed that enteric-coated capsule could improve the intestinal absorption of insulin, leading to a considerable hypoglycemic effect.

1.2.1.2.2.4. Silica nanoparticles

There are few studies in the literature based on silica nanoparticles for oral delivery of insulin. Some studies only report the use of silica as coating agent, as the case of liposomes coated with silica for improving the vesicle stability, as well as the insulin encapsulation efficacy (Dwivedi et al., 2010). Silica coating was synthesized by polymerization reaction of silica source under acid catalysis at room temperature. The anionic silanol groups interact with cationic phosphatidylcholine (PC) leading to silica coat over insulin-encapsulated PC vesicles. The acidic catalyzed polymerization reaction can improve the formulation stability, as well as prevents the insulin denaturation. In addition, *in vivo* studies demonstrated that insulin remains biologically active, reducing, thus, the glucose levels in comparison to standard insulin by parental route.

Mesoporous silica structures with different pore sizes have also been investigated for insulin delivery. Tozuka and co-workers demonstrated the possibility of insulin adsorption on silica mesoporous by freeze-thaw method (Tozuka et al., 2010). Concerning the pore size, the desired insulin release profile can be achieved (e.g. smaller pore size lead to fast release of insulin).

However, although these investigations demonstrate the application of silica for oral insulin delivery, they do not provide any information about the structural integrity and pharmacological activity of insulin.

1.3. Aims of the work

The main aim of this work was the design and characterization of nanoparticles for safe and efficient insulin delivery using the sol-gel technology under mild conditions. The nanoparticles were composed of silica matrix as the comprising core and mucoadhesive polymers as the outer layers. The polymers used for silica nanoparticles coating were chitosan, sodium alginate, PEG 6000 and PEG 20000 and a comparative study between these different coatings on insulin structure, release and permeation was also assessed.

1.4. Outline of the work

Based on the aims, the experimental sections were structured as follows:

In Chapter II, the production of silica nanoparticles was optimized by sol-gel technology applying a 2^2 factorial design approach. Here, the influence of tetraethyl orthosilicate (TEOS) and the different homogenization speeds on mean average size (Z-Ave) and polydispersity index (PI) was assessed. Further, freeze drying process was applied and the appearance and size distribution of re-dispersed of the optimized formulation were also evaluated.

In Chapter III, the influence of freeze-drying process on the physical properties of the resulting silica nanoparticles was checked varying the type, concentration and ratio of several cryoprotective agents (trehalose, mannitol and sorbitol).

In Chapter IV, coated silica nanoparticles with mucoadhesive polymers (chitosan, sodium alginate, PEG 6000 and PEG 20000) were developed and characterized. The interaction between insulin and silica nanoparticles coated with different mucoadhesive polymers was examined by X- ray diffraction, Differential scanning calorimetry (DSC) and Infra-red (IR) analysis.

In Chapter V, structural integrity of insulin, as well as its thermal stability after dissolution in mucoadhesive polymers for nanoparticles preparation were examined. The mucoadhesive properties of produced nanoparticles were also evaluated by interaction between them and mucin in aqueous solution. In addition, the biophysical interaction between the particles and biological membranes was carried out using model membrane systems based on phospholipid bilayers (DPPC).

In Chapter VI, the influence of coating of the particles on the insulin release and permeation through biomembranes was studied. Insulin release behavior from different nanoparticles was described applying several mathematic modeling. In addition, insulin permeation through everted rat intestine was also evaluated.

In Chapter VII, the biocompatibility of uncoated and coated silica nanoparticles was evaluated in two cell lines, namely, a Human colon adenocarcinoma (Caco-2) and a Human hepatocellular carcinoma (HepG2).

Chapter VIII summarizes the main general conclusions of the work.

1.5. References

Accomasso, L., Rocchietti, C.E., Raimondo, S., Catalano, F., Alberto, G., Giannitti, A., Minieri, V., Turinetto, V., Orlando, L., Saviozzi, S., Caputo, G., Geuna, S., Martra, G., Giachino, C., 2012. Fluorescent silica nanoparticles improve optical imaging of stem cells allowing direct discrimination between live and early-stage apoptotic cells. Small 8, 3192-3200.

Agarwal, V., Reddy, I.K., Khan, M.A., 2000. Oral deliveryof proteins: effect of chicken and duck ovomucoid on the stability of insulin in the presence of alfa-chymotripsin and trypsin. Pharm Pharmacol Commum 6, 223-227.

Ahrén, B., Burke, B., 2012. Using albumin to improve the therapeutic properties of diabetes treatments. Diabetes Obes Metab 14, 121-129.

Al-Qadi, S., Grenha, A., Carrión-Recio, D., Seijo, B., Remuñán-López, C., 2012. Microencapsulated chitosan nanoparticles for pulmonary protein delivery: In vivo evaluation of insulin-loaded formulations. J Control Release 157, 383-390.

Alfredsson, V., Anderson, M.W., 1996. Structure of MCM-48 revealed by transmission electron microscopy. Chem Mater 8, 1141-1146.

Amiri, H., Bordonali, L., Lascialfari, A., Wan, S., Monopoli, M.P., Lynch, I., Laurent, S., Mahmoudi, M., 2013. Protein corona affects the relaxivity and MRI contrast efficiency of magnetic nanoparticles. Nanoscale 5, 8656-8665.

Anagnostis, P., Athyros, V.G., Adamidou, F., Panagiotou, A., Kita, M., Karagiannis, A., Mikhailidis, D.P., 2011. Glucagon-like peptide-1-based therapies and cardiovascular disease: looking beyond glycaemic control. Diabetes Obes Metab 13, 302-312.

Anderson, J.M., Van Itallie, C.M., 1995. Tight junctions and the molecular basis for regulation of paracellular permeability. Am J Physiol 269, G467- G475.

Andrade, J.D., Hlady, V., Jeon, S.I., 1996. Poly(ethylene oxide) and protein resistance: Principles, problems, and possibilities. Adv Chem Ser 248, 51-59.

Andreani, T., Silva, A.M., Souza, A.L.R., Souto, E.B., Lopes, C.M., 2011. The GLP-1 system: Biochemistry, physiological effects and the role of DDP-IV inhibitor in the management of type 2 Diabetes *Mellitus.* Revista da Faculdade de Ciências da Saúde-Universidade Fernando Pessoa 7, 6-18.

Andreani, T., Silva, A.M, Souto, E.B., 2012a. Cell scaffolds and fabrication technologies for tissue engineering, in "Advanced Functional Polymers and Composites: Materials, Devices and Allied Applications" (Inamuddin, Ed), Nova Science Publishers, Inc, USA.

Andreani, T., Souza, A.L.R., Silva, A.M., Souto, E.B., 2012b. Sol-gel carrier system: A novel controlled drug delivery. In Patenting Nanomedicines: Emerging Threats versus Grant Opportunities. Heidelberg, Germany: Springer.

Angelopoulou, A., Efthimiadou, E.K., Kordas, G., 2012. Dextran modified pH sensitive silica hydro-xerogels as promising drug delivery scaffolds. Mat Lett 74, 50-53.

Aravind, A., Veeranarayanan, S., Poulose, A.C., Nair, R., Nagaoka, Y., Yoshida, Y., Maekawa, T., Kumar, D.S., 2012. Aptamer-functionalized silica nanoparticles for targetd cancer therapy. BioNanoScience 2, 1-8.

Ashcroft, F.M., Gribble, F.M., 1999. ATP-sensitive K+ channels and insulin secretion: their role in health and disease. Diabetologia 42, 903-919.

Astrup, A., Rössner, S., Van Gaal, L.F., Rissanen, A., Niskanen, L., Hakim, A.L.M., Madsen, J. Rasmussen, M.F., Lean, M.E.J., 2009. Effects of liraglutide in the treatment of obesity: a randomized, double-blind, placebo-controlled study. Lancet 374, 1606-1616.

Atabaev, T.S., Lee, J.H., Han, D.-W., Hwang, Y.-H., Kim, H.K., 2012. Cytotoxicity and cell imaging potentials of submicron color-tunable yttria particles. J Biomed Mater Res 100A, 227-2294.

Baca, H.K., Carnes, E., Singh, S., Ashhey, C., Lopez, D., Brinker, C.J., 2007. Cell-directed assembly of bio/nano interfaces - a new scheme for cell immobilization. Acc Chem Res 40, 836-845.

Bagwe, R.P., Yang, C., Hilliard, L.R., Tan, W., 2004. Optimization of dye-doped silica nanoparticles prepared using a reverse microemulsion method. Langmuir 20, 8336-8342.

Balena, R., Robert, R., Berria, R., Asnaghi, V., Grant, R., Snaith, J., Boldrin, M., Nauck, M., 2008. Eight weeks of treatment with the long acting, human GLP-1 analogue r1583 improves glycemic control and lowers body weight in subjects with type 2 diabetes *mellitus* (T2DM) treated with metformin: a double-blind placebo-controlled phase 2 study. 68th Annual Meeting of the American Diabetes Association, San Francisco, US.

Banting, F.G., Best, C.H., 1922. The internal secretion of the pancreas. J Lab Clin Med 7, 251-266.

Barbe, C., Bartlett, J., Kong, L.G., Finnie, K., Lin, H.Q., Larkin, M., Calleja, S., Bush, A., Calleja, G., 2004. Silica particles: A novel drug-delivery system. Adv Mater 16, 1959-1966.

Barbe, J.C., Kong, L., Finnie, K.S., Calleja, S., Hanna, J.V., Drabarek, E., Cassidy, D.T., Blackford, M.G., 2008. Sol–gel matrices for controlled release: from macro to nano using emulsion polymerisation. J Sol-Gel Sci Technol 46, 393-409.

Barrington, P., Chien, J.Y., Showalter, H.D.H., Schneck, K., Cui, S., Tibaldi, F., Ellis, B., Hardy, T.A., 2011.A 5-week study of the pharmacokinetics and pharmacodynamics of LY2189265, a novel, long-acting glucagon-like peptide-1 analogue, in patients with type 2 diabetes. Diabetes Obes Metab 13, 426-433.

Baumann, C.A., Ribon, V., Kanzaki, M., Thurmond, D.C., Mora, S., Shigematsu, S., Bickel, P.E., Pessin, J.E., Saltiel, A.R., 2000. CAP defines a second signaling pathway required for insulin-stimulated glucose transport. Nature 407, 202-207.

Bell, G.I., Sanchez-Pescador, R., Laybourn, P.J., Najarian, R.C., 1983. Exon duplication and divergence in the human preproglucagon gene. Nature 304, 368 - 371.

Bhatia, R.B., Brinker, C.J., Gupta, A.K., Singh, A.K., 2000. Aqueous sol-gel process for protein encapsulation. Chem Mater 12, 2434-2441.

Black, C., Donnelly, P., McIntyre, L., Royle, P.L., Shepherd, J.P., Thomas, S., 2007.Meglitinide analogues for type 2 diabetes *mellitus*. Cochrane Database Syst Rev. doi: 10.1002/14651858.CD004654.

Blase, E., Deng, W., Walsh, B., Fineman, M.S., Rhodes, C., 2008. Intranasal administration of exenatide in patients with type 2 diadetes: pharmacokinetics, pharmacodynamics, safety and tolerability. American and Diabetes Association (ADA) 68th Scientific Sessions, San Francisco, CA.

Bode, B., 2012. An overview of the pharmacokinetics, efficacy and safety of liraglutide. Diabetes Res Clin Pract 97, 27-42.

Bosi, E., Camisasca, R.P., Collober, C., Rochotte, E., Garber, A., PHD3, 2007. Effect of vildagliptin on glucose control over 24 weeks in patients with type 2 diabetes inadequately controlled with metformin. Diabetes Care 30, 890-895.

Botella, P., Abasolo, I., Fernandez, Y., Muniesa, C., Miranda, S., Quesada, M., Ruiz, J., Schwartz Jr, S., Corma, A., 2011. Surface-modified silica nanoparticles for tumor-targeted delivery of camptothecin and its biological evaluation. J Control Release 156, 246-257.

Brubacker, L.P., 2007. Incretin-based therapies: mimetics versus protease inhibitors. Trends Endocrinol Metab 18, 240-245.

Burcelin, R., Dejager, S., 2010. GLP-1: What is known, new and controversial in 2010? Diabetes Metab 36, 503-509.

Buse, J.B., Henry, R.R., Han, J., Kim, D.D., Fineman, M.S., Baron, A.D., 2004. Effects of exenatide (exendin-4) on glycemic control over 30 weeks in sulfonylurea-treated patients with type 2 diabetes. Diabetes Care 27, 2628-2635.

Buse, J.B., Rosenstock, J., Sesti, G., Schmidt, W.E., Montanya, E., Brett, J.H., Zychma, M., Blonde, L., 2009. Liraglutide once a day versus exenatide twice a day for type 2 diabetes: a 26-week randomised, parallel-group, multinational, open-label trial (LEAD-6). Lancet 374, 39-47.

Buteau, J., 2008. GLP-1 receptor signaling: effects on pancreatic β-cell proliferation and survival. Diabetes Metab 34, S73-S77.

Caputo, G., Scognamiglio, M., De Marco, I., 2012. Nimesulide adsorbed on silica aerogel using supercritical carbon dioxide. Chem Eng Res Des 90, 1082-1089.

Carino, G.P., Mathiowitz, E., 1999. Oral insulin delivery. Adv Drug Deliv Rev 35, 249-257.

Carturan, G., Dal Toso, R., Boninsegna, S., Dal Monte, R., 2004. Encapsulation of functional cells by sol–gel silica: actual progress and perspectives for cell therapy. J Mater Chem 14, 2087-2098.

Cauda, V., Engelke, H., Sauer, A., Arcizet, D., Brauchle, C., Radler, J., Bein, T., 2010. Colchicine-loaded lipid bilayer-coated 50 nm mesoporous nanoparticles efficiently induce microtubule depolymerization upon cell uptake. Nano Lett 10, 2484-–2492.

Chalasani, K.B., Russell-Jones, G.J., Jain, A.K., Diwan, P.V., Jain, S.K., 2007a. Effective oral delivery of insulin in animal models using vitamin B12-coated dextran nanoparticles. J Control Release 122, 141-150.

Chalasani, K.B., Russell-Jones, G.J., Yandrapu, S.K., Diwan, P.V., Jain, S.K., 2007b. A novel vitamin B12-nanosphere conjugate carrier system for peroral delivery of insulin. J Control Release 117, 421-429.

Chang, G., Tatsu, Y., Goto, T., Imaishi, H., Morigaki, K., 2010. Glucose concentration determination based on silica sol-gel encapsulated glucose oxidase optical biosensor arrays. Talanta 83, 61-65.

Cheatham, B., Kahn, C.R., 1995. Insulin action and the insulin signaling network. Endo Rev 16, 117-142.

Cheatham, B., Vlahos, C.J., Cheatham, L., Wang, L., Blenis, J., Kahn, C.R., 1994. Phosphatidylinositol 3-kinase activation is required for insulin stimulation of pp70 S6 kinase, DNA synthesis, and glucose transporter translocation. Mol Cell Biol 14, 4902-4911.

Chen, A.M., Zhang, M., Wei, D., Stueber, D., Taratula, O., Minko, T., He, H., 2009. Co-delivery of doxorubicin and Bcl-2 siRNA by mesoporous silica nanoparticles enhances the efficacy of chemotherapy in multidrug-resistant cancer cells. Small 5, 2673-2677.

Choi, S., Baudys, M., Kim, S., 2004. Control of blood glucose by novel GLP-1 delivery using biodegradable triblock copolymer of PLGA-PEG-PLGA in type 2 diabetic rats. Pharm Res 21, 827-831.

Clemens, D.L., Lee, B.-Y., Xue, M., Thomas, C.R., Meng, H., Ferris, D., Nel, A.E., Zink, J.I., Horwitz, M.A., 2012. Targeted intracellular delivery of antituberculosis drugs to mycobacterium tuberculosis-Infected macrophages via functionalized mesoporous silica nanoparticles. Antimicrob Agents Chemother 56, 2535-2545.

Clement, S., Dandona, P., Still, J.G., Kosutic, G., 2004. Oral modified insulin (HIM2) in patients with type 1 diabetes *mellitus*: results from a phase I/II clinical trial. Metabolism 53, 54-58.

Conconi, M.T., Bellini, S., Teoli, D., de Coppi, P., Ribatti, D., Nico, B., Simonato, E., Gamba, P.G., Nussdorfer, G.G., Morpurgo, M., Parnigotto, P.P., 2009. In vitro and in vivo evaluation of acellular diaphragmatic matrices seeded with muscle precursors cells and coated with VEGF silica gels to repair muscle defect of the diaphragm. J Biomed Mater Res Part A 89A, 304-316.

Conroy, J.F.T., Power, M.E., Martin, J., Earp, B., Hosticka, B., Daitch, C.E., et al., 2000. Cell in sol-gel. A cytocompatibility route for the production of macroporous silica gels. J Sol-gel Sci Technol 18, 269-283.

Costache, M.C., Vaughan, A.D., Qu, H., Ducheyne, P., Devore, D.I., 2013. Tyrosine-derived polycarbonate-silica xerogel nanocomposites for controlled drug delivery. Acta Biomater 9, 6544-6552.

Damgé, C., Maincent, P., Ubrich, N., 2007. Oral delivery of insulin associated to polymeric nanoparticles in diabetic rats. J Control Release 117, 163-170.

Dave, N., Hazra, P., Khedkar, A., Manjunath, H.S., Iyer, H., Suryanarayanan, S., 2008. Process and purification for manufacture of a modified insulin intended for oral delivery. J Chromatogr A 1177, 282-286.

DeFronzo, R.A., Fleck, P.R., Wilson, C.A., Mekki, Q., Group, A.S., 2008. Efficacy and safety of the dipeptidyl peptidase-4 inhibitor alogliptin in patients with type 2 diabetes and inadequate glycemic control: A randomized, double-blind, placebo-controlled study. Diabetes Care 31, 2315-2317.

DeFronzo, R.A., Hissa, M.N., Garber, A.J., Gross, J.L., Duan, R.Y., Ravichandran, S., Chen, R.S., Group, S.S., 2009. The efficacy and safety of saxagliptin when added to metformin therapy in patients with inadequately controlled type 2 diabetes with metformin alone. Diabetes Care 32, 1649-1655.

DeFronzo, R.A., Ratner, R.E., Han, J., Kim, D.D., Fineman, M.S., Baron, A.D., 2005. Effects of exenatide (exendin-4) on glycemic control and weight over 30 weeks in metformin treated patients with type 2 diabetes. Diabetes Care 28, 1092-1100.

Del Prato, S., Barnett, A.H., Huisman, H., Neubacher, D., Woerle, H.J., Dugi, K.A., 2011. Effect of linagliptin monotherapy on glycaemic control and markers of β-cell function in patients with inadequately controlled type 2 diabetes: a randomized controlled trial. Diabetes Obes Metab 13, 258-267.

Deng, Y.-H., Wang, C.-C., Hu, J.-H., Yang, W.-L., Fu, S.-K., 2005. Investigation of formation of silica-coated magnetite nanoparticles via sol-gel approach. Colloid Surf A: Physicochem Eng Aspects 262, 87-93.

Derfus, A.M., Chan, W.C.W., Bhatia, S.N., 2004a. Intracellular delivery of quantum dots for live cell labeling and organelle tracking. Adv Mater 16, 961-966.

Derfus, A.M., Chan, W.C.W., Bhatia, S.N., 2004b. Probing the cytotoxicity of semiconductor quantum dots. Nano Lett 4, 11-18.

Du, H., Hamilton, P.D., Reilly, M.A., D'Avignon, A., Biswas, P., Ravi, N., 2009.A facile synthesis of highly water-soluble, core–shell organo-silica nanoparticles with controllable size via sol–gel process. J Colloid Interf Sci 340, 202-208.

During, M.J., Cao, L., Zuzga, D.S., Francis, J.S., Fitzsimons, H.L., Jiao, X., Bland, R.J., Klugmann, M., Banks, W.A., Drucker, D.J., Haile, C.N., 2003. Glucagon-like peptide-1 receptor is involved in learning and neuroprotection. Natural Medicine 9, 1173-1179. doi: 10.1155/2010/652048.

Ferrer, M.L., del Monte, F., Levy, D., 2002. A novel and simple alcohol-free sol-gel route for encapsulation of labile proteins. Chem Mater 14, 3619-3621.

Fonseca, V., Kipnes, M., Durrwell, L., Hoekstra, J., Boldrin, M., Balena, R., 2012. Efficacy and safety of taspoglutide monotherapy in drug-naive type 2 diabetic patients after 24 weeks of treatment results of a randomized, double-blind, placebo-controlled phase 3 study (T-emerge 1). Diabetes Care 35, 485-487.

Fonte, P., Nogueira, T., Gehm, C., Ferreira, D., Sarmento, B., 2011. Chitosan-coated solid lipid nanoparticles enhance the oral absorption of insulin. Drug Deliv Transl Res 1, 299-308.

Gao, Z., Tang, Y., Chen, J., Bai, R., Zhang, Q., Hou, Y., Lu, Y., Bai, G., 2009a. A novel DPP-IV-resistant analog of glucagon-like peptide-1 (GLP-1): KGLP-1 alone or in combination with long-acting PLGA microspheres. Peptides 30, 1874-1881.

Gao, Z., Bai, G., Chen, J., Zhang, Q., Pan, P., Bai, F., Geng, P., 2009b. Development, characterization, and evaluation of a fusion protein of a novel glucagon-like peptide-1 (GLP-1) analog and human serum albumin in *Pichia pastoris*. Biosci Biotechnol Biochem 73, 688-694.

Garber, A., 2012. Novel GLP-1 receptor agonists for diabetes. Expert Opin Investig Drugs 21, 45-57.

Geho, B.W., Geho, H.C., Lau, R.J., Gana, T.J., 2009. Hepatic-directed vesicle insulin: A review of formulation development and preclinical evaluation. J Diabetes Sci Technol 3, 1451-1459.

Gehrke, S.H., Lee, P.I., 1990. Hydrogels for drug delivery systems. In: Tyle, P. (Ed.), Specialized Drug Delivery Systems. Marcel Dekker, pp. 333-392.

Ghach, W., Etienne, M., Billard, P., Jorand, F.P.A., Walcarius, A., 2013. Electrochemically assisted bacteria encapsulation in thin hybrid sol–gel films. J Mater Chem B 1, 1052-1059.

Giovino, C., Ayensu, I., Tetteh, J., Boateng, J.S., 2012. Development and characterisation of chitosan films impregnated with insulin loaded PEG-b-PLA nanoparticles (NPs): A potential approach for buccal delivery of macromolecules. Int J Pharm 428, 143-151.

Graves, P.M., Eisenbarth, G.S., 1999. Pathogenesis, prediction and trials for the prevention of insulin-dependent (type 1) diabetes *mellitus*. Adv Drug Deliv Rev 35, 143-156.

Guibault, G., 1984. Analytical uses of immobilized enzymes. Marcel Dekker, New York.

Guo, X., Canet, J.L., Boyer, D., Gautier, A., Mahiou, R., 2012. Sol–gel emulsion synthesis of biphotonic core–shell nanoparticles based on lanthanide doped organic–inorganic hybrid materials. J Mater Chem 22, 6117-6122.

Gutniak, M., Orskov, C., Holst, J.J., Ahrén, B., Efendic, S., 1992. Antidiabetogenic effect of glucagons-like peptide-1 (7-36) amide in normal subjects and patients with diabetes *mellitus*. New Engl J Med 326, 1316-1322.

Hanato, J., Kuriyama, K., Mizumoto, T., Debari, K., Hatanaka, J., Onoue , S., Yamada, S., 2009. Liposomal formulations of glucagon-like peptide-1: Improved bioavailability and anti-diabetic effect. Int J Pharm 382, 111-116.

Haus, J.M., Kashyap, S.R., Kasumov, T., Zhang, R., Kelly, K.R., DeFronzo, R.A., Kirwan, J.P., 2009. Plasma ceramides are elevated in obese subjects with type 2 diabetes and correlate with the severity of insulin resistance. Diabetes 58, 337 - 343.

He, W.-T., Xue, Y.-N., Liu, W.-M., Huang, S.-W., Zhuo, R.-X., 2011. One-pot preparation of polyethlyenimine/silica hybride nanoparticles as serum-resistant gene delivery vectors: Transfection and intracellular trafficking. J Control Release 152, e145-e146.

Heine, R.J., Van Gaal, L.F., Johns, D., Mihm, M.J., Widel, M.H., Brodows, R.G., 2005. Exenatide versus insulin glargine in patients with suboptimally controlled type 2 diabetes: a randomized trial. Ann Intern Med 143, 559-569.

Heinemann, L., 2008. The failure of Exubera: Are we beating a dead horse? J Diabetes Sci Technol 2, 518-529.

Heinemann, L., 2011. New ways of insulin delivery. Int J Clin Pract 65, 31-46.

Hermann, L.S., 1979. Metformin: a review of its pharmacological properties and therapeutic use. Diabete Metab 5, 233-245.

Herr, J.K., Smith, J.E., Medley, C.D., Shangguan, D.H., Tan, W.H., 2006. Aptamer-conjugated nanoparticles for selective collection and detection of cancer cells. Anal Chem 78, 2918-2924.

Hervé, K., Douziech-Eyrolles, K.L., Munnier, E., Cohen-Jonathan, S., Soucé, M., Marchais, H., Limelette, P., Warmont, F., Saboungi, M.L., Dubois, P., Chourpa, I., 2008. The development of stable aqueous suspensions of PEGylated SPIONs for biomedical applications. Nanotechnology 19. doi: 10.1088/0957-4484/19/46/465608.

Holst, J.J., Orskov, C., 2001. Incretin hormones—an update. Scand J Clin Lab Invest. Suppl (234), 75-85.

Hou, S., Ou, Z., Chen, Q., Wu, B., 2012. Amperometric acetylcholine biosensor based on self-assembly of gold nanoparticles and acetylcholinesterase on the sol-gel/multi-walled carbon nanotubes/choline oxidase composite-modified platinum electrode. Biosensors Bioelectron 33, 44-49.

Huang, J., Li, J., Yang, Y., Wang, X., Wu, B., Anzai, J.-I., Osa, T., Chen, Q., 2008. Development of an amperometric l-lactate biosensor based on l-lactate oxidase immobilized through silica sol-gel film on multi-walled carbon nanotubes/platinum nanoparticle modified glassy carbon electrode. Mater Sci Eng C 28, 1070-1075.

Hwang, Y.J., Oh, C., Oh, S.G., 2005. Controlled release of retinol from silica particles prepared in O/W/O emulsion: The effects of surfactants and polymers. J Control Release 106, 339-349.

Iller, R.K., 1979.The chemistry of silica.Wiley, New York.Wiley, New York.

Itani, S.I., Ruderman, N.B., Schmieder, F., Boden, G., 2002. Lipid-induced insulin resista nce in human muscle is associated with changes in diacylglycerol, protein kinase C, and I kappa B-alpha. Diabetes 51, 2005 - 2011.

Jafarzadeh, M., Rahman, I.A., Sipaut, C.S., 2009. Synthesis of silica nanoparticles by modified sol–gel process: the effect of mixing modes of the reactants and drying techniques. J Sol-Gel Sci Technol 50, 328-336.

Jean, M., Alameh, M., Buschmann, M.D., Merzouki, A., 2011. Effective and safe gene-based delivery of GLP-1 using chitosan/plasmid-DNA therapeutic nanocomplexes in an animal model of type 2 diabetes. Gene Ther 18, 807-816.

Kadowaki, T., Yamauchi, T., Kubota, N., Hara, K., Ueki, K., Tobe, K., 2006. Adiponectin and adiponectin receptors in insulin resistance, diabetes, and the metabolic syndrome. J Clin Invest 116, 1784-1792.

Kendall, D.M., Riddle, M.C., Rosenstock, J., Zhaung, D., Kim, D.D., Fineman, M.S., Baron, A.D., 2005. Effect of exenatide (exendin-4) on glycaemic control over 30 weeks in patients with type 2 diabetes treated with metformin and sufonylurea. Diabetes Care 28, 1083-1091.

Khafagy, E.-S., Kamei, N., Nielsen, E.J.B., Nishio, R., Takeda-Morishita, M., 2013. One-month subchronic toxicity study of cell-penetrating peptides for insulin nasal delivery in rats. Eur J Pharm Biopharm 85, 736-743.

Kim, J., Kim, H.S., Lee, N., Kim, T., Kim, H., Yu, T., Song, I.C., Moon, W.K., Hyeon, T., 2008. Multifunctional uniform nanoparticles composed of a magnetite nanocrystal core and a mesoporous silica shell for magnetic resonance and fluorescence imaging and for drug delivery. Angew Chem Int Ed 47, 8438-8441.

Kim, J.K., Fillmore, J.J., Chen, Y., Moore, I.K., Pypaert, M., Lutz, E.P., Kako, Y., Velez-Carrasco, W., Goldberg, I.J., Breslow, J.L., Shulman, G.I., 2001. Tissue- specific overexpression of lipoprotein lipase causes tissue-specific insulin resistance. PNAS 98, 7522-7527.

Kim, T.-W., Chung, P.W., Lin, V.S.Y., 2010. Facile synthesis of monodisperse spherical MCM-48 mesoporous silica nanoparticles with controlled particle size. Chem Mater 22, 5093-5104.

Kim, T., Lee, M., Kim, S.W., 2012. Efficient GLP-1 gene delivery using two-step transcription amplification plasmid system with a secretion signal peptide and arginine-grafted bioreducible polymer. J Control Release 157, 243-248.

Kim, W., Egan, J.M., 2008.The role of incretins in glucose homeostasis and diabetes treatment. Pharmacol Rev 60, 470-512.

Klonoff, D.C., Buse, J.B., Nielsen, L.L., Guan, X., Bowlus, C.L., Hoscombe, J.H., Wintle, M.E., Mags, D.G., 2008. Exenatide effects on diabetes, obesity, cardiovascular risk factors and hepatic biomarkers in patients with type 2 diabetes treated for at least 3 years. Cur Med Res Opin 24, 275-286.

Knudsen, L.B., Nielsen, O.P.F., Huusfeldt, P.O., Johansen, N.L., Madsen, K., Pedersen, F.Z., Thøgersen, H., Wilken, M., Agersø, H., 2000. Potent derivatives of glucagon-like peptide-1 with pharmacokinetic properties suitable for once daily administration. J Med Chem 43, 1664-1669.

Kolterman, O.G., Kim, D.D., Shen, L., Rugles, J.A., Nielsen, L.L., Fineman, M.S., Baron, A.D., 2005. Pharmacokinetics, pharmacodynamics, and safety of exenatide in patients with type 2 diabetes *mellitus*. Am J Health-Syst Pharm 62, 173-181.

Kortesuo, P., Ahola, M., Kangas, M., Yli-Urpo, A., Kiesvaara, J., Marvola, M., 2001. In vitro release of dexmedetomidine from silica xerogel monoliths: effect of sol-gel synthesis parameters. Int J Pharm 221, 107-114.

Kortesuo, P., Ahola, M., Minna, K., Mika, J., Tiina, L., Lauri, V., Sirpa, L., Juha, K., Antti, Y., Martti, M., 2002. Effect of synthesis parameters of the sol-gel-processed spray-dried silica gel microparticles on the release rate of dexmedetomidine. Biomaterials 23, 2795-2801.

Krentz, A.J., Bailey, C.J., 2005. Oral antidiabetic agents: current role in type 2 diabetes *mellitus*. Drugs 653, 385-411.

Kruger, D.F., Gloster, M.A., 2004. Pramlintide for the treatment of insulin-requiring diabetes *mellitus*: rationale and review of clinical data. Drugs 64, 1419-1432.

Kuncová, G., Prodazky, O., Ripp, S., Trogl, J., Sayler, G.S., Demnerova, K., Vankova, R. 2004. Monitoring of the viability of cells immobilized by sol-gel process. J Sol-gel Sci Technol 31, 335-342.

Lawal, M., 2008. Management of diabetes *mellitus* in clinical practice. Brit J Nurs 17, 1106 - 1113.

Lebovitz, H.E., 1998. α-Glucosidase inhibitors as agents in the treatment of diabetes. Diabetes Rev 6, 132-145.

Lee, J.E., Lee, N., Kim, H., Kim, J., Choi, S.H., Kim, J.H., Kim, T., Song, I.C., Park, S.P., Moon, W.K., Hyeon, T., 2009. Uniform mesoporous dye-doped silica nanoparticles decorated with multiple magnetite nanocrystals for simultaneous enhanced magnetic resonance imaging, fluorescence imaging, and drug delivery. J Am Chem Soc 132, 552-557.

Leone-Bay, A., Grant, M., Greene, S., Stowell, G., Daniels, S., Smithson, A., Villanueva, S., Cope, S., Carrera, K., Reyes, S., Richardson, P., 2009. Evaluation of novel particles as an inhalation system for GLP-1. Diabetes Obes Metab 11, 1050-1059.

Li, M., Lam, J.W.Y., Mahtab, F., Chen, S., Zhang, W., Hong, Y., Xiong, J., Zheng, J., Zheng, Q., Tang, B.Z., 2013. Biotin-decorated fluorescent silica nanoparticles with aggregation-induced emission characteristics: fabrication, cytotoxicity and biological applications. J Mater Chem B 1, 676-684.

Li, T., Yao, Z., Ding, L., 2004. Development of an amperometric biosensor based on glucose oxidase immobilized through silica sol-gel film onto Prussian Blue modified electrode. Sensors and Actuators B: Chemical 101, 155-160.

Liang, Y., Gong, J.-L., Huang, Y., Zheng, Y., Jiang, J.-H., Shen, G.-L., Yu, R.-Q., 2007. Biocompatible core-shell nanoparticle-based surface-enhanced Raman scattering probes for detection of DNA related to HIV gene using silica-coated magnetic nanoparticles as separation tools. Talanta 72, 443-449.

Liu, S., Jin, M.-n., Quan, Y.-s., Kamiyama, F., Katsumi, H., Sakane, T., Yamamoto, A., 2012. The development and characteristics of novel microneedle arrays fabricated from hyaluronic acid, and their application in the transdermal delivery of insulin. J Control Release 161, 933-941.

Lu, J., Liong, M., Li, Z., Zink, J.I., Tamanoi, F., 2010. Biocompatibility, biodistribution, and drug-delivery efficiency of mesoporous silica nanoparticles for cancer therapy in animals. Small 6, 1794-1805.

Luzio, S.D., Dunseath, G., Lockett, A., Broke-Smith, T.P., New, R.R., Owens, D.R., 2010. The glucose lowering effect of an oral insulin (Capsulin) during an isoglycaemic clamp study in persons with type 2 diabetes. Diabetes Obes Metab 12, 82-87.

Macmillan, A.M., Panek, D., McGuinness, C.D., Pickup, J.C., Graham, D., Smith, W.E., Birch, D.J.S., Karolin, J., 2009. Improved biocompatibility of protein encapsulation in sol–gel materials. J Sol-Gel Sci Technol 49, 380-384.

Makhlof, A., Tozuka, Y., Takeuchi, H., 2011. Design and evaluation of novel pH-sensitive chitosan nanoparticles for oral insulin delivery. Eur J Pharm Sci 42, 445-451.

Malkov, D., Angelo, R., Wang, H., Flandes, E., Tang, H., Gomez-Orellana, I., 2005. Oral delivery of insulin with the eligen technology: mechanistic studies. Curr Drug Deliv 2, 191-197.

Mentis, N., Vardarli, I., Köthe, L.D., Holst, J.J., Deacon, C.F., Theodorakis, M., Meier, J.J., Nauck, M.A., 2011. GIP does not potentiate the antidiabetic effects of GLP-1 in hyperglycemic patients with type 2 diabetes. Diabetes 60, 1270-1276.

Mesiha, M., Plakogiannis, F., Vejosoth, S., 1994. Enhanced oral absorption of insulin from desolvated fatty acid-sodium glycocholate emulsions. Int J Pharm 111, 213-216.

Meunier, C.F., Dandoy, P., Su, B.-L., 2010. Encapsulation of cells within silica matrixes: Towards a new advance in the conception of living hybrid materials. J Colloid Interf Sci 342, 211-224.

Mevorat-Kaplan, K., Levin, G., Sacks, H., Stern, M., 2011. Transdermal system for extended delivery of incretins and incretin mimetic peptides. World patent WO2010010555 A2.

Miller, S.A., St Onge, E.L., Accardi, J.R., 2009. Sitagliptin as combination therapy in the treatment of type 2 diabetes *mellitus*. Diabetes Metab Syndr Obes 2, 23-30.

Mohanan, J.L., Arachchige, I.U., Brock, S.L., 2005. Porous semiconductor. Chalcogenide Aerogels. Science 21, 397-400.

Moller, D.E., 2000. Potential role of TNF-α in the pathogenesis of insulin resistance and type 2 diabetes. Trends endocrinol metab 11, 212-217.

Moodie, S.A., Alleman-Sposeto, J., Gustafson, T.A., 1999. Identification of the APS protein as a novel insulin receptor substrate. J Biol Chem 274, 11186-11193.

Moore, J., 2000. Type 2 diabetes is a major drain on resources (Letter). British Medical J 320, 732.

Moretto, T.J., Milton, D.R., Ridge, T.D., MacConell, L.A., Okerson, T., Wolka, A.M., Brodows, R.G., 2008.Efficacy and tolerability of exenatide monotherapy over 24 weeks in antidiabetic drug-naive patients with type 2 diabetes: A randomized, double-blind, placebo-controlled, parallel-group study. ClinTher 30, 1448-1460.

Mulakayala, N., Reddy, U., Iqbal.J., Pal, M., 2010. Synthesis of dipeptidyl peptidase-4 inhibitors: a brief overview. Tetrahedron 66, 4919-4938.

Na, H.-K., Kim, M.-H., Park, K., Ryoo, S.-R., Lee, K.E., Jeon, H., Ryoo, R., Hyeon, C., Min, D.-H., 2012. Efficient functional delivery of siRNA using mesoporous silica nanoparticles with ultralarge pores. Small 8, 1752-1761.

Nauck, M., Frid, A., Hermansen, K., Shah, N., Tankova, T., Mitha, I.H., Zdravkovic, M., Düring, M., Matthews, D.R., 2009. Efficacy and safety comparison of liraglutide, glimepiride, and placebo, all in combination with metformin, in type 2 diabetes: the LEAD (Liraglutide Effect and Action in Diabetes)-2 study. Diabetes Care 32, 84-90.

Nauck, M.A., Bartels, E., Orskov, C., Ebert, R., Creutzfeldt, W., 1993a. Additive insulinotropic effects of exogenous synthetic human gastric inhibitory polypeptide and glucagon-like peptide-1-(7–36) amide infused at near physiological insulinotropic hormone and glucose concentrations. J Clin Endocrinol Metab 74, 912-812.

Nauck, M.A., Kleine, N., Orskov, C., Holst, J.J., Willms, B., Creutzfeldt, W., 1993b. Normalization of fasting hyperglycemia by exogenous glucagons-like peptide 1(6–36) amide in type 2 (non-insulin dependent) diabetic patients. Diabetologia 36, 741-744.

Nauck, M.A., Niedereichholz, U., Ettler, R., Holst, J.J., Orskov, C., Ritzel, R., Schmiegel, W.H., 1997. Glucagon-like peptide 1 inhibition of gastric emptying outweighs its insulinotropic effects in healthy humans. Am J Physiol 273, E981-E988.

Nguyen, H.-N., Wey, S.P., Juang, J.H., Sonaje, K., Ho, Y.C., Chuang, E.Y., Hsu, C.W., Yen, T.C., Lin, K.J., Sung, H.W., 2011. The glucose-lowering potential of exendin-4 orally delivered via a pH-sensitive nanoparticle vehicle and effects on subsequent insulin secretion in vivo. Biomaterials 32, 2673-2682.

Nieto, A., Areva, S., Wilson, T., Viitala, R., Vallet-Regi, M., 2009. Cell viability in a wet silica gel. Acta Biomaterialia 5, 3478-3487.

Nikolaidis, L.A., Mankad, S., Sokos, G.G., Miske, G., Shah, A., El ahi, D., Shannon, R.P., 2004. Effects of glucagon-like peptide-1 in patients with acute myocardial infarction and left ventricular dysfunction after successful reperfusion. Circulation 109, 962-965.

Niu, M., Lu, Y., Hovgaard, L., Guan, P., Tan, Y., Lian, R., Qi, J., Wu, W., 2012. Hypoglycemic activity and oral bioavailability of insulin-loaded liposomes containing bile salts in rats: The effect of cholate type, particle size and administered dose. Eur J Pharm Biopharm 81, 265-272.

Nyström, T., Gutniak, M.K., Zhang, Q., Holst, J.J., Ahrén, B., Sjöholm, A., 2004. Effects of glucagon-like peptide-1 on endothelial function in type 2 diabetes patients with stable coronary artery disease. Am J Physiol (Endocrinol Metab) 287, E1209-E1215.

Oh, S., Lee, M., Ko, K.S., Choi, S., Kim, S.W., 2003. GLP-1 gene delivery for the treatment of type 2 diabetes. Mol Ther 7, 478-483.

Ow, H., Larson, D.R., Srivastana, M., Baird B.A., Webb, W.W., Wiesner, U., 2004. Bright and stable core-shell fluorescent silica nanoparticles. Nano Lett 5, 113-117.

Owens, D.R., Zinman, B., Bolli, G., 2003. Alternative routes of insulin delivery. Diabetic Medicine 20, 886-898.

Park, S.K., Kim, K.D., Kim, H.T., 2002. Preparation of silica nanoparticles: determination of the optimal synthesis conditions for small and uniform particles. Colloid Surf A: Psysicochem Eng Aspect 197, 7-17.

Parveen, S., Misra, R., Sahoo, S.K., 2012. Nanoparticles: a boon to drug delivery, therapeutics, diagnostics and imaging. Nanomedicine 8, 147-166.

Pattzi, H.M.R., Pitale, S., Alpizar, M., Bennett, C., O'Farrell, A.M., Li, J., Cherrington, J.M., Guler, H.P., Group, P.-P.S., 2010. Dutogliptin, a selective DPP4 inhibitor, improves glycaemic control in patients with type 2 diabetes: a 12-week, double-blind, randomized, placebo-controlled, multicentre trial. Diabetes Obes Metab 12, 348-355.

Pek, Y.S., Wan, A.C.A., Ying, J.Y., 2010. The effect of matrix stiffness on mesenchymal stem cell differentiation in a 3D thixotropic gel. Biomaterials 31, 385-391.

Peppas, N.A., Kavimandan, N.J., 2006. Nanoscale analysis of protein and peptide absorption: Insulin absorption using complexation and pH-sensitive hydrogels as delivery vehicles. Eur J Pharma Sci 29, 183-197.

Peppas, N.A., Mikos, A.G., 1986. Preparation methods and structure of hydrogels. In: Peppas, N.A. (Ed.), Hydrogels in Medicine and Pharmacy. CRC Press, Boca Raton, FL, pp. 1-27.

Perfetti, R., Zhou, J., Doyle, M.E., Egan, J.M., 2000. Glucagon-like peptide-1 induces cell proliferation and pancreatic duodenum homeobox-1 expression an increase endocrine cell mass in the pancreas of old, glucose-intolerant rats. Endocrinology 141, 4600-4605.

Peters, A., 2010. Incretin-based therapies: review of current clinical trial data. Am J Med 123, S28-S37.

Philippe, J., 2010. How to minimize weight gain associated with insulin treatment. Rev Med Suisse 6, 1199-1202.

Philippe, J., Raccah, D., 2009. Treating type 2 diabetes: how safe are current therapeutic agents? Int J Clin Pract 63, 321-332.

Pi-Sunyer, F.X., 2008. The effects of pharmacologic agents for type 2 diabetes *mellitus* on body weight. Postgrad Med 120, 5-17.

Pierre, A.C., Pajonk, G.M., 2002. Chemistry of aerogels and their applications. Chem Rev 102, 4243-4265.

Plamboeck, A., Holst, J.J., Carr, R.D., Deacon, C.F., 2005. Neutral endopeptidases 24.11 and dipeptidyl peptidase IV are both mediators of the degradation of glucagon-like peptide-1 in the anaesthetized pig. Diabetologia 48, 1882-1890.

Poologasundarampillai, G., Yu, B., Tsigkou, O., Valliant, E., Yue, S., Lee, P.D., Hamilton, R.W., Stevens, M.M., Kasuga, T., Jones, J.R., 2012. Bioactive silica–poly(γ-glutamic acid) hybrids for bone regeneration: effect of covalent coupling on dissolution and mechanical properties and fabrication of porous scaffolds. Soft Matter 12, 4822-4832.

Popat, A., Liu, J., Lu, G.Q., Qiao, S.Z., 2012. A pH responsive drug delivery system based on chitosan coated mesoporous silica nanoparticles. J Mater Chem 22, 11173-11178.

Prokopowicz, M., 2009a. Correlation between physicochemical properties of doxorubicin-loaded silica/polydimethylsiloxane xerogel and in vitro release of drug. Acta Biomaterialia 5, 193-207.

Rahman, I.A., Vejayakumaran, P., Sipaut, C.S., Ismail, J., Abu Bakar, M., Adnan, R., Chee, C.K., 2004.An optimized sol–gel synthesis of stable primary equivalent silica particles. Colloid Surf A: Physicochem Eng Aspects 294, 102–110.

Ratner, R., Nauck, M., Kapitza, C., Asnaghi, V., Boldrin, M., Balena, R., 2008. Safety and tolerability of high doses of the long acting, human GLP-1 analogue r1583 in diabetic subjects treated with metformin: a double-blind, placebo-controlled phase 2 study. 68th Annual Meeting of the American Diabetes Association, San Francisco, USA

Ravichandran, S., Chacra, A.R., Tan, G.H., Apanovitch, A., Chen, R., 2008. Saxagliptin added to a sulfonylurea is safe and more effective than up-titrating a sulfonylurea in patients with type 2 diabetes [abstract]. Diabetologia 51, S342.

Reis, C.P., Ribeiro, A.J., Houng, S., Veiga, F., Neufeld, R.J., 2007. Nanoparticulate delivery system for insulin: Design, characterization and in vitro/in vivo bioactivity. Eur J Pharm Sci 30, 392-397.

Reis, C.P., Veiga, F.J., Ribeiro, A.J., Neufeld R.J., C., D., 2008. Nanoparticulate biopolymers deliver insulin orally eliciting pharmacological response. J Pharm Sci 97, 5290-5305.

Richter, B., Bandeira-Echtler, E., Bergerhof f, K., Lerch, C.L., 2008. Dipeptidyl peptidase-4 (DPP-4) inhibitors for T2DM *mellitus*. Cochrane Database Syst Rev 16. doi: 10.1002/14651858.CD006739.pub2.

Ritger, P.L., Peppas, N., 1987. Fickian and non-Fickian release from non-swellable devices in the form of slabs, spheres cylindersor discs. J Control Release 5, 23-36.

Rosen, M., 1989. Surfactants and interfacial phenomena, 2nd ed. Wiley, New York.

Rosenstock, J., Reusch, J., Bush, M., Yang, F., Stewart, M., 2009. The potential of albiglutide, a long-acting GLP-1 receptor agonist, in type 2 diabetes: A randomized controlled trial exploring weekly, biweekly, and monthly dosing. Diabetes Care 32, 1880-1886.

Rosenstock, J., Sankoh, S., List, J.F., 2008. Glucose-lowering activity of the dipeptidyl peptidase-4 inhibitor saxagliptin in drug-naive patients with type 2 diabetes. Diabetes Obes Metab 10, 376-386.

Roth, R.A., Cassel, M.P., 1983. Insulin receptor: evidence that it is a protein kinase. Science 219, 299-301.

Rotter, V., Nagaev, I., Smith, U., 2003. Interleukin-6 (IL-6) induces insulin resistance in 3T3-L1 Adipocytes and is, like IL-8 and tumor necrosis factor alpha, overexpressed in human fat cells from insulin-resistant subjects. J Biol Chem 278, 45777-45784.

Russel-Jones, D., Cuddihy, R.M., Hanefeld, M., Kumar, A., González, J.G., Chan, M., Wolka, A.M., Boardman, M., PHARMD, Group, D.-S., 2012. Efficacy and safety of exenatide once weekly versus metformin, pioglitazone and sitagliptin used as monotherapy in drug-naive patients with type 2 diabetes (DURATION-4). Diabetes Care 35, 252-258.

Sabetsky, V., Ekblom, J., 2010. Insulin: A new era for an old hormone. Pharmacol Res 61, 1-4.

Sabri, F., Cole, J.A., Scarbrough, M.C., Leventis, N., 2010. Investigation of polyurea - crosslinked silica aerogels as a neuronal scaffold: A pilot study. PLoS ONE 7.

Sadhukha, T., Wiedmann, T.S., Panyam, J., 2013. Inhalable magnetic nanoparticles for targeted hyperthermia in lung cancer therapy. Biomaterials 34, 5163-5171.

Samuel, V.T., Shulman, G.I., 2012. Mechanisms for insulin resistance: Common threads and missing links. Cell 148, 852-871.

Sarmento, B., Martins, S., Ferreira, D., Souto, E.B., 2007a. Oral insulin delivery by means of solid lipid nanoparticles. Int J Nanomedicine 2, 743-749.

Sarmento, B., Ribeiro, A., Veiga, F., Sampaio, P., Neufeld, R., Ferreira, D., 2007b. Alginate/chitosan nanoparticles are effective for oral insulin delivery. Pharm Res 24, 2198-2206.

Sarmento, B., Mazzaglia, D., Bonferoni, M.C., Neto, A.P., do Céu Monteiro, M., Seabra, V., 2011. Effect of chitosan coating in overcoming the phagocytosis of insulin loaded solid lipid nanoparticles by mononuclear phagocyte system. Carbohydr Polym 84, 919-925.

Sasaoka, T., Kobayashi, M., 2000. The Functional significance of Shc in insulin signaling as a substrate of the insulin receptor. Endocr J 47, 373-381.

Sato, S., Murakata, T., Suzuki, T., Ohgawara, T., 1990. Control of pore size distribution of silica gel through sol-gel process using water soluble polymers as additives. J Mater Sci 254, 4880-4885.

Scheen, A.J., Charpentier, G., Östgren, C.J., Hellqvist, A., Gause-Nilsson, I., 2010. Efficacy and safety of saxagliptin in combination with metformin compared with sitagliptin in combination with metformin in adult patients with type 2 diabetes *mellitus*. Diabetes Metab Res Rev 26, 540-549.

Scherbaum, W.A., Schweizer, A., Mari, A., Nilsson, P.M., Lalanne, G., Jauffret, S., Foley, J.E., 2008. Efficacy and tolerability of vildagliptin in drugnaïve patients with type 2 diabetes and mild hyperglycaemia. Diabetes Obes Metab 10, 675-682.

Scott, R., Loeys, T., Davies, M.J., Engel, S.S., 2008. Efficacy and safety of sitagliptin when added to ongoing metformin therapy in patients with type 2 diabetes. Diabetes Obes Metab 10, 959-969.

Scott, R., Wu, L., Sanchez, M., Stein, P., 2007. Efficacy and tolerability of the dipeptidyl peptidase-4 inhibitor sitagliptin as monotherapy over 12 weeks in patients with type 2 diabetes. Int J Clin Pract 61, 171-180.

Shah, D., Shen, W.-C., 1996. Transcellular delivery of an insulin-transferrin conjugate in enterocytes-like caco-2 cells. J Pharm Sci 85, 1306-1311.

Slowing, I.I., Vivero-Escoto, J.L., Wu, C.-W., Lin, V.S.Y., 2008. Mesoporous silica nanoparticles as controlled release drug delivery and gene transfection carriers. Adv Drug Deliv Rev 60, 1278-1288.

Smith, J.E., Medley, C.D., Tang, Z.W., Shangguan, D.H., Lofton, C., Tan, W.H., 2007. Aptamer-conjugated nanoparticles for the collection and detection of multiple cancer cells. Anal Chem 79, 3075-3082.

Solanki, P.R., Kaushik, A., Ansari, A.A., Tiwari, A., Malhotra, B.D., 2009. Multi-walled carbon nanotubes/sol-gel-derived silica/chitosan nanobiocomposite for total cholesterol sensor. Sensors Actuators B 137, 727-735.

Sonaje, K., Chen, Y.-J., Chen, H.-L., Wey, S.-P., Juang, J.-H., Nguyen, H.-N., Hsu, C.-W., Lin, K.-J., Sung, H.-W., 2010. Enteric-coated capsules filled with freeze-dried

chitosan/poly(gamma-glutamic acid) nanoparticles for oral insulin delivery. Biomaterials 31, 3384-3394.

Sonaje, K., Lin, Y.H., Juang, J.H., Wey, S.P., Chen, C.T., Sung, H.W., 2009. In vivo evaluation of safety and efficacy of self-assembled nanoparticles for oral insulin delivery. Biomaterials 30, 2329-2339.

Steensgaard, D.B., Thomsen, J.K., Olsen, H.B., Knudsen, L.B., 2008. The molecular basis for the delayed absorption of the once-daily human GLP-1 analogue, liraglutide. Diabetes 57 (Suppl. 1), A164.

Stober, W., Fink, A., Bohn, E., 1968. Controlled growth of monodisperse silica spheres in micro size range. J Colloid Interf Sci 26, 62.

Su, F.-Y., Lin, K.-J., Sonaje, K., Wey, S.-P., Yen, T.-C., Ho, Y.-C., Panda, N., Chuang, E.-Y., Maiti, B., Sung, H.-W., 2012. Protease inhibition and absorption enhancement by functional nanoparticles for effective oral insulin delivery. Biomaterials 33, 2801-2811.

Suwalski, A., Dabboue, H., Delalande, A., Bensamoun, S.F., Canon, F., Midoux, P., Saillant, G.r., Klatzmann, D., Salvetat, J.-P., Pichon, C., 2010. Accelerated Achilles tendon healing by PDGF gene delivery with mesoporous silica nanoparticles. Biomaterials 31, 5237-5245.

Takahashi, R., Sato, S., Sodesawa, T., Kawakita, M., Ogura, K., 2000. High surface-area silica with controlled pore size prepared from nanocomposite of silica and citric acid. J Phys Chem B 104, 12184-12191.

Tan, B.H., Santos, E.M., Ducheyne, P., 1996. Ultramicroscopic pore size and porosity of xerogels for controlled release of biological molecules. Fifth World Biomaterials Congress, Toronto, Canada, p. 191.

Teng, Z., Han, Y., Li, J., Yan, F., Yang, W., 2010. Preparation of hollow mesoporous silica spheres by a sol–gel/emulsion approach. Microp Mesop Mater 127, 67–72.

Terra, S.G., Somayaji, V., Schwartz, S., Lewin, A.J., Teeter, J.G., Dai, H., Nguyen, T.T., Calle, R.A., 2011. A dose ranging study of the DDP-IV inhibitor PF-734200 added to metformin in subjects with type 2 diabetes. Exp Clin Endocrinol Diabetes 119, 401-407.

Todoroff, J., Vanbever, R., 2011. Fate of nanomedicines in the lungs. Cur Opin Coll Interf Sci 16, 246-254.

Tozuka, Y., Sugiyama, E., Takeuchi, H., 2010. Release profile of insulin entrapped on mesoporous materials by freeze–thaw method. Int J Pharm 386, 172-177.

Turinske, A., Nelson, S., Stojilovic, N., Ali, S., Dordevic, S., Evans, E., 2013. Formation of ZnO within flexible polymer fibers. J Sol-Gel Sci Tech 65, 283-286.

Umpierrez, G.E., Blevins, T., Rosenstock, J., Cheng, C., Anderson, J.H., Bastyr, E.J., 2011. The effects of LY2189265, a long-acting glucagon-like peptide-1 analogue, in a randomized, placebo-controlled, double-blind study of overweight/obese patients with type 2 diabetes: the EGO study. Diabetes Obes Metab 13, 418-425.

Verdich, C., Flint, A., Gutzwiller, J.P., Naslund, E., Beglinger, C., Hellstrom, P.M., Long, S.J., Morgan, L.M., Holst, J.J., Astrup, A., 2001. A meta-analysis of the effect of glucagon-like peptide-1 (7–36) amide on ad libitum energy intake in humans. J Clin Endocrinol Metab 86, 4382-4389.

Vilsboll, T., Krarup, T., Deacon, C.F., Madsbad, S., Holst, J.J., 2001. Reduced post-prandial concentrations of intact biologically active glucagon-like peptide 1 in type 2 diabetic patients. Diabetes 50, 609-613.

Vilsboll, T., Zdravkovic, M., Le-Thi, T., Krarup, T., Schmitz, O., Courrèges, J.P., Verhoeven, R., Bugánová, I., Madsbad, S., 2007. Liraglutide, a long-acting human glucagon-like peptide-1 analog, given as monotherapy signifi cantly improves glycemic control and lowers body weight without risk of hypoglycemia in patients with type 2 diabetes. Diabetes Care 30, 1608-1610.

Virkamäki, A., Ueki, K., Kahn, C.R., 1999. Protein–protein interaction in insulin signaling and the molecular mechanisms of insulin resistance. J Clin Invest 103, 931-943.

Voss, R., Brook, M.A., Thompson, J., Chen, Y., Pelton, R.H., Brennan, J.D., 2007. Non-destructive horseradish peroxidase immobilization in porous silica nanoparticles. J Mater Chem 17, 4854-4863.

Wang, D., Qian, J., Cai, F., He, S., Han, S., Mu, Y., 2012. Green'-synthesized near-infrared PbS quantum dots with silica–PEG dual-layer coating: ultrastable and biocompatible optical probes for in vivo animal imaging. Nanotechnology 23. doi:10.1088/0957-4484/23/24/245701.

Wang, G., Xu, J.-J., Chen, H.-Y., Lu, Z.-H., 2003. Amperometric hydrogen peroxide biosensor with sol-gel/chitosan network-like film as immobilization matrix. Biosens Bioelectron 18, 335-343.

Wang, T., Zhang, L., Su, Z., Wang, C., Liao, Y., Fu, Q., 2011. Multifunctional hollow mesoporous silica nanocages for cancer cell detection and the combined chemotherapy and photodynamic therapy. Appl Mater Interfaces 3, 2479-2486.

Wright, R.J., Frier, B.M., Deary, I.J., 2009. Effects of acute insulin-induced hypoglycemia on spatial abilities in adults with type 1 diabetes. Diabetes Care 32, 1503-1506.

Wu, Z., Joo, H., Lee, T.G., Lee, K., 2005. Controlled release of lidocaine hydrochloride from the surfactant-doped hybrid xerogels. J Control Release 104, 497-505.

Wu, Z.M., Zhou, L., Guo, X.D., Jiang, W., Ling, L., Qian, Y., Luo, K.Q., Zhang, L.J., 2012. HP55-coated capsule containing PLGA/RS nanoparticles for oral delivery of insulin. Int J Pharm 425, 1-8.

Xia, T., Kovochich, M., Liong, M., Meng, H., Kabehie, S., George, S., Zink, J.I., Nel, A.E., 2009. Polyethyleneimine coating enhances the cellular uptake of mesoporous silica nanoparticles and allows safe delivery of siRNA and DNA constructs. ACS Nano 3, 3273-3286.

Xiong, X.Y., Li, Y.P., Li, Z.L., Zhou, C.L., Tam, K.C., Liu, Z.Y., Xie, G.X., 2007. Vesicles from Pluronic/poly(lactic acid) block copolymers as new carriers for oral insulin delivery. J Control Release 120, 11-17.

Yagüe, C., Morosa, M., Grazúa, V., Arruebo, M., Santamaría, J., 2008. Synthesis and stealthing study of bare and PEGylated silica micro- and nanoparticles as potential drug-delivery vectors. Chem Eng J 137, 45-53.

Yang, C., Xie, H., Li, Y., Zhang, J.-K., Su, B.-L., 2013. Direct and rapid quantum dots labelling of Escherichia coli cells. J Colloid Interf Sci 393, 438-444.

Yu, M., Moreno, C., Hoagland, K.M., Dahly, A., Ditter, K., Mistry, M., Roman, R.J., 2003. Antihypertensive effect of glucagon-like peptide 1 in Dahl salt-sensitive rats. J Hypertens 21, 1125-1135.

Yu, Z., Jin, T., 2010.New insights into the role of cAMP in the production and function of the incretin hormone glucagon-like peptide-1 (GLP-1). Cellular Signalling 22, 1-8.

Zhang, C., Hou, T.A., Chen, J.F., Wen, L.X., 2010. Preparation of mesoporous silica microspheres with multi-hollow cores and their application in sustained drug release. Particuology 8, 447-452.

Zhang, L., Wang, T., Li, L., Wang, C., Su, Z., Li, J., 2012. Multifunctional fluorescent-magnetic polyethyleneimine functionalized Fe3O4–mesoporous silica yolk–shell nanocapsules for siRNA delivery. Chem Commum 48, 8706-8708.

Zhang, N., Ping, Q.N., Huang, G.H., Xu, W.F., 2005. Investigation of lectin-modified insulin liposomes as carriers for oral administration. Int J Pharm 294, 247-259.

Zhang, X., Sun, M., Zheng, A., Cao, D., Bi, Y., Sun, J., 2012. Preparation and characterization of insulin-loaded bioadhesive PLGA nanoparticles for oral administration. Eur J Pharm Sci 45, 632-638.

Zhao, D.Y, Huo, Q., Feng, J.L., Chmelka, B.F., D. Stucky, G.D., 1998a. Nonionic triblock and star diblock copolymer and oligomeric surfactant syntheses of highly ordered, hydrothermally stable, mesoporous silica structures. J Am Chem Soc 120, 6024-6036.

Zhao, D.Y., Feng, J.L., Huo, Q.S., Melosh, N., Fredrickson, G.H., Chmelka, B.F., Stucky, G.D., 1998b. Triblock copolymer synthesis of mesoporous silica with periodic 50 to 300 angstrom pores. Science 279, 448-552.

Zhao, X.J., Tapec-Dytioco, R., Wang, K.M., Tan, W.H., 2003. Collection of trace amounts of DNA/mRNA molecules using genomagnetic nanocapturers. Anal Chem 75, 3476-3483.

Zimmet, P., Alberti, K.G.M.M., Shaw, J., 2001. Global and societal implications of the diabetes epidemic. Nature 414, 782-787.

Zou, Y., Xiang, C., Sun, L.-X., Xu, F., 2008. Glucose biosensor based on electrodeposition of platinum nanoparticles onto carbon nanotubes and immobilizing enzyme with chitosan-SiO2 sol-gel. Biosens Bioelectron 23, 1010-1016.

Chapter II
Design of silica nanoparticles

2.1. Introduction

In the present work, SiNP were selected as a potential carrier for oral insulin delivery. The choice of SiNP for this purpose was based on important characteristics that makes them a promising system for biomolecule association, such as (i) silica present large surface area which allows high interaction with drugs (Salonen et al., 2008), (ii) silica matrices can act as drug reservoir by possessing high porosity allowing efficient drug loading (Chen et al., 2004), (iii) silica materials are known to be biocompatible *in vivo* application (Arruebo et al., 2006; Dormer et al., 2005), (iii) silica materials are no subjected to microbial attack (Weetal, 1970), (iv) these materials can be synthesized at low temperature (Kneuer et al., 2000), and (v) possess residual silanol groups (SiOH) at their surface which can be functionalized by different organic groups (Westcott et al., 1998).

One of the most used methods for synthesizing SiNP is the Stöber method. This method allows obtain monodisperse SiNP for a range of the initial reactant concentrations for TEOS (0.1-0.5 M), for H_2O (0.5-17 M) and for NH_3 (0.1-3.0 M) (Bogush et al., 1988). Two models have been proposed to elucidate the mechanism of SiNP growth. The formation of SiNP can be divided in two stages: nucleation and growth. Being the source of monomer, TEOS concentration will generate nuclei or primary particles present in aqueous medium. Generally, two models are used to describe silica particle growth. The monomer addition model supports a LaMer-like mechanism (La Mer, 1952) where, after an initial burst of nucleation, growth occurs through the addition of hydrolyzed monomers to the nuclei surface which occurs throughout primary particle aggregation to form secondary particles (larger particles). In contrast, the second model is based on controlled aggregation, in which nucleation occurs continuously throughout the reaction. In this case, the primary particles (or nuclei) aggregate with one another or with larger aggregates leading to a narrow size distribution (Bogush et al., 1988; Green et al., 2003).

In the present work, for preparing SiNP, a modified Stöber method was applied, involving the hydrolysis and condensation of TEOS, using ammonium as catalyst agent. For dissolving TEOS in aqueous medium, low concentration of ethanol was used. Since Stöber method is based on sol-gel process, we adopted the sol-gel terminology in all experimental sections.

The development of particles, in particular for oral delivery, dispersion and agglomeration should be critically controlled since these factors influence the quality of

particles, as well as the particle cell uptake. It has been found that the size of particles plays a key role in cellular uptake, influencing their absorption (He et al., 2012; Morishita et al., 2004; Schleh et al., 2012), adhesion (Goto et al., 2006) and transfection (Prabha et al., 2002) properties.

In this context, the formulations were optimized with the aim of achieving suitable mean particle size (Z-Ave) and polydispersity (PI) indices for oral delivery using high shear homogenization (HSH). HSH was chosen because it is a method widely used for producing nanoparticles with diameter below 1 μm with high monodispersity. The influence of TEOS and different homogenization speeds on Z-Ave and PI was assessed by a 2^2 factorial design approach. The choice of TEOS was based on the fact that its hydrolysis can lead to ethanol production that is less toxic than methanol, which would be generated by TMOS hydrolysis. The other parameters, such as ammonium and ethanol concentration, were not evaluated due to two reasons. Firstly, ethanol was used for dissolving TEOS in aqueous medium. Secondly, although the concentration of ammonium can influence the diameter of nanoparticles, in the present study, a minimum amount of ammonium was used only for decreasing the hydrolysis reaction time.

Several external factors, such as heating, mixing, pH variations or chemical reactions (e.g., hydrolysis and demidation), can compromise the conformational structure of the proteins resulting in loss of their biological activity and risk of adverse effects (Bilati et al., 2005). Therefore, to overcome possible protein instability after its association to nanoparticles, as well as to achieve an acceptable shelf-life of the product, freeze drying process was applied and the appearance and size distribution of re-dispersed optimized formulation were also evaluated.

2.2. Materials and methods

2.2.1. Materials

Tetraethyl orthosilicate (TEOS, 98 %) and NH_3 25 % were purchased from Merck (Darmstadt, Germany). Ethanol 99.9 % was purchased from Sigma-Aldrich (Steinhein, Germany). Ultra-purified water was obtained from Milli® Q Plus system (Millipore, Germany).

2.2.2. Experimental factorial design

To maximize the yield of production with a minimum of experiments, a factorial design approach was applied (Araújo et al., 2009). The influence of TEOS and different homogenization speeds on the particle properties were evaluated using a 2^2 factorial design with triplicate of central point, composed of 2 variables which were set at 2-levels each. The design required a total of 7 experiments. Each factor, the lower and higher values of the lower and upper levels were represented by a (−1) and a (+1) and the central point was represented by (0), as summarized in Table 2.1. The independent variables were the concentration of TEOS and the HSH homogenization speeds. The established dependent variables were Z-Ave and PI. The data were analyzed using STATISTICA 7.0 (Stafsoft, Inc.) software. All the results were obtained with 95 % confidence using ANOVA test.

Table 2. 1. Initial 2^2 factorial design, providing the lower (−1), upper (+1) and central point (0) level values for each variable.

Variables	**Levels**		
	-1	0	+1
TEOS ($mol.L^{-1}$)	0.43	0.69	0.95
HSH speed (rpm)	3000	4000	5000

2.2.3. Synthesis of silica nanoparticles

SiNP were prepared by a well established sol-gel method at room temperature using NH_3 as catalytic agent. In the experimental procedure, TEOS, ethanol and NH_3 were mixed under high shear homogenization (Ultra-Turrax®Ika T25, Germany) using an 18G impeller (Ika T25, Darmstadt, Germany) for 2 hours. The resulting nanoparticles were recovered by centrifuging and washing with a mixture of ethanol 99.9 % and ultra-purified water (1:1, v,v) by 2 cycles at 12,000 rpm (Spectrafuge 16M, Lambnet International, Inc.) for 5 min.

2.2.4. Preparation of freeze dried nanoparticles

SiNP suspension was frozen at −80 ºC for 24 h and freeze-dried at −45 ºC/184 mT for 48 h (Dura-dry TM). Before size measurements, nanoparticles in powder form were reconstituted with ultra-purified water.

2.2.5. Size and size distribution analysis

The average hydrodynamic diameter (Z-Ave) of nanoparticles was determined through dynamic light scattering (DLS, Zetasizer Nano ZS, Malvern Instruments, Malvern, UK). DLS is also known as photon correlation spectroscopy (PCS) that allows the measurement of molecules and/or particles due to Brownian motion in submicron region (Goldburg, 1999). Each sample was diluted with ultra-purified water before measuring the Z-Ave and polydispersity index (PI). Values reported are the mean ± SD of three different measurements of each sample.

2.2.6. Transmission electron microscope (TEM) analysis

The morphology of nanoparticles after freeze-drying was checked by transmission electron microscopy (TEM) (LEO 906E). The nanoparticles were dispersed in ethanol and placed on copper grids covered with carbon coating for TEM observations.

2.3. Results and discussions

2.3.1. Effect of TEOS concentration and different HSH speeds

To evaluate the effect of TEOS concentration and the HSH speeds on Z-Ave and PI of developed SiNP, seven experiments were conducted by 2^2 full factorial design to assure the existence of uniformity between the results and, thus to minimize the number of experiments need to find the dependence on these parameters.

Table 2.2 shows the obtained values of Z-Ave and PI for SiNP formulations produced by different concentrations of TEOS and HSH speeds. The Z-Ave of the formulations ranged from 183.9 nm ± 11.1 to 366.4 ± 18.1 nm, while the PI varied from 0.218 ± 0.074 to 0.505 ± 0.082. Mean values were calculated from a pool of 3 experiments from each formulation.

Table 2.2. Influence of TEOS ($mol.L^{-1}$) and HSH speed (rpm) on the formation of silica nanoparticles.

TEOS	HSH speed	Mean size ± S.D. (nm)	PI ± S.D.
0.43	5000	256.6 ± 20.3	0.218 ± 0.074
0.43	3000	356.4 ± 112.2	0.443 ± 0.006
0.69	4000	200.7 ± 13.5	0.308 ± 0.021
0.69	4000	292.7 ± 15.2	0.334 ± 0.058
0.69	4000	291.5 ± 35.3	0.349 ± 0.030
0.95	5000	366.4 ± 18.1	0.381 ± 0.005
0.95	3000	183.9 ± 11.1	0.505 ± 0.082

Abbreviation: SD, Standard Deviation

For TEOS concentration and HSH speed, analysis of variance (ANOVA) was performed.

Eearlier studies provided controversial data about the effect of TEOS concentration on particle size and distribution. Stöber and co-workers reported that TEOS concentration had no influence on the final particle size (Stober et al., 1968), while other studies indicated that

increasing TEOS concentration, the particle size decreased (Van Helden et al., 1981) or, on the other hand, larger particles were produced (Bogush et al., 1988). Most recent studies indicate that the formation of uniform-sized SiNP highly depends on the reaction parameters, namely TEOS concentration, catalytic agent concentration, effect of solvent and temperature (Rahman et al., 2007).

Although the parameters studied did not show a significant effect on Z-Ave of SiNP (Table 2.3) and (Figure 2.1A), smaller particles were produced with high TEOS concentration and high HSH speeds (Figure 2.2A).

Regarding to high TEOS concentration, the production of smaller particles can be attributed to the presence of lower water concentration which decreases the nucleation rate and consequently the TEOS hydrolysis rate, as well as the condensation rate of hydrolyzed monomers. Therefore, the formation of sub-particles during a short period was reduced and no aggregation was observed as reported by others (Park et al., 2002).

Table 2.3. Analysis of the Z-Ave by ANOVA statistical test.

Evaluated factors and their interactions	**Sum of squares**	**Degrees of freedom**	**Mean square**	***F*-value**	***p*-value**
(1) TEOS concentration	982.82	1	982.82	0.419361	0.563396
(2) HSH speed	1709.82	1	1709.82	0.729565	0.455805
1 by 2	19923.32	1	19923.32	8.501088	0.061713
Error	7030.86	3	2343.62		
Total	29646.83	6			

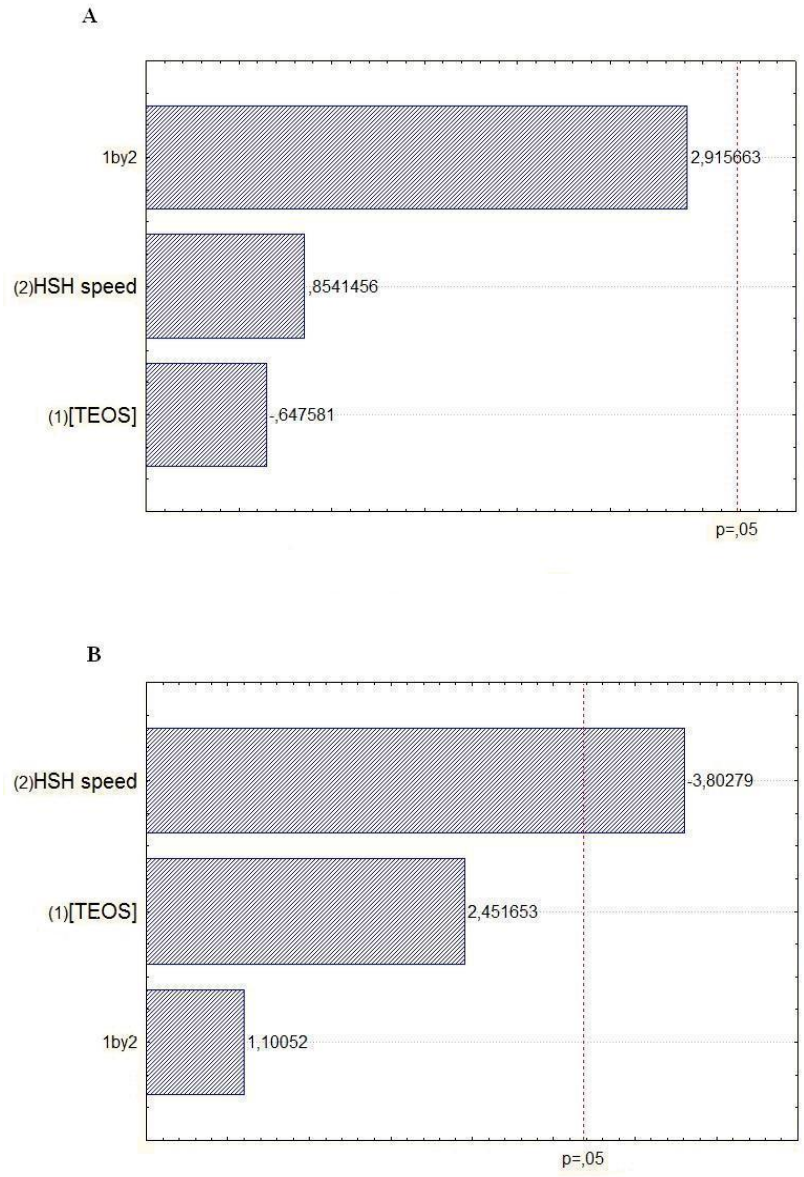

Figure 2.1. Pareto chart of the Z-Ave (A) and PI (B) for silica nanoparticles.

From Table 2.4 and Figure 2.1B, only HSH speed had a significant effect on PI (*p*-value < 0.05). An increase of HSH speed led to a decrease of size and PI (Figure 2.2A and 2.2B). As expected, a decrease of nanoparticles size was correlated to an increase of HSH speed. It is known that high speed is required to form silica homogenous dispersion and consequently to obtain smaller particles due to the higher input of energy (Enomoto et al., 1996).

Table 2.4. Analysis of PI by ANOVA statistical test.

Evaluated factors and their interactions	**Sum of squares**	**Degrees of freedom**	**Mean square**	***F*-value**	***p*-value**
(1) TEOS concentration	0.012656	1	0.012656	6.01060	0.091545
(2) HSH speed	**0.030450**	**1**	**0.030450**	**14.46118**	**0.031944**
1 by 2	0.002550	1	0.002550	1.21114	0.351489
Error	0.006317	3	0.002106		
Total	0.051974	6			

Since Z-Ave and PI are important parameters for producing nanoparticles with suitable physicochemical characteristics, the main purpose of the factorial design approach was to optimize a formulation for loading therapeutic proteins. Therefore, from obtained results, the optimal values were 0.43 $mol.L^{-1}$ of TEOS and a homogenization speed with 5000 rpm, depicting a Z-Ave of 256.6 ± 20.3 nm and a PI of 0.218 ± 0.074.

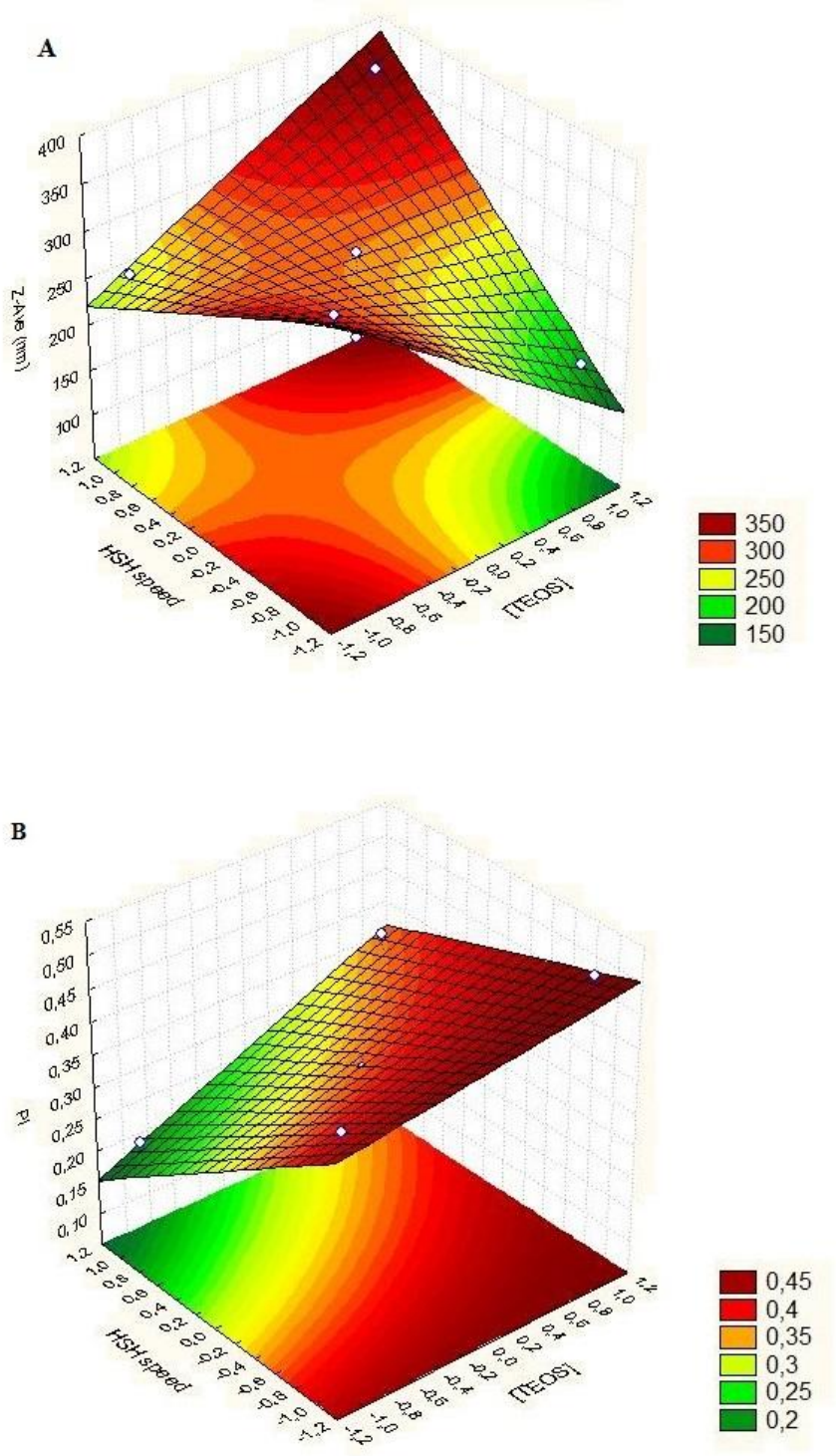

Figure 2. 2. Surface response chart of the effect of TEOS concentration and HSH speed on Z-Ave (A) and PI (B) of SiNP.

2.3.2. Analysis of lyophilized nanoparticles

Freeze-drying has been routinely applied to nanoparticles for increasing their stability upon storage. Few studies are reported in the literature regarding to the lyophilization of SiNP (Sameti et al., 2003).

The optimized formulation was lyophilized in the absence of cryoprotectants followed by sample reconstitution in ultra pure water. The visual inspection of the final lyophilized nanoparticles showed that they were brittle and white with strong signs of collapse and shrinkage. For the nanoparticles reconstitution in water, several additional forces were tested, such as vortexing, shaking, magnetic stirring or ultrasonication to achieve full resuspension of lyophilized nanoparticles. However, any additional forces were able of allowing complete nanoparticles dissolution. Large aggregates were macroscopically visible and a drastic increase of PI was also observed by DLS analysis (data not shown). According to Abdelwahed and co-workers (Abdelwahed et al., 2002), during the freeze-drying, the concentration of nanoparticles increases, favoring the condensation of SiOH groups present at silica surface into Si-O-Si bridges, leading to the irreversible particle aggregation.

2.3.3. TEM analysis

TEM micrographs were recorded to investigate the effect of freeze drying on the morphology of optimized SiNP (Figure 2.3). The images show that freeze drying process lead to stronger nanoparticle agglomeration, with no individual particles, confirming thus, the results obtained by DLS.

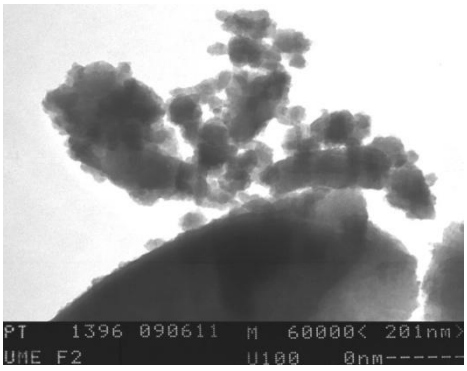

Figure 2.3. TEM images of optimized SiNP synthesized by HSH after freeze-drying process in the absence of cryoprotectants agents.

2.4. Conclusions

Silica nanoparticles were successfully prepared by sol-gel technology at room temperature from the hydrolysis and condensation of TEOS. The full factorial design was applied to find out which parameters could influence the mean size and size distribution of nanoparticles. The factors studied were the concentration of TEOS and the HSH speed. Higher concentration of TEOS and higher HSH speeds resulted in smaller SiNP. Based on these observations, the optimal formulation was obtained using 0.43 $mol.L^{-1}$ of TEOS and 5000 rpm with low degree of particle agglomeration.

The effect of freeze-drying process on the mean size and size distribution of nanoparticles was also evaluated. The optimized formulation was lyophilized in the absence of cryoprotectants followed by sample reconstitution in ultra-purified water. In this case, the Z-Ave and PI were strongly affected during the freeze-drying process. TEM images could confirm the results obtained from DLS, showing that freeze-drying can generate severe particle agglomeration due to the condensation of SiOH groups present at silica surface.

2.5. References

Abdelwahed, M., Boufi, S., Ben, S., Naceur, B., Gandini, A., 2002. Interaction of silane coupling agents with cellulose. Langmuir 18, 3203-3208.

Araújo, J., Vega, E., Lopes, C., Egea, M.A., Garcia, M.L., Souto, E.B., 2009. Effect of polymer viscosity on physicochemical properties and ocular tolerance of FB-loaded PLGA nanospheres. Colloids Surf B: Biointerf 72, 48-56.

Arruebo, M., Galan, M., Navascues, N., Tellez, C., Marquina, C., Ibarra, M.R., Santamaria, J., 2006. Development of magnetic nanostructured silica-based materials as potential vectors for drug-delivery applications. Chem Mater 18, 1911-1919.

Bilati, U., Allémann, E., Doelker, E., 2005. Strategic approaches for overcoming peptide and protein instability within biodegradable nano- and microparticles. Eur J Pharm Biopharm 59, 375-388.

Bogush, G.H., Tracy, M.A., Zukoski, C.F., 1988. Preparation of monodisperse silica particles: Control of size and mass fraction. J Non-Cryst Solids 104, 95-106.

Chen, J.-F., Ding, H.-M., Wang, J.-X., Shao, L., 2004. Preparation and characterization of porous hollow silica nanoparticles for drug delivery application. Biomaterials 25, 723-727.

Dormer, K., Seeney, C., Lewelling, K., Lian, G., Gibson, D., Johnson, M., 2005. Epithelial internalization of superparamagnetic nanoparticles and response to external magnetic field. Biomaterials 26, 2061-2072.

Enomoto, N., Koyano, T., Nakagawa, Z., 1996. Effect of ultrasound on synthesis of spherical silica. Ultrasonics Sonochemistry 3, S105-S109.

Goldburg, W.I., 1999. Dynamic light scattering. Am J Phys 67, 1152-1160.

Goto, T., Morishita, M., Kavimandan, N.J., Takayama, K., Peppas, N.A., 2006. Gastrointestinal transit and mucoadhesive characteristics of complexation hydrogels in rats. J Pharm Sci 95, 462-469.

Green, D.L., Lin, J.S., Lam, Y.-F., Hu, M.Z.C., Schaefer, D.W., Harris, M.T., 2003. Size, volume fraction, and nucleation of Stober silica nanoparticles. J Colloid Interf Sci 266, 346-358.

He, C., Yin, L., Tang, C., Yin, C., 2012. Size-dependent absorption mechanism of polymeric nanoparticles for oral delivery of protein drugs. Biomaterials 33, 8569-8578.

Kneuer, C., Sameti, M., Haltner, E.G., Schiestel, T., Schirra, H., Schmidt, H., Lehr, C.-M., 2000. Silica nanoparticles modified with aminosilanes as carriers for plasmid DNA. Int J Pharm 196, 257-261.

La Mer, V., 1952. Nucleation in phase transitions. Ind Eng Chem 44, 1270-1277.

Morishita, M., Goto, T., Peppas, N.A., Joseph, J.I., Torjman, M.C., Munsick, C., Nakamura, K., Yamagata, T., Takayama, K., Lowman, A.M., 2004. Mucosal insulin delivery systems based on complexation polymer hydrogels: effect of particle size on insulin enteral absorption. J Control Release 97, 115-124.

Park, S.K., Kim, K.D., Kim, H.T., 2002. Preparation of silica nanoparticles: determination of the optimal synthesis conditions for small and uniform particles. Colloids Surf A: Psysicochem Eng 197, 7-17.

Rahman, I.A., Vejayakumaran, P., Sipaut, C.S., Ismail, J., Bakar, M.A., Adnan, R., Chee, C.K., 2007. An optimized sol–gel synthesis of stable primary equivalent silica particles. Colloids Surf A: Physicochem Eng 294, 102-110.

Salonen, J., Kaukonen, A.M., Hirvonen, J., Lehto, V., 2008. Mesoporous silicon in drug delivery applications. J Pharm Sci 97, 632-653.

Sameti, M., Bohr, G., Ravi Kumar, M.N.V., Kneuer, C., Bakowsky, U., Nacken, M., Schmidt, H., Lehr, C.M., 2003. Stabilisation by freeze-drying of cationically modified silica nanoparticles for gene delivery. Int J Pharm 266, 51-60.

Stober, W., Fink, A., Bohn, E., 1968. Controlled growth of monodisperse silica spheres in micro size range. J Colloid Interf Sci 26, 62.

Van Helden, A.K., Jansen, J.W., Vrij, A., 1981. Preparation and characterization of spherical monodisperse silica dispersions in nonaqueous solvents. J Colloid Interf Sci 81, 354-368.

Weetal, H.H., 1970. Starage stability of water insiluble enzymes covalently coupled to organic and inorganic carriers. Biochim Biophys Acta 212, 1-7.

Westcott, S.L., Oldenburg, S.J., Lee, T.R., Halas, N.J., 1998. Formation and adsorption of clusters of gold nanoparticles onto functionalized silica nanoparticle surfaces. Langmuir 14, 5396-5401.

Chapter III

Effect of cryoprotectants on reconstitution of silica nanoparticles

3.1. Introduction

As described in the previous chapter, SiNP were successfully produced by sol-gel technology within the nanometer range and low degree of agglomeration. However, the freeze-drying process in the absence of cryoprotectant agents demonstrated to be inefficient for nanoparticle stabilization, with an increase of the Z-Ave and PI in comparison to the wet formulation. Therefore, it was essential to preserve the size of SiNP during freeze-drying process.

Freeze-drying, also known as lyophilization, is a well-established process used to preserve the original properties of biological molecules (Chang et al., 2005). Recently, this process has been applied to improve the stabilization of colloidal systems in the pharmaceutical field, such as nanoparticles (Han et al., 2013; Holzer et al., 2009; Varshosaz et al., 2012). However, during the freezing and drying steps, some stresses can be generated due to the phase separation into ice and concentrated particles suspension. The high concentration of particles may induce an irreversible aggregation, affecting the texture and morphology of the particulate system.

In the literature, several excipients are used to preserve the primary physical and chemical characteristics of the formulation. Such excipients can be classified as: (i) cryoprotectant agents that protect the product from freezing step or (ii) lyoprotectant agents, which are able of avoiding the stress induced by the drying process (Abdelwahed et al., 2006). Typically, sugars, including glucose, sucrose, dextrose and trehalose are used as cryoprotectants for stabilizing nanoparticle formulations (Beck-Broichsitter et al., 2012; Tang et al., 2013; Varshosaz et al., 2012).

The protective effect of cryoprotectants can be explained by several factors. Since freezing is carried out below sugar *T*g (glass transition temperature), there is an immobilization of particles within a glassy matrix of the cryoprotectants leading to an increase of product stabilization (Slade L and H, 1991). A different approach to preserve the native structure of nanoparticles is based on water replacement (Crowe JH et al., 1993). This mechanism suggests the interaction between the polar groups at the particle surface and stabilizer molecules by hydrogen bonds, due to water lost during drying. Therefore, these stabilizers preserve the nanoparticle properties by acting as water substitutes. Also, the addition of cryoprotectant agents may suppress the formation of ice crystals due to the rise of

viscosity in the solution. Thus, the isolation of individual particles prevents the aggregation during freezing above *T*g (Allison et al., 2000).

Only few studies reporting lyophilization of SiNP are available in the literature. A more systematic study with these particles was performed using 5, 10 or 20 % of different cryoprotectans to investigate their effect on the reconstitution of cationically modified SiNP (Sameti et al., 2003). In these studies, trehalose and glycerol demonstrated to be more efficient for particle diameter and DNA-binding activity preservation.

In the present study, trehalose, sorbitol and mannitol were used as cryoprotectant agents for freeze drying of SiNP. The selection of these agents was based on their availability on our laboratory, as well as on previous works that show the preservative effect of these cryoprotectants on size and size distribution of nanoparticles (Anhorn et al., 2008; Wu et al., 2012). Therefore, the influence of freeze-drying process in the presence of several cryoprotective agents with different concentrations and ratios on the resulting nanoparticles was evaluated.

3.2. Materials and methods

3.2.1. Materials

Tetraethyl orthosilicate (TEOS, 98 %) and NH_3 25 % were purchased from Merck (Darmstadt, Germany). Trehalose dehydrate, mannitol, sorbitol and ethanol 99.9 % were obtained from Sigma-Aldrich (Steinhein, Germany). Ultra-purified water was obtained from Milli® Q Plus system (Millipore, Germany).

3.2.2. Synthesis of silica nanoparticles

SiNP were prepared by sol-gel technology at room temperature using NH_3 as catalytic agent. In the experimental procedure TEOS, ethanol and NH_3 were mixed under high shear homogenization (Ultra-Turrax®Ika T25, Germany) using an 18G impeller (Ika T25, Darmstadt, Germany) for 2 hours (Table 3.1) at 5000 rpm. The resulting nanoparticles were recovered by centrifuging and washing with a mixture of ethanol and ultra-purified water (1:1, v/v) by 2 cycles at 12,000 rpm (Spectrafuge16M, Lambnet International, Inc.) for 5 min.

Table 3.1. Controlled parameters applied for the synthesis of nanoparticles.

Parameters	**Optimal Value**
[TEOS] ($mol.L^{-1}$)	0.43
[NH_3] ($mol.L^{-1}$)	2.20
[Ethanol] ($mol.L^{-1}$)	10.30
[H_2O]/[TEOS]	39.00

3.2.3. Preparation of freeze-dried nanoparticles

Nanoparticle suspension was mixed with the desired amount of cryoprotectant solution, e.g., mannitol, sorbitol or trehalose to prevent aggregation. The cryoprotectant agents were added to the suspension at concentrations of 5 and 10 % (w/v) in different ratios followed by freezing at –80 ºC for 24 h. Finally, the samples were dried at freeze dryer Labconco FreeZone® Freeze Dry Systems during 48 h at a pressure of 0.06 mbar. Before the

measurements, nanoparticles in powder form were reconstituted with ultra-purified water by vortex.

3.2.4. Size and size distribution analysis

The average hydrodynamic diameter (Z-Ave) of nanoparticles was determined through dynamic light scattering (DLS, Zetasizer Nano ZS, Malvern Instruments, Malvern, UK). DLS is also known as Photon correlation spectroscopy (PCS) that allows the measurement of molecules and/or particles due to Brownian motion in submicron region (Goldburg, 1999). Each sample was dissolved with ultra-purified before measuring the Z-Ave and polydispersity index (PI). Values reported are the mean ± SD of three different measurements of each sample.

3.2.5. Atomic force microscopy (AFM) studies

AFM is a scanning probe microscope able to resolving surface detail down to the atomic level for the observation of images with high resolution.

In the AFM, the dominant interactions at probe-sample distance are Van der Waals forces. There are 3 primary imaging modes in AFM: (i) Contact AFM (repulsive Van der Waals forces); (ii) Tapping mode and (iii) Non-contact mode (attractive Van der Waals forces). In tapping mode, fast oscillating amplitude is employed to obtain the surface image, minimizing the inelastic surface deformation by reducing the duration of tip-sample contact (Magonov, et al., 1997).

To investigate the morphological aspect of SiNP after freeze-drying, AFM micrographs were taken. AFM experiments were performed with a Multimode microscope (Veeco, Santa Barbara, California) controlled by Nanoscope IIIa electronics (Veeco). The images were done in tapping mode at 25 °C. Samples were prepared by depositing 5 µL of the samples after re-dispersion in water, on silicon substrate followed by drying overnight at 25 ^{o}C.

3.2.6. Thermal analysis

Differential scanning calorimetry (DSC) is a frequent thermal analysis used for the physical and energetic characterization of pharmaceutical compounds. DSC is used for studying the heat loss or gain occurring within a sample as a function of the temperature. Therefore, several thermal events can be determined by DSC, such as melting, boiling, desolvatation, glass transition, decomposition and recrystallization. The samples contained in pans are heating in a raised platform on the constant discs. Heat is transferred through the disc and through the sample pan to the contained sample and reference (Ford and Timmins, 1989).

The thermal analysis of the cryoprotectants and nanoparticles in the presence of sorbitol, mannitol or trehalose were performed using a TA Instrument (TA Instruments, New Castle, USA). For this purpose, 5 mg of lyophilized nanoparticles were accurately weighted in 40 μL aluminium pans. DSC scans have been recorded from 25 to 350 ºC at a heating constant rate of 10 ºC/min under purging of nitrogen at 20 mL/min using an empty pan as reference. Data were obtained from the peaks areas using a TA instrument software.

3.2.7. X-ray diffraction (XRD) analysis

X-ray is used for determining the atomic structure of a compound. This technique allows that crystalline and amorphous materials to be differentiated. Crystalline compounds display many diffractions bands, whereas amorphous compounds show a more or less regular baseline. When a X-ray beam interacts with a crystalline compound, a diffraction pattern is produced in particular directions, which are related to the position of the atoms in the crystalline lattice.

The physical structure of cryoprotectants and nanoparticles in the presence of sorbitol, mannitol or trehalose was performed at 25 ºC using a Siemens D5000 diffractometer system (Siemens, Germany) with a copper anode (Cu-Kα radiation , $\lambda = 0.1542$ nm) at angles $2\theta = 4$-70º.

3.3. Results and discussions

3.3.1. Size and size distribution analysis

Freeze-drying is a widely used method to improve the stability of the nanoparticulate systems in order to maintain the primary structure of the formulation. A variety of excipients, such as sugar and sugar alcohols have been employed to achieve the chemical and physical stability of nanoparticles during freeze-drying. However, there are no rules for the selection of a suitable cryoprotectant agent. Some studies show that high cryoprotectant concentrations can stabilize or even lead to the aggregation of the system depending on the type of nanoparticles and the freeze drying conditions (Bildstein et al., 2009; Lee et al., 2009; Shi et al., 2012).

In the present study, mannitol, sorbitol and trehalose were used in different concentrations and ratios to evaluate their influence on the physicochemical properties of SiNP during freeze drying process.

The results from DLS measurements are presented in Figure 3.1. Nanoparticles prepared by sol-gel method exhibited a Z-Ave of 285.60 ± 20.38 nm and PI of 0.218 ± 0.074 which indicate a monodisperse distribution of colloidal system. For prior experiments, nanoparticles were freeze dried either without cryoprotectants or in the presence of mannitol, sorbitol or trehalose with a concentration of 5 and 10 % (w/v) at a volume ratio cryoprotectants:nanoparticles of (1:1) and (2:1).

For nanoparticles lyophilized in the presence of trehalose, a fine powder occupying the same shape and volume as the original frozen suspension was obtained. In contrast, nanoparticles without cryoprotectant and or in the presence of sorbitol or mannitol, the final freeze-dried cake was partially collapsed. Reconstitution of lyophilized nanoparticles using equal volume of ultra pure water (the same volume solution before the freeze drying process) showed that in the absence of any cryoprotectant, large aggregates were macroscopically visible and a drastic increase of PI was also observed. On the other hand, nanoparticles in the presence of trehalose, exhibited a rapid rehydration rate compared to the formulation without cryoprotectants or with that treated with sorbitol or mannitol.

The explanation for this phenomenon may be due to the interaction between SiNP surface and the cryoprotectant. During freeze-drying, the condensation of SiOH groups into Si-O-Si bridges occurs, leading to the particle aggregation. Thus, hydroxyl groups present in

sugars and sugar alcohol can react with SiOH by hydrogen bonds, protecting the nanoparticles from agglomeration (Abdelwahed et al., 2002).

In the presence of 5 or 10 % (w/v) of cryoprotectants at both ratios (1:1or 2:1), mannitol and sorbitol demonstrated to be inefficient for nanoparticle stabilization, with an increase of the Z-Ave and PI in comparison to wet formulation (Figure 3.1). The aggregation of nanoparticles after freeze-drying process using mannitol is due to the possible crystallization of mannitol and the formation of eutectics with ice leading to the separation from the system. Therefore, the crystals formed by the interaction between mannitol and water may exert a mechanical force on the nanoparticles causing the particles destabilization. Previous reports also state the sorbitol unavailability to preserve biomolecules due to its crystallization during freeze-drying process (Piedmonte et al., 2007).

Unlike other cryoprotectants tested, trehalose preserved Z-Ave and PI of SiNP. It is generally known that high concentrations of cryoprotectant can lead to better reconstitution of nanoparticles (Anhorn et al., 2008). As shown in Figure 3.1, high concentrations of trehalose (10 %) proved to be more effective for nanoparticle stabilization. Better results were obtained at a ratio of (1:1) when compared with the ratio of (2:1). Therefore, increasing cryoprotectant amount to a certain level, a limit of stabilization or even a destabilization of nanoparticles can occur. Similar observations have been reported during freeze drying of poly (lactic acid-co-ethylene oxide) (PLE) using trehalose as cryoprotective agent (De Jaeghere et al., 1999).

Since SiNP depict SiOH groups at their surface, we hypothesize that trehalose interacts strongly with the SiOH than sorbitol and mannitol, which demonstrate its ability to avoid nanoparticle aggregation.

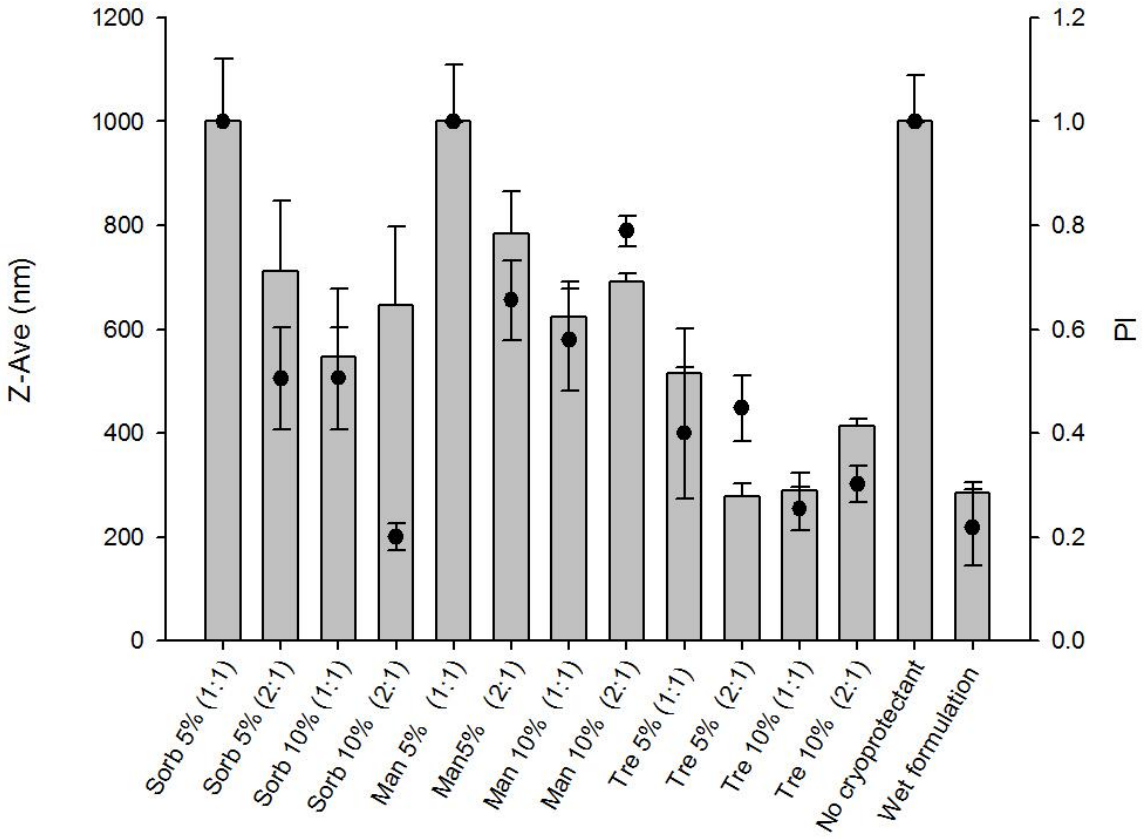

Figure 3.1. Z-Ave (nm) ± SD and PI ± SD (●) of SiNP in the presence of different cryoprotectants. The % (w/v) as well as the ratio cryoprotectants:nanoparticles (v/v) are indicated for each cryoprotectant agents. Sorb: sorbitol; Man: mannitol; Tre: trehalose.

3.3.2. AFM studies

The morphological characterization of nanoparticles with 10 % trehalose (1:1) by AFM showed homogeneity and spherical shape of the particles with size similar to that recorded by DLS (Figure 3.2), indicating that the cryoprotectant is able of preserving the physicochemical properties of the nanoparticles during freeze-drying process.

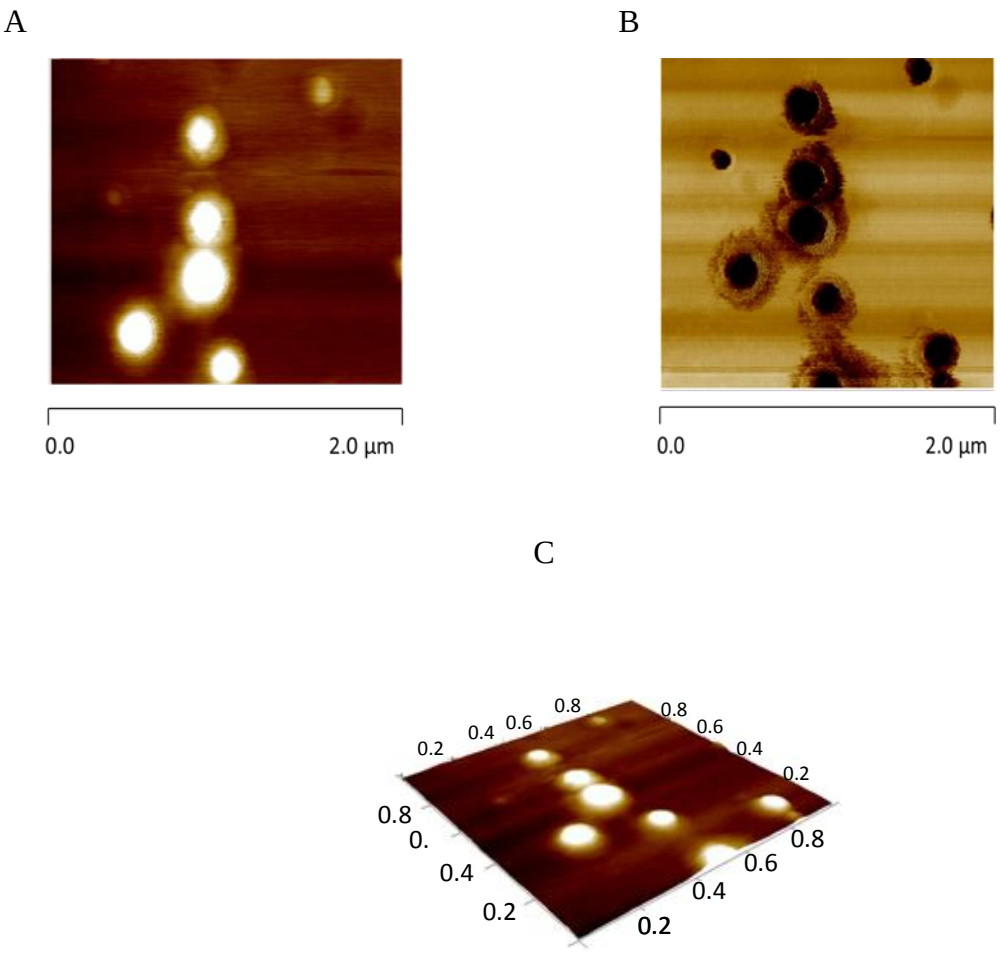

Figure 3.2. Morphological characterization of SiNP in the presence of trehalose 10 % (1:1, v/v). AFM height image (A), phase image (B) and 3D image (C).

3.3.3. DSC analysis

DSC thermograms of lyophilized nanoparticles with 10 % (w/v) of cryoprotectant at ratio of (1:1) are shown in Figure 3.3A. The DSC parameters for sorbitol, mannitol and trehalose show an endothermic peak at 98.76, 167.88 and 94.57 ºC, respectively (Table 3.2). Upon addition of SiNP to three different cryoprotectant solutions a melting peak at 164.97 °C for SiNP-Mannitol (SiNP-Man), 78.30 °C for SiNP-Sorbitol (SiNP-Sorb) and 77.90 °C for SiNP-Trehalose (SiNP-Tre) were clearly observed (Figure 3.3A). This could be attributed to the presence of bulk materials in the freeze-dried nanoparticles.

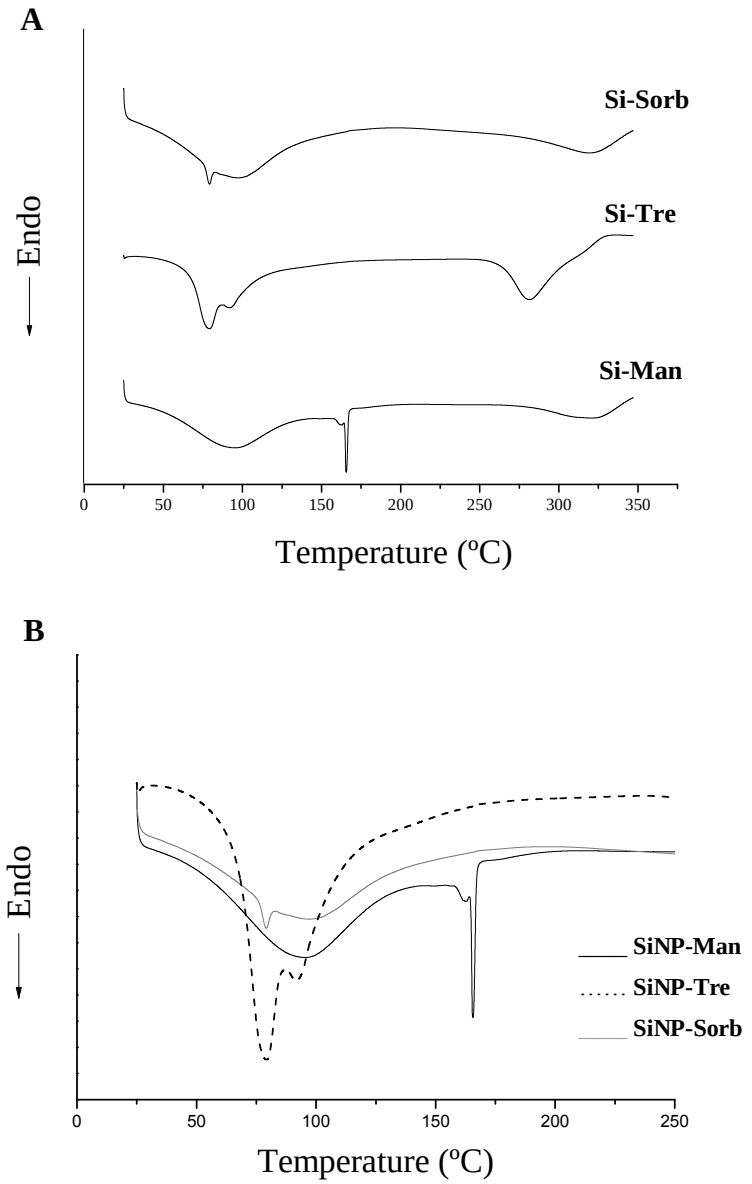

Figure 3.3. DSC patterns of the freeze-dried SiNP in the presence of different cryoprotectant agents (10 %, 1:1). The superposition of the 3 DSC curves of SiNP and different cryoprotectants (B).

By analyzing the DSC curves of SiNP-Sorb and SiNP-Tre, a shift in the melting point of the cryoprotectants to lower temperature and a decrease of enthalpy were observed (Figure 3.3A and 3.3B). These results may be ascribed to the interaction of SiNP with sorbitol or trehalose. Therefore, the hydroxyl groups of sorbitol or trehalose can combine with SiOH groups present at silica surface. In contrast, mannitol molecules crystallized and separated from the nanoparticulate system during freeze drying process, resulting in nanoparticles aggregation.

Table 3.2. DSC parameters for cryoprotectant agents and their mixture with SiNP.

	Melting Peak (ºC)	**Onset (ºC)**	**Enthalpy (J/g)**
Man	165.02	167.88	244.80
Sorb	101.52	98.76	158.30
Tre	101.51	94.57	129.70
SiNP-Man (10 %, 1:1)	166.17	164.97	10.45
SiNP-Sorb (10 %, 1:1)	78.83	77.00	1.18
SiNP-Tre (10 %, 1:1)	77.90	71.25	40.39

3.3.4. XRD analysis

The X-ray diffraction patterns of dried nanoparticles and the cryoprotectants involved in freeze drying process (mannitol, sorbitol and trehalose) are shown in Figure 3.4. Specific diffraction peaks of mannitol, sorbitol and trehalose occurred, demonstrating the crystalline nature of the sugars. However, SiNP in the presence of mannitol, showed a more crystalline behavior in comparison to nanoparticles with sorbitol or trehalose. Based on the position of the peaks, the crystallized compound was identified as mannitol (Figure 3.4B). These results can justify the nanoparticle aggregation containing mannitol during freeze-drying process.

It is known that an amorphous sugar has the ability to protect the material to be preserved due to its high viscosity, which avoids the mobility of the nanoparticles, increasing their stability (Imamura et al., 2001). The drying step of a concentrated solution leads to the formation of a syrup, then into a viscoelastic rubber, and finally into a stable glass (Sun et al., 1996). Therefore, SiNP containing mannitol did not transform into a glass state during the freeze-drying process, due to the regular rearrangement of alcohol sugar crystal lattice. Consequently, there is a concentrated of organized sugar molecular and other with nanoparticles. Since nanoparticles were not kept well dispersed, the aggregation occurred.

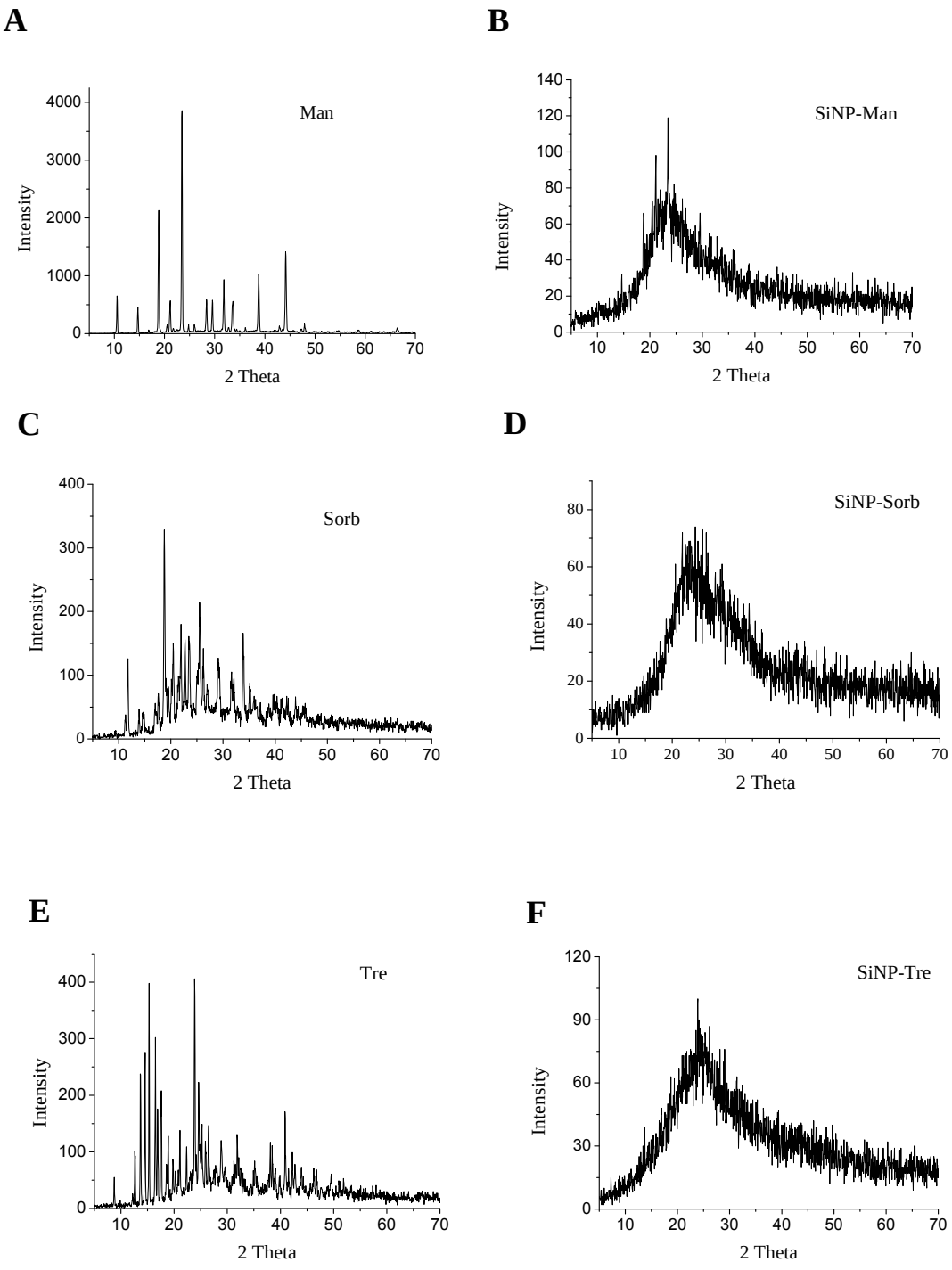

Figure 3.4. X-ray diffraction patterns of the cryoprotectant agents alone and of their mixture with silica nanoparticles after freeze-drying process.

On the other hand, no distinct peaks for sorbitol were observed (Figure 3.4D) in the XRD of SiNP in the presence of sorbitol. It suggests that the crystal lattice of sorbitol was

rearranged irregularly, and the sugar remained bound to nanoparticles. Thus, the crystallization process is inhibited and the glass state is created. However, the effective stabilization of nanoparticles is only achieved by trehalose during freeze-drying process. Although SiNP-Sorb show predominantly amorphous XRD patterns, sorbitol did not preserve the particle size. It may suggest that the structure of cryoprotectant agents may influence in their preservative properties. In the XRD patterns of freeze-dried nanoparticles in the presence of trehalose, a peak in the SiNP-Tre was observed (Figure 3.4F). These results are in agreement with DSC studies, since all cryoprotectants decreased their crystallinity in the presence of SiNP. However, trehalose was more efficient in preserving the particle size nanoparticles during the freeze-drying process. The structure of trehalose can be considered as annular, while of the mannitol and sorbitol is linear. Therefore, the interaction between trehalose and SiOH groups is more intense, due to higher spatial resistance of layer. In contrast, mannitol and sorbitol molecules can be less effective as cryoprotectants possible due to their linear shape, forming a layer with low spatial resistance.

3.4. Conclusions

Generally, nanoparticles show a poor long-term stability in aqueous suspension due to several physical (aggregation/fusion phenomena) and chemical (pH or temperature) factors that may destabilize the colloidal systems. Freeze-drying is widely applied to increase the shelf-life of labile drug solutions and/or colloidal carriers.

Based on the obtained results, SiNP in the presence of mannitol, showed a more crystalline behavior in comparison to nanoparticles with sorbitol or trehalose that could be confirmed by DSC and XRD. SiNP in the presence of trehalose demonstrated a structure more crystalline than that in the presence of sorbitol. However, trehalose was more efficient in preserving the particle size of nanoparticles during the freeze-drying process. The optimal concentration of trehalose for preserving SiNP was 10 % (w/v) at a ratio of (1:1, v/v). During the freeze-drying process, trehalose can replace water molecules due to the strong interaction via hydrogen bounds between SiOH groups present in SiNP surface and the sugar, forming a stable layer around the particle and thus, preserving the particle physical properties.

3.5. References

Abdelwahed, M., Boufi, S., Ben, S., Naceur, B., Gandini, A., 2002. Interaction of silane coupling agents with cellulose. Langmuir 18, 3203-3208.

Abdelwahed, W., Degobert, G., Stainmesse, S., Fessi, H., 2006. Freeze-drying of nanoparticles: Formulation, process and storage considerations. Adv Drug Deliv Rev 58, 1688-1713.

Allison, S.D., Molina, M.D.C., Anchordoquy, T.J., 2000. Stabilization of lipid/DNA complexes during the freezing step of the lyophilization process: the particle isolation hypothesis. Biochim Biophys Acta 1468, 127-138.

Anhorn, M.G., Mahler, H.-C., Langer, K., 2008. Freeze drying of human serum albumin (HSA) nanoparticles with different excipients. Int J Pharm 363, 162-169.

Beck-Broichsitter, M., Kleimann, P., Schmehl, T., Betz, T., Bakowsky, U., Kissel, T., Seeger, W., 2012. Impact of lyoprotectants for the stabilization of biodegradable nanoparticles on the performance of air-jet, ultrasonic, and vibrating-mesh nebulizers. Eur J Pharm Biopharm 82, 272-280.

Bildstein, L., Hillaireau, H., Desmaële, D., Lepêtre-Mouelhi, S., Dubernet, C., Couvreur, P., 2009. Freeze-drying of squalenoylated nucleoside analogue nanoparticles. Int J Pharm 381, 140-145.

Chang, L., Shepherd, D., Sun, J., Ouellette, D., Grant, K.L., Tang, X., Pikal, M.J., 2005. Mechanism of protein stabilization by sugars during freeze-drying and storage: Native structure preservation, specific interaction, and/or immobilization in a glassy matrix? J Pharm Sci 94, 1427-1444.

Crowe JH, Crowe LM, JF, C., 1993. Preserving dry biomaterials: The water replacement hypothesis. Part 1. BioPharm 6, 28-29.

De Jaeghere, F., Allémann, E., Leroux, J.-C., Stevels, W., Feijen, J., Doelker, E., Gurny, R., 1999. Formulation and lyoprotection of poly(lactic acid-co-ethylene oxide) nanoparticles: influence on physical stability and in vitro cell uptake. Pharm Res 16, 859-866.

Ford, J., Timmins, P., 1989. Pharmaceutical thermal analysis. In Rubinstein, M.H. (Ed). Ellis Horwood Limited, UK.

Goldburg, W.I., 1999. Dynamic light scattering. Am J Phys 67, 1152-1160.

Han, J., Zhou, C., Wu, Y., Liu, F., Wu, Q., 2013. Self-assembling behavior of cellulose nanoparticles during freeze-drying: effect of suspension concentration, particle size, crystal structure, and surface charge. Biomacromolecules 14, 1529-1540.

Holzer, M., Vogel, V., Mäntele, W., Schwartz, D., Haase, W., Langer, K., 2009. Physico-chemical characterisation of PLGA nanoparticles after freeze-drying and storage. Eur J Pharm Biopharm 72, 428-437.

Imamura, K., Iwai, M., Ogawa, T., Sakiyama, T., Nakanishi, K., 2001. Evaluation of hydration states of protein in freeze-dried amorphous sugar matrix. J Pharm Sci 90, 1955-1963.

Lee, M.K., Kim, M.Y., Kim, S., Lee, J., 2009. Cryoprotectants for freeze drying of drug nano-suspensions: Effect of freezing rate. J Pharm Sci 98, 4808-4817.

Magonov, S.N., Elings, V., Whangbo, M.-H., 1997. Phase imaging and stiffness in tapping-mode atomic force microscopy. Surf Sci 375, L385-L391.

Piedmonte, D., Summers, C., McAuley, A., Karamujic, L., Ratnaswamy, G., 2007. Sorbitol crystallization can lead to protein aggregation in frozen protein formulations. Pharm Res 24, 136-146.

Sameti, M., Bohr, G., Ravi Kumar, M.N.V., Kneuer, C., Bakowsky, U., Nacken, M., Schmidt, H., Lehr, C.M., 2003. Stabilisation by freeze-drying of cationically modified silica nanoparticles for gene delivery. Int J Pharm 266, 51-60.

Shi, A.-M., Wang, L.-J., Li, D., Adhikari, B., 2012. The effect of annealing and cryoprotectants on the properties of vacuum-freeze dried starch nanoparticles. Carbohydr Polym 88, 1334-1341.

Slade L, H, L., 1991. Beyond water activity: Recent advances based on an alternative approach to the assessment of food quality and safety. Crit Rev Food Sci Nutrition 30, 115-360.

Sun, W.Q., Leopold, A.C., Crowe, L.M., Crowe, J.H., 1996. Stability of dry liposomes in sugar glasses. Biophys J 70, 1769-1776.

Tang, K.S., Hashmi, S.M., Shapiro, E.M., 2013. The effect of cryoprotection on the use of PLGA encapsulated iron oxide nanoparticles for magnetic cell labeling. Nanotechnol 24.

Varshosaz, J., Eskandari, S., Tabbakhian, M., 2012. Freeze-drying of nanostructure lipid carriers by different carbohydrate polymers used as cryoprotectants. Carbohydr Polym 88, 1157-1163.

Wu, Z.M., Zhou, L., Guo, X.D., Jiang, W., Ling, L., Qian, Y., Luo, K.Q., Zhang, L.J., 2012. HP55-coated capsule containing PLGA/RS nanoparticles for oral delivery of insulin. Int J Pharm 425, 1-8.

Chapter IV

Coating of silica nanoparticles with mucoadhesive polymers

4.1. Introduction

The main objective of the present work was the development of SiNP for potential oral insulin delivery. For this purpose, sol-gel technology was select to produce nanoparticles with suitable physical properties, applying a factorial design approach. During the freeze-drying process, a severe nanoparticles aggregation occurred. However, the addition of trehalose as cryoprotectant agent was able to preserve the physicochemical properties of nanoparticles.

A strategy to improve the bioavailability is to develop drug delivery systems that prolong the gastrointestinal residence time. This effect can be achieved by using bioadhesive polymers.

Bioadhesion is a general term which defines the adhesion of natural or synthetic materials to the surface of biological tissues. Mucoadhesive drug delivery systems utilize the ability of bioadhesion of the material to adhere to mucus membranes (Nagai and Machida, 1985), targeting a drug to a particular mucus tissue for an extended period of time (Kamath and Park, 1994).

Mucoadhesion is a complex phenomenon and the mechanisms responsible in the formation of bioadhesive bonds are not fully known. However, these mechanisms can be described by the combination of several theories, such as electronic (Derjaguin et al., 1977), adsorption (Tabor, 1977), diffusion (Mikos and Peppas, 1986), wetting (Helfand and Tagami, 1972) and fracture (Ponchel et al., 1987).

Various factors can affect the mucoadhesion, including the polymer properties and the physiological features, such as mucus turnover, mucus thickness, intestinal fluid volumes, pathological conditions and pH (Mikos and Peppas, 1986; Mortazavi and Smart, 1993; Rubinstein and Tirosh, 1994; Siccardi et al., 2005; Varum et al., 2008).

For the first generation of bioadhesive polymers, such as chitosan, alginate and carbopols, the mechanism of mucoadhesion is based on the physicochemical interactions. Due to the presence of negative charges in the mucin, opposite electric charges are required to increase the residence time of particles and consequently to achieve better drug absorption (George and Abraham, 2006). However, some studies have reported that the use of anionic polymers leads to better mucosal adhesion than cationic polymers or non-ionic polymers (Chickering and Mathiowitz, 1995). This observation can be attributed to the presence of numerous surface carboxyl groups on anionic polymers, generating strong bioadhesive

interactions by hydrogen bonds with oligosaccharide chains of the mucin (Bernkop-Schnurch, 2002).

Recently, various groups have suggested that a good mucoadhesive polymer has to bind to the mucosa surface than mucin. This theory is based on the fact that the interaction between polymer and mucin in the gastrointestinal lumen may prevent its direct contact with the intestinal cells (Efremova et al., 2002). Therefore, the use of polymers that can avoid the mucin interaction, such as PEG, has been widely exploited as permeation enhancers for oral protein delivery (Rekha and Sharma, 2008).

Based on these previous considerations, after optimizing the formulation, the next step was to coat SiNP with mucoadhesive polymers to develop a hybrid system intended for oral insulin administration by combining the advantages of SiNP and the mucoadhesive properties of hydrophilic polymers. The presence of residual SiOH at silica surface can act as reactive site for its surface modification by convenient organic groups (Westcott et al., 1998). The polymers selected were chitosan, sodium alginate and PEG with two different molecular weights (6000 and 20000 Da). The choice of these polymers was based on their mucoadhesive properties which have already been widely explored for mucosal delivery (Yin et al., 2009).

Chitosan is a linear polysaccharide, derived from chitin, consisting of D-glucosamine and N-acetyl glucosamine units (George and Abraham, 2006). It has been reported that chitosan binds to mucin due to the affinity of positive charged amino groups of the polymer to the negatively charged sialic acid residues of glycoprotein or by forming hydrogen bonds between mucin and chitosan (Deacon et al., 2000; Dedinaite et al., 2005; Qaqish and Amiji, 1999). Indeed, chitosan can increase the paracellular permeability by affecting the structure of the proteins associated to the tight junctions (Schipper NG et al., 1997).

Sodium alginate is the sodium salt of alginic acid, being a water-soluble linear polysaccharide composed of two blocks of (1-4)-linked β-D-mannuronic acid residues (M) and α-L-guluronic (G) residues (George and Abraham, 2006). Alginate is a biopolymer that also possesses bioadhesive properties. Unlike chitosan, alginate prolongs the drug residence time in the mucosa due to the presence of numerous carboxyl groups leading to a strong bioadhesive interaction by hydrogen bonds between anionic polymer and the mucin (Park and Robinson, 1984).

PEG is considered a water soluble, non-ionic and biodegradable polymer (Zhu et al., 2007). The use of PEG in therapeutic applications has been widely investigated. PEG can promote the mucoadhesion by the penetration of its chains in the intestinal mucosa (Peppas,

1998). It is also known that the PEG coating can stabilize the nanoparticles in the gastric and intestinal fluids due to the inhibition of the plasma protein adsorption (Tobío et al., 2000). This inhibition can be explained by two approaches: excluded volume and mixing interaction effects. The former is based on the loss of conformation entropy. The contact of protein leads to the reduction of each polymer segment and repulse forces occur owing to the loss of PEG chain conformation (Atha and Ingham, 1981). In the case of mixing interaction, when a protein gets close to PEG chains, the conformation of PEG segments is reduced due to a compression or interpenetration of the protein molecule, resulting in an osmotic repulsive force between the protein and PEG chains. (Alcantar et al., 2000). In addition, the hydrophilic properties of PEG can prolong the circulation time of drugs by forming a hydrated outer layer, reducing or avoiding the natural blood opsonization process (Rio-Echevarria et al., 2010).

Therefore, in this chapter, the interaction between insulin and SiNP coated with different mucoadhesive polymers (chitosan, sodium alginate, PEG 6000 or PEG 20000) was examined by X- ray diffraction, differential scanning calorimetry (DSC) and Fourier transform infrared (FTIR) analysis.

4.2. Materials and methods

4.2.1. Materials

Tetraethyl orthosilicate (TEOS, 98 %), NH_3 25 %, PEG with M_w of 6000 and 20 000 Da (PEG 6000; PEG 20 000) were purchased from Merck (Darmstadt, Germany). Chitosan low molecular weight (235 g/mol; degree of deacetylation of 78.5 %), ethanol 99.9 %, trehalose dehydrate and bovine serum albumin (BSA) were purchased from Sigma-Aldrich (Steinhein, Germany). Sodium alginate (198.11 g/mol) was purchased from VWR Portugal (Carnaxide, Portugal). Solution of 100 IU/mL of human insulin (Humulin® R) was purchased from Eli Lilly (Lisbon, Portugal). Ultra-purified water was obtained from Milli® Q Plus system (Millipore, Germany).

4.2.2. Synthesis of nanoparticles

SiNP were synthesized by sol-gel technology at room temperature via hydrolysis and condensation of TEOS under high shear homogenization (Ultra-Turrax, IKA, T25) using NH_3 as catalytic agent. The obtained nanoparticles were centrifuged and washed with a mixture of ethanol and ultra-purified water (1:1, v/v) by 2 cycles at 12,000 rpm for 5 min (Spectrafuge16M, Lambnet International, Inc.) as described in chapter II.

For coating nanoparticles, a solution of chitosan (CH) (0.3 %, w/v) at pH 4.5, or sodium alginate (SA) (0.3 % , w/v) at pH 4.5, or PEG 6000 or PEG 20000 (2 %, w/v) at pH 6.8 were added to nanoparticles, stirred for 30 min and centrifuged as described above. The percentage of mucoadhesive polymers was selected according to previous experiments in the laboratory of Cell biology and bioenergetics at UTAD, demonstrating smaller mean size and low PI of the coated nanoparticles (data not shown).

For insulin associated to SiNP, 1.0 mL of human insulin (100 IU/mL, pH 7.0) was added to 10 mg of uncoated SiNP under gentle stirring (300 rpm) for 30 min into ice bath.

For coated insulin-SNP, 1.0 mL of human insulin (100 IU/mL, pH 7.0) was dissolved in 2 mL of the hydrophilic polymer solutions, mixed for 30 min under magnetic stirring and then added to SiNP (10 mg) under gentle stirring (300 rpm) for more 30 min into ice bath. The nanoparticles were centrifuged at 5000 rpm for 5 min and the pellet was freeze-dried during 24 h with trehalose (10 %, w/v) as cryoprotectant agent to prevent particle aggregation. The obtained nanoparticles were stored at 4 °C until further use.

4.2.3. Particle size and zeta potential analysis

The Z-Ave of the different nanoparticles were determined as described in chapter II (please, see the section 3.2.4). Zeta potential (ZP) of nanoparticles was also measured in ultra-purified water adjusting the conductivity (50 µS/cm) with sodium chloride solution (0.9 %, w/v). The ZP was calculated from the electrophoretic mobility using the Helmholtz-Smoluchowski equation (Deshiikan and Papadopoulos, 1998). Values reported are the mean ± SD of three different measurements of each sample.

4.2.4. Association efficacy

The amount of insulin associated to nanoparticles was determined using the Bradford method and bovine serum albumin (BSA) as a standard. Thirty milligrams of lyophilized nanoparticles were incubated in 3 mL of phosphate buffer solution (PBS) at pH 6.8 (FP VIII) without enzymes under magnetic stirring (150 rpm) at 30 min followed by centrifugation for 5 min. The supernatant containing released insulin was collected for protein quantification using a spectrophotometer (Genesys 10S UV-Vis, Thermo Scientific) to read the absorbance at 595 nm. The preparation of samples by Bradford method is described in Supplement I. The following equation (Eq. 4.1) was used to calculate the insulin association efficacy (AE):

$$AE\ (\%) = \frac{Total\ amount\ of\ insulin - insulin\ in\ supernatant}{Total\ amount\ of\ insulin}\ x\ 100 \qquad \text{Equation 4.1}$$

4.2.5. Differential scanning calorimetry (DSC) analysis

Thermograms were obtained using a TA Instrument (New Castle, USA). Accurately, 5 mg of lyophilized nanoparticles were weighted in 40 µL aluminium pans and sealed. DSC scans have been recorded from 25 to 350 ºC at a heating constant rate of 10 ºC/min under purging of nitrogen at 20 mL/min using an empty pan as reference. Data were obtained from the peaks areas using a TA instrument analysis.

4.2.5. Fourier transform infrared (FTIR) analysis

Infrared (IR) spectroscopy is one of the most common spectroscopic methods for structural elucidation and compound identification. This technique is based on molecular vibrations, such as stretching, twisting and rotating. Specific functional groups can be determined by IR technique, such as C=O, O–H, S–H, COO^- and –COOH. Infrared radiation can be represented by wavenumbers from roughly 13,000 to 10 cm^{-1} or by wave lengths from 1 to 1000 μm (Haris and Severcan, 1999). IR technique has been widely applied for characterization of polymers and their interaction, as well as for determining the secondary structure of the proteins (Elliott and Ambrose, 1950; Guo et al., 2010; Jiang et al., 2011; Sarmento et al., 2006a).

FTIR-spectra were performed using a Shimadzu® Europe - Prestige-21 spectrometer. Uncoated and coated nanoparticles containing insulin were gently mixed with a suitable amount of micronized KBr powder and compressed into discs at a force of 10 kN using a manual tablet presser. For each spectrum a 128-scan interferogram was collected with a 4 cm^{-1} resolution in the mid-IR region at 25 °C.

4.2.6. X-ray diffraction (XRD) analysis

X-Ray diffraction patterns of bulk materials and nanoparticles were performed using Siemens D5000 diffractometer system (Siemens, Germany) with a copper anode (Cu-Kα radiation, $\lambda = 0.1542$ nm) at angles $2\theta = 4\text{-}70^{\circ}$.

4.3. Results and discussions

4.3.1. Size and zeta potential analysis

SiNP surface was coated with different mucoadhesive polymers by physical adsorption. The interaction between silica nanoparticles and the polymers or insulin can be explained by the fact that SiOH can be used as reactive sites for coatings and/or for protein adsorption.

The measured Z-Ave, PI, ZP and AE of Ins-SiNP in the absence and in the presence of different mucoadhesive polymers are summarized in Table 4.1.

Table 4.1. Physicochemical properties of different insulin-associated nanoparticles.

Samples	**Z-Ave ± SD (nm)**	**PI ± SD**	**ZP ± SD (mV)**	**Insulin AE ± SD (%)**
Ins-SiNP	289.6 ± 28.24	0.251 ± 0.081	–25.0 ± 0.1	71.7 ± 2.4
Ins-SiNP-PEG 6000	493.7 ± 89.10	0.580 ± 0.010	–15.2 ± 0.0	85.4 ± 4.5
Ins-SiNP-PEG 20000	625.2 ± 20.21	0.315 ± 0.030	–13.8 ± 0.1	82.5 ± 3.4
Ins-SiNP-CH	576.7 ± 14.97	0.329 ± 0.077	+19.9 ± 1.7	90.8 ± 5.6
Ins-SiNP-SA	349.1 ± 14.75	0.371 ± 0.056	–11.9 ± 0.9	84.6 ± 5.3

Abbreviation: Ins, insulin; CH, chitosan; SA, sodium alginate.

The Z-Ave of the developed formulations synthesized by sol-gel technology under mild conditions varied from 289.6 ± 28.24 nm (Ins-SiNP) to 625.2 ± 20.2 nm (Ins-SiNP-PEG 20000), whereas PI varied from 0.251 ± 0.081 (Ins-SiNP) to 0.580 ± 0.010 (Ins-SiNP-PEG 6000). The Z-Ave, as well the PI of the particles increased after coating with the mucoadhesive polymers. Concerning to the PEGylation, the particle size tends to increase with increasing the chain length of PEG due to the increase of the extending PEG layer on the final nanoparticles.

The ZP values represent the electrical charge of the surface of the nanoparticles. The measurement of ZP is an indirect analysis which represents an important criterion for the long-term physical stability and mucoadhesion properties of colloidal systems (Patil et al., 2007). Higher positive or negative ZP values mean that nanoparticles will have greater long-

term stability. The electrostatic repulsion between nanoparticles with the same electrical charge avoids the occurrence of aggregation (Feng and Huang, 2001).

The ZP values of negatively charged nanoparticles varied from –25 ± 0.1 mV (Ins-SiNP) to −11.9 ± 0.9 mV (Ins-SiNP-SA). Ins-SiNP-CH showed positive ZP values (Table 4.1). The high negative ZP value of SiNP is attributed to the presence of deprotonated silanol molecules on the nanoparticle surface (Cauda et al., 2010). The ZP was also influenced by different coatings used for synthesizing the nanoparticles. The ZP of nanoparticles decreased after coating with sodium alginate and PEG polymers. On the other hand, after coating with chitosan, the surface charge of SiNP was reverted to positive values around +19 mV. These results indicated that the SiNP surface was completely adsorbed by polymer molecules and they are in agreement with previous data on silica hybrids (Prokopowicz and Łukasiak, 2010; Witoon et al., 2009).

It is known that particle uptake is strongly influenced by surface charge of particles. When in contact with cell surface, the particles ZP may be affected by influencing of the ions adsorption in the medium or by shifting the shear plane from the particle surface (Zhang et al., 2008). There is a controversial opinion about the interaction of nanoparticles and biological surfaces. Due to the presence of negative charges in the mucin, opposite electric charges are required to increase the residence time of particles and consequently to achieve better drug absorption (George and Abraham, 2006). However, high interactions between positively charged nanoparticles and mucin can lead to a decrease in their absorption and consequently their uptake by intestinal mucosa. In addition, as described above, some studies have reported that the use of anionic polymers leads to better mucosal adhesion than cationic polymers or non-ionic polymers (Chickering and Mathiowitz, 1995) due to the presence of numerous surface carboxyl groups on anionic polymers, generating strong biodhesive interactions by hydrogen bonds with the mucin.

4.3.2. Association Efficacy (AE)

Association Efficacy (AE) for all nanoparticles is shown in Table 4.1. After coating, the AE of SiNP increased, showing the high affinity of the protein to the hydrophilic polymer chains.

The high AE of insulin using PEG as coating was attributed to the compatibility of the hydrophilic protein with the PEG chains.

In this study, the final pH after the addition of insulin solution to SiNP was 7.2. Therefore, insulin was less efficiently associated to the SiNP, which might be related to both insulin and nanoparticles having net negative charges at this pH (silica pI = 2.0; insulin pI = 5.3).

In particular, the AE of insulin can be modulated by changing the pH of chitosan or sodium alginate solutions, which can lead to ionic interaction between protein and protonated amino groups of chitosan or between insulin and deprotonated carboxyl groups of alginate. In this study, the final pH after the addition of insulin to chitosan or sodium alginate solutions was 5.5. In this context, the high insulin AE of Ins-SiNP-CH can be attributed to the ionic interaction between negative charge of insulin and positive charge of chitosan (pK_a approximately 6.3) (Allan and Peyron, 1995) above the isoelectric point of insulin (Ma et al., 2002).

The possibility of electrostatic interaction between alginate and insulin is low, since both present negative charges in the experimental conditions (the pK_a of sodium alginate is approximately 3.5) (Harnsilawat et al., 2006). But, the synthesis conditions (stirring and long time of nanoparticles preparation) can allow the physical adsorption of insulin by other mechanisms such as hydrogen binding or hydrophobic interactions. Also, due to the presence of higher concentration of alginate, the ionic equilibrium between insulin and alginate could be dislocated to the associated complex (Sarmento et al., 2006b).

4.3.3. DSC analysis

In this study, DSC was used for evaluating the influence of different coatings on SiNP. Table 4.2 presents a summary of the peak temperature and enthalpies associated with each peak for the various bulk materials and nanoparticles produced by sol-gel technology.

Typical DSC thermograms of sodium alginate, SiNP-SA and Ins-SiNP-SA are representatively illustrated in Figure 4.1. Themogram of sodium alginate depicts an endothermic peak at 97.00 ºC followed by an exothermic transition at 239.74 ºC. The exothermic peaks attributed to a polymer can be associated to the degradation phenomena due to depolymerization or oxidation reactions (Mimmo et al., 2005; Zohuriaan and Shokrolahi, 2004).

Table 4.2. DSC parameters of the polymers and unloaded and loaded-nanoparticle produced by sol-gel technology.

Samples	**Temperature (ºC)**			***ΔH* (J/g)**
	Initial	**Peak**	**Final**	
PEG 6000	58.50	63.04	73.57	163.40
PEG 20000	51.97	54.43	62.95	101.70
Sodium alginate	43.99	97.00	153.31	238.00
	220.78	239.74	273.67	202.70
Chitosan	45.17	88.94	139.72	124.40
	286.32	304.03	338.78	117.00
SiNP-PEG 6000	32.05	83.41	133.08	89.24
	268.72	287.30	347.28	145.40
SiNP-PEG 20000	40.84	94.84	159.43	123.40
	263.37	287.89	347.07	209.60
SiNP-SA	77.65	139.91	199.85	65.41
	210.11	253.51	279.06	26.69
	282.50	311.55	345.00	120.10
SiNP-CH	40.09	93.05	155.48	94.81
	201.29	229.84	306.84	126.20
Ins-SiNP-PEG 6000	59.63	92.10	114.01	128.70
Ins-SiNP-PEG 20000	69.28	101.17	142.21	146.10
Ins-SiNP-SA	78.23	102.16	129.77	132.30
	287.90	292.99	297.72	53.43
Ins-SiNP-CH	53.41	91.29	150.92	234.80
	193.02	204.98	230.12	133.30

Upon coating of SiNP with SA, the endothermic peak was shifted to 139.91 °C associated to an enthalpy of 65.41 J/g (Figure 4.1 (b)). Also, the addition of SA onto SiNP surface shifted the exothermic peak to higher temperatures in comparison to SA. The shift of melting point and the exothermic peak in SiNP-SA may ascribe to the interaction between silica and sodium alginate resulting in higher thermal stability of the system. The second

endothermic peak at 253.51 °C may be attributed to the removal of the absorbed water in the sample under heating.

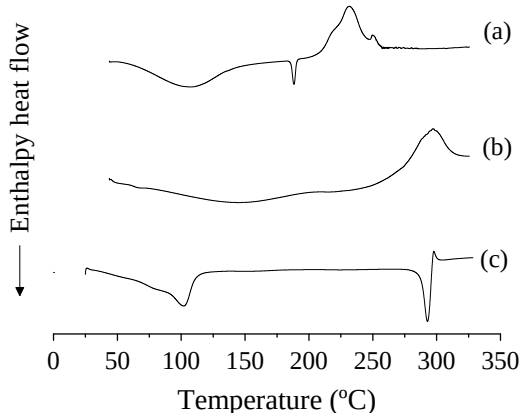

Figure 4.1. Thermograms of (a) sodium alginate, (b) SiNP-SA and (c) Ins-SiNP-SA.

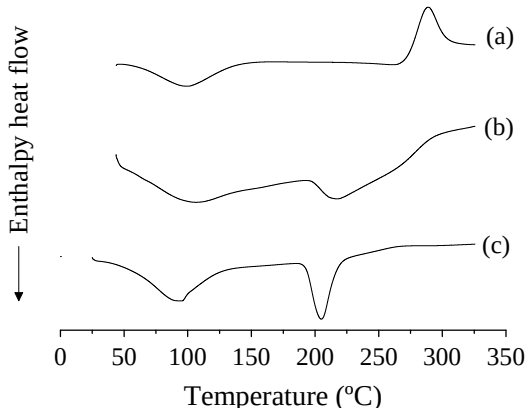

Figure 4.2. Thermograms of (a) chitosan, (b) SiNP-CH and (c) Ins-SiNP-CH.

From the DSC results, Ins-SiNP-SA (Figure 4.1 (c) and Table 4.2) showed the endothermic peak at different temperature values comparing to the one obtained with unloaded nanoparticles (Figure 4.1 (b)). The endothermic peak started at lower temperature. Therefore, it is confirmed that the presence of insulin changed the thermal behavior of nanoparticles due to the interaction between the protein and the polymer.

As shown in Figure 4.2 (a), chitosan exhibits a sharp endothermic event, ascribing to the melting peak around 88.94 ºC and an exothermic event at 304.03 ºC. The coating of SiNP with chitosan (Figure 4.2 (b)) changed the thermal behavior of the polymer with respect to the bulk material, shifting the endothermic transition to higher temperatures (93.05 °C), indicating the formation of strong hydrogen bonding between silica and chitosan (Lai et al., 2006). Also, the exothermic peak of chitosan disappeared. Upon insulin association to SiNP-CH (Figure 4.2 (c)), the endothermic peak is still present, almost unmodified. It can be concluded that the coating of SiNP with chitosan resulted in higher stability of the system, requiring more energy to break the interactions between silica and the polymer, as well as during the thermal decomposition of the nanoparticles. Again, the second endothermic peak at 204.98 ºC after coating with chitosan can be due to the removal of adsorbed water. No signal of insulin peak was detectable after its incorporation in SiNP-CH. This result suggests that insulin is completely dissolved in the polymer chains leading to an interaction between insulin and the polyelectrolyte.

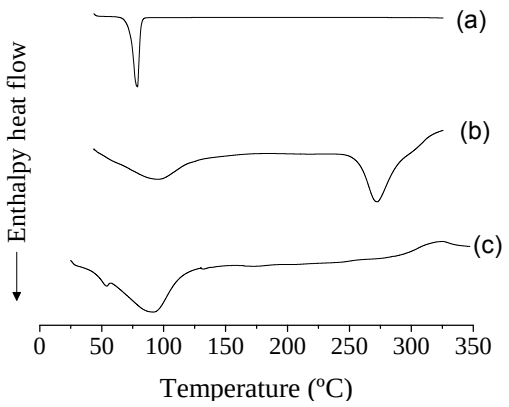

Figure 4.3. Thermograms of (a) PEG 6000, (b) SiNP-PEG 6000 and (c) Ins- SiNP-PEG 6000.

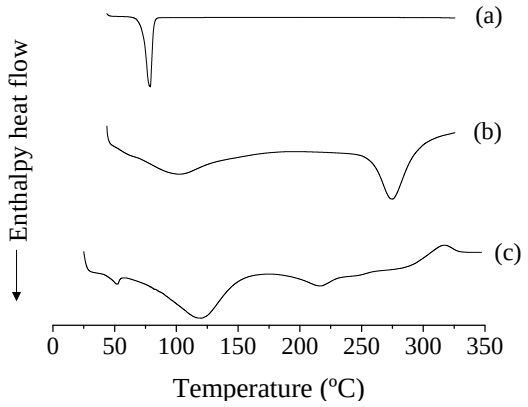

Figure 4.4. Thermograms of (a) PEG 20000, (b) SiNP-PEG 20000 and (c) Ins-SiNP-PEG 20000.

Concerning the effect of PEGylation on SiNP, the thermal behavior of nanoparticles using PEG 6000 was similar to that using PEG 20000 (Figure 4.3 and Figure 4.4, respectively). Pure PEG 6000 and PEG 20000 melt at 63.04 and 54.43 ºC, respectively. The coating of SiNP with PEG 6000 and PEG 20000 shifted the endothermic peak of the polymers to higher temperatures about 83.41 ºC and 94.84 ºC, respectively (Figure 4.3 (b) and Figure 4.4 (b)). This result may be attributed to the fact that PEG chains in PEG-SiNP are less flexible than those in pure PEG due to the interaction between silica and PEG segments. In other words, SiNP could act as nucleating agent, promoting the orientation of PEG chains and consequently leading to the high formation of crystal. In the presence of insulin, the endothermic peaks were registered at 92.10 ºC for Ins-SiNP-PEG 6000 and at 102.17 ºC for Ins-SiNP-PEG 20000, respectively (Figure 4.3 (c) and Figure 4.4 (c)).

However, the peak around 50 ºC observed in both PEGylated formulations can be related to the transition midpoint (T_m) of insulin. T_m of insulin in the absence of nanoparticles was found to be 77.64 ºC (Please, see chapter V, section 5.3.4). Therefore, it is clear that PEG decreased the stability of insulin. These results are in agreement with other studies that indicate that PEGs interact with the protein molecules by hydrophobic interactions being responsible for the destabilization of the protein structure (Arakawa and Timasheff, 1985).

The thermal analysis of the interaction between insulin and mucoadhesive polymers will be discussed in more details in the chapter V.

4.3.4. X-ray analysis

X-ray diffraction spectra indicate that sodium alginate (Figure 4.5 (c)), chitosan (Figure 4.6 (c)), PEG 6000 (Figure 4.7 (c)) and PEG 20000 (Figure 4.8 (c)) are present as a crystalline material. However, the intensity of the peaks in SiNP coating with the polymers is decreased, reflecting less ordered structure of the nanoparticles (Figures 4.5 (b), 4.6 (b), 4.7 (b) and 4.8 (b)). The association of insulin to nanoparticles also supports high crystallinity of the nanoparticles in comparison to unloaded nanoparticles. Probably, the solubilization of insulin into the polymers solutions may have a tendency to crystallize the formulations during the storage leading to a change in the physical properties of the nanoparticles.

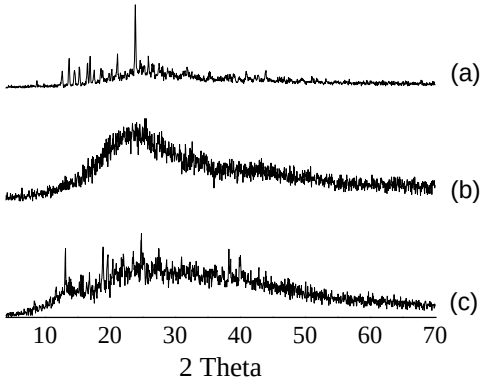

Figure 4.5. XRD patterns of (a) Ins-SiNP-SA, (b) SiNP-SA and (c) sodium alginate.

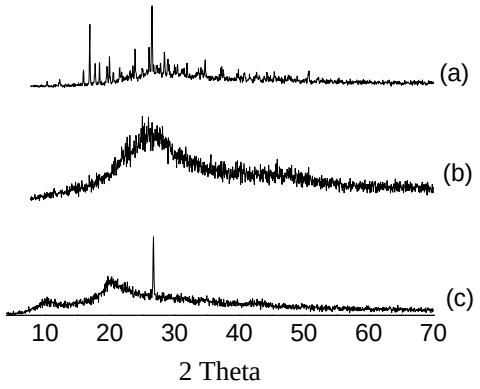

Figure 4.6. XRD patterns of (a) Ins-SiNP-CH, (b) SiNP-CH and (c) chitosan.

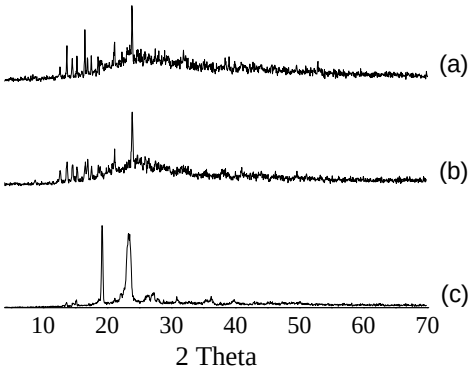

Figure 4.7. XRD patterns of (a) Ins-SiNP-PEG, (b) SiNP-PEG 6000 and (c) PEG 6000.

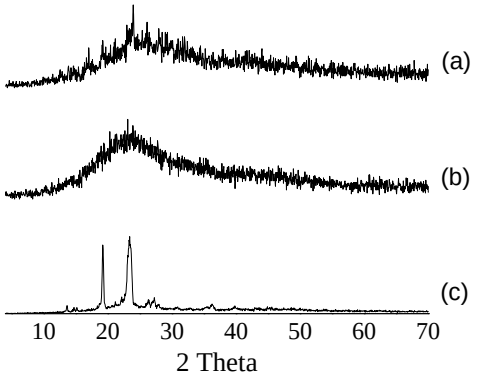

Figure 4.8. XRD patterns of (a) Ins-SiNP-PEG 20000, (b) SiNP-PEG 20000 and (c) PEG 20000.

4.3.5. FTIR analysis

Figure 4.9 shows the FTIR spectra relative to the Ins-SiNP-CH (a), Ins-SiNP-SA (b), Ins-SiNP-PEG 6000 (c), Ins-SiNP-PEG 20000 (d) and Ins-SiNP (e).

The FTIR spectra of Ins-SiNP (Figure 4.9 (e)) showed a peak of free O–H stretching vibration around 3500 cm^{-1} (H-bonded H_2O, hydroxyl terminals, H-bonded OH vibrations of alcohol and H-bonded Si–OH in chain), a peak of Si–O stretching vibration around 1040 cm^{-1}, a peak Si-OH at 980 cm^{-1}, and a peak of Si–O-Si bending around 600 cm^{-1} (Kioul and Mascia, 1994; Kusakabe et al., 1996; Beganskienė et al., 2004).

The spectra of Ins-SiNP-CH (Figure 4.9 (a)) showed the presence of peaks around 1600, 1500 and 1400 cm^{-1}, probably related to amide bond, to vibration of protonated amine group and $–CH_2$ bending, respectively. The absorption bands at 1000 cm^{-1} (skeletal vibrations involving the C–O stretching) are characteristics of its saccharide structure (Yin et al., 1999). A characteristic band at 3440 cm^{-1} was assigned to O–H stretching, indicating intermolecular hydrogen bonding which is overlapped in the same region to the stretching vibration of N–H.

The bands around 1600 and 1400 cm^{-1} present in the FTIR spectrum of Ins-SiNP-SA (Figure 4.9 (b)) are assigned to symmetric and asymmetric stretching vibrations of carboxylate salt groups. In addition, the bands around 1300 cm^{-1} (C–O stretching), 1100 cm^{-1} (C–C stretching) and 1000 cm^{-1} (C–O stretching) are attributed to its saccharide structure (Sartori et al., 1997).

The representative FTIR spectra of Ins-SiNP-PEG 6000 and of Ins-SiNP-PEG 20000 were quite similar (Figure 4.9 (c) and (d), respectively). The region between 3300 and 3600 cm^{-1} corresponds to O–H stretching, the band ranging from 2800 to 2900 cm^{-1} corresponds to C–H stretching and the band between 1000 and 1200 cm^{-1} is assigned to C–O stretching. The addition of PEG increased the relative intensity of the OH band indicating the increase of degree of hydration of the samples (Prokopowicz and Łukasiak, 2010).

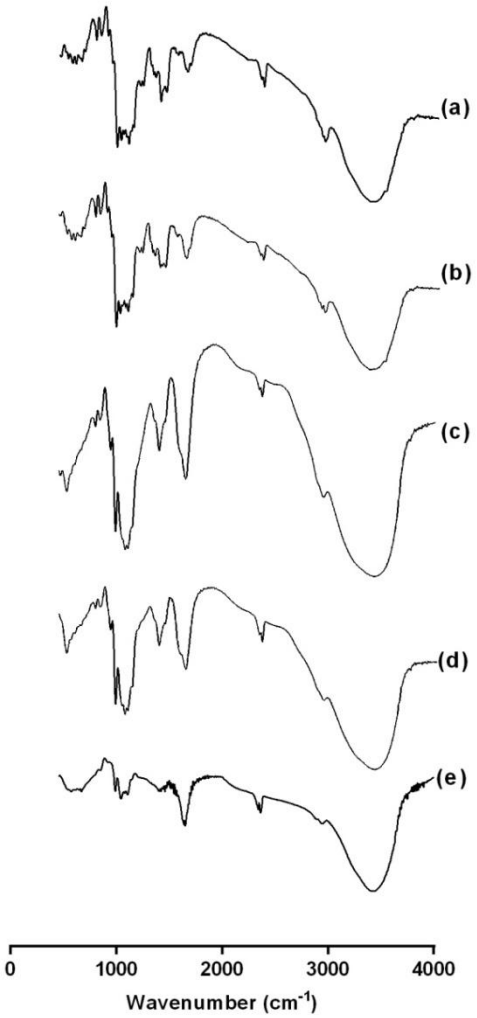

Figure 4.9. FTIR spectra of (a) Ins-SiNP-CH, (b) Ins-SiNP-SA, (c) Ins-SiNP-PEG 20000, (d) Ins-SiNP-PEG 6000 and (e) Ins-SiNP.

Comparing the spectra, changes observed in the absorption band of O–H can be assumed to a possible interaction that would occur between OH groups of SiNP and OH groups of PEG, as well as between OH groups and carboxyl of alginate or amino groups of chitosan. These results suggest an effective interaction between silica and the polymers. Finally, a band indicative of amide I at 1645 cm^{-1} (C=O stretching) was observed in all samples, which is characterized by the presence of α-helical content (Zhang et al., 2008).

4.4. Conclusions

In the present work, Ins-SiNP have been successfully coated with mucoadhesive polymers (alginate, chitosan, PEG 6000 and PEG 20000) by sol-gel technology with particles within the nanometer range. Also, this technology showed the ability to associate insulin with high efficacy.

The association efficacy was higher for SiNP coated with mucoadhesive polymers due to the affinity of insulin to hydrophilic chains of the polymers.

DSC, X-ray and infrared were used for evaluating the influence of different coatings on Ins-SiNP. In the DSC studies, the endothermic and the exothermic peaks of pure polymers were shifted to higher temperatures in all coated SiNP, probably due to the interaction by hydrogen bounds between SiOH groups of SiNP and specific functional groups of PEG (OH), chitosan (NH) or sodium alginate (COOH). This shift resulted in higher nanoparticles stability. In addition, no signal of insulin peak was detected after its incorporation into chitosan and sodium alginate solutions, indicating that insulin is completely dissolved in the polymer chains. On the other hand, the incorporation of insulin into PEG solutions resulted in a decrease of insulin stability.

The X-ray diffraction showed that coated SiNP displayed less ordered structure compared with pure polymers. On the other hand, the association of insulin to nanoparticles resulted in more crystalline structure, probably due to the solubilization of insulin into the polymers solutions leading to the crystallization of the nanoparticles during the storage.

The FTIR analysis also demonstrated the high efficiency of different coatings on SiNP. In addition, characteristic band of amide I was found in all infrared spectra which indicate the adsorption of the protein onto nanoparticles surface.

4.5. References

Alcantar, N.A., Aydil, E.S., Israelachvili, J.N., 2000. Polyethylene glycol–coated biocompatible surfaces. J Biomed Mater Res 51, 343-351.

Allan, G.G., Peyron, M., 1995. Molecular weight manipulation of chitosan I: kinetics of depolymerization by nitrous acid. Carbohydr Res 277, 257-272.

Arakawa, T., Timasheff, S.N., 1985. Mechanism of poly(ethyelene glycol) interaction of proteins. Biochemistry 24, 6756–6762.

Atha, D.H., Ingham, K.C., 1981. Mechanism of precipitation of proteins by polyethylene glycols: Analysis in terms of excluded volume. J Biol Chem 256, 2108-2117.

Beganskienė, A., Sirutkaitis, V., Kurtinaitienė, M., Juškėnas, R., Kareiva, A., 2004. FITR, TEM and NMR investigations of Stöber silica nanoparticles. Mater Sci 10, 287-290.

Bernkop-Schnurch, A., 2002. Mucoadhesive polymers. *In*: Dumitriu, S. (Ed.), Polymer Biomaterial. Marcel Decker, New York, pp. 147-165.

Cauda, V., Argyo, C., Schlossbauer, A., Bein, T., 2010. Controlling the delivery kinetics from colloidal mesoporous silica nanoparticles with pH-sensitive gates. J Mater Chem 20, 4305-4311.

Chickering, D.E., Mathiowitz, E., 1995. Bioadhesive microspheres: I. A novel electrobalance-based method to study adhesive interactions between individual microspheres and intestinal mucosa. J Control Release 34, 251-262.

Deacon, M.P., McGurk, S., Roberts, C.J., Williams, P.M., Tendler, S.J.B., Davies, M.C., Davis, S.S., Harding, S.E., 2000. Atomic force microscopy of gastric mucin and chitosan mucoadhesive systems. Biochem J 348, 557 - 563.

Dedinaite, A., Lundin, M., Macakova, L., Auletta, T., 2005. Mucin-chitosan complexes at the solid-liquid interface: Multilayer formation and stability in surfactant solutions. Langmuir 21, 9502-9509.

Derjaguin, B.V., Toporov, Y.P., Muller, V.M., Aleinikova, I.N., 1977. On the relationship between the molecular component of the adhesion of elastic particles to a solid surface. J Colloid Interface Sci 58, 528-533.

Deshiikan, S.R., Papadopoulos, K.D., 1998. Modified booth equation for the calculation of zeta potential. Colloid Polym Sci 276, 117-124.

Efremova, N.V., Huang, Y., Peppas, N.A., Leckband, D.E., 2002. Direct measurement of interactions between tethered poly(ethylene glycol) chains and adsorbed mucin layers. Langmuir 18, 836-845.

Elliott, A., Ambrose, E.J., 1950. Structure of synthetic polypeptides. Nature 165, 921−922.

Feng, S.S., Huang, G., 2001. Effects of emulsifiers on the controlled release of paclitaxel (Taxol ®) from nanospheres of biodegradable polymers. J Control Release 71, 53-69.

George, M., Abraham, T.E., 2006. Polyionic hydrocolloids for the intestinal delivery of protein drugs: Alginate and chitosan — a review. J Control Release 114, 1-14.

Guo, L., Sato, H., Hashimoto, T., Ozaki, Y., 2010. FTIR study on hydrogen-bonding interactions in biodegradable polymer blends of poly(3-hydroxybutyrate) and poly(4-vinylphenol). Macromolecules 43, 3897-3902.

Haris, P.I., Severcan, F., 1999. FTIR spectroscopic characterization of protein structure in aqueous and non-aqueous media. J Molecular Catal B 7, 207-221.

Harnsilawat, T., Pongsawatmanit, R., McClements, D.J., 2006. Characterization of β-lactoglobulin–sodium alginate interactions in aqueous solutions: A calorimetry, light scattering, electrophoretic mobility and solubility study. Food Hydrocoll 20, 577-585.

Helfand, E., Tagami, Y., 1972. Theory of interface between immiscible polymers. J Chem Phys 57, 1812-1813.

Jiang, Y., Li, C., Nguyen, X., Muzammil, S., Towers, E., Gabrielson, J., Narhi, L., 2011. Qualification of FTIR spectroscopic method for protein secondary structural analysis. J Pharm Sci 100, 4631-4641.

Kamath, K.R., Park, K., 1994. Mucosal adhesive preparations. In: Swarbrick, J., Boylan, J.C. (Eds.), Encyclopedia of Pharmaceutical Technology. Marcel Dekke, New York.

Kioul, A., Mascia, L., 1994. Compatibility of polyimide-silicate ceramers induced by alkoxysilane coupling agents. J Non-Cryst Solids 175.

Kusakabe, K., Ichiki, K., Hayashi, J.-I., Maeda, H., Morooka, S., 1996. Preparation and characterization of silica-polyimide composite membranes coated on porous tubes for CO2 separation. J Membr Sci 115, 65-75.

Lai, S.M., Yang, A.J.M., Chen, W.C., Hsiao, J.F., 2006. The properties and preparation of chitosan/silica hybrids using sol-gel process. Polym Plast Technol Eng 45, 997-1003.

Ma, Z., Yeoh, H.H., Lim, L.-Y., 2002. Formulation pH modulates the interaction of insulin with chitosan nanoparticles. J Pharm Sci 91, 1396-1404.

Mikos, A., Peppas, N.A., 1986. Systems for controlled release of drugs V. Bioadhesive systems. STP Pharma Sci 2, 705-716.

Mimmo, T., Marzadori, C., Montecchio, D., Gessa, C., 2005. Characterisation of Ca- and Al-pectate gels by thermal analysis and FTIR spectroscopy. Carbohydr Res 340, 2510-2519.

Mortazavi, S.A., Smart, J.D., 1993. An investigation into the role of water movement and mucus gel dehydration im mucoadhesion. J Control Release 25, 197-203.

Nagai, T., Machida, Y., 1985. Mucosal adhesive dosage forms. Pharm Int 6, 196-200.

Park, K., Robinson, J.R., 1984. Bioadhesive polymers as plataforms for oral-controlled drug delivery: Method to study bioadhesion. Int J Pharm 19, 107-127.

Patil, S., Sandberg, A., Heckert, E., Self, W., Seal, S., 2007. Protein adsorption and cellular uptake of cerium oxide nanoparticles as a function of zeta potential. Biomaterials 28, 4600-4607.

Peppas, N.A., 1998. Molecular calculations of poly(ethylene glycol) transport across a swollen poly(acrylic acid)/mucin interface. J Biomater Sci Polymer Edn 9, 535-542.

Ponchel, G., Touchard, F., Duchêne, D., Peppas, A., 1987. Bioadhesive analysis of controlled-release systems. I. Fracture and interpenetration analysis in poly(acrylic acid)-containing systems. J Control Release 5, 129-141.

Prabha, S., Zhou, W.-Z., Panyam, J., Labhasetwar, V., 2002. Size-dependency of nanoparticle-mediated gene transfection: studies with fractionated nanoparticles. Int J Pharm 244, 105-115.

Prokopowicz, M., Łukasiak, J., 2010. Synthesis and in vitro characterization of freeze-dried doxorubicin-loaded silica/PEG composite. J Non-Cryst Solids 356, 1711-1720.

Qaqish, R., Amiji, M., 1999. Synthesis of a fluorescent chitosan derivative and its application for the study of chitosan–mucin interactions. Carbohydr Polym 38, 99-107.

Rekha, M.R., Sharma, C.P., 2008. Phthalyl chitosan-poly(ethylene oxide) semi-interpenetrating polymer network microparticles for oral protein delivery: an in vitro characterization. J Appl Polym Sci 110, 2787-2795.

Rio-Echevarria, I.M., Selvestrel, F., Segat, D., Guarino, G., Tavano, R., Causin, V., Reddi, E., Papini, E., Mancin, F., 2010. Highly PEGylated silica nanoparticles: "ready to use" stealth functional nanocarriers. J Mater Chem 20, 2780-2787.

Rubinstein, A., Tirosh, B., 1994. Mucus gel thickness and turnover in the gastrointestinal tract of the rat: response to cholinergic stimulus and implication for mucoadhesion. Pharm Res 11, 794-799.

Sarmento, B., Ferreira, D., Veiga, F., Ribeiro, A., 2006a. Characterization of insulin-loaded alginate nanoparticles produced by ionotropic pre-gelation through DSC and FTIR studies. Carbohydr Polym 66, 1-7.

Sarmento, B., Ribeiro, A., Veiga, F., Ferreira, D., 2006b. Development and characterization of new insulin containing polysaccharide nanoparticles. Coll Surf B 53 193-202.

Sartori, C., Finch, D.S., Ralph, B., Gilding, K., 1997. Determination of the cation content of alginate thin films by FTIR spectroscopy. Polymer 38, 43-51.

Schipper NG, Olsson S, Hoogstraate JA, deBoer AG, Varum KM, P., A., 1997. Chitosans as absorption enhancers for poorly absorbable drugs 2: mechanism of absorption enhancement. Pharm Res 14, 923-929.

Schleh, C., Semmler-Behnke, M., Lipka, J., Wenk, A., Hirn, S., Schäffler, M., Schmid, G.n., Simon, U., Kreyling, W.G., 2012. Size and surface charge of gold nanoparticles determine absorption across intestinal barriers and accumulation in secondary target organs after oral administration. Nanotoxicology 6, 36-46.

Siccardi, D., Turner, J.R., Mysny, R.J., 2005. Regulation of intestinal epithelial function: a link between opportunities for macromolecular drug delivery and inflammatory bowel disease. Adv Drug Del Rev 57, 219-235.

Tabor, D., 1977. Surface forces and surface interactions. J Colloid Interface Sci 58, 2-13.

Tobío, M., Sánchez, A., Vila, A., Soriano, I.I., Evora, C., Vila-Jato, J.L., Alonso, M.J., 2000. The role of PEG on the stability in digestive fluids and in vivo fate of PEG-PLA nanoparticles following oral administration. Colloids Surf B 18, 315-323.

Varum, F.J.O., McConnell, E.L., Souza, J.J.S., Veiga, F., Basit, A.W., 2008. Mucoadhesion and gastrointestinal tract. Crit Rev Ther Drug Carrier Sys 25, 207-258.

Westcott, S.L., Oldenburg, S.J., Lee, T.R., Halas, N.J., 1998. Formation and adsorption of clusters of gold nanoparticles onto functionalized silica nanoparticle surfaces. Langmuir 14, 5396-5401.

Witoon, T., Chareonpanich, M., Limtrakul, J., 2009. Effect of acidity on the formation of silica–chitosan hybrid materials and thermal conductive property. J Sol-Gel Sci Technol 51, 146-152.

Yin, L., Ding, J., He, C., Cui, L., Tang, C., Yin, C., 2009. Drug permeability and mucoadhesion properties of thiolated trimethyl chitosan nanoparticles in oral insulin delivery. Biomaterials 30, 5691-5700.

Yin, Y.J., Yao, K.D., Cheng, G.X., Ma, J.B., 1999. Properties of polyelectrolyte complex films of chitosan and gelatin. Polym Int 48, 429-432.

Zhang, X.G., Teng, D.Y., Wu, Z.M., Wang, X., Wang, Z., Yu, D.M., Li, C.X., 2008. PEG-grafted chitosan nanoparticles as an injectable carrier for sustained protein release. J Mater Sci Mater Med 19, 3525-3533.

Zhang, Y., Yang, M., Portney, N., Cui, D., Budak, G., Ozbay, E., Ozkan, M., Ozkan, C., 2008. Zeta potential: a surface electrical characteristic to probe the interaction of nanoparticles with normal and cancer human breast epithelial cells. Biomed Microdevices 10, 321-328.

Zhu, S., Qian, F., Zhang, Y., Tang, C., Yin, C., 2007. Synthesis and characterization of PEG modified N-trimethylaminoethylmethacrylate chitosan nanoparticles. Eur Polym J 43, 2244-2253.

Zohuriaan, M.J., Shokrolahi, F., 2004. Thermal studies on natural and modified gums. Polymer Testing 23, 575-579.

Chapter V
Coated silica nanoparticles for mucosal adhesion

5.1. Introduction

In the previous chapter, a comparative physicochemical study has been described for the interaction between SiNP and mucoadhesive polymers after insulin association. SiNP were successfully coated with chitosan, sodium alginate or PEG in order to obtain a mucoadhesive system for insulin delivery.

One of the most important challenges for protein encapsulation/association in nanoparticles is its stability. The structure of the protein should be kept during the designing, manufacturing, storage or release. Therefore, the development of protein formulations which maintain the physical and chemical stabilities and maintain the biological activity of native protein is desired.

Compared to conventional drugs, proteins have several additional obstacles in preserving their biological activity as a result of their complexity due to the numerous reactive groups and delicate three-dimensional structures. Currently, protein stability is an important issue in the pharmaceutical field, since the development of commercial therapeutic protein products increases.

The protein conformation can be degraded by chemical and physical processes. Chemical degradation involves covalent changes in amino acid sequences resulting in one or two products with smaller weight. These chemical processes are characterized by deamidation, oxidation, hydrolysis and disulfide exchange (Bilati et al., 2005). Protein physical degradation generally refers to reversible or irreversible denaturation with loss of three-dimensional conformation of the protein (Manning et al., 1989). The physical degradation involves denaturation, aggregation and precipitation of the protein.

Several biophysical characterization methods can be applied for detecting disturbances of the protein structure. Among them, spectroscopic techniques, such as near and far-ultraviolet (UV) circular dichroism (CD) spectroscopy, fluorescence, Raman and FTIR analysis are the main analytical methods to ensure the integrity and stability of the protein structures (Keating et al., 1998; Sanchez et al., 2011; Sarmento et al., 2007; Shafaat et al., 2008).

Generally, micro or nano differential scanning calorimetry (μDSC or nDSC) is used to verify the transition temperature T_m, as well as to obtain information on the thermodynamics of native and denatured state of the protein, since μDSC or nDSC improves the sensitivity in comparison to the conventional DSC (Matheus et al., 2006). μDSC or nDSC can describe and

study the interaction of proteins with ligands, ions or matrices (Huus et al., 2005; Robertson and Murphy, 1997). Therefore, the effect of matrices on melting temperature of insulin can be detect and quantified by these techniques.

In the present chapter, the structural integrity of insulin and its thermal stability after its dissolution in mucoadhesive polymers for nanoparticles preparation were examined by CD and nDSC, respectively.

In addition to the stability of insulin, another concern of this work was demonstrated the ability of the obtained nanoparticles to interact with the biological systems. Taking into account the complexity of studying the behavior of nanoparticles when in contact with the cell cultures, the prediction of the biophysical interaction between the particles and biological membranes can be carried out using model membrane systems based on phospholipid bilayers, such as that produced with dipalmitoylphosphatidylcholine (DPPC) (Montenegro et al., 2012). DPPC liposomes have well-defined thermotropic properties, and thus, any variations in these structures can be easily detected by DSC (Musumeci et al., 2006).

The *in vitro* evaluation of the mucoadhesive properties of a polymeric system is a first step in the development of a mucoadhesive drug delivery system. Optimum contact between the carrier and the biological surfaces is essential to increase the drug absorption. The mucoadhesive properties of a polymer can be examined by the interaction between the polymer and the mucin molecules. Mucin is a key component in mucus layer composed by branched and unbranched blocks secreted by surface epithelium (goblet cells) and submucosal glands (mucous cells) (Thornton and Sheehan, 2004). Mucin is an extracellular glycoprotein with molecular weight ranging from 0.5 to 20 MDa, being characterized by blocks containing protein backbone chains covalently attached to sugar residues, such as galactose, fucose, *N*-acetylglucosamine, *N*-acetylgalactosamine and sialic acid residues (Thornton et al., 2008).

After the initial contact between the polymeric system and the mucin, the polymer adheres to the mucosal surface due to the surface forces between the molecules of two surfaces. This interaction is due to van der Waals bonds, hydrogen bonds, electrostatic and hydrophobic interactions (Smart, 2005). In the present study, the adsorption of mucin molecules on the different nanoparticles was determined by DLS. One of the methods for measuring the resulting charges of the mucin adsorption onto nanoparticles is the zeta potential meter. In this context, we evaluated the ability of different nanoparticles to adsorb mucin at acidic (pH 2.0) and neutral (pH 6.8) conditions.

5.2. Materials and methods

5.2.1. Materials

Tetraethyl orthosilicate (TEOS, 98 %), NH_3 25 %, PEG with M_w of 6000 and 20 000 Da (PEG 6000; PEG 20 000) were purchased from Merck (Darmstadt, Germany). Chitosan low molecular weight (235 g/mol, degree of deacetylation of 78.5 %), ethanol 99.9 %, porcine stomach mucin, type II and trehalose dehydrate were purchased from Sigma-Aldrich (Steinhein, Germany). Sodium alginate (198.11 g/mol) was purchased from VWR Portugal (Carnaxide, Portugal). Solution of 100 IU/mL of human insulin (Humulin® R) was purchased from Eli Lilly (Lisbon, Portugal). DPPC was purchased from Avantis Polar Lipids (Alabama, USA). Ultra-purified water was obtained from Milli® Q Plus system (Millipore, Germany).

5.2.2. Synthesis of nanoparticles

SiNP were synthesized by a well established sol-gel method at room temperature using NH_3 as catalytic agent. In the experimental procedure TEOS, ethanol and NH_3 were mixed under high shear homogenization (Ultra-Turrax®Ika T25, Germany) using an 18G impeller (Ika T25, Darmstadt, Germany) for 2 hours. The resulting nanoparticles were centrifuged and washed with a mixture of ethanol and ultra-purified water (1:1, v/v) by 2 cycles at 12,000 rpm (Spectrafuge16M, Lambnet International, Inc.) for 5 min. Insulin (1.0 mL, 100 IU/mL, pH 7.0) was added to 10 mg of uncoated SiNP under gentle stirring (300 rpm) for 30 min into ice bath. For the association of insulin to hydrophilic polymers, 1.0 mL of insulin was dissolved in 2.0 mL of the polymer solutions: at pH 4.5 for CH (0.3 %, w/v) and SA (0.3 %, w/v) or at pH 6.8 for PEG (2 %, w/v); mixed for 30 min under magnetic stirring and then added to SiNP under gentle stirring (300 rpm) for more 30 min, into ice bath. The nanoparticles were centrifuged at 5000 rpm for 5 min and the pellet was freeze-dried during 24 h with trehalose (10 %, w/v) as cryoprotectant agent to prevent particle aggregation. The obtained nanoparticles were stored at 4 °C until further use.

5.2.3. Size and zeta potential analysis

The Z-Ave and ZP of nanoparticles as described in chapter II and IV (please, see the section 2.2.5 and 4.2.3).

5.2.4. Association efficacy (AE)

The AE of insulin in nanoparticles was determined as described in chapter IV (please see, section 4.2.4).

5.2.5. Analysis of insulin secondary structure

The far-UV CD signals of a protein (240 nm and below) generally reflect its secondary structure composition (α-helix, β-sheet, turns and random coil). The far-UV CD spectrum is due mainly to the peptide bond. There is $n \rightarrow \pi^*$ transition around 220 nm and a more pronounced $\pi \rightarrow \pi^*$ transition centered around 190 nm (Whitmore and Wallace, 2008). With respect to insulin, the negative band at 223 nm is based on its anti-parallel β-structure and is mainly due to its monomeric form. The negative band at 208 nm is assigned to its α-helical structure and is due to its dimer (Pocker and Biswas, 1980; Woody, 1996). On the other hand, the CD signals in the near-UV (260-320 nm) assign the protein tertiary structure arising from aromatic residues (Kelly et al., 2005).

The CD spectra of insulin (70 µg/mL) dissolved in KCl/HCl buffer (FP VIII), chitosan, sodium alginate, PBS (FP VIII), PEG 6000 or PEG 20000 solutions were obtained at 25 ºC using a Jasco Spectropolarimeter J-815 (Tokyo, Japan). CD spectra were recorded in a 0.1 cm cell from 250-195 nm. For all spectra, an average of 5 scans was obtained. CD spectra of all samples were recorded and subtracted from the reference spectra (polymer solution in the respective pH). Spectra are expressed as mean residual ellipticity [θ] ($deg.cm^2.dmol^{-1}$). Deconvolution of CD spectra was obtained by the SELCON3 method (Sreerama and Woody, 2000).

5.2.6. Thermal analysis of insulin

Thermal analysis of insulin denaturation after insulin association to hydrophilic polymers was performed by nano DSC instrument (TA Instruments, New Castle, DE). Insulin was dissolved into the respective polymer solution (chitosan, sodium alginate, PEG 6000 and PEG 20000) according to the synthesis procedure as described above. All protein scans were performed from 25 to 100 °C at a scan rate of 1 °C/min. All samples and references were degassed immediately before use. Data analysis was carried out using Nanoanalyze® software (TA Instruments, New Castle, DE).

5.2.7. Interaction studies between nanoparticles and biomembrane models

DPPC multilamellar liposomes were prepared by film hydration (Bangham et al., 1965). DPPC was solubilized in chloroform in a round-bottomed flask and the solvent was removed under vacuum rotoevaporation. The resulting film was then hydrated with 3.0 mL of water at 51 ºC and maintained in water bath at the same temperature during 1 h. The biomembrane suspension was left at 25 ºC for 2 h to anneal the bilayer structures. 25 µL of SiNP and SiNP coated with mucoadhesive polymers were incubated in 2.2 mg/mL of liposomes suspension. The interaction between nanoparticles and liposomes was investigated using nDSC instrument (TA Instruments, New Castle, DE). All the samples were degassed under vacuum before loading into the cells. nDSC thermograms were collected from 25 ºC to 60 ºC at a scan rate of 1 ºC/min. The samples scan was subtracted from the reference scan (ultra-purified water) during the nDSC analysis. All data analysis was performed using Nanoanalyze® software (TA Instruments, New Castle, DE).

5.2.8. *In vitro* interaction between mucin and different nanoparticles

To analyze the interaction between mucin and nanoparticles at gastrointestinal-simulated fluid, mucin was dispersed in HCl/KCl buffer (pH 2.0) and PBS (pH 6.8) to make stock solutions of 100, 250 and 500 µg/mL. Nanoparticles (286 µL) were dispersed in the above mucin solutions followed by the incubation by shaking at 37 ºC during 30 min. Afterwards, ZP of each sample was determined by ZetaSize Nano ZS at a temperature of 37 ºC.

5.3. Results and discussions

5.3.1. Size and zeta potential analysis

The uncoated and coated nanoparticles produced by sol-gel technology were characterized in terms of Z-Ave, PI, ZP and AE. The measured Z-Ave, PI, ZP and AE of SiNP prepared in the absence and presence of different mucoadhesive polymers are summarized in Table 5.1. The average hydrodynamic diameter of the nanoparticles increased after coating. Such observations can be due to an increase of the extending polymer layers on the final nanoparticles as discussed in Chapter IV.

The results presented on Table 5.1 also show that the ZP was affected by the kind of polymer used for synthesizing the nanoparticles. The adsorption of PEG and alginate influences the distribution of charge in the diffuse part of the electrical double layer, reducing the ZP. On the other hand, coating with chitosan resulted in an inversion of ZP. These results indicate that the selected mucoadhesive polymers were successfully adsorbed onto SiNP as described in Chapter IV.

Table 5.1. Z-Ave, PI and ZP and EA of different insulin-associated nanoparticles.

Samples	**Z-Ave ± SD (nm)**	**PI ± SD**	**ZP ± SD (mV)**	**Insulin AE ± SD (%)**
Ins-SiNP	289.6 ± 28.24	0.251 ± 0.081	–25.0 ± 0.1	71.7 ± 2.4
Ins-SiNP-PEG 6000	493.7 ± 89.10	0.580 ± 0.010	–15.2 ± 0.0	85.4 ± 4.5
Ins-SiNP-PEG 20000	625.2 ± 20.21	0.315 ± 0.030	–13.8 ± 0.1	82.5 ± 3.4
Ins-SiNP-CH	576.7 ± 14.97	0.329 ± 0.077	+19.9 ± 1.7	90.8 ± 5.6
Ins-SiNP-SA	349.1 ± 14.75	0.371 ± 0.056	–11.9 ± 0.9	84.6 ± 5.3

5.3.2. Association Efficacy (AE) of insulin

After coating, the AE of nanoparticles increased, showing the high affinity of insulin for the hydrophilic properties of the polymers (Table 5.1). Also, the high insulin AE of Ins-SiNP-CH can be attributed to the ionic interaction between negative charge of insulin and positive charge of chitosan as described in chapter IV.

5.3.3. Analysis of insulin secondary structure

The maintenance of the structural integrity of therapeutic proteins is crucial for their biological efficacy. The secondary structure of insulin in solution during the process of nanoparticles formation was determined by circular dichroism (CD). The effect of solubilizing insulin in aqueous dilute solutions of HCl/KCl buffer (pH 4.5), CH (pH 4.5), SA (pH 4.5), PBS (pH 6.8), PEG 6000 (pH 6.8) or PEG 20000 (pH 6.8) on its conformational stability was evaluated.

Figure 5.1 shows the CD spectra of human insulin dissolved in PBS (black line), PEG 6000 (black dotted line) and PEG 20000 (grey line) at pH 6.8. The CD spectrum of insulin dissolved in PBS display two minima at 209 and 222 nm, which is assigned to helical peptide conformation (Ettinger and Timasheff, 1971; Lu et al., 2012).

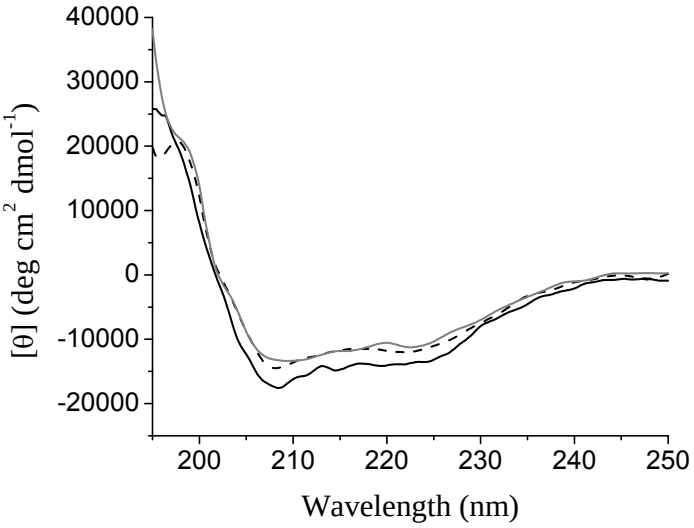

Figure 5.1. Far-UV CD spectra of native insulin in PBS (black line), insulin associated to PEG 6000 (black dotted line) and insulin associated to PEG 20000 (grey line).

After dissolving insulin in PEG 6000 or PEG 20000 solution, minor differences were observed in the insulin spectra. The obtained result demonstrates that the dissolution of insulin in PEG polymers during nanoparticles preparation did not change its conformation.

Slight differences can be seen in the content of α-helix, β-sheet, β-turn, and random coil for the secondary structure of the insulin dissolved in PBS and in PEG 6000 (Table 5.2). For insulin dissolved in PEG 20000, the content of β-sheet increased from 6.5 to 11.7 %. This

change can be attributed to a possible aggregation of insulin (Nielsen et al., 2001). The increase occurred only with high PEG molecular weight indicating that PEG 20000 could interact with insulin by hydrogen bonding and by hydrophobic interactions due to a higher contact area between long PEG chains and the protein (Wu et al., 2013).

Table 5.2. Observed parameters of secondary structure of insulin dissolved in PBS, PEG 6000 or PEG 20000.

Samples	α-helix (%)	β-sheet (%)	β-turn (%)	random coil (%)
Ins-PBS	54.4	6.5	13.7	26.2
Ins-PEG 6000	51.5	6.1	13.5	27.8
Ins-PEG 20000	47.8	11.7	15.6	26.8

The addition of insulin in chitosan solution affects the circular dichroism band in comparison to insulin dissolved in HCl/KCl at the same pH (Figure 5.2 and Table 5.3). The slight shift might be due to interference from the polymer on insulin structure due to the ionic interaction between the protein and chitosan. However, the overall spectral shape was essentially retained, which indicates that the secondary structure was kept.

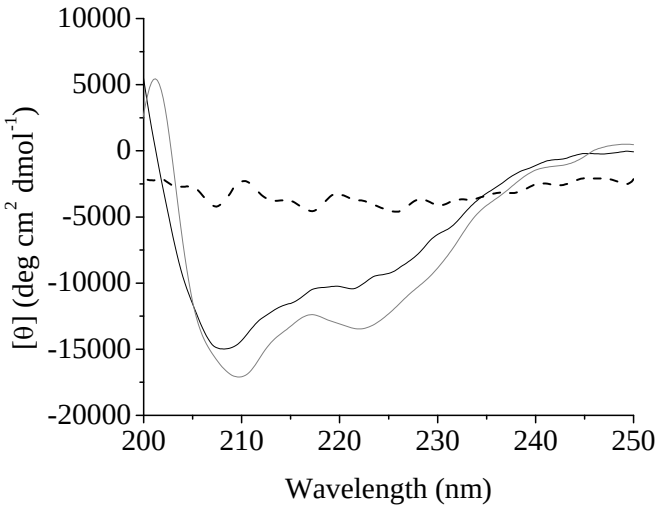

Figure 5.2. Far-UV CD spectra of native insulin in HCl/KCl buffer (black line), insulin associated to sodium alginate (black dotted line) and insulin associated to chitosan (grey line).

After dissolving insulin in SA solution, higher differences in insulin spectrum were observed in comparison to insulin dissolved in HCl/KCl at pH 4.5 (Figure 5.2 and Table 5.3).

Probably, this occurs due to the interference from SA solution on the insulin spectrum, since this polymer absorb in the wavelength range of 190-250 nm (De'Nobili et al., 2013; Khouri and Buss, 2011). Moreover, it is known that SA binding may cause conformation changes to insulin structure, which is usually detected by CD spectra (Wallace, 2009).

Table 5.3. Observed parameters of secondary structure of insulin dissolved in HCl/KCl buffer, chitosan and sodium alginate.

Samples	α-helix (%)	β-sheet (%)	β-turn (%)	Random coil (%)
Ins-HCl/KCl	44.6	8.5	16.5	29.5
Ins-CH	32.1	11.5	17.3	33.5
Ins-SA	11.9	42.9	24.9	21.3

5.3.4. Thermal analysis of insulin

The thermodynamics of insulin folding was investigated by nDSC. Table 5.4 summarizes the thermodynamic results, where T_{max} was defined as the peak maximum of temperature and ΔH was the enthalpy change associated with each peak for human insulin solution, insulin associated to chitosan, sodium alginate, PEG 6000 and SiNP and Figure 5.3 shows the obtained nDSC curves.

The curves were recorded from 25 ºC to 100 ºC at heating rate 1 ºC/min, which is sufficient to record the occurrence of insulin denaturation. From Figure 5.3 (e), the nDSC showed two endothermic peaks at 77.64 ºC and 91.31 ºC for human insulin solution. This thermogram pattern is in agreement with other reported in literature (Huus et al., 2005).

The mean peak of denaturation after insulin association to alginate (Figure 5.3 (b)) and to chitosan (Figure 5.3 (c)) became lower in comparison to free insulin. Insulin associated to alginate or chitosan led to a shift of endothermic peak to lower temperature. It has been therefore assumed that the shift of T_{max} to lower temperatures is consequence of the interaction between the protein and the polymers. Shifts of endothermic peak are usually associated with interactions between drug-loaded and poly-electrolytes. It was therefore demonstrated that chitosan and sodium alginate solutions decrease the thermal stability of insulin, as shown by the decreasing of T_{max}.

The peak related to insulin associated to PEG 6000 remains unchanged (Figure 5.3 (a)), suggesting that PEG 6000 does not influence in the thermal behavior of insulin. Farrugia and co-workers showed that high molecular weight PEG have greater stabilizing effect on

protein structure (Farruggia et al., 1997), probably due to the perturbation of protein surface by modifying the layer of water. This perturbation is allowed by compact structure of PEG, which penetrates easily into the hydration layer of the protein.

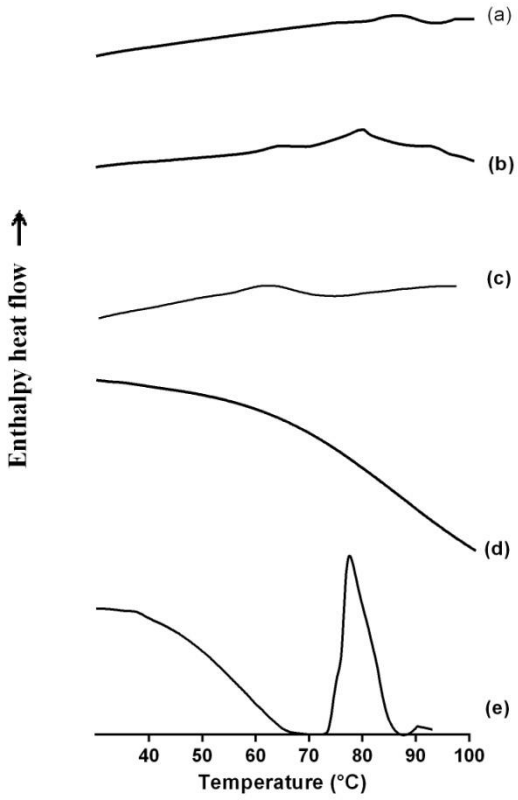

Figure 5.3. DSC transition profiles of insulin associated to PEG 6000 (a), to SA (b), to CH (c), to SiNP (d) and human insulin solution (e).

Regard to insulin associated to uncoated SiNP, the T_{max} of insulin disappears (Figure 5.3 (d)). Therefore, SiNP can shift the endothermic peak of insulin to higher temperatures, above the range of experimental conditions (100 °C), increasing the protein thermal stability (Vanea et al., 2013; Zhao et al., 2013).

Table 5.4. Calorimetric parameters of human insulin and insulin associated to SiNP, SA, CH and PEG 6000.

Samples	T_{max} **(ºC)**	ΔH **(kJ.mol^{-1})**
Insulin sulution	77.64	45.09
Ins-SiNP	-	-
Ins-AS	74.77	2.28
Ins-CH	67.41	0.65
Ins-PEG 6000	77.85	0.68

5.3.5. Interaction studies between nanoparticles and biomembrane models

An *in vitro* interaction study between the carriers and biomembranes allow getting information for understanding the mechanism by which nanoparticles interact with cell membranes. To evaluate the influence of different nanoparticles on DPPC liposomes properties an nDSC analysis was carried out.

The nDSC thermograms of DPPC liposomes in the absence or in the presence of nanoparticles are showed in Figure 5.4. nDSC scan of DPPC liposomes demonstrated two signals, which are associated with two phase transition (Figure 5.4, curve (e)). A small endothermic pre-transition was showed at 35.36 °C. This pre-transition can be attributed to the conversion of lamellar gel-phase to a hexagonal ripple gel phase, due to the conformation changes in phosphodiester groups and glycerol backbone and due to the rotation of the polar heads of phospholipids. The mean peak observed at 41.41 °C is associated to the conversion of gel-phase to lamellar liquid crystal phase due to an increase of trans-gauche isomerization of acyl chains (Yi et al., 2012).

The thermograms, shown in Figure 5.4 indicated that after the incorporation of all nanoparticles in DPPC liposomes, the thermal behavior of DPPC bilayer was not affected. After the dispersion of nanoparticles in DPPC vesicles, there were no changes in pre-transition peak, indicating a weak and superficial interaction between nanoparticles and outer bilayers of liposomes.

However, an increase of ΔH associate to main phase transition of DPPC liposomes was observed only by SiNP and SiNP-PEG 6000 as shown in Table 5.5.

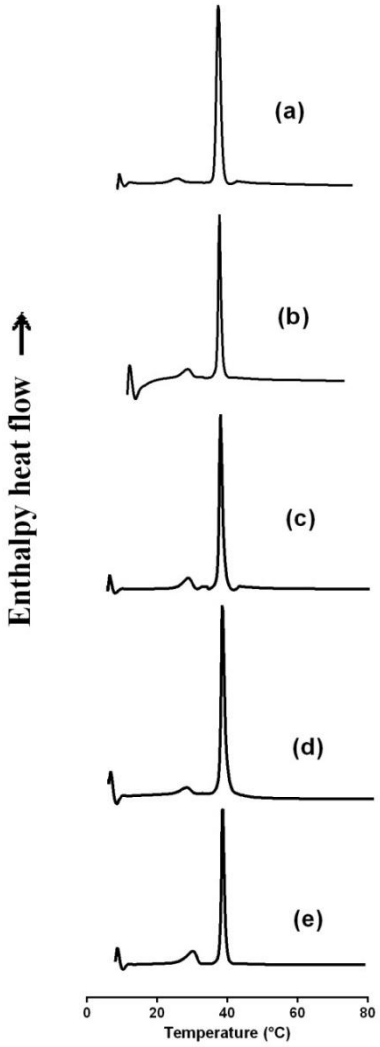

Figure 5.4. DSC transition profiles of interaction between DPPC and different nanoparticles. DPPC liposomes in the presence of SiNP (curve a), SiNP-PEG 6000 (curve b), SiNP-CH (curve c) SiNP-AS (curve d) and in the absence of nanoparticles (curve e).

The increase of ΔH values is ascribed to a strong association of SiNP and SiNP-PEG 6000 with DPPC polar heads by forming hydrogen bonds and/or by electrostatic interaction, leading to an increase of Van der Waals interaction between lipid chains due to a reduction of electrostatic repulsion among choline groups.

Such findings can be also demonstrated by different scans carried out with SiNP (Figure 5.5). With increasing of scan numbers, an increase of ΔH associated to main transition phase occurred (Table 5.6). Therefore, these nanoparticles could be situated close or adsorbed to the polar head of the lipid chains.

Table 5.5. Calorimetric parameters of DPPC liposomes in the presence of different nanoparticles.

Samples	**Pre-transition temperature (°C)**	***ΔH* (kJ.mol^{-1}) Pre-transition**	**Main transition temperature (ºC)**	***ΔH* (kJ.mol^{-1}) main transition**
Liposomes	35.56	2.52	41.41	23.84
SiNP	34.07	1.50	41.08	26.07
SiNP-CH	35.41	2.00	41.41	23.27
SiNP-AS	34.96	1.69	41.27	23.61
SiNP-PEG 6000	33.76	1.53	41.09	28.21

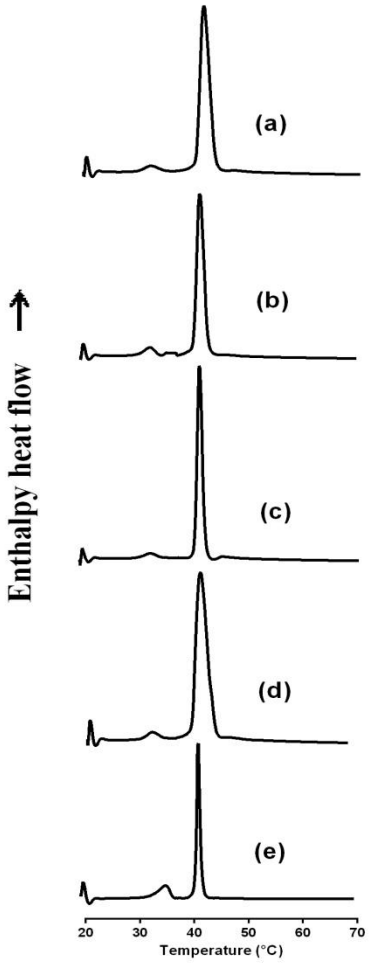

Figure 5.5. DSC curves of DPPC liposomes in contact with SiNP in different scans (a) 1 scan, (b) 2 scan, (c) 3 scan, (d) 4 scan and in the absence of nanoparticles (e).

Table 5.6. Calorimetric parameters of DPPC liposomes in the presence of SiNP at different scans.

Samples	**Pre-transition temperature (°C)**	***ΔH* (kJ.mol^{-1}) Pre-transition**	**Main transition temperature (ºC)**	***ΔH* (kJ.mol^{-1}) main transition**
Liposomes	35.56	2.52	41.41	23.84
SiNP 1 scan	34.07	1.50	41.08	26.07
SiNP 2 scan	32.58	2.19	41.25	42.02
SiNP 3 scan	32.56	1.87	41.40	46.47
SiNP 4 scan	32.88	1.49	41.55	47.59
SiNP 5 scan	33.43	0.94	41.60	50.76

5.3.6. *In vitro* interaction between mucin and different nanoparticles

Figure 5.6 shows the ZP of the *in vitro* interaction between nanoparticles and mucin either in acidic (pH 2.0) or neutral (pH 6.8) conditions. The concentration of mucin varied from 100 to 500 μg/mL.

Under acidic or neutral medium (Figure 5.6A, 6B), it was shown that only SiNP-CH or SiNP-SA demonstrated the ability to interact with mucin in all concentrations. The ZP of SiNP-CH and SiNP-SA decreased with increasing mucin concentration. These results confirm that chitosan and sodium alginate have the ability to adsorb mucin. The high degree of mucin adsorption to the surface of these nanoparticles was expectable taking in account the bioadhesive properties of the polymers. This is indicative of a more specific adsorption process where electrostatic interaction is involved. The adsorption of mucin to chitosan was more pronounced at pH 6.8 (Figure 5.6B). At pH 6.8, sialic mucin residues are negatively charged and the electrostatic attraction between mucin and positively charged chitosan is favored. On the other hand, sodium alginate could interact with mucin mainly by hydrogen bonds (Chickering and Mathiowitz, 1995) due to the presence of numerous surface carboxyl groups on anionic polymers, resulting to high bioadhesive interactions by hydrogen bonds with mucin.

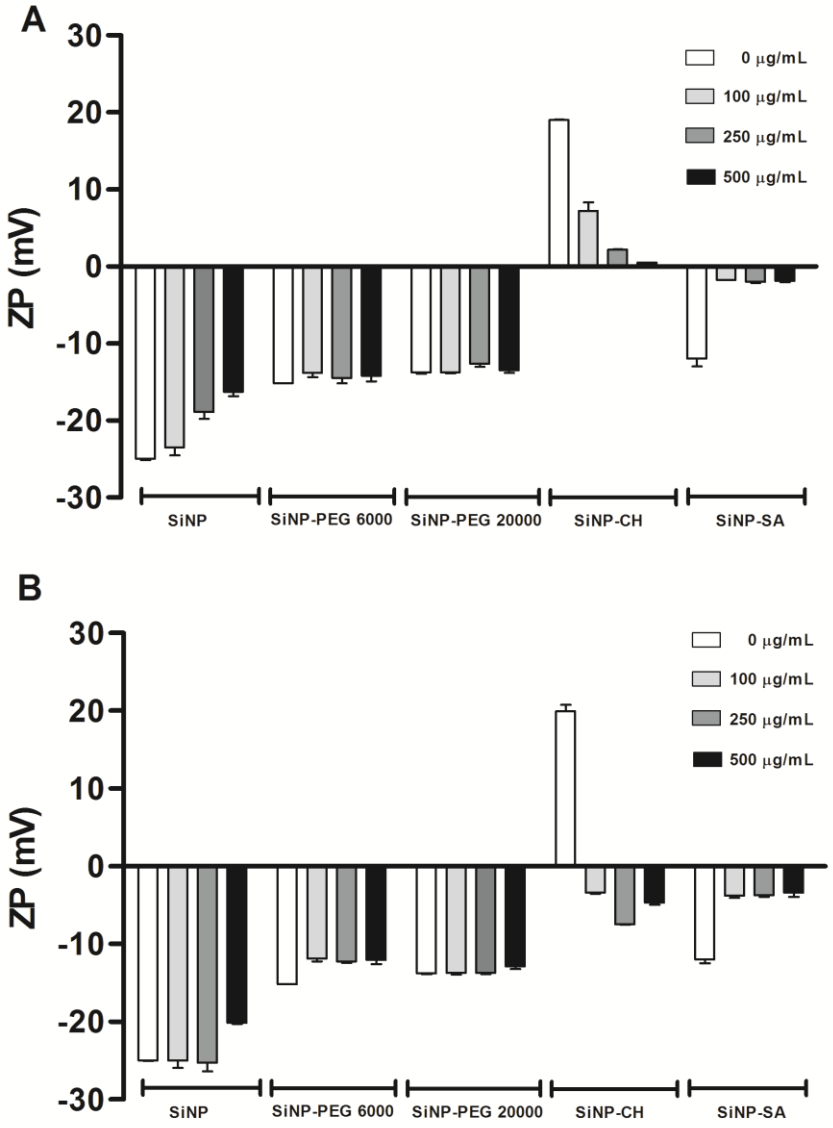

Figure 5.6. Influence of mucin on the nanoparticle ZP. Different concentrations of mucin in μg/mL: 0 (white bars), 100 (light-grey bars), 250 (dark-grey bars) and 500 (black filled bars), and several coating agents, as denoted in the graph, at two different pH environment, pH 2.0 (A) and pH 6.8 (B). Measurements were performed after 30 min incubation (mean ± SD, n=3).

The ZP of SiNP coated with PEG 6000 or PEG 20000 was not influenced by mucin concentrations at both pH values. The steric hindrance of PEG surface can lead to lower level of mucin adsorption (Sanders et al., 2002). Similar results were obtained by Yoncheva and co-workers (Yoncheva et al., 2005) describing that lower interaction of PEG 2000-coated

nanoparticles with mucin may increase their adhesion to intestinal surface due to the permeation properties of PEG chains.

SiNP showed more intensive interaction with mucin at acidic pH (Figure 5.5A). This pH is close to pI of SiNP (pI = 2.0) and mucin (pI = 2.6). On the other hand, at pH 6.8, the interaction between SiNP and mucin is disfavored due to the negatively charged SiNP and the glycoprotein.

5.4. Conclusions

In order to develop a system for oral administration of insulin, coating with different hydrophilic polymers was carried out. Coated SiNP were successfully prepared by sol-gel technology under hydrolysis and condensation of TEOS, showing suitable mean size and high insulin association efficacy.

CD spectra showed that insulin structure was slightly affected by coating. However, some interference due to sodium alginate could be affected the CD spectrum of insulin associated to this polymer.

nDSC was used to collect information about the interaction between the nanoparticles and biomembrane model (liposomes) and about the thermal stability of insulin dissolved in different polymers (chitosan, sodium alginate, PEG 6000 and PEG 20000) for nanoparticles preparation. The interaction between the different nanoparticles and biomembrane models showed that SiNP could promote better interaction with the polar head groups of liposomes. Also SiNP were more effective in protecting insulin from thermal denaturation followed by PEG 6000.

Regarding to *in vitro* interaction with mucin, SiNP coated with chitosan or sodium alginate showed better ability in adsorb mucin in comparison to uncoated nanoparticles and silica nanoparticles coated with PEG as demonstrated by ZP analysis. The ZP of SiNP-CH and SiNP-SA decreases with increasing mucin concentration. However, as previously described the low interaction between PEG-coated nanoparticles and mucin can facilitate the directed contact with intestinal cells.

5.5. References

Bangham, F., Standish, M.W., Watkins, J.C., 1965. Diffusion of univalent ions across the lamellae of swollen phospholipids. J Mol Biol 13, 238-252.

Bilati, U., Allémann, E., Doelker, E., 2005. Strategic approaches for overcoming peptide and protein instability within biodegradable nano- and microparticles. Eur J Pharm Biopharm 59, 375-388.

Chickering, D.E., Mathiowitz, E., 1995. Bioadhesive microspheres: I. A novel electrobalance-based method to study adhesive interactions between individual microspheres and intestinal mucosa. J Control Release 34, 251-262.

De'Nobili, M.D., Curto, L.M., Delfino, J.M., Soria, M., Fissore, E.N., Rojas, A.M., 2013. Performance of alginate films for retention of l-(+)-ascorbic acid. Int J Pharm 450, 95-103.

Ettinger, M.J., Timasheff, S.N., 1971. Optical activity of insulin. I. On the nature of the circular dichroism bands. Biochemistry 10, 824–840.

Farruggia, B., Garcia, G., D'Angelo, C., Picó, G., 1997. Destabilization of human serum albumin by polyethylene glycols studied by thermodynamical equilibrium and kinetic approaches. Int J Biol Macromol 20, 43-51.

Huus, K., Havelund, S., Olsen, H.B., van de Weert, M., Frokjaer, S., 2005. Thermal dissociation and unfolding of insulin. Biochemistry 44, 11171-11177.

Keating, C.D., Kovaleski, K.M., Natan, M.J., 1998. Protein: Colloid conjugates for surface enhanced Raman scattering: stability and control of protein orientation. J Phys Chem B 102, 9404-9413.

Kelly, S.M., Jess, T.J., Price, N.C., 2005. How to study proteins by circular dichroism. Biochim Biophys Acta 1751, 119-139.

Khouri, S.J., Buss, V., 2011. Interaction of cationic cyanine dye with algal alginates: evidence for a polymer bound dye dimer. J Biophys Chem 2, 380-385.

Lu, X., Gao, H., Li, C., Yang, Y.-W., Wang, Y., Fan, Y., Wu, G., Ma, J., 2012. Polyelectrolyte complex nanoparticles of amino poly(glycerol methacrylate)s and insulin. Int J Pharm 423, 195-201.

Manning, M.C., Patel, K., Borchardt, R.T., 1989. Stability of protein pharmaceuticals. Pharm Res 6, 903-918.

Matheus, S., Friess, W., Mahler, H.-C., 2006. FTIR and nDSC as analytical tools for high-concentration protein formulations. Pharm Res 23, 1350-1363.

Montenegro, L., Ottimo, S., Puglisi, G., Castelli, F., Sarpietro, M.G., 2012. Idebenone loaded Solid Lipid Nanoparticles interact with biomembrane models: Calorimetric evidence. Mol Pharmaceutics 9, 2534−2541.

Musumeci, T., Ventura, C.A., Giannone, I., Ruozi, B., Montenegro, L., Pignatello, R., Puglisi, G., 2006. PLA/PLGA nanoparticles for sustained release of docetaxel. Int J Pharm 325, 172-179.

Nielsen, L., Frokjaer, S., Carpenter, J.F., Brange, J., 2001. Studies of the structure of insulin fibrils by Fourier transform infrared (FTIR) spectroscopy and electron microscopy. J Pharm Sci 90, 29-37.

Pocker, Y., Biswas, S.B., 1980. Conformational dynamics of insulin in solution. Circular dichroic studies. Biochemistry 19, 5043-5049.

Robertson, A.D., Murphy, K.P., 1997. Protein structure and the energetics of protein stability. Chem Rev 97, 1251-1267.

Sanchez, K.M., Kang, G., Wu, B., Kim E, J., 2011. Tryptophan-lipid interactions in membrane protein folding probed by ultraviolet resonance Raman and fluorescence spectroscopy. Biophys J 100, 2121-2130.

Sanders, N.N., De Smedt, S.C., Cheng, S.H., Demeester, J., 2002. Pegylated GL67 lipoplex retain their gene transfection activity after exposure to components of CF mucus. Gene Ther 9, 363-371.

Sarmento, B., Ferreira, D.C., Jorgensen, L., van de Weert, M., 2007. Probing insulin's secondary structure after entrapment into alginate/chitosan nanoparticles. Eur J Pharm Biopharm 65, 10-17.

Shafaat, H.S., Sanchez, K.M., Neary, T.J., Kim, J.E., 2008. Ultraviolet resonance Raman spectroscopy of a membrane-bound beta-sheet peptide as a model for membrane protein folding. J Raman Spectrosc 40 1060-1064.

Smart, J.D., 2005. The basics and underlying mechanism of mucoadhesion. Adv Drug Deliv Rev 57, 1556-1568.

Sreerama, N., Woody, R., 2000. Estimation of protein secondary structure from circular dichroism spectra: Comparison of CONTIN. SELCON and CDSSTR methods with an expanded reference set. Anal Biochem 287, 252-260.

Thornton, D.J., Karine Rousseau, K., McGuckin, M.A., 2008. Structure and function of the polymeric mucins in airways mucus. Annu Rev Physiol 70, 459-486.

Thornton, D.J., Sheehan, J.K., 2004. From mucins to mucus: toward a more coherent understanding of this essential barrier. Proc Am Thorac Soc 1, 54-61.

Vanea, E., Moraru, C., Vulpoi, A., Cavalu, S., Simon, V., 2013. Freeze-dried and spray-dried zinc-containing silica microparticles entrapping insulin. J Biomater Appl. (in press) doi: 10.1177/0885328213501216

Wallace, B.A., 2009. Protein characterisation by synchrotron radiation circular dichroism spectroscopy. Quarterly Rev Biophys 42, 317-370.

Whitmore, L., Wallace, B.A., 2008. Protein secondary structure analyses from circular dichroism spectroscopy: Methods and reference databases. Biopolymers 89, 392-400.

Woody, R.W., 1996. Circular dichroism and the conformational analysis of biomolcules. Plenum Press, New York.

Wu, J., Wang, Z., Lin, W., Chen, S., 2013. Investigation of the interaction between poly(ethylene glycol) and protein molecules using low field nuclear magnetic resonance. Acta Biomaterialia 9, 6414-6420.

Yi, Z., Nagao, M., Bossev, D.P., 2012. Effect of charged lidocaine on static and dynamic properties of model bio-membranes. Biophys Chem 160, 20−27.

Yoncheva, K., Lizarraga, E., Irache, J.M., 2005. Pegylated nanoparticles based on poly(methyl vinyl ether-co-maleic anhydride): preparation and evaluation of their bioadhesive properties. Eur J Pharm Sci 24, 411-419.

Zhao, X., Shan, C., Zu, Y., Zhang, Y., Wang, W., Wang, K., Sui, X., Li, R., 2013. Preparation, characterization, and evaluation in vivo of Ins-SiO2-HP55 (insulin-loaded silica coating HP55) for oral delivery of insulin. Int J Pharm 454, 278-284.

Chapter VI

In vitro insulin release and permeation from nanoparticles

6.1. Introduction

The objective of the present chapter was the determination of the *in vitro* insulin release pattern from the different nanoparticles, as well as the *in vitro* permeation studies through everted rat intestine.

By modulation of SiNP surface properties and composition, the desired release profile of the drug could be achieved. Concerning the drug release pattern, one of the most commonly used methods involves the Franz-type cells (Franz, 1975; McCarron et al., 2000; Morales et al., 2004). Therefore, for the study of insulin release profile, Franz diffusion cells were used at gastric and intestinal conditions. The diffusion process across an inert membrane can be described by Fick's first law, according to the following equation (equation 6.1):

$$J = \frac{DK}{h} C_v \qquad \text{Equation 6.1}$$

where, J is the flux (solute quantity (mol) per unit time per unit area crossing the membrane), D is the diffusion-coefficient, K is the membrane vehicle partition coefficient, h is the diffusional path length and C_v is the concentration of the diffused vehicle.

The use of mathematical models is an important tool for describing the pharmacokinetic profile of a drug formulated in these carriers in order to develop new drug delivery systems with better knowledge about drug bioavailability and bioequivalence (Mohamad and Dashevsky, 2007).

The dissolution process is controlled by the affinity between the drug and solvent and its release form (Craig, 2002). The drug solubility is a very important parameter regarding to pre-formulation studies.The *in vitro* kinetics is desirable in order to reduce the number of bio-analysis, and also to establish *in vitro-in-vivo* correlations, since the performance of the drug release profile may change *in vivo* experiments.

The quantitative interpretation of values obtained in dissolution tests can be accomplished by a general equation which mathematically translates the dissolution curve versus time, and includes the influence of some parameters related to the pharmaceutical form. The type of drug, polymorphic form, crystallinity, drug size, solubility and amount of

the drug loaded in a matrix may influence the release kinetics (Escudero et al., 2010; Hiremath and Saha, 2008).

Several models can be applied to predict the drug pharmacokinetic profile from a matrix, including zero order kinetics, first order kinetics, Weibull, Higuchi, Korsmeyer-Peppas, Baker-Lonsdale and independent model methods that use the difference factor (f_1) and the similarity factor (f_2) (Rescigno, 1992) to check if differences exist between the dissolution profiles, relating the percentage of dissolved drug, the area under the dissolution curve (AUC) and the time of dissolution. In the present study, the kinetic evaluation of the insulin release profile from the different nanoparticles was made using several mathematic modelling, such as zero order, first order, second order, hyperbola and Boltzmann models.

Also, in this work, the influence of coating on *in vitro* insulin permeation through everted rat intestine was examined. This technique is a simple and efficient *in vitro* model widely used for evaluating the nutrient uptake and transport in the intestine (Nomoto et al., 1998; Wilson and Wiseman, 1954). However, an extension of this method has been applied for studying the intestinal absorption of the drugs (Souza et al., 2014), as well as to measure the bioadhesion of a matrix (Santos et al., 1999).

In addition, other studies were also carried out, regarding to nanoparticles morphology, using atomic force microscopy (AFM) and to insulin integrity after the release test applying the circular dichroism (CD) technique.

6.2. Materials and methods

6.2.1. Materials

Tetraethyl orthosilicate (TEOS, 98 %), NH_3 25 %, PEG with M_w of 6000 and 20000 Da (PEG 6000; PEG 20000) were purchased from Merck (Darmstadt, Germany). Chitosan low molecular weight (235 g/mol, degree of deacetylation of 78.5 %), ethanol 99.9 %, trehalose dehydrate and bovine serum albumin (BSA) were purchased from Sigma-Aldrich (Steinhein, Germany). Sodium alginate (198.11 g/mol) was purchased from VWR Portugal (Carnaxide, Portugal). Solution of 100 IU/mL of human insulin (Humulin® R) was purchased from Eli Lilly (Lisbon, Portugal). Pentobarbital Sodium was purchased from Abbott (Rio de Janeiro, Brazil). Ultra-purified water was obtained from Milli® Q Plus system (Millipore, Germany).

6.2.2. Synthesis of nanoparticles

SiNP were synthesized by sol-gel technology at room temperature via hydrolysis and condensation of TEOS, under high shear homogenization (Ultra-Turrax, IKA, T25), using NH_3 as catalytic agent. The obtained nanoparticles were centrifuged and washed with a mixture of ethanol and ultra-purified water (1:1, v/v) by 2 cycles at 12,000 rpm for 5 min (Spectrafuge16M, Lambnet International, Inc.) as described in chapter II.

For coating SiNP, a solution of chitosan (CH) (0.3 %, w/v) at pH 4.5, or sodium alginate (SA) (0.3 % , w/v) at pH 4.5, or PEG 6000 or PEG 20000 (2 %, w/v) at pH 6.8 were added to nanoparticles, stirred for 30 min and centrifuged as described above. The percentage of mucoadhesive polymers was selected according to previous experiments in the laboratory of Cell biology and bioenergetics at UTAD, demonstrating smaller mean size and low polydispersity index of the coated nanoparticles (data not shown).

To produce insulin associated to SiNP, 1.0 mL of human insulin (100 IU/mL, pH 7.0) was added to 10 mg of uncoated SiNP under gentle stirring (300 rpm) for 30 min into ice bath.

For coated insulin-SiNP, 1.0 mL of human insulin (100 IU/mL, pH 7.0) was dissolved in 2.0 mL of the mucoadhesive polymer solutions, mixed for 30 min under magnetic stirring and then added to SiNP (10 mg) under gentle stirring (300 rpm) for more 30 min into ice bath.

The nanoparticles were centrifuged at 5000 rpm for 5 min and the pellet was freeze-dried during 24 h with trehalose (10 %, w/v) as cryoprotectant agent to prevent particle aggregation. The obtained nanoparticles were stored at 4 °C until further use.

6.2.3. Apparatus and chromatography system

The chromatography system consisted of a Waters 1525 pump (Waters, Milford, Massachusetts) with a UV-Vis 2487 detector (Waters®). C18 column (5 μm, 250 × 4.6 mm, Phenomenex®) with a flow rate of 1.0 mL/minute was used. The mobile phase consisted of acetonitrile- water with 0.1 % trifluoroacetic acid (TFA; 40:60, v/v), the injection volume was 100 μL and a total run time of 12 minutes. The absorbance of insulin was recorded at 220 nm, and the area under the curve was measured for calculation of insulin concentration based on the calibration curves.

6.2.4. Insulin assay by high performance liquid chromatography (HPLC)

The validation method for the insulin quantification was described in the Supplement II.

6.2.5. *In vitro* insulin release from nanoparticles

In vitro release studies of insulin from uncoated and coated SiNP were performed using Franz glass diffusion cells. These cells consisted of donor and receptor chambers between which a cellulose nitrate membrane with an average pore size of 0.2 μm is positioned. Phosphate-buffered saline (PBS) at pH 6.8 (FP VIII) or HCl/KCl buffer at pH 2.0 (FP VIII) were used as receptor fluid and maintained at 37 °C. A volume of 300 μL of nanoparticles was applied to the donor compartment, containing 7 mL of buffer. During all the experiment, a magnetic bar was stirring in each cell. At determined times, 1.0 mL of the samples were collected and the same volume was replaced with buffer. The insulin collected was analyzed by HPLC.

6.2.6. Release profile analysis

The insulin release data were also kinetically evaluated applying the Akaike's approach (Doménech et al., 1998). The empirical models were selected based on the Akaike Information Criteria (AIC). The model associated to the smallest value of AIC is considered as giving the best fit of the set of data. The AIC was calculated according to equation 6.2:

$$AIC = n \ln SSQ + 2p \qquad \text{Equation 6.2}$$

where, n is the number of pairs of experimental values, SSQ is the residual sum of squares and p is the number of parameters of the model.

The mean release time (MRT) of insulin from different nanoparticles was also arithmetically assessed from experimental data by using the equation 6.3:

$$MRT = \frac{\sum t_i . \Delta Q}{Q_\infty} \qquad \text{Equation 6.3}$$

where, Q_∞ is the asymptote of the dissolved amount of drug and $\sum t_i . \Delta Q$ is the area between the cumulative release and Q_∞.

6.2.7. Circular dichroism (CD)

The secondary structure of insulin was determined by circular dichroism (CD). The CD spectra of native insulin and insulin released into buffers at pH 2.0 and pH 6.8 from nanoparticles were recorded in a 0.1 cm cell from 250-190 nm at 25 °C using a Jasco Spectropolarimeter J-815 (Tokyo, Japan). CD spectra of all samples were acquired and subtracted from the reference spectra (polymer solution in the respective pH). Each spectrum represents an average of 6 successive scans and is expressed as the mean residual ellipticity [θ] (deg.cm^2.dmol^{-1}). Deconvolution of CD spectra was obtained by the SELCON3 method (Sreerama and Woody, 2000).

6.2.8. Permeation studies through everted rat intestine

Male Wistar rats, weighing approximately 250-270 g were provided by São Carlos Federal University (Animal Ethics Committee, protocol number 003/2011). Rats fasted overnight with free access to water were anesthetized by an intraperitoneal injection of pentobarbital sodium (0.5 mL/kg) and killed by cervical dislocation immediately after removing the small intestine *via* an abdominal incision. Small intestine (ca. 6 cm) was removed, rinsed several times with oxygenated TC-199 buffer solution without lactose at 10 °C and gently everted. One end of the gut sac was clamped and the whole length of the intestine was filled with TC-199 buffer and sealed with braided silk sutures. The everted gut sacs were placed into Erlenmeyer flasks containing a solution of TC-199 buffer with lactose (20 mL) and nanoparticles (loaded with insulin) and incubated at 37 °C. The solution was continually aerated. After 60 min, the sacs were removed, washed with TC-199 and cut open. The content of the sacs were then filtered via cellulose acetate membrane (0.22 µm). The cumulative amount of insulin permeated through the gut sac was analyzed by HPLC. The TC-199 buffer is composed of NaCl (145 mM), KCl (4.56 mM), $CaCl_2.2H_2O$ (1.25 mM) and $NaHPO_4$ (5 mM). The TC-199 buffer containing lactose has the same composition described above with 10 mM of lactose.

6.2.9. Morphological studies

Nanoparticles were examined morphologically using an atomic force microscopy (AFM). AFM experiments were performed with a Multimode microscope (Veeco, Santa Barbara, California) controlled by Nanoscope IIIa electronics (Veeco). The images were done in tapping mode at 25 °C. Samples were prepared by depositing 5 µL of the samples after redispersion in water on silicon substrate followed by drying overnight at 25 ºC.

6.2.10. Statistical analysis

Statistically evaluation of data was performed using a one-way analysis of variance (ANOVA) test. Bonferroni's Multiple Comparison test was carried out to compare the significance between the different groups. A p-value < 0.05 was considered statistically significant.

6.3. Results and discussions

6.3.1. *In vitro* insulin release and modeling

The insulin release studies from uncoated and coated SiNP were conducted in HCl/KCl buffer or PBS at 37 ºC and the *in vitro* release profiles are displayed in Figure 6.1 (A and B). At both pH, only SiNP and SiNP-PEG 6000 affected significantly the insulin release pattern ($p < 0.05$).

Insulin-loaded SiNP synthesized in the absence of coating displayed lower rate of release drug from colloidal system in comparison to that coated SiNP with different mucoadhesive polymers at both pH. This result can be best described by the fact that insulin could be easily bound to silanol groups present onto the silica surface leading to a lower insulin release rate. With the addition of mucoadhesive polymers, the number of sites for insulin association decreased, resulting in faster protein release. The results also show that the released amount depended on the insulin associated to nanoparticles. Higher insulin association resulted in more insulin release, which is due to the higher insulin adsorption on the surface of nanoparticles, leading to a faster release rate. Therefore, the insulin association to coated nanoparticles was higher than uncoated SiNP, contributing to a higher amount of insulin release.

PEG coating can lead to an increase of drug release due to the hydration process of PEG layers in the dispersion medium which favors the protein diffusion (Quellec et al., 1998). The experimental results showed that PEG 6000 provided a slower insulin release compared with PEG 20000. This can be attributed due to the enhancement properties leading to the protein release by diffusion mechanism related to the channels and the pores formed by the PEGylation process (Elvassore et al., 2001).

At low pH, insulin was rapidly release from SiNP coated with chitosan (SiNP-CH), sodium alginate (SiNP-SA) and PEG 20000 (SiNP-PEG 20000) (Figure 6.1A). Theoretically, the release of macromolecules from alginate matrices under acidic conditions is reduced due to the conversion of sodium alginate into alginic acid (George and Abraham, 2006). However, in the present study, this conversion could result in the loss of the interaction between negative charge of alginate and positive charge of insulin leading to the faster insulin release. In the case of chitosan, at low pH, the chitosan polymer chains become positively charged

with the protonated amino groups. Therefore there is a weak interaction forces between insulin and chitosan and thus, insulin is rapidly released.

The retention time of particles in stomach is considered to be about 1 to 2 h. In the present study, the amount of insulin released at pH 2.0 (~ 60%), after 2 h, indicates that it is important to optimize the system in order to provide a minimum contact between the protein and the gastric environment, thus avoiding a possible protein denaturation.

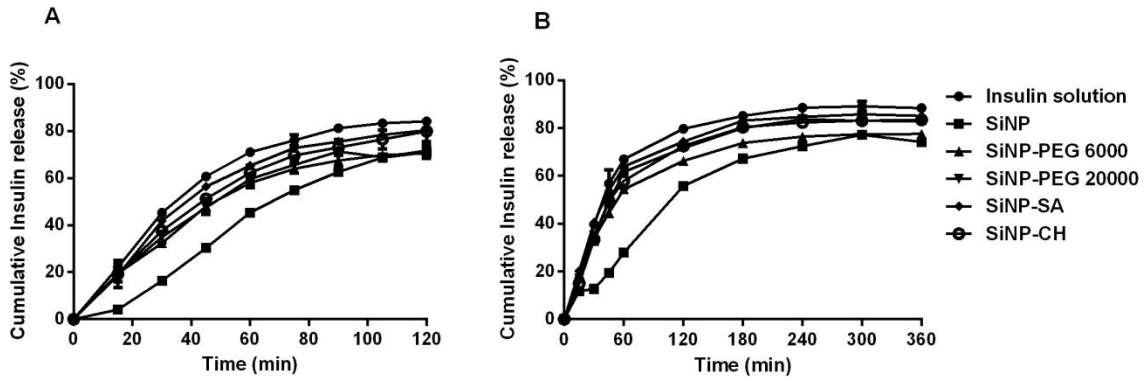

Figure 6.1. Cumulative release profiles of insulin from different nanoparticles. Experiments were conducted in HCl/KCl buffer at pH 2.0 (A) and in PBS at pH 6.8 (B) (n = 6 ± SD).

A different situation emerges from studies with buffer at pH 6.8 simulating intestinal conditions for insulin released from uncoated SiNP (Figure 6.1B). When PBS was used, lower insulin release from SiNP was observed in the first 1 h in comparison to insulin released in the acidic pH. This result can be attributed to the fact that low pH disfavors the polycondensation reactions resulting in faster dissolution of silica matrix (Kortesuo et al., 2002). In addition, insulin is more soluble at low pH.

On the other hand, the presence of sodium alginate and chitosan onto SiNP surface contributed to a higher amount of insulin release and no significant differences were found in comparison to insulin solution, as well as in comparison to SiNP-CH and SiNP-SA at low pH ($p > 0.05$). This result is probably due to the fact that at pH 6.8, sodium alginate swells forming a soluble salt and the polymeric matrix is totally disintegrated (Sarmento et al., 2007). At this pH, the amine groups of chitosan are deprotonated and insulin show negative charges and, thus the ionic interaction between them is less pronounced leading to a faster insulin release.

SiNP, SiNP-PEG 6000 and SiNP-PEG 20000 were selected for insulin kinetic studies. This selection was based on the fact that SiNP and SiNP-PEG 6000 showed better profile for insulin release. The choice of SiNP-PEG 20000 was for comparing them with SiNP-PEG 6000 and to verify the influence of Mw on the kinetic dissolution.

Comparing the values of half-lives, at both acidic and neutral pH, insulin solution showed a slower half-live resulting in slower time for insulin release (Table 6.1 and Table 6.2). Insulin solution showed a faster diffusion followed by SiNP-PEG 20000, Si-PEG 6000 and SiNP. Therefore the association of insulin to SiNP considerably prolongs its half-life.

Table 6.1 and Table 6.2 also show the MRT for insulin and different nanoparticles at both gastric and intestinal pH, respectively. The MRT obtained with uncoated and coated silica nanoparticles increases compared with insulin solution, confirming that the association of insulin to nanoparticles modified its release time.

Table 6.1. MRT and half-life for insulin solution, Ins-SiNP and Ins-SiNP-PEG 6000 at gastric pH.

Gastric	**Insulin solution**	**Ins-SiNP**	**Ins-SiNP-PEG 6000**
MRT (min)	34.10 ± 0.9	52.80 ± 0.3	36.2 ± 1.2
Half-live (min)	30.32	194.90	35.05

The statistically different formulations are: Insulin solution vs Ins-SiNP: $p < 0.0001$; Ins-SiNP vs Ins-SiNP-PEG 6000: $p < 0.0001$; Insulin solution vs Ins-SiNP-PEG 6000: $p < 0.05$; Insulin solution vs Ins-SiNP-PEG 20000: $p < 0.05$.

Table 6.2. MRT and half-life for insulin solution, Ins-SiNP and Ins-SiNP-PEG 6000 at intestinal pH.

Intestinal	**Insulin solution**	**Ins-SiNP**	**Ins-SiNP-PEG 6000**
MRT (min)	50.0 ± 0.4	86.6 ± 2.0	57.5 ± 2.1
Half-life (min)	33.45	89.24	36.16

The statistically different formulations are: Insulin solution vs Ins-SiNP: $p < 0.0001$; Ins-SiNP vs Ins-SiNP-PEG 20000: $p < 0.0001$; Ins-SiNP vs Ins-SiNP-PEG 6000: $p < 0.0001$; Insulin solution vs Ins-SiNP-PEG 6000: $p < 0.001$; Insulin solution vs Ins-SiNP-PEG 20000: $p < 0.05$; Ins-SiNP-PEG 6000 vs Ins-SiNP-PEG 20000: $p < 0.01$.

Table 6.3 lists the model and their corresponding dissolution parameters for insulin solution and different nanoparticles at pH 2.0 and pH 6.8. According to lower AIC values, at pH 2.0, for insulin solution, the best model was found to be first order, and for SiNP and SiNP coated with PEG 6000 or PEG 20000 the best model was found to be second order. At intestinal condition (pH 6.8) the best fitting was first-order for all formulation, except for SiNP and insulin solution, which showed a Boltzmann behavior.

Table 6.3. Mathematic modeling for insulin release at gastric and intestinal conditions.

Release condition	**Formulations**	**Zero-order**		**First-order**		**Second order**		**Boltzmann**		**Hiperbola**	
		AIC	**r^2**	**AIC**	**r^2**	**AIC**	**r^2**	**AIC**	**r^2**	**AIC**	**r^2**
Gastric	Insulin free	39.86	0.9738	18.29	0.9982	19.02	0.9985	*	*	81.51	0.9962
	Ins-SiNP	31.45	0.9929	29.58	0.9944	13.01	0.9994	14.94	0.9999	102.75	0.9943
	Ins-SiNP-PEG 20000	36.90	0.9767	20.05	0.9972	12.43	0.9991	16.57	0.9993	79.89	0.9954
	Ins-SiNP-PEG 6000	35.42	0.9798	16.27	0.9982	9.09	0.9994	14.79	0.9999	67.85	0.9967
Intestinal	Insulin free	61.09	0.9427	29.70	0.9986	52.51	0.9801	28.41	0.9992	39.04	0.9937
	Ins-SiNP	54.21	0.9761	35.06	0.9973	29.70	0.9983	25.75	0.9993	39.17	0.9947
	Ins-SiNP-PEG 20000	58.73	0.9492	26.12	0.9989	48.44	0.9852	29.00	0.9990	34.81	0.9954
	Ins-SiNP-PEG 6000	54.75	0.9570	12.06	0.9997	42.60	0.9896	*	*	22.01	0.9984

*Kinetic fitting model interrupted

6.3.2. Circular dichroism (CD)

For the same reason, as described in the previous section, the structure of insulin after release was performed comparing insulin solution, SiNP-PEG 6000 and SiNP-PEG 20000. The structure of insulin was studied after release from nanoparticles at pH 2.0 and pH 6.8 using CD spectroscopy (Figure 6.2A, 6.2B). CD spectra of insulin released from all nanoparticles at pH 2.0 and pH 6.8 revealed a slight difference compared with native insulin solution.

Parameters of the secondary structure of insulin, including α-helix, β-sheet, β-turn, and random coil, are summarized in Table 6.4 and Table 6.5, at pH 2.0 and pH 6.8, respectively. At both pH, some differences can be seen comparing the secondary structure of insulin solution with the insulin release from SiNP-PEG 6000 and SiNP-PEG 20000. The content of α-helix decreases, while the content of β-sheet increases. The content of β-turn and random coil does not obviously change.

Table 6.4. Observed parameters of secondary insulin solution structure and of insulin release from SiNP-PEG 6000 and SiNP-PEG 20000 at pH 2.0.

Samples	α-helix (%)	β-sheet (%)	β-Turn (%)	Random coil (%)
Insulin solution	66.8	1.7	10.2	23.4
SiNP-PEG 2000	59.1	3.6	14.9	23.7
SiNP-PEG 6000	53.6	4.7	14.0	30.6

Table 6.5. Observed parameters of secondary insulin solution structure and of insulin release from SiNP-PEG 6000 and SiNP-PEG 20000 at pH 6.8.

Samples	α-helix (%)	β-sheet (%)	β-Turn (%)	Random coil (%)
Insulin solution	66.8	1.7	10.2	23.4
SiNP-PEG 20000	50.0	6.6	17.5	29.0
SiNP-PEG 6000	39.7	15.6	15.5	29.3

These results can be attributed to the adsorption of insulin on the surface of particles because of the affinity of the protein with the hydrophilic chains of PEG, as confirmed by high AE. The association of insulin to the hydrophilic polymers could make the α-helix draw and extend into β-sheet (Liu et al., 2007). Regardless of slight difference of the spectra intensity and fractional composition of secondary parameters, the line shape of the spectrum

of insulin released was similar to that of the native insulin, indicating that the association of insulin to nanoparticles did not influence the conformation of the protein.

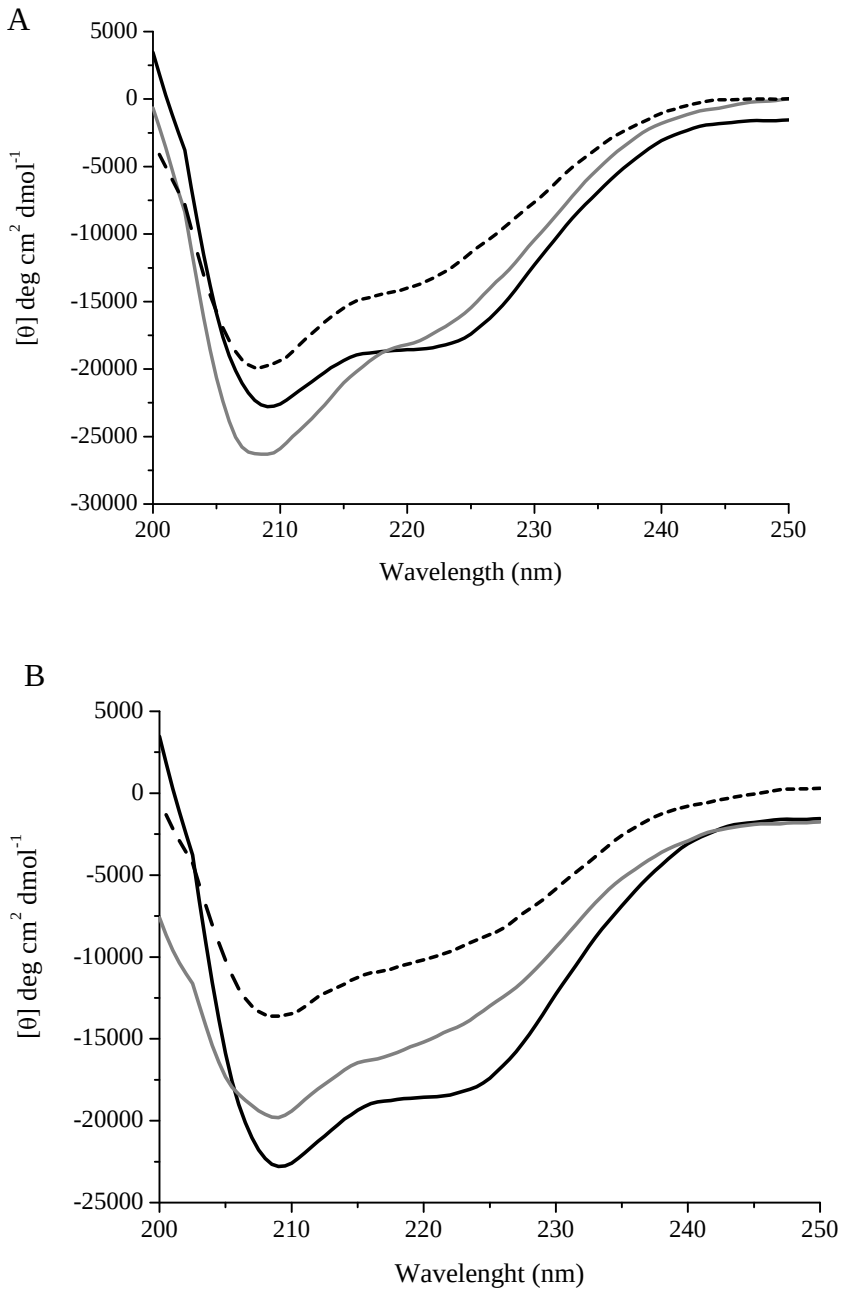

Figure 6.2. Far-UV CD spectrum of native insulin (black line), insulin released from SiNP-PEG 6000 (black dotted line) and SiNP-PEG 20000 (grey line) at pH 2.0 (A) and pH 6.8 (B) buffers.

6.3.3. Permeation studies through everted rat intestine

Permeation studies were carried out to investigate the influence of PEG coatings on insulin transport through the intestinal mucosa. The results of mean percentage of insulin permeation were 46.50 % ± 4.82, 42.46 % ± 5.08, 48.70 % ± 3.86 and 40.13 % ± 2.77 for insulin solution, SiNP, SiNP-PEG 6000 and SiNP-PEG 20000 respectively (Figure 6.3).

Although PEG is a polymer that may increase the drug absorption through intestinal mucosa, the presence of PEG onto the silica surface did not significantly change the permeation behavior of insulin through the small intestinal mucosa ($p > 0.05$)

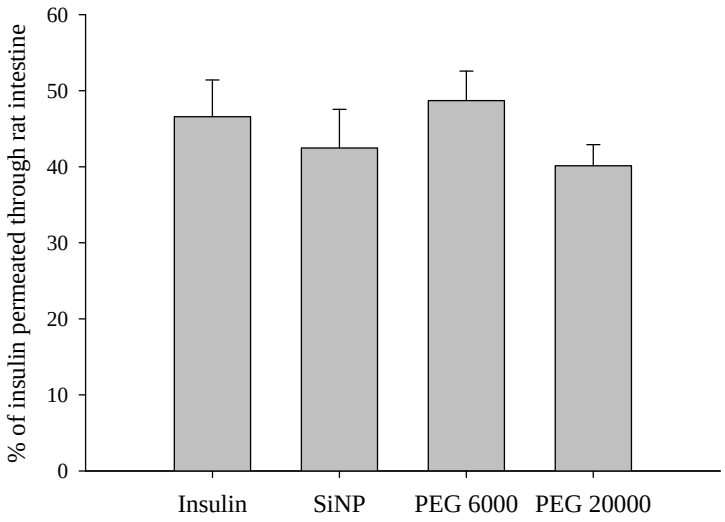

Figure 6.3. The influence of SiNP and PEG-coated SiNP on insulin permeation from everted gut sacs incubated in TC-199 buffer over 60 min (n = 6 ± SD).

Several studies have demonstrated that the conjugation of low Mw PEGs to drugs can enhance the absorption. However, the effect of PEG on protein permeation in intestinal mucosa is strongly associated to the polymer structure, to the molecular weight of PEG, as well as to the percentage of polymer used for coating strategy. Also, in order to avoid the limiting factors of the use of everted rat intestine studies, such as loss of protein, *in vivo* models should be applied for better results of nanoparticles permeation.

6.3.4. Morphological studies

AFM studies were conducted to investigate the morphology of prepared nanoparticles (Figure 6.4). AFM observations showed individualized spherical-shaped SiNP with minor deformation and aggregation (Figure 6.4, left). Coating with PEG did not affect the particle shape. However, from the images, partial aggregation of nanoparticles was observed after coating with PEG 6000 (Figure 6.4, right). Also, SiNP have a smaller size in comparison to that observed by DLS characterization, probably due to the shrinkage and collapse of silica nanoparticles and PEG layer in the drying process. For In-SiNP-PEG 6000, the particle surface is very smooth and no signal of insulin is visible.

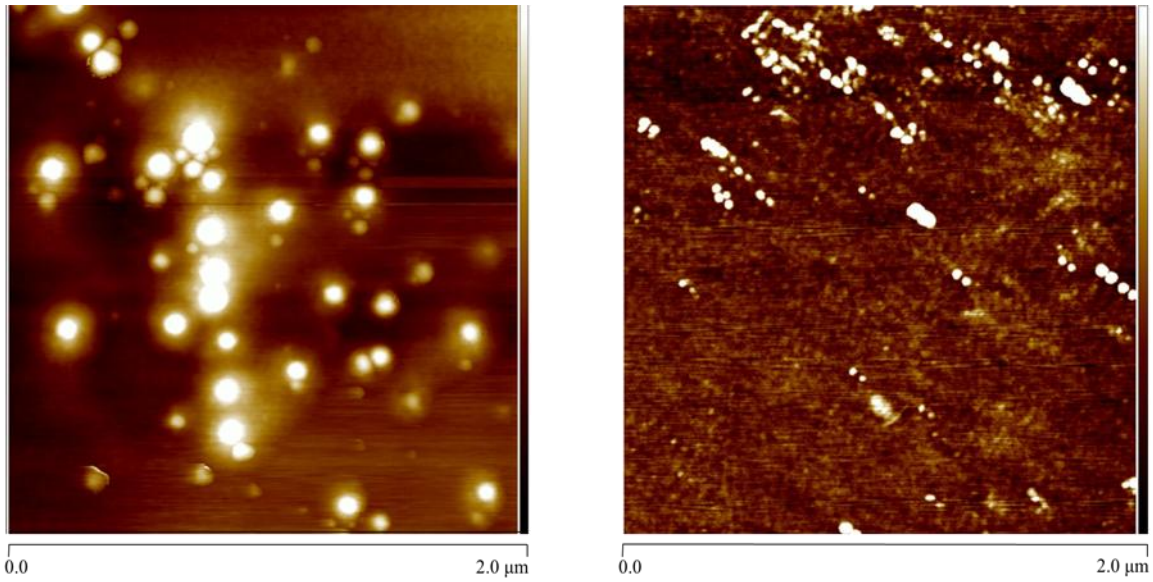

Figure 6.4. Morphological characterization of SiNP (left) and Ins-SiNP coated with PEG 6000 (right).

6.4. Conclusions

A major problem during the development of drug delivery systems is the drug burst release observed in the first minutes of contact with aqueous medium. In the case of oral protein delivery, the difficulty is more pronounced, since the system has to show the ability in protecting the protein from gastric pH as well as from proteolytic enzymes present in stomach and intestine.

Uncoated and coated SiNP with mucoadhesive polymers (chitosan, PEG 6000, PEG 20000 or sodium alginate) were selected to evaluate the performance of these nanoparticles on *in vitro* insulin release and permeation.

Concerning to *in vitro* release studies at pH 2.0 and pH 6.8, the coating of nanoparticles with mucoadhesive polymers resulted in faster insulin release in comparison to uncoated nanoparticles due to the low interaction between insulin and SiOH groups present onto the silica surface. In addition, the insulin association to coated nanoparticles was higher than uncoated nanoparticles, contributing to a higher amount of insulin release.

The insulin release profile was only significantly affected by uncoated nanoparticles and SiNP coated with PEG 6000. The insulin release from uncoated nanoparticles at intestinal condition was lower in comparison to gastric conditions due to the fact that low pH disfavors the polycondensation reactions resulting in faster dissolution of silica matrix. Also, the CD spectra showed that insulin structure was not affected after protein release from nanoparticles coated with PEG 6000 or PEG 20000.

The *in vitro* insulin permeation studies trough everted rat intestine indicated that the coating did not affect significantly the insulin absorption, probably due to the molecular weight of PEG or the percentage of polymer used for coating process.

AFM observations showed that uncoated and nanoparticles coated with PEG resulted in individualized spherical-shaped nanoparticles with minor deformation and aggregation.

6.5. References

Craig, D.Q.M., 2002. The mechanisms of drug release from solid dispersions in water-soluble polymers. Int J Pharm 231, 131-144.

Doménech, J., Martínez, J., Plá, J.M., 1998. Biofarmacia y Farmacocinética II. Síntesis, Madrid.

Elvassore, N., Bertucco, A., Caliceti, P., 2001. Production of insulin-loaded poly(ethylene glycol)/ poly(l-lactide) (PEG/PLA) nanoparticles by gas antisolvent techniques. J Pharm Sci 90, 1628-1636.

Escudero, J.J., Ferrero, C., Jimenez-Castellanos, M.R., 2010. Compaction properties, drug release kinetics and fronts movement studies from matrices combining mixtures of swellable and inert polymers II. Effect of HPMC with different degrees of methoxy/hydroxypropyl substitution. Int J Pharm 387, 56-64.

Franz, T.J., 1975. Percutaneous absorption and the relevance of in vitro data. J Invest Derm 64, 190-195.

George, M., Abraham, T.E., 2006. Polyionic hydrocolloids for the intestinal delivery of protein drugs: Alginate and chitosan-a review. J Control Release 114, 1-14.

Hiremath, P.S., Saha, R.N., 2008. Oral controlled release formulations of rifampicin. Part II: effect of formulation variables and process parameters on in vitro release. Drug Deliv Transl Res 15, 159 -168.

Kortesuo, P., Ahola, M., Kangas, M., Jokinen, M., Leino, T., Vuorilehto, L., Laakso, S., Kiesvaara, J., Yli-Urpo, A., Marvola, M., 2002. Effect of synthesis parameters of the sol-gel processed spray-dried silica gel microparticles on the release rate of dexmedetomidine. Biomaterials 23, 2795-2801.

Liu, T., Guo, R., Hua, W., Qiu, J., 2007. Structure behaviors of hemoglobin in PEG 6000/Tween 80/Span 80/H2O niosome system. Colloid Surf B 293, 255-261.

McCarron, P.A., Woolfson, A.D., Keating, S.M., 2000. Sustained release of 5-fluorouracil from polymeric nanoparticles. J Pharm Pharmacol 52, 1451-1459.

Mohamad, A., Dashevsky, A., 2007. In vitro and in vivo performance of a multiparticulate pulsatile drug delivery system. Drug Dev Ind Pharm 33, 113-119.

Morales, M.E., Gallardo Lara, V., Calpena, A.C., Doménech, J., Ruiz, M.A., 2004. Comparative study of morphine diffusion from sustained release polymeric suspensions. J Control Release 95, 75-81.

Nomoto, M., Yamada, K., Haga, M., Hayashi, M., 1998. Improvement of intestinal absorption of peptide drugs by glycosylation: Transport of tetrapeptide by the sodium ion-dependent D-glucose transporter. J Pharm Sci 87, 326-332.

Quellec, P., Gref, R., Perrin, L., Dellacherie, E., Sommer, F., Verbavatz, J.M., Alonso, M.J., 1998. Protein encapsulation within polyethylene glycol-coated nanospheres I. Physicochemical characterization. J Biomed Mater Res 42, 45-54.

Rescigno, A., 1992. Bioequivalence Pharm Res 9, 925-928

Santos, C.A., Jacob, J.S., Hertzog, B.A., Freedman, B.D., Press, D.L., Harnpicharnchai, P., Mathiowitz, E., 1999. Correlation of two bioadhesion assays: the everted sac technique and the CAHN microbalance. J Control Release 61, 113-122.

Sarmento, B., Ribeiro, A., Veiga, F., Sampaio, P., Neufeld, R., Ferreira, D., 2007. Alginate/chitosan nanoparticles are effective for oral insulin delivery. Pharm Res 24, 2198-2206.

Souza, A.L.R.d., Andreani, T., de Oliveira, R.N., Kiill, C.P., Santos, F.K.d., Allegretti, S.M., Chaud, M.V., Souto, E.B., Silva, A.M., Gremião, M.P.D., 2014. In vitro evaluation of permeation, toxicity and effect of praziquantel-loaded solid lipid nanoparticles against Schistosoma mansoni as a strategy to improve efficacy of the schistosomiasis treatment. Int J Pharm 463, 31-37.

Sreerama, N., Woody, R., 2000. Estimation of protein secondary structure from circular dichroism spectra: Comparison of CONTIN. SELCON and CDSSTR methods with an expanded reference set. Anal Biochem 287, 252-260.

Wilson, T.H., Wiseman, G., 1954. The use of sacs of inverted small intestine for the study of the transferance of substances from the mucosal to the serosal surface. J Physiol 123, 116-125.

Chapter VII

Comparative cytotoxicity response of nanoparticles

7.1. Introduction

In the previous chapter, the coating of SiNP affected significantly the insulin release profile. The association of insulin to uncoated SiNP and PEG 6000-coated SiNP considerably prolongs its half-life at simulated gastric and intestinal conditions in comparison to SiNP coated with chitosan, sodium alginate or PEG 20000. However, the potential toxicity of these nanoparticles is not well understood. Although nanomaterials are attractive systems for biomedical applications, the human exposure and the environmental impact of these systems are still not well known but are of great interest.

The concept of nanotoxicology has emerged recently, after the rapid development and introduction of a significant number of nanoparticles in the industrial processes and consequently in the market (Donaldson et al., 2004). Therefore, the exposure of organism to nanoparticles has become an interesting field of research, in order to evaluate their interaction with cell membranes, their cell uptake, as well as their transport into cells.

It is well established that nanoparticles show several individual characteristics, such as particle size, hydrophobicity and surface properties and surface functionalization that can be different compared to the corresponding bulk materials of the same composition.

Many studies suggest that the physicochemical properties of SiNP might provide potential risk to human health, causing toxic effects especially in the liver (Kumar et al., 2010; Sun et al., 2011; Ye et al., 2010; Yu et al., 2009). The adverse events of SiNP exposure are still unclear. Some investigators have hypothesized that nanoparticles aggregation could not only increase their size but also modify their surface area (Ahamed et al., 2008), being the surface area the main characteristic for cytotoxic activity of disperse nanoparticles (Rabolli et al., 2010). Both aggregated and non-aggregated SiNP demonstrated the same cytotoxic activity, probably due to the unmodified surface area of aggregated particles (Borm et al., 2006), indicating that the greater surface area of stable monodisperse particles is maintained in the aggregates, and thus, the toxicity is not influenced (Rabolli et al., 2011).

Recently, several studies have shown the cytotoxicity effects of SiNP, including reduction of cell viability and oxidative damage in cellular membrane (Lin et al., 2006; Napierska et al., 2009). For example, it was confirmed that SiNP could induce oxidative stress, pro-inflammatory responses and clusters of topoisomerase I in the cellular nucleoplams, as well as, they could promote fibrogenesis in Wistar rats (Park and Park, 2009;

Wang et al., 2009). In addition, long term exposure to SiNP could also accumulate in embryonic cells (Park et al., 2009).

In the present work, the *in vitro* cytotoxicity of uncoated nanoparticles and coated SiNP with different mucoadhesive polymers (chitosan, sodium alginate, PEG 6000 and PEG 20000) was investigated. The objective was to evaluate and compare the potential biological effects produced by different SiNP in two cell lines: the HepG2 (human hepatocyte model cell line, obtained from a human hepatocellular carcinoma) and Caco-2 (human enterocyte model cell line, obtained from colorectal adenocarcinoma), which represent the target tissues and routes for exposure to oral insulin-nanoparticles. For this purpose, to elucidate the relationship between cell damage and modified SiNP, Alamar Blue method was used. Alamar Blue is a sensitive oxidation-reduction indicator added to the cell medium which can be measured either by colorimetric or fluorimetric determinations upon reduction by living cells. The reduction of Alamar Blue can be mediated by mitochondrial, cytosolic and microsomal enzymes (Gonzalez and Tarloff, 2001; O'Brien et al., 2000). For these reasons, Alamar Blue has been considered superior to classical dyes for cell viability, such as (4,5-dimethylthiazol-2-yl)-2,5-diphenyl-tetrazolium bromide (MTT), which kills the cells to obtain measurements (Ahmed et al., 1994).

Although, the toxicity of silica, chitosan, sodium alginate and PEG is well-know, few studies with the effect of modified SiNP on cell viability have been reported (Chang et al., 2007; Kneuer et al., 2000; Lebret et al., 2008; Ruizendaal et al., 2009).

7.2. Materials and methods

7.2.1. Materials

Tetraethyl orthosilicate (TEOS, 98 %), NH_3 25 %, PEG with M_w of 6000 and 20000 Da (PEG 6000; PEG 20000) were purchased from Merck (Darmstadt, Germany). Chitosan low molecular weight (235 g/mol, degree of deacetylation of 78.5 %), ethanol 99.9 %, trehalose dehydrate and bovine serum albumin (BSA) were purchased from Sigma-Aldrich (Steinhein, Germany). Sodium alginate (198.11 g/mol) was purchased from VWR Portugal (Carnaxide, Portugal). Solution of 100 IU/mL of human insulin (Humulin® R) was purchased from Eli Lilly (Lisbon, Portugal). Dulbecco's Modified Eagle's Medium (DMEM), foetal bovine serum (FBS), penicillin/streptomycin, L-glutamine, 0.05 % tripsin-EDTA and Alamar Blue (AB) were purchased from Gibco (Alfagene, Invitrogen, Portugal). Ultra-purified water was obtained from Milli® Q Plus system (Millipore, Germany).

7.2.3. Synthesis of nanoparticles

SiNP were synthesized by sol-gel technology at room temperature via hydrolysis and condensation of TEOS under high shear homogenization (Ultra-Turrax, IKA, T25) using NH_3 as catalytic agent. The obtained nanoparticles were centrifuged and washed with a mixture of ethanol and ultra-purified water (1:1, v/v) by 2 cycles at 12,000 rpm for 5 min (Spectrafuge16M, Lambnet International, Inc.) as described in chapter II.

For coating SiNP, a solution of chitosan (CH) (0.3 %, w/v) at pH 4.5, or sodium alginate (SA) (0.3 % , w/v) at pH 4.5, or PEG 60002 or PEG 20000 (2 %, w/v) at pH 6.8 were added to nanoparticles, stirred for 30 min and centrifuged as described above.

For insulin associated to SiNP, 1 mL of human insulin (100 IU/mL, pH 7.0) was added to 10 mg of uncoated SiNP under gentle stirring (300 rpm) for 30 min into ice bath.

For coated insulin-SNP, 1.0 mL of human insulin (100 IU/mL, pH 7.0) was dissolved in 2 mL of the hydrophilic polymer solutions, mixed for 30 min under magnetic stirring and then added to SiNP (10 mg) under gentle stirring (300 rpm) for more 30 min into ice bath. The nanoparticles were centrifuged at 5000 rpm for 5 min and the pellet was freeze-dried during 24 h with trehalose (10 %, w/v) as cryoprotectant agent to prevent particle aggregation. The obtained nanoparticles were stored at 4 °C until further use.

7.2.4. Cell cultures and maintenance

The experiments were conducted at the Cell Biology and Bioenergetic Laboratory of the Center for Research and Technology of Agro-Environmental and Biological Sciences, Vila Real, Portugal. HepG2 (Human hepatocellular carcinoma cell line; ATCC® Number: HB-8065 ™; were a gift from Professor Carlos Palmeira, CNC-UC, Coimbra, Portugal) and Caco-2 (Human colon adenocarcinoma cell line; Cell Line Service, CLS Cell Lines Service, Eppelheim, Germany) cells were used as cell models to perform the cytotoxicity assay of different nanoparticles. HepG2 and Caco-2 cells were maintained in DMEM (Dulbecco's Modified Eagle Medium) supplemented with 10 % (v/v) foetal bovine serum (FBS), antibiotics (100 U/mL of penicillin and 100 µg/mL of streptomycin) and 1 mM L-glutamine in an atmosphere of 5 % CO_2 /95 % air, at 37 °C with controlled humidity.

7.2.5. *In vitro* cytotoxicity assay

The cytotoxicity of nanoparticles was evaluated by comparing the proliferation rate and viability of non-exposed HepG2 and Caco-2 cells (control) with exposed HepG2 and Caco-2 cells, to appropriate concentrations during defined periods of time (see later), using the AB reduction method.

For the cytotoxicity assay cells were detached from the culture flaks with trypsin, counted and seeded in 96-well microplates at a density of 5×10^4 cells/mL (100 µL/well). Lyophilized nanoparticles were diluted in FBS-free culture media to various concentrations, ranging from 50 to 500 µg/mL (0, 50, 200, 500 µg/mL). Then, 24 h after seeding, the culture media was removed and replaced by media containing the nanoparticles (at defined concentrations). For each concentration of nanoparticles, different microplates were prepared for 24 h and 48 h of exposure. After the exposure time, the media containing the nanoparticles (and the control) was removed and replaced by FBS-free medium supplemented with 10 % (v/v) of AB. The absorbance readings occurred about 4 h after AB addition, at 570 and 620 nm using a microplate reader (Multiskan Ascent). The percentage of AB reduction was calculated according to the equation 7.1:

$$\%\ AB\ reduction = \frac{(\varepsilon_{ox}\lambda_2)(\mathrm{A}\lambda_1) - (\varepsilon_{ox}\lambda_1)(\mathrm{A}\lambda_2)}{(\varepsilon_{red}\lambda_1)(\mathring{\mathrm{A}}\lambda_2) - (\varepsilon_{red}\lambda_2)(\mathring{\mathrm{A}}\lambda_1)}\ x\ 100 \qquad \text{Equation 7.1}$$

where, $\varepsilon_{ox}\lambda_1$ is the molar extinction coefficient of oxidized AB at 570 nm, $\varepsilon_{ox}\lambda_2$ is the molar extinction coefficient of oxidized AB at 620 nm, $\varepsilon_{red}\lambda_1$ is the molar extinction coefficient of reduced AB at 570 nm, $\varepsilon_{red}\lambda_2$ is the molar extinction coefficient of reduced AB at 620 nm, $A\lambda_1$ and $A\lambda_2$ are the absorbance of test wells at 570 and 620 nm, respectively, and $A\lambda_1$ and $A\lambda_2$are the absorbance of the negative control wells (media plus AB but no cells) at 570 and 620 nm, respectively.

7.2.6. Evaluation of alterations on cell morphology

The morphology of Caco-2 cells was evaluated by observation using an inverted microscope (Olympus IX51) equipped with a digital camera and a program for image analysis (Cell^A; Olympus). Cells were incubated with the various coated and uncoated nanoparticles for 48 h at 37 ºC, and cells were observed and compared with non-exposed cells (control). Pictures from all conditions were taken, using the Cell^A image software (Olympus), and visually analyzed.

7.2.7. Statistical analysis

Results are expressed in terms of viability as percentage of control (untreated cells), and are a mean of octuplicates ± S.D. Statistically evaluation of data was performed using a one-way analysis of variance (ANOVA) test. Bonferroni's Multiple Comparison test was carried out to compare the significance between the different groups. A *p*-value < 0.05 was considered statistically significant.

7.3. Results and discussions

In this study, the toxicity of the different nanoparticles was evaluated by AB reduction assay using HepG2 and Caco-2 cell lines. The viability of Caco-2 (leftmost columns) and HepG2 (rightmost columns) cells after 48 h exposure to uncoated SiNP is shown on Figure 7.1. Figure 7.2 shows the effect of SiNP coated with chitosan (a) and SiNP coated with sodium alginate (b) and Figure 7.3 shows the results of and SiNP coated with PEG 6000 (a) and PEG 20000 (b), at different concentrations ranging from 50 to 500 µg/mL. For each condition, we also evaluated the toxicity of unloaded and insulin-loaded nanoparticles (Ins-SiNP, Ins-SiNP-CH, Ins-SiNP-SA, Ins-SiNP-PEG 6000 and Ins-SiNP-PEG 20000). Results are compared to unexposed cells (control).

For uncoated SiNP, cell viability ranged from 97.67 ± 0.19 % (for 50 µg/mL) to 108.97 ± 2.17 % (for 200 µg/mL) for Caco-2 cells (Figure 7.1, left) and from 92.63 ± 1.04 % (for 50 µg/mL) to 101.45 ± 3.41 % (for 200 µg/mL) for HepG2 cells (Figure 7.1, right). No significant changes, compared with the control group, were observed in both cell lines and at all tested concentrations after 48 h exposure to uncoated SiNP ($p > 0.05$). These results can be attributed to the two factors: the size or the surface charge of nanoparticles. In general, it is know that there is a correlation between the size of the particles and cell toxicity. As a particle decreases in size, its surface area per unit mass increases leading to an increase of surface energy which in turn makes it biologically more reactive (Nel et al., 2009). According to Li and co-workers (Li et al., 2011) smaller SiNP (~19 nm) possess high toxicity effects resulting in several morphological damages on HepG2 cells, including cellular shrinkage, lack of cell connection and nuclear condensation. In the present work, the low cytotoxicity observed with SiNP in both cell lines can be attributed to the size of SiNP (~280 nm). However, in the present study, the size of nanoparticles was only measured in aqueous media. The cell culture media for *in vitro* studies present an environment with high ionic strength, fixed pH and proteins that can affect the stability of the nanoparticles (Napierska et al., 2009b; Thomassen et al., 2009). Probably, in the present study, SiNP could form aggregates after their dispersion in DMEM leading to a smaller surface area and consequently to a reduced cell toxicity. Other parameter that can be considered is the role of the particle surface. In this case, SiNP have negative charge at pH 7. Several studies have reported that negatively charged nanoparticles exert very little or no toxicity on biological membranes, in comparison to positively charged particles (Bhattacharjee et al., 2010). In Figure 7.1 (a), a slight decrease in cell viability is

observed when they are exposed to insulin-loaded nanoparticles, compared to control. The decrease in more evident in Caco-2 cells than in HepG2, but the differences are minimal.

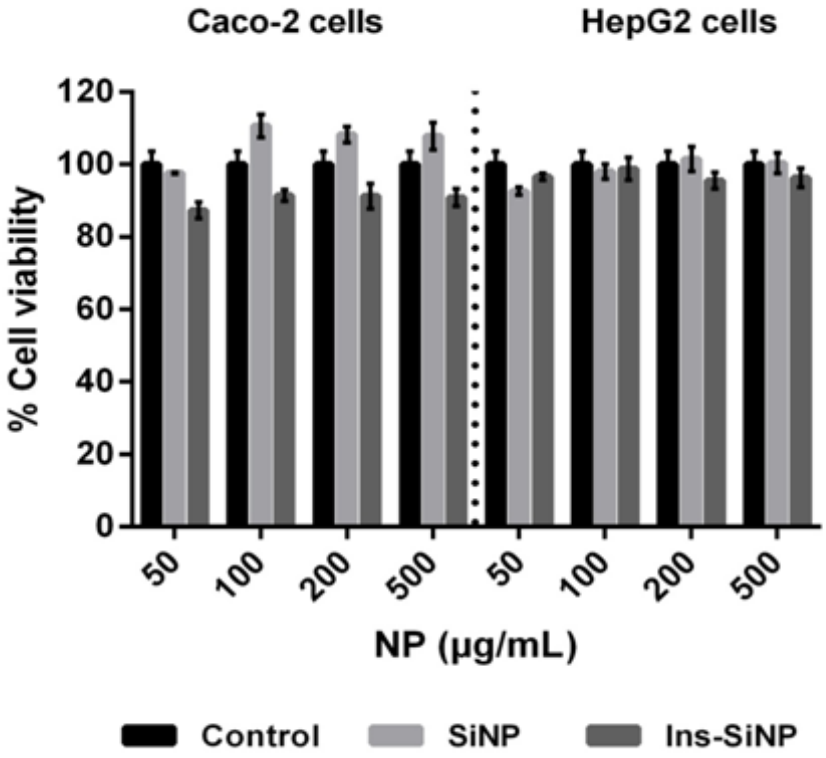

Figure 7.1. Viability of Caco-2 (leftmost columns) and HepG2 (rightmost columns) cells after 48 h exposure to 50, 100, 200 and 500 µg/mL of uncoated SiNP, unloaded (light grey bars) and insulin-loaded (dark grey bars). Cell viability is expressed as % of control (untreated cells). For each cell line, three independent experiments (each with 8 replicates) were carried out.

The biological effects of the nanoparticles can be modified by the reactive groups inserted onto the particle surface. It is important to consider that the coating of the nanoparticles with chitosan, sodium alginate or PEG may alter the toxicity of the free polymers. For SiNP coated with chitosan, the cell viability ranged from 76.68 ± 1.17 % (for 500 µg/mL) to 96.84 ± 0.97 % (for 50 µg/mL) for Caco-2 cell (Figure 7.2 (a, left) and from 85.99 ± 8.99 % (for 200 µg/mL) to 99.44 ± 2.91 % (for 50 µg/mL) for HepG2 cells (Figure 7.2 (a, right). As shown in Figure 7.2 (a, right), compared with the control group, all concentrations reduced significantly the cell viability ($p < 0.05$), although reduction in not higher than 25 %. In addition, increasing the nanoparticles concentration, the cell viability is

reduced. These results suggest that higher concentration lead to higher cytotoxicity. On the other hand, in HepG2 cells, only the concentration of 50 μg/mL is not statistically different from control, after 48 h exposure of SiNP-CH (Figure 7.2 (a, left). Comparing with uncoated SiNP, it is clearly observed that SiNP coated with chitosan showed higher toxicity in both cell lines. Although, *in vitro* evaluation of chitosan and chitosan nanoparticles has been performed in a wide range of cell lines demonstrating low cytotoxicity (Huang et al., 2004), cationic compounds can cause cell damage. The presence of the positive charges on the SiNP-CH consequently affects the interaction with cells leading to a decrease of cell viability. Many studies suggest that cationic polymers imply higher toxicity due to the interactions with the membrane plasma and/or with negatively charged cell components and proteins (Choksakulnimitr et al., 1995; Fischer et al., 2003). Also, some works have showed that chitosan coated nanoparticles can induce cell apoptosis in some extend (Zhu et al., 2009). In this case, insulin-loaded nanoparticles decreased the cytotoxicity of SiNP-CH after 48 h of incubation at higher concentrations being more evident in Caco-2 cells. This phenomenon can be related to the possible decrease of the interaction between the positively charged amino groups of chitosan with the anionic components of the glycoproteins on the cell membrane surface, leading to higher cell viability.

Regarding to SiNP-SA, Caco-2 cells were also more susceptible than HepG2 cells to SiNP coated with sodium alginate exposure (Figure 7.2 (b)). All concentrations of the nanoparticles reduced significantly the viability of Caco-2 cells, compared to control (Figure 7.2 (b), left). However, only the concentration of 500 μg/mL of SiNP-SA reduced significantly HepG2 viability (Figure 7.2 (b), right). Similar results were obtained by Douglas and co-workers (Douglas et al., 2006), demonstrating that high concentrations of alginate-chitosan nanoparticles resulted in a significant decrease of 293 T cells viability after 24 h of incubation in comparison to chitosan polymer.

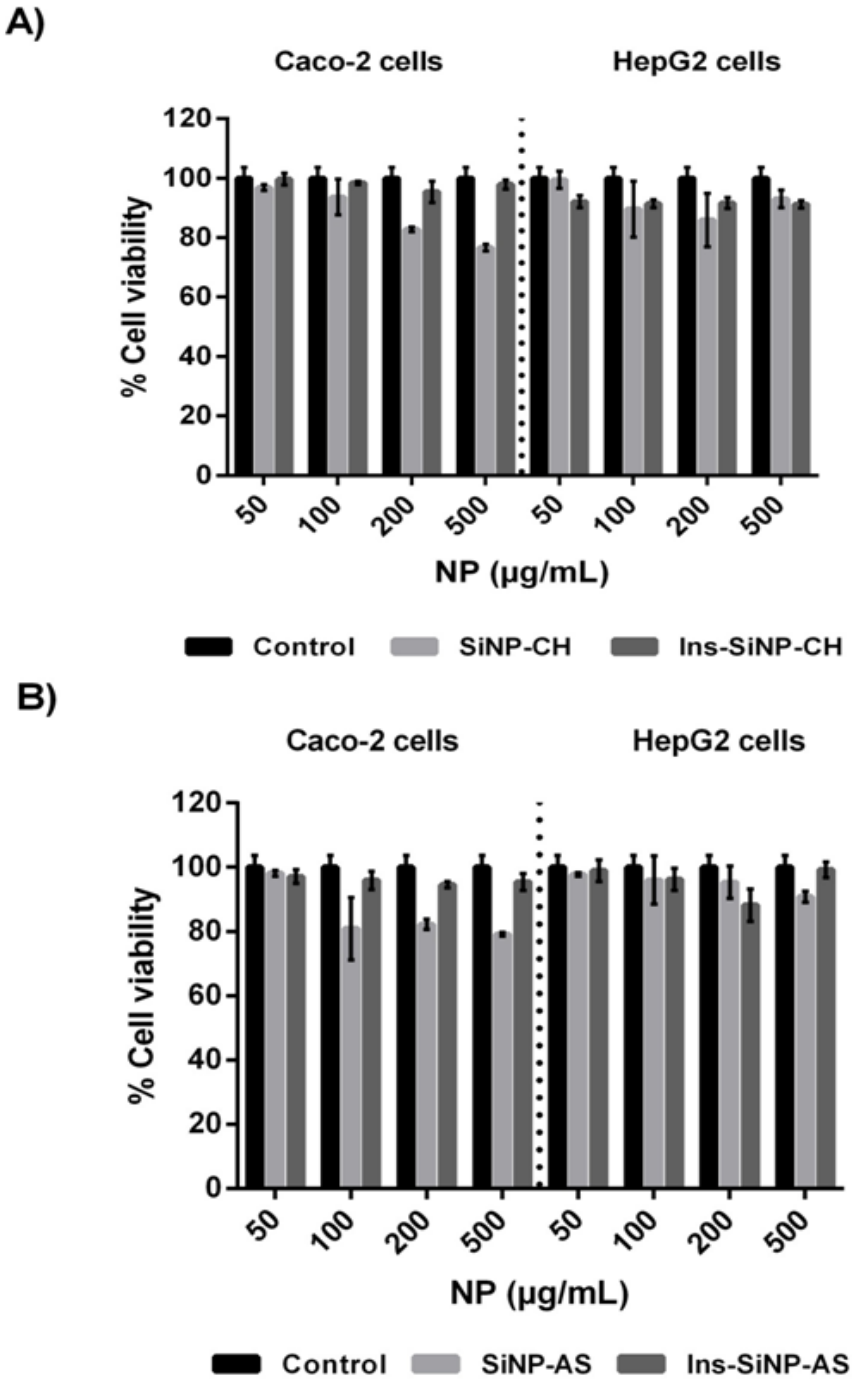

Figure 7.2. Viability of Caco-2 (leftmost columns) and HepG2 (rightmost columns) cells after 48 h exposure to 50, 100, 200 and 500 µg/mL of SiNP coated with chitosan (a) and sodium alginate (b). Cell viability is expressed as % of control (untreated cells). For each cell line, three independent experiments (each with 8 replicates) were carried out.

After insulin incorporation into SiNP-SA, all concentrations tested show low cytotoxicity on Caco-2 (Figure 7.2 (b), left) and HepG2 cells (Figure 7.2 (b), right). These

results are in evident agreement with other studies demonstrating high biocompatibility of alginate as a coating or even as a carrier (Borges et al., 2006).

In general we can observe a low degree of toxicity for all particles at the concentration range tested. Although, for the unloaded nanoparticles, a reduction in the cell viability is observed which is concentration dependent, and more evident for Caco-2 cells, as observed for SiNP-CH (Figure 7.2 (a)) and for SiNP-SA (Figure 7.2 (b)).

Concerning to the coating with PEG, two different PEG polymers were studied differing on chain extent and thus on MW, the PEG 6000 and PEG 20000 were used. The viability of Caco-2 and HepG2 cells after exposure to SiNP-PEG 6000 and SiNP-PEG 20000 is shown in Figure 7.3 (a) and Figure 7.3 (b), respectively. Regard to the nanoparticles concentration effect on cytotoxicity, we could note that high concentrations of SiNP-PEG 6000 (200 and 500 µg/mL) induced high cytotoxic events on both cell lines (Figure 7.3 (a)), while SiNP-PEG 20000 did not significantly affect the HepG2 and Caco-2 cell viability (Figure 7.3 (b)). In general, conjugation of PEG to nanoparticles is recognized as being nontoxic by all routes of administration. However, comparing to uncoated SiNP, the concentrations of 200 and 500 µg/mL of SiNP-PEG 6000, in both cell lines, reduced significantly cell viability. Cho and co-workers (Cho et al., 2009) showed that gold nanoparticles coated with PEG 5000 can induce acute inflammation and apoptosis in the mouse liver. Higher cell viability, especially at concentration of 200 and 500 µg/mL was observed for SiNP-PEG 20000 compared to that of SiNP-PEG 6000 (Figure 7.3 (a) and (b)). This result can be attributed to the long chain structure of PEG 20000 leading to a higher steric effect. The flexibility of a long PEG chain like PEG 20000 was supposed to make it cover greater surface areas. Similar observations were obtained by Mao and co-workers (Mao et al., 2005) that verified lower cytotoxicity effect of trimethyl chitosan (TMC) grafted by PEG 5 kDa in comparison to TMC grafted by PEG 550 Da. However, some studies showed that low PEG chain length used for poly(ethylene imine) (PEI) coating induced low cytotoxic and oxidative stress response in lung cell line (Beyerle et al., 2010).

No cytotoxicity effect on cell proliferation and viability was observed after the incorporation of insulin into SiNP-PEG 6000 (Figure 7.3 (a)) and SiNP-PEG 20000 (Figure 7.3 (b)) for both cell lines.

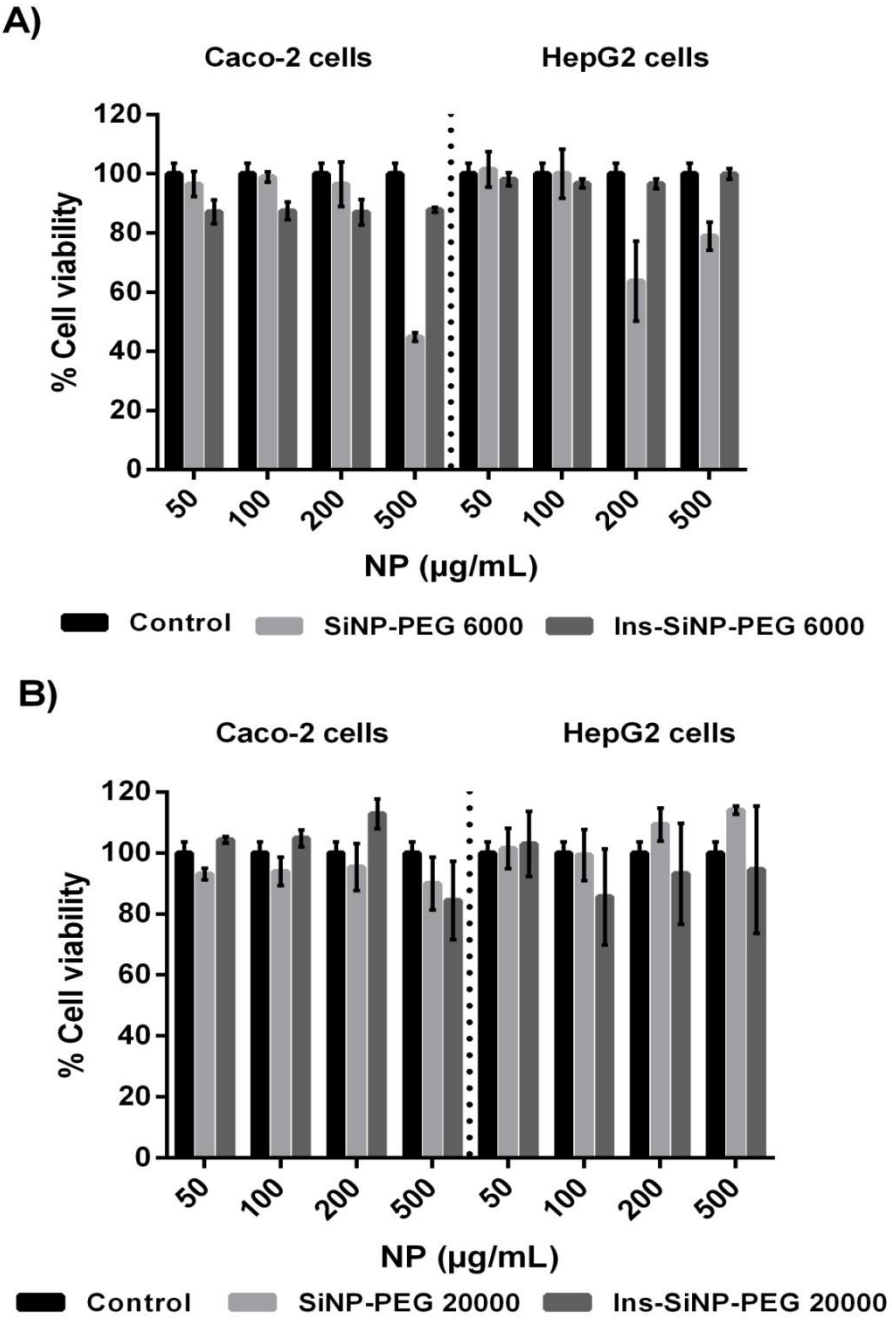

Figure 7.3. Viability of Caco-2 (leftmost columns) and HepG2 (rightmost columns) cells after 48 h exposure to 50, 100, 200 and 500 µg/mL of SiNP coated with PEG 6000 (a) and SiNP coated with PEG 20000 (b). Cell viability is expressed as % of control (untreated cells). For each cell line, three independent experiments (each with 8 replicates) were carried out.

Figure 7.4 shows two pictures of Caco-2 cells, one of unexposed cells (control, Figure 7.4 (a) and after the treatment with SiNP-PEG 6000 at 500 µg/mL (Figure 7.4, (b)). In Figure 7.4 (b) we can observe the formation of vacuole-like stuctures in the Caco-2 cell body after

the treatment of SiNP-PEG 6000 at 500 µg/mL, indicating a possible endocytosis of these particles. In the presence of insulin, the endocytosis of SiNP-PEG 6000 could be inhibited, probably due to the contact of insulin with its specific cell surface receptor, protecting, thus the cell against the harmful effects due to endocytosis (Gupta et al., 2003). As a result, Ins-SiNP-PEG 6000 increased Caco-2 viability compared to SiNP-PEG 6000 at 500 µg/mL concentration.

The presence of vacuoles was observed only for Caco-2 cells exposed to SiNP-PEG 6000 at the higher concentrations. We also can observe that the cell-to-cell adhesions are mostly lost indicating that cell physiology was altered.

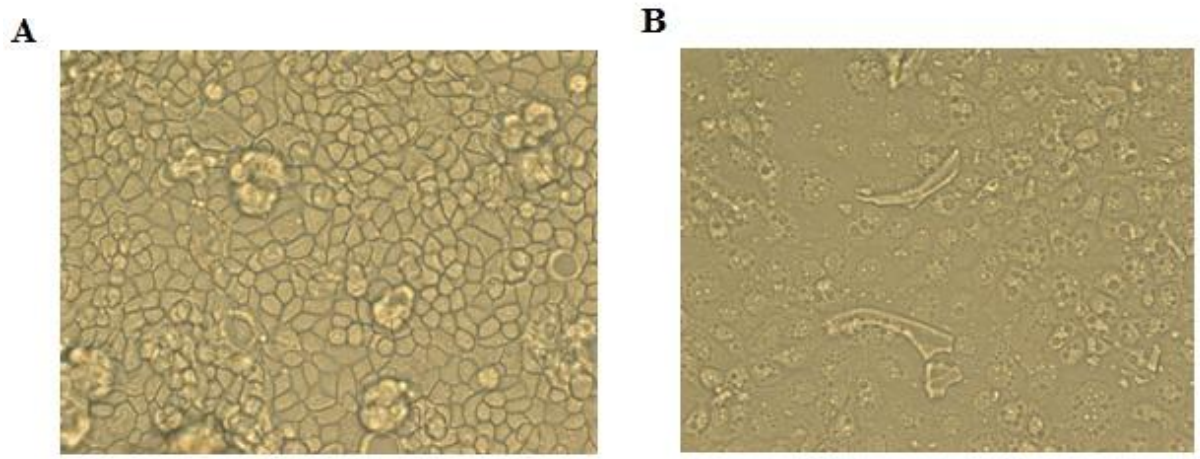

Figure 7.4. Appearance of Caco-2 cells observed under optical inverted microscope. (A) control cells and (B) cells incubated with SiNP-PEG 6000 at 500 µg/mL (amplification 400x).

7.4. Conclusions

One of the major concerns of the present work was to develop an efficient and safe formulation as a vehicle to deliver proteins and peptides orally. In this context, insulin was incorporated into SiNP with distinct surface characteristics. The surface modification of SiNP was achieved by coating with different mucoadhesive polymers (chitosan, sodium alginate, PEG 60000 and PEG 20000) *via* sol-gel technology.

The potential toxicity and hazardous effects of nanoparticles are of great concern as previous mentioned. Therefore, in this chapter, the emphasis was to evaluate the toxicity of SiNP with novel coatings for potential oral insulin delivery. For this purpose, the viability of HepG2 and Caco-2 cell lines after the incubation with nanoparticles was performed by Alamar Blue assay.

From these results, the cell toxicity studies demonstrated that uncoated or coated nanoparticles provide high biocompatibility. For unloaded nanoparticles, the reduction in cell viability was concentration dependent only for SiNP-CH and SiNP-SA, being more evident for Caco-2 cells. It can be concluded that in general there was no toxicity of different nanoparticles in all tested concentrations for both cell lines, except for SiNP-PEG 6000 at high concentrations. This observation can be attributed to the possible endocytosis of these particles due to the presence of vacuoles in the Caco-2 cell body which was confirmed by microscope observations.

Further extensive studies, such as cell internalization and *in vivo* performance of the developed formulations are required to confirm these preliminary results.

7.5. References

Ahamed, M., Karns, M., Goodson, M., Rowe, J., Hussain, S.M., Schlager, J.J., Hong, Y., 2008. DNA damage response to different surface chemistry of sil-ver nanoparticles in mammalian cells. Toxicol. Appl Pharmacol 233, 404-410.

Ahmed, S.A., Gogal, R.M., Walch, J.E., 1994. A new rapid and simple non-radioactive assay to monitor and determine the proliferation of lymphocytes: an alternative to [^{3}H]thymidine incorporation assay. J Immunol Methods 170, 211-224.

Beyerle, A., Merkel, O., Stoeger, T., Kissel, T., 2010. PEGylation affects cytotoxicity and cell-compatibility of poly(ethylene imine) for lung application: Structure–function relationships. Toxicol Appl Pharmacol 242, 146-154.

Bhattacharjee, S., de Haan, L., Evers, N., Jiang, X., Marcelis, A., Zuilhof, H., Rietjens, I., Alink, G., 2010. Role of surface charge and oxidative stress in cytotoxicity of organic monolayer-coated silicon nanoparticles towards macrophage NR8383 cells. Particle Fibre Toxicol 7, 25.

Borges, O., Cordeiro-da-Silva, A., Romeijn, S.G., Amidi, M., de Sousa, A., Borchard, G., Junginger, H.E., 2006. Uptake studies in rat Peyer's patches, cytotoxicity and release studies of alginate coated chitosan nanoparticles for mucosal vaccination. J Control Release 114, 348-358.

Borm, P.J., Robbins, D., Haubold, S., Kuhlbusch, T., Fissan, H., Donaldson, K., Schins, R., Stone, V., Kreyling, W., Lademann, J., Krutmann, J., Warheit, D., Oberdorster, E., 2006. The potential risks of nanomaterials: a review carried out for ECETOC. Part. Fibre Toxicol 3:11.

Chang, J.-S., Chang, K.L.B., Hwang, D.-F., Kong, Z.-L., 2007. In vitro cytotoxicitiy of silica nanoparticles at high concentrations strongly depends on the metabolic activity type of the cell line. Environ SciTechnol 41, 2064-2068.

Cho, W.-S., Cho, M., Jeong, J., Choi, M., Cho, H.-Y., Han, B.S., Kim, S.H., Kim, H.O., Lim, Y.T., Chung, B.H., Jeong, J., 2009. Acute toxicity and pharmacokinetics of 13 nm-sized PEG-coated gold nanoparticles. Toxicol Appl Pharmacol 236, 16-24.

Choksakulnimitr, S., Masuda, S., Tokuda, H., Takakura, Y., Hashida, M., 1995. In vitro cytotoxicity of macromolecules in different cell culture systems. J Control Release 34, 233-241.

Donaldson, K., Stone, V., Tran, C.L., Kreyling, W., Borm, P.J., 2004. Nanotoxicology. Occup Environ Med 61, 727 -728.

Douglas, K.L., Piccirillo, C.A., Tabrizian, M., 2006. Effects of alginate inclusion on the vector properties of chitosan-based nanoparticles. J Control Release 115, 354-361.

Fischer, D., Li, Y., Ahlemeyer, B., Krieglstein, J., Kissel, T., 2003. In vitro cytotoxicity testing of polycations: influence of polymer structure on cell viability and hemolysis. Biomaterials 24 1121-1131.

Gonzalez, R.J., Tarloff, J.B., 2001. Evaluation of hepatic subcellular fractions for Alamar blue and MTT reductase activity. Toxicol in Vitro 15, 257-259.

Gupta, A.K., Berry, C., Gupta, M., Curtis, A., 2003. Receptor-mediated targeting of magnetic nanoparticles using insulin as a surface ligand to prevent endocytosis. IEEE Trans Nanobioscience 2, 255-261.

Huang, M., Khor, E., Lim, L.-Y., 2004. Uptake and cytotoxicity of chitosan molecules and nanoparticles: effects of molecular weight and degree of deacetylation. Pharm Res 21, 344-353.

Kneuer, C., Sameti, M., Bakowsky, U., Schiestel, T., Schirra, H., Schmidt, H., Lehr, C.-M., 2000. A nonviral DNA delivery system based on surface modified silica-nanoparticles can efficiently transfect cells in vitro. Bioconjugate Chem 11, 926-932.

Kumar, R., Roy, I., Ohulchanskky, T.Y., Vathy, L.A., Bergey, E.J., Sajjad, M., Prasad, P.N., 2010. In vivo biodistribution and clearance studies using multimodal organically modified silica nanoparticles. ACS Nano 4, 699-708.

Lebret, V., Raehm, L., Durand, J.-O., Smaïhi, M., Werts, M.V., Blanchard-Desce, M., Méthy-Gonnod, D., Dubernet, C., 2008. Surface functionalization of two-photon dye-doped mesoporous silica nanoparticles with folic acid: cytotoxicity studies with HeLa and MCF-7 cancer cells. J Sol-Gel Sci Technol 48, 32-39.

Li, Y., Sun, L., Jin, M., Du, Z., Liu, X., Guo, C., Li, Y., Huang, P., Sun, Z., 2011. Size-dependent cytotoxicity of amorphous silica nanoparticles in human hepatoma HepG2 cells. Toxicol in Vitro 25, 1343-1352.

Lin, W., Huang, Y.-w., Zhou, X.-D., Ma, Y., 2006. In vitro toxicity of silica nanoparticles in human lung cancer cells. Toxicol Appl Pharmacol 217, 252-259.

Mao, S., Shuai, X., Unger, F., Wittmar, M., Xie, X., Kissel, T., 2005. Synthesis, characterization and cytotoxicity of poly(ethylene glycol)-graft-trimethyl chitosan block copolymers. Biomaterials 26, 6343-6356.

Napierska, D., Thomassen, L.C., Rabolli, V., Lison, D., Gonzalez, L., Kirsch-Volders, M., Martens, J.A., Hoet, P.H.R.S., 2009a. Size-dependent cytotoxicity of monodisperse silica nanoparticles in human endothelial cells. Small 5, 846-853.

Nel, A.E., Madler, L., Velegol, D., Xia, T., Hoek, E.M., Somasundaran, P., Klaessig, F., Castranova, V., Thompson, M., 2009. Understanding biophysicochemical interactions at the nano-bio interface. Nat Mater 8, 543-557.

O'Brien, J., Wilson, I., Orton, T., Pognan, F., 2000. Investigation of the Alamar Blue (resazurin) fluorescent dye for the assessment of mammalian cell cytotoxicity. Eur J Biochem 267, 5421-5426.

Park, E.J., Park, K., 2009. Oxidative stress, pro-inflammatory responses induced by silica nanoparticles in vivo and in vitro. Toxicology Letters 184, 18-25.

Park, M.V.D.Z., Annema, W., Salvati, A., Lesniak, A., Elsaesser, A., Barnes, C., McKerr, G., Howard, C.V., Lynch, I., Dawson, K.A., Piersma, A.H., de Jong, W.H., 2009. In vitro developmental toxicity test detects inhibition of stem cell differentiation by silica nanoparticles. Toxicol Appl Pharmacol 240, 108-116.

Rabolli, V., Thomassen, L.C., Princen, C., Napierska, D., Gonzalez, L., Kirsch-Volders, M., Hoet, P.H., Huaux, F., Kirschhock, C.E., Martens, J.A., Lison, D., 2010. Influence of size, surface area and microporosity on the in vitro cytotoxic activity of amorphous silica nanoparticles in different cell types. Nanotoxicology 4(3):307-18

Rabolli, V., Thomassen, L.C.J., Uwambayinema, F., Martens, J.A., Lison, D., 2011. The cytotoxic activity of amorphous silica nanoparticles is mainly influenced by surface area and not by aggregation. Toxicol Lett 206 197-203.

Ruizendaal, L., Bhattacharjee, S., Pournazari, K., Rosso-Vasic, M., de Haan, L.H.J., Alink, G.M., Marcelis, A.T.M., Zuilhof, H., 2009. Synthesis and cytotoxicity of silicon nanoparticles with covalently attached organic monolayers. Nanotoxicology 3, 339-347.

Sun, L., Li, Y., Liu, X., Jin, M., Zhang, L., Du, Z., Guo, C., Huang, P., Sun, Z., 2011. Cytotoxicity and mitochondrial damage caused by silica nanoparticles Toxicol In Vitro. 25(8):1619-1629

Thomassen, L.C.J., Aerts, A., Rabolli, V., Lison, D., Gonzalez, L., Kirsch-Volders, M., Napierska, D., Hoet, P.H., Kirschhock, C.E.A., Martens, J.A., 2009. Synthesis and characterization of stable monodisperse silica nanoparticle sols for in vitro cytotoxicity testing. Langmuir 26, 328-335.

Wang, F., Gao, F., Lan, M., Yuan, H.R.S., Huang, Y., Liu, J., 2009. Oxidative stress contributes to silica nanoparticle-induced cytotoxicity in human embryonic kidney cells. Toxicol In Vitro 23, 808-815.

Ye, Y., Liu, J., Xu, J., Sun, L., Chen, M., Lan, M., 2010. Nano-SiO_2 induces apoptosis via activation of p53 and Bax mediated by oxidative stress in human hepatic cell line. Toxicol In Vitro 24, 751-758.

Yu, K., Grabinski, C., Schrand, A., Murdock, R., Wang, W., Gu, B., Schlager, J., Hussain, S., 2009. Toxicity of amorphous silica nanoparticles in mouse keratinocytes. Nanopart Res 11, 15-24.

Zhu, L., Ma, J., Jia, N., Zhao, Y., Shen, H., 2009. Chitosan-coated magnetic nanoparticles as carriers of 5-Fluorouracil: Preparation, characterization and cytotoxicity studies. Colloids Surf B 68, 1-6.

Chapter VIII
General conclusions

8.1. Conclusion remarks of current study

Insulin therapy by subcutaneous injection is the most common treatment for Diabetes. However, due to their sensitivity to enzymatic degradation in the gastrointestinal tract, susceptibility to gastric pH and low intestinal permeability, the vast majority of the therapeutic proteins are administrated by parenteral route. Until now, the subcutaneous administration of insulin has been the main delivery route of insulin for the treatment of Diabetes type 1. Patients suffering from type 1 Diabetes *mellitus* do not synthesize enough insulin to sustain life and, thus, they depend on exogenous insulin for survival. Among the numerous advances in the biotechnology field, oral delivery is considered the most and convenient route for insulin administration because it can overcome the difficulties associated to subcutaneous route, such as, dairy injections, pain, risk of infection, edema, and fat deposition on the local of injection and it would have a great advantage of mimicking the natural insulin secretion pathway and, thus, of avoiding the hypoglycemic effect.

The rapid progress of nanotechnology in biomedical and biotechnology fields leads to the development of new drug delivery systems. Optimal pharmacokinetic performance and high bioavailability of pharmaceutical proteins might be of general interest for the design of novel and more efficient delivery technologies for oral peptide delivery. The association of therapeutic proteins with drug carriers, such as nanoparticles, has been extensively investigated for oral delivery because these systems can provide enteric protection of biomolecules from metabolic degradation, allow intimate contact with the absorption sites, as well as can improve protein absorption through the intestinal epithelium. Recently, due to their high porosity, specific surface area, biocompatibility and ease of surface functionalization, silica nanoparticles have been considered an excellent option as delivery systems for proteins. The presence of residual silanol groups at silica surface acts as reactive site for its surface modification by convenient organic groups.

In the present research, the properties of SiNP were modified by coating nanoparticle surface with mucoadhesive polymers, such as chitosan, sodium alginate and PEG in order to prolong and/or to intensify the contact between the system and the gut mucosa.

The first step involved the synthesis of SiNP. For preparing SiNP, a modified Stöber method at room temperature was applied, involving the hydrolysis and condensation of TEOS, using ammonium as catalyst agent. The formulations were optimized with the aim of achieving suitable Z-Ave and PI index using high shear homogenization. The influence of

TEOS and different homogenization speeds on Z-Ave and PI was assessed by a 2^2 factorial design approach. Higher concentration of TEOS and higher HSH speeds resulted in smaller silica nanoparticles. The optimal formulation was obtained using 0.43 $mol.L^{-1}$ of TEOS and 5000 rpm with low degree of particle agglomeration. However, the lyophilization in the absence of cryoprotectants agents of the optimized formulation resulted in severe particle aggregation due to the condensation of SiOH groups present at silica surface. Therefore, different cryoprotectants, such as trehalose, mannitol and sorbitol at several concentrations and ratios were selected to evaluate their ability in preserving silica nanoparticles during freeze-drying process. The developed SiNP could be successfully lyophilized using trehalose 10 % (v/w) at a ratio of (1:1) as cryoprotectants followed by sorbitol and mannitol. During the freeze-drying process, trehalose can replace water molecules due to the strong interaction via hydrogen bounds between silanol groups present in SiNP surface and the sugar, forming a stable layer around the particles and thus, preserving the particle physicochemical properties.

Bioadhesive polymers have been extensively used as strategy to improve the bioavailability of the drugs by prolonging their intestinal residence time. In this context, in the present study, chitosan, sodium alginate and PEG with two different molecular weights (6000 and PEG 20 000 Da) were selected for coating SiNP. The process of insulin association to nanoparticles consisted of simple adsorption. For coated SiNP, insulin was dissolved into polymeric solution and then added to SiNP. The association efficacy of insulin could be modulated by ionic interaction between the protein and nanoparticles. Insulin was less efficiently associated to uncoated silica nanoparticles due to the negative charges of both insulin and silica at pH 7.2. On the other hand, higher association efficacies were achieved for coated nanoparticles (~ 80%), demonstrating high affinity of insulin to the chains of hydrophilic polymers. Ionic interaction between negative charge of insulin and positive charge of the protonated amino groups of chitosan was favored at pH 5.5 leading to an association efficacy around of 90 %. The interaction between insulin and different nanoparticles was confirmed by DSC, X-ray and FTIR.

The structural integrity of insulin and its thermal stability after its dissolution in mucoadhesive polymers for nanoparticles preparation were examined by CD and nDSC, respectively. CD spectra showed that coating of silica nanoparticles did not affect the insulin structure. The thermal analysis demonstrated that SiNP were more effective in protecting insulin from thermal denaturation followed by PEG 6000. On the other hand, insulin

associated to alginate or chitosan led to a shift of endothermic peak to lower temperature as consequence of the interaction between the protein and the polymers. Therefore, chitosan and sodium alginate decreased the thermal stability of insulin.

In vitro biophysical interaction study between nanoparticles and biological membranes was carried out using model membrane systems based on phospholipid bilayers, such as that produced with DPPC. The influence of different nanoparticles on DPPC liposomes properties was assessed by nDSC analysis. This technique showed an increase of ΔH associate to main phase transition of DPPC liposomes when in contact with SiNP and SiNP-PEG 6000, suggesting a strong association of these nanoparticles with DPPC polar heads by forming hydrogen bonds and/or by electrostatic interaction, leading to an increase of Van der Waals interaction between lipid chains due to a reduction of electrostatic repulsion among choline groups.

The interaction of nanoparticles and mucin at pH 2.0 and 6.8 was assessed by measuring the zeta potential (ZP) of nanoparticles after mucin adsorption. The ZP of SiNP-CH and SiNP-SA decreased with increasing mucin concentration at both pH. The adsorption of mucin to chitosan was more pronounced at pH 6.8. At this pH, sialic mucin residues are negatively charged and the electrostatic attraction between mucin and positively charged chitosan is favored. In the case SiNP-SA, the interaction with mucin can be mainly mediated by hydrogen bonds, due to the presence of numerous surface carboxyl groups on anionic polymers, generating strong bioadhesive interactions by hydrogen bonds with the mucin. However, uncoated SiNP showed higher interaction with mucin at low pH. At pH 6.8, the interaction between SiNP and mucin was low due to the negative charges present at silica and mucin surfaces. On the other hand, the ZP of PEG-coated silica nanoparticles was not influenced by mucin concentrations at both pH values. This result can be attributed to the steric hindrance of PEG layers leading to lower adsorption of mucin molecules.

The insulin release profile was only significantly affected by uncoated SiNP and SiNP coated with PEG 6000 in comparison to insulin solution. The coating of nanoparticles with mucoadhesive polymers resulted in faster insulin release at gastric and intestinal conditions in comparison to uncoated nanoparticles due to the low interaction between insulin and silanol groups present onto the silica surface. However, the presence of PEG onto the silica surface did not significantly change the permeation behavior of insulin through the small intestinal mucosa of rats.

The surface modifications of SiNP resulted in different cytotoxicity responses. All nanoparticles showed to be biocompatible, demonstrating low toxicity in different human cancer cell lines (HepG2 and Caco-2), except for PEG 6000-coated nanoparticles at high concentrations. Microscope images revealed the formation of vacuoles in the Caco-2 cell body, indicating a possible endocytosis of these nanoparticles.

In summary, these results support the following conclusions:

(i) SiNP could be successfully coated with mucoadhesive polymers by sol-gel method which is a simple, of low cost and environmental friendly technology;

(ii) Higher insulin association efficacy was achieved for SiNP coated with mucoadhesive polymers in comparison to uncoated silica nanoparticles;

(iii) In general, for all tests carried out in this study, uncoated SiNP demonstrated to be the best formulation with improved physicochemical properties for oral insulin administration followed by PEG 6000-coated SiNP. Uncoated SiNP was more effective to protect insulin from thermal degradation, demonstrated better interaction with polar head groups of the biomembrane models, decreased insulin release at both gastric and intestinal pH, showed low interaction with mucin, as well as, low toxicity in the selected cell lines (HepG2 and Caco-2) for this study.

The results of the present thesis provided valuable data in assessing the *in vitro* performance of SiNP containing insulin coated with mucoadhesive polymers.

Chapter IX
Supplements

Supplement 1: Bradford method for insulin quantification

The amount of insulin associated to nanoparticles was determined by Bradford method, which is a simple, rapid and accurate method for the estimation of protein concentration (Bradford, 1976). The Bradford method is based on the binding of the dye Coomassie Blue G250 to arginyl and lysyl residues of proteins at acidic solutions (Compton and Jones, 1985). The cationic red and green forms have absorbance at 470 nm and 650 nm, respectively. When in the presence of proteins, the dye donates its free electron to ionizable groups on the protein and a complex between anionic form of the dye and amine groups of the protein is formed. Therefore, the binding of protein stabilize the anionic blue form of the dye. The protein-dye complex causes a shift in the absorption maximum of the dye to 595 nm.

S1. Experimental procedures

S1.1. Preparation of Bradford reagent

The Bradford reagent was prepared according to the protocol described by Bradford (Bradford, 1976) with some modifications added by others (Walker and Kruger, 2009). Firstly, 100 mg of Coomassie Blue Brilliant G-250 (Merck) were dissolved in 50 mL of ethanol 99.9 %. Afterwards, an amount of water was added to the mixture followed by the addition of 100 mL of phosphoric acid (85 %, w/v). Under ice bath, water was added to the solution to complete 1 L. The solution was then filtered through in a 0.45 μm cellulose membrane and stored in dark bottle at 4 °C.

S1.2. Sample preparation

A standard curve was prepared in PBS at pH 6.8 (FP VIII) (Figure S1.1) in triplicate, using bovine serum albumin (BSA) as the standard protein with concentrations ranging from 100 to 500 μg/mL.

For insulin association efficacy (AE), thirty milligrams of lyophilized nanoparticles were incubated in 3 mL of PBS at pH 6.8 without enzymes under magnetic stirring (150 rpm) at 30 min followed by centrifugation for 5 min. The supernatant containing released insulin (100 μL) was collected, added to 900 μL of Bradford reagent and incubated for 10 min at

room temperature for protein quantification using a spectrophotometry (Genesys 10S UV-Vis, Thermo Scientific) at 595 nm.

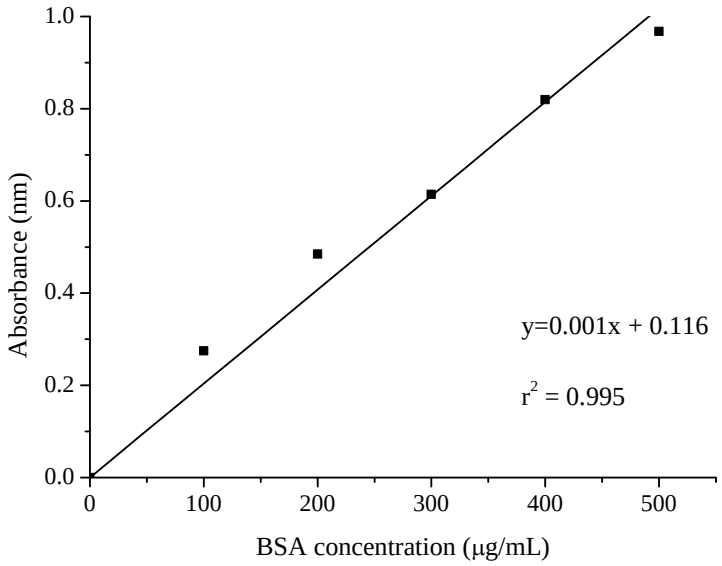

References

Bradford, M. M., 1976. A rapid and sensitive method for the quantitation of microgram quantities of protein utilizing the principle of protein-dye binding. Anal Biochem 72, 248-254.

Compton, S. J. and C. G. Jones, 1985. Mechanism of dye response and interference in the Bradford protein assay. Anal Biochem 151, 369-374.

Walker, J. and N. Kruger, 2009. The Bradford method for protein quantitation. The protein protocols handbook, Humana Press: 17-24.

Supplement 2: HPLC validation for insulin assay

A validation for the insulin quantification and permeation test was then required and undertaken in agreement with International Conference on Harmonization guidelines (ICH, 1996). The validation method was carried out in KCl/HCl buffer (pH 2.0) (FP VIII), PBS (pH 6.8) (FP VIII) and TC-199 buffer without glucose (pH 7.2). The analytical parameters analyzed were linearity, precision, accuracy and specificity.

S2.1. Linearity

The linearity of the method was defined by the slopes, Y-intercept of the calibration curve and the correlation coefficients. The mean peak areas *versus* concentration of each standard were treated by least-squares linear regression analysis. Calibration curves from seven human insulin standard solutions of different concentrations ranging from 1.96 to 98 µg/mL were prepared in HCl/KCl, PBS and TC-199 buffers. The linear regression equations for insulin in HCl, PBS and TC-199 buffers are demonstrated in Table S2.1. The results showed an excellent linearity between the insulin peak under curve and all standard concentrations within the concentrations range indicated above. The r^2 obtained was higher than 0.999, as frequently recommended (Épshtein, 2004).

Table S2.1. Linear regression equations obtained from validation process.

Calibration curves	**Equation**	r^2
HCl/KCl buffer at pH 2.0	$y = 212957.35x - 92104.14$	0.999
PBS at pH 6.8	$y = 213123.34x - 103899.26$	0.999
TC-199 buffer at pH 7.2	$y = 200583.62x - 43289.48$	0.999

S2.2. Specificity

The specificity of the method was confirmed by the analysis of placebo samples (buffers without insulin) to determine possible interferences. The set of chromatograms confirms that the peaks of the impurities were sufficiently well separated from insulin peak (Figures S2.1, S2.2, S2.3, S2.4, S2.5 and S2.6).

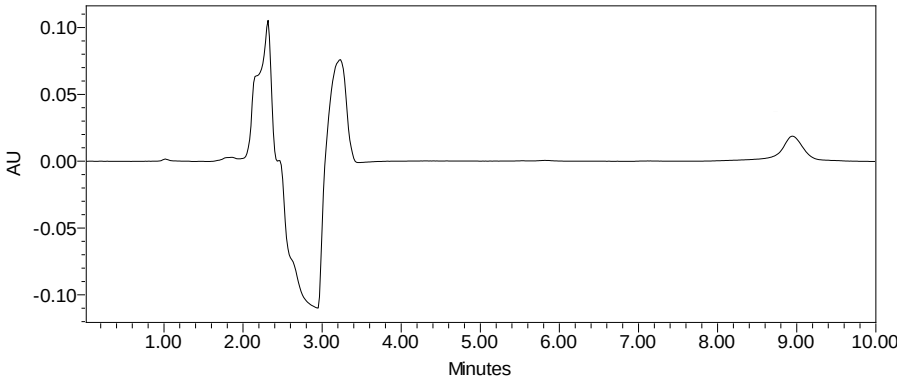

Figure S2.1. Representative chromatogram of insulin at 2 µg/mL in HCl/KCl buffer (pH 2.0).

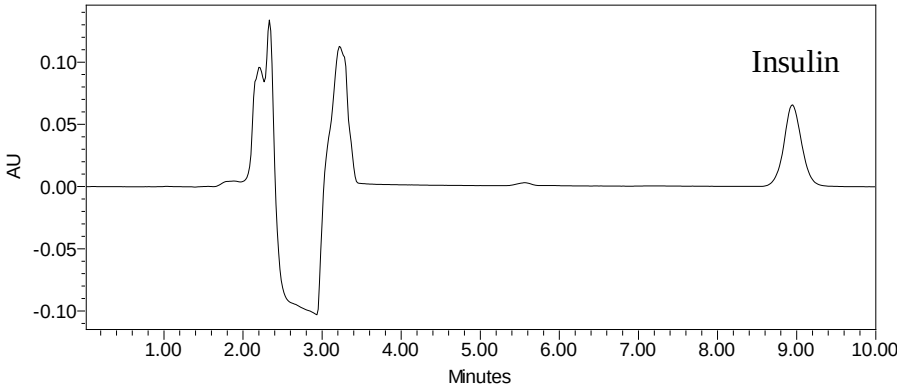

Figure S2.2. Representative chromatogram of insulin at 2 µg/mL in PBS (pH 6.8).

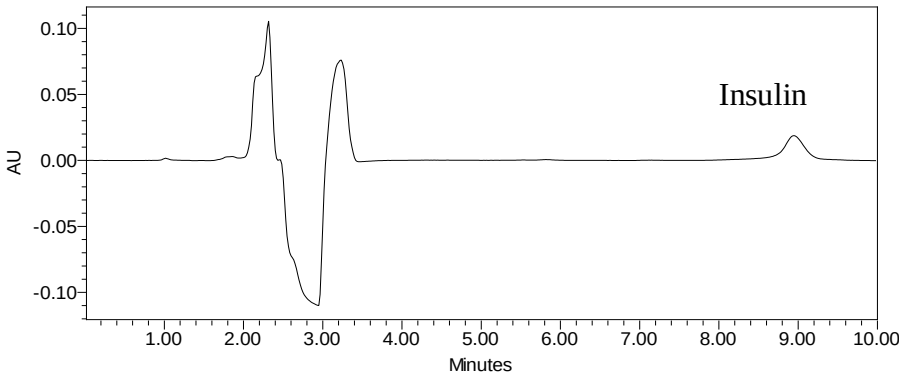

Figure S2.3. Representative chromatogram of insulin at 2 µg/mL in TC-199 buffer (pH 7.2).

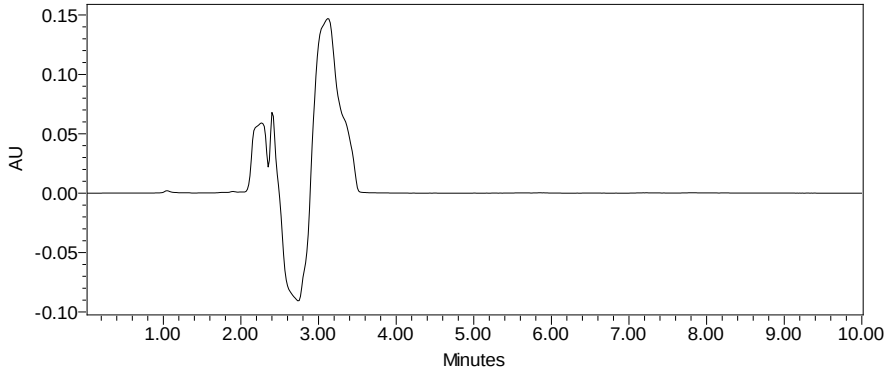

Figure S2.4. Representative chromatogram of HCl/KCl buffer (pH 2.0).

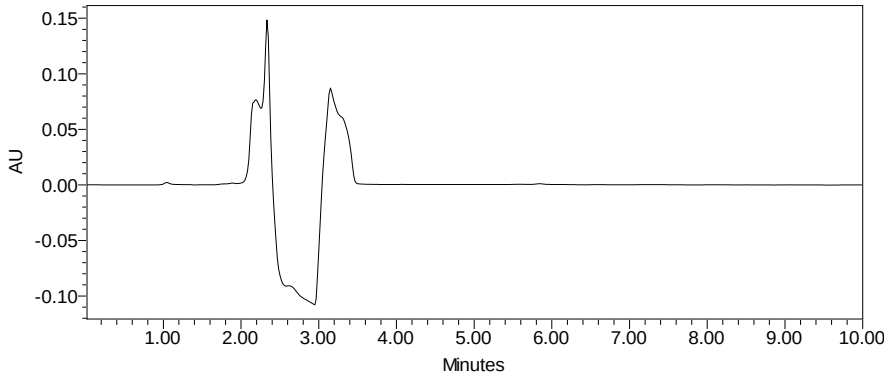

Figure S2.5. Representative chromatogram of PBS (pH 6.8).

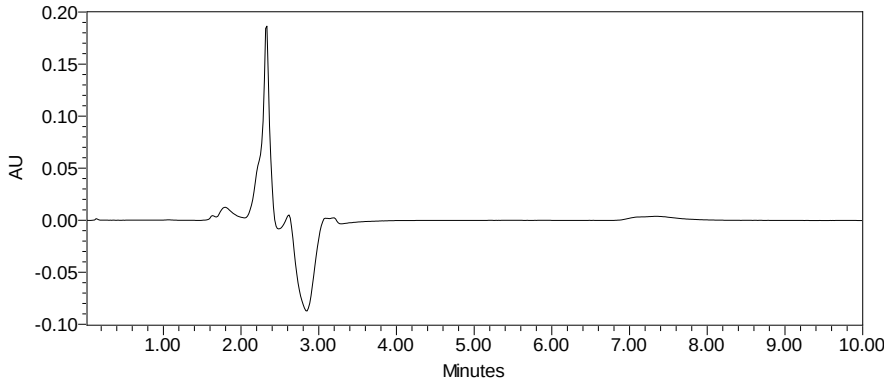

Figure S2.6. Representative chromatogram of TC-199 without lactose buffer (pH 7.2).

S2.3. Precision

Precision intra-assay was evaluated by performing repeatability. For this test, two concentrations (medium and high of the curve) were injected three times in the same day. From the data obtained, the developed HPLC method was found to be precise. The results were expressed as the percentage of relative standard deviation (RSD) and recovery (Table S2.2).

Table S2.2. Results of precision test for insulin from standard concentrations in HCl/KCl (pH 2.0), PBS (pH 6.8) and in TC-199 without lactose (pH 7.2) buffers (n = 3).

	HCl/KCl		**PBS**		**TC-199**	
Standard solutions (µg/mL)	**RSD (%)**	**Recovery (%)**	**RSD (%)**	**Recovery (%)**	**RSD (%)**	**Recovery (%)**
24.5	2.45	95.03	3.45	101.36	0.42	106.44
98.0	1.10	92.00	0.17	94.21	0.73	100.36

S2.4. Accuracy

Accuracy of the method was defined as the percentage recoveries of mean of a known amount of insulin, which is assessed as standardized agreement between the measured value and the true value by determination of the RSD.

The recovery varied from 91.91 to 106.12 % for HCl/KCl buffer, from 83.16 to 99.46 % for PBS and from 88.94 to 102.74 % for TC-199 buffer (Table S2.3, Table S2.4 and Table S2.5, respectively).

Table S2.3. Validation parameters for insulin quantification in HCl/KCl buffer (pH 2.0).

Theoretical concentration (µg/mL)	Experimental concentration (µg/mL)	Standard deviation (SD)	Recovery (%)	RSD (%)
1.96	1.99	0.07	101.53	3.55
4.90	5.20	0.11	106.12	2.22
9.80	9.40	0.12	95.91	1.34
24.5	24.23	0.32	98.89	1.34
49.0	48.31	0.51	98.59	1.05
73.5	73.51	1.93	100.00	2.62
98.0	98.16	3.02	100.16	3.08

Table S2.4. Validation parameters for insulin quantification in PBS (pH 6.8).

Theoretical concentration (µg/mL)	Experimental concentration (µg/mL)	Standard deviation (SD)	Recovery (%)	RSD (%)
1.96	1.63	0.10	83.16	6.14
4.90	4.52	0.09	92.24	2.08
9.80	8.73	0.10	89.08	1.18
24.5	23.56	0.26	96.16	1.12
49.0	48.14	0.42	98.24	0.87
73.5	72.84	1.57	99.10	2.16
98.0	97.48	2.46	99.46	2.53

Table S2.5. Validation parameters for insulin quantification in TC-199 buffer (pH 7.2).

Theoretical concentration (µg/mL)	Experimental concentration (µg/mL)	Standard deviation (SD)	Recovery (%)	RSD (%)
1.96	1.74	0.05	88.94	3.28
4.90	4.91	0.03	100.34	0.65
9.80	9.97	0.39	101.74	1.79
24.5	24.30	0.57	99.20	1.47
49.0	48.91	0.55	99.82	0.68
73.5	73.54	0.64	100.06	0.58
98.0	98.09	1.79	100.09	1.14

References

Épshtein, N., 2004. Validation of HPLC techniques for pharmaceutical analysis. Pharm Chem J 38, 212-228.

International conference on harmonization (ICH) of technical requirements for the registration of pharmaceuticals for human use, 1996. Validation of Analytical Procedures: Methodology (ICB-Q2B).

Chapter X
Publication list

The work presented on this thesis, or parts of it, permitted: i) the publication of two book chapters (one already published, other in press), ii) the preparation of several manuscripts that have been submitted for appreciation, and iii) the participation on several national and international meetings, being the respective abstracts published in the abstract book/ proceedings of the respective meeting.

Book Chapters

Andreani, T., Souza, A.L.R., Silva, A.M., Souto, E.B. Sol-gel carrier system: A novel controlled drug delivery. *In* Patenting Nanomedicines: Emerging Threats versus Grant Opportunities. Ed. Springer, Heidelberg, Germany (2012), Chap. 5, pp. 151 - 166. Doi 10.1007/978-3-642-29265-1_5.

Andreani, T., Venkatesh, N., Ferreira, S.F., Silva, A.M., Souto, E.B. Emerging Technologies of Polymers for Nanomedicine Applications. *In* Nanotechnology and Drug Delivery: Vol. 2 Nano-Engineering Strategies and Nanomedicines against Severe Diseases. J. L. Arias Mediano (Ed.), CRC Press, Taylor & Francis Group, Boca Raton, FL, USA. (in press, March 2015). ISBN 9781482262711.

Publications in ISI Journals (published, submitted or in preparation)

Andreani, T., Doktorovová, S., Lopes, C.M., Souto, E.B. Nano-biotechnology approaches for targeted delivery of pharmaceutics and cosmetics ingredients. Int J Nanotechnol, 8 (1/2), pp. 66-83, 2011.

Andreani, T., Souza, A.L.R., Kiill, C.P., Lorenzón, E.N., Fangueiro, J.F., Calpena, A.C., Chaud, M.V., García, M.L., Gremião, M.P.D., Silva, A.M., Souto, E.B. PEG-coated silica nanoparticles by sol-gel technology as potential oral insulin delivery. Int J Pharm (in press). DOI: 10.1016/j.ijpharm.2014.07.049.

Andreani, T. Silva, A.M., Souto, E.B. Silica-based matrices: State of the art and new perspective for biomedical and bioengineering applications. Biochem Eng J (2014)

(submitted: BEJ-S-14-00288).

Andreani, T., Kiill, C.P., Souza, A.L.R., Fangueiro, J.F., Doktorovová, S., García, M.L., Gremião, M.P.D., Silva, A.M., Souto, E.B. Effect of cryoprotectants on the reconstitution of silica nanoparticles produced by sol-gel technology. Central Eur J Chem (2014) (submitted: CEJC-S-14-00363).

Andreani, T., Miziara, L., Lorenzón, E.N., Souza, A.L.R., Kiill, C.P., Fangueiro, J.F., García, M.L., Gremião, M.P.D., Silva, A.M., Souto, E.B. A comparative study of the potential of silica hybrid nanoparticles as carriers for oral insulin delivery. Eur J Pharm Sci (2014) (submitted: EJPS-S-14-00291).

Andreani, T., Fangueiro, J.F., Silva, A.M., Jose, S., Souto, E.B. Swellable polymers for oral drug delivery: Mathematical modelling for pharmacokinetic analysis. Biomech Model Mechanobiol (2014) (submitted: BMMB-S-14-00087).

Andreani, T., Severino, P., Silva, A.M., Souto, E.B. Production of silica nanoparticles in acidic medium and colloidal stabilization by hydrophilic polymers (in preparation).

Andreani, T., Kiill, C.P., Souza, A.L.R., Fangueiro, J.F., García, M.L., Fernandes, L., Almeida M., Gremião, M.P.D., Souto, E.B., Silva, A.M. Surface engineering of silica nanoparticles for oral insulin delivery: characterization and cell toxicity assessment (in preparation).

Publications in other peer-reviewed Journals (published or submitted)

Andreani, T., Silva, A.M., Souza, A.L.R., Souto, E.B., Lopes, C.M. The GLP-1 system: Biochemistry, physiological effects and the role of DDP-IV inhibitor in the management of type 2 Diabetes *Mellitus.* RFCS-Universidade Fernando Pessoa (UFP), nº 7, pp. 6-18, 2011.

AndreaniI, T., Souto, E.B., Silva, A.M., Lopes, C.M. Miméticos do glucagon like peptide -1 (GLP-1) e seu potencial farmacêutico no controlo da diabetes tipo 2 e obesidade. RFCS-UFP, nº 6, pp. 94-102, 2009.

Silva, A.M., Lopes, C.M., Misler, S., Cooper, G.D., **Andreani, T**., Souto, E.B. Glucagon like peptide-1: Biochemistry, secretion and main physiological effects. RFCS-UFP, nº 6, pp.104-113, 2009.

Poster Presentations in International Congresses

Andreani, T., Kiill, C.P., Souza, A.L.R., Doktorovová, S., Gaivão, I., Souto, E.B., Silva, A.M. Genotoxicity study of silica nanoparticles in HepG2 cells. 3rd Conference on Innovation in Drug Delivery – Advances in Local Drug Delivery. Pisa, Italy, 22-25 September 2013.

Andreani, T., Vieira, V., Silva, A.M., Souto, E.B. Synthesis and characterization of silica scaffolds for small hydrophilic peptides. 9th Central European Symposium of Pharmaceutical Technology. Dubrovnik, Croatia, 2012.

T. Andreani, A.L.R. de Souza, A.M. Silva, E.B, Souto. Effect of PEGylation of sílica gel nanoparticles (nanogels) by sol-gel technology. World Meeting. Istambul, 2012. P 107.

Andreani T, Ribeiro de Souza A.L, Silva A.M., Souto E.B. Synthesis and characterization of chitosan-silica nanogels for oral peptide delivery. 12th International symposium of Controlled Release Society (Indian Chapter), 9 - 10 February. Mumbai, India. 2012. P 50.

T. Andreani, E.B.Souto, A.M. Silva. Particle characterization and cell toxicity assessment of silica nanoparticles for biomolecules delivery. New Trends in Pharmaceutical Sciences. Porto, 2011.

T. Andreani, C.M. Lopes, P. Boonme, E.B. Souto, A.M. Silva. Influence of TEOS concentration on the formation of silica gel nanoparticles for bioactive loading. UKPharmSci, 2011.

Andreani, T., Souza, A.L.R., Silva, A.M., Martins, C.L., Souto, E.B. Effects of mixing mode of the formation of silica nanoparticles synthesized via aqueous sol-gel process. 8th Central

European Symposium of Pharmaceutical Technology. Graz, Austria, 2010.